Technical Report Documentation Page

1. Report No.	2. Government Accession No.	3. Recipient's Catalog No.
FHWA/TX-0-1776-2		

4. Title and Subtitle	5. Report Date
Increasing the Flexural Capacity of Typical Reinforced Concrete Bridges in Texas Using Carbon Fiber Reinforced Polymers	*May 2001*
	6. Performing Organization Code
7. Author(s)	8. Performing Organization Report No.
Sergio F. Breña, Sharon L. Wood, and Michael E. Kreger	Research Report 1776-2
9. Performing Organization Name and Address	10. Work Unit No. (TRAIS)
Center for Transportation Research The University of Texas at Austin 3208 Red River, Suite 200 Austin, TX 78705-2650	11. Contract or Grant No. Research Project 0-1776
12. Sponsoring Agency Name and Address	13. Type of Report and Period Covered
Texas Department of Transportation Research and Technology Transfer Office P.O. Box 5080 Austin, TX 78763-5080	Research Report (9/97-10/00)
	14. Sponsoring Agency Code

15. Supplementary Notes

16. Abstract

A large portion of the off-system bridges and some on-system bridges in Texas were constructed in the 1950s using vehicle loads that are less than the current design standards. As a result, the legal load that is permitted to cross these bridges is often limited and many are scheduled for replacement. The use of carbon fiber reinforced polymer (CFRP) composites to increase the flexural capacity of reinforced concrete bridges was investigated in this research project. The overall goal was to develop design procedures for strengthening existing bridges using CFRP to avoid replacement of bridges that have been functioning satisfactorily for many years.

The third phase of the research project is described in this report. Four full-scale specimens representative of bridge construction during the 1950s in Texas were constructed, strengthened, and tested in the laboratory to assess the effectiveness of the CFRP composites for increasing the flexural capacity. Results from the laboratory tests indicate that the composite materials may be used successfully to strengthen existing bridges. The strength of all specimens was controlled by debonding of the CFRP composites from the surface of the concrete.

An analytical model was verified using the measured response of the laboratory specimens. The model was able to reproduce the overall response of the specimens, but did not reproduce the local modes of failure. Therefore, the model may be used to design strengthening systems for reinforced concrete bridges, but the maximum strain in the CFRP composites must be limited to reflect the observed modes of failure. Design guidelines for CFRP systems are presented.

17. Key Words	18. Distribution Statement
pan-girder bridges, flat-slab bridges, design guidelines, pultruded CFRP plate, unidirectional CFRP fabric, debonding	No restrictions. This document is available to the public through the National Technical Information Service, Springfield, Virginia 22161.

19. Security Classif. (of report)	20. Security Classif. (of this page)	21. No. of pages	22. Price
Unclassified	Unclassified	282	

Form DOT F 1700.7 (8-72) Reproduction of completed page authorized

INCREASING THE FLEXURAL CAPACITY OF TYPICAL REINFORCED CONCRETE BRIDGES IN TEXAS USING CARBON FIBER REINFORCED POLYMERS

by

Sergio F. Breña, Sharon L. Wood, and Michael E. Kreger

Research Report 1776-2

Research Project 0-1776

DEVELOPMENT OF METHODS TO STRENGTHEN EXISTING STRUCTURES WITH COMPOSITES

conducted for the

Texas Department of Transportation

in cooperation with the

U.S. Department of Transportation
Federal Highway Administration

by the

CENTER FOR TRANSPORTATION RESEARCH
BUREAU OF ENGINEERING RESEARCH
THE UNIVERSITY OF TEXAS AT AUSTIN

May 2001

Research performed in cooperation with the Texas Department of Transportation and the U.S. Department of Transportation, Federal Highway Administration.

ACKNOWLEDGEMENTS

This research project was sponsored by the Texas Department of Transportation (TxDOT) under Project No. 0-1776. The involvement of Mark Steves and Richard Wilkison from TxDOT were extremely important for the successful completion of the research project.

Manufacturers of the composite systems that participated in the project donated the composites that were used to strengthen the laboratory specimens. The support from the representatives of the different organizations is recognized. The assistance of Bill Light, Sika Corporation; Howard Kliger and Bob Snider, Master Builders Technology; Paul Gugenheim, Delta Structural Technology, Inc. (Fyfe Co.), and Ali Ganjehlou, Mitsubishi/Sumitomo Corp. is appreciated.

The pan-girder specimens were built using the steel forms that are used for construction of pan-girder bridges in the field. Donnie Liska of Liska Construction loaned the research team the pan forms required for this project. We extend our gratitude for his assistance.

This research project was conducted at the Ferguson Structural Engineering Laboratory (FSEL). The assistance of laboratory technicians and administrative staff was fundamental for the completion of this project. Many students participated at different times during the duration of this project. Regan Bramblett presented the results of the first phase of the investigation as her Masters Thesis. Michaël Benouaich participated in the construction, testing, and data reduction of the beams subjected to repeated loads. Nicole García, Sarah Orton, and Janna Renfro participated during the fabrication and testing of specimens at different phases of the project. Testing would have taken much longer without their assistance.

DISCLAIMER

NOTICE

S. L. Wood, Texas P.E. #83804

M. E. Kreger, Texas P.E. #65541

Research Supervisors

TABLE OF CONTENTS

LIST OF FIGURES

LIST OF TABLES

SUMMARY

A large portion of the off-system bridges and some on-system bridges in Texas were constructed in the 1950s using vehicle loads that are less than the current design standards. As a result, the legal load that is permitted to cross these bridges is often limited and many are scheduled for replacement. The use of carbon fiber reinforced polymer (CFRP) composites to increase the flexural capacity of reinforced concrete bridges was investigated in this research project. The overall goal was to develop design procedures for strengthening existing bridges using CFRP to avoid replacement of bridges that have been functioning satisfactorily for many years.

The third phase of the research project is described in this report. Four full-scale specimens representative of bridge construction during the 1950s in Texas were constructed, strengthened, and tested in the laboratory to assess the effectiveness of the CFRP composites for increasing the flexural capacity. Results from the laboratory tests indicate that the composite materials may be used successfully to strengthen existing bridges. The strength of all specimens was controlled by debonding of the CFRP composites from the surface of the concrete.

An analytical model was verified using the measured response of the laboratory specimens. The model was able to reproduce the overall response of the specimens, but did not reproduce the local modes of failure. Therefore, the model may be used to design strengthening systems for reinforced concrete bridges, but the maximum strain in the CFRP composites must be limited to reflect the observed modes of failure. Design guidelines for CFRP systems are presented.

Chapter 1: Introduction

1.1 BACKGROUND

A comprehensive research program was conducted at the University of Texas to investigate the effectiveness of carbon fiber reinforced polymer (CFRP) composites to strengthen existing reinforced concrete bridges. The first two phases of the research project involved testing strengthened rectangular beams under static or fatigue loads. In these two phases of the project, different materials and strengthening schemes were used to evaluate the response of the different specimens. The results of the first two phases of the research project are presented in a companion report by Breña, et al. (2001).

The need to evaluate the applicability of these techniques to full-size specimens was identified as an important component of the project at the early stages. This report concentrates on the description and testing of four full-scale bridge components conducted in the Ferguson Structural Engineering Laboratory. However, a summary of the results from the rectangular beam tests is presented in Section 1.3.

1.2 IDENTIFICATION OF CANDIDATE BRIDGES

A large percentage of the total number of bridges in Texas is part of off-system roadways. Pan-girder and flat-slab bridges are commonly found along these roads. Approximately 30% of the total number of pan-girder bridges and 20% of the total number of flat-slab bridges were not designed using the current design truck (HS-20). Therefore, many of these bridges are load posted and do not meet the TxDOT criteria for roadway widening discussed in the companion report of this project [Breña et al., 2001]. Because of the large number of these types of bridges, pan-girder and flat-slab bridges were selected as candidates for the application of the strengthening methods investigated in this research project.

1.3 OBJECTIVES AND SCOPE OF RESEARCH

The objectives of this research project were to investigate the effectiveness of composite materials to strengthen reinforced concrete bridges, and to develop design guidelines for the safe implementation of these materials in existing bridges. The use of the guidelines presented in this report is limited to bridges that do not show signs of damage or deterioration. The bridges considered in this investigation were inspected recently, and there were no indications that the original capacity has been compromised.

To meet the goals of this project, a comprehensive research program was developed in coordination with TxDOT engineers. The overall research project was divided into three phases. A summary of the most important results from phase 1 and 2 are presented in Sections 1.3.1 and 1.3.2, respectively. Only the results from phase 3 are presented in detail in this report, but results from the other phases are referenced throughout.

1.3.1 Summary of Results from Beams Subjected to Static Loads

Twenty-two rectangular beams were tested in the first phase of the research project to investigate the effect of CFRP composites on the flexural strength of reinforced concrete elements. Composites supplied by four different manufacturers were used in this part of the project. The main objective of this phase of the research project was to develop strengthening schemes using CFRP composites that would produce

reliable and repeatable response of the strengthened elements (Fig. 1.1). The effects of placement of the composite on the reinforced concrete element, external anchorage using transverse composites straps, and long-term wetting and drying cycles were among the variables included in these tests. Breña et al. [2001] give a detailed discussion of the results obtained from the beams tested in phase 1. Therefore, only a summary of the most important research findings are presented here.

The laboratory tests were initially designed to determine the bond length required to develop the rupture stress of the composite before the CFRP composites debonded from the surface of the concrete. The CFRP was bonded to the tension face to maximize the contribution to the flexural capacity of the beams. All beams were simply supported and were subjected to four-point loading (Fig. 1.2). The bond length was measured from a critical section, where a crack was pre-formed in the beams, to the end of the composite. The critical section also corresponded to the position of one of the applied loads on the beams (Figure 1.1b). However, the results from these tests indicated that debonding of the CFRP composites from the surface of the concrete was the controlling mode of failure for all specimens, even when the composites were bonded along the entire span.

The tests with composites applied to the bottom face of the specimens revealed that debonding predominantly initiated from the flexural crack closest to the critical section on the shear span of the beams. The combination of shear and moment caused the crack to open and simultaneously generate a vertical offset on the surface of the concrete (Fig. 1.2). This phenomenon triggered local debonding of the composite in the vicinity of the crack due to prying action. Therefore, ways to control the detrimental effects of local debonding due to vertical offset of the surface of the beam were investigated.

The addition of transverse composite straps along the bonded length of the laminate arrested the debonding crack and prevented it from spreading along the entire length. This technique was initially implemented on beams with composites attached to the bottom face (Figure 1.1c).

Another strengthening configuration was investigated to delay local debonding caused by the vertical offset at flexural cracks. In this scheme the CFRP composites were attached to the side faces of the beams to eliminate the prying action that caused local debonding (Figure 1.1d). Also, a combination of the schemes presented in Figure 1.1c and Figure 1.1d was tested in some beams. Transverse CFRP woven fabric was wrapped around the CFRP pultruded plates that were attached to the sides of the beams (Figure 1.1e).

The test results indicated that debonding was delayed by the addition of transverse straps along the span of the specimens. In most cases, however, failure of the beams was still controlled by debonding of the CFRP composites. The measured strains on the composites in beams with transverse straps were larger than the strains on the composites developed in beams with the composites bonded to the bottom surface. In some specimens, although debonding had initiated at several locations, failure was controlled by CFRP rupture. This event indicated that the maximum composite strain was reached before total debonding from the surface of the concrete occurred. This technique was only used for beams strengthened using wet-layup composite systems.

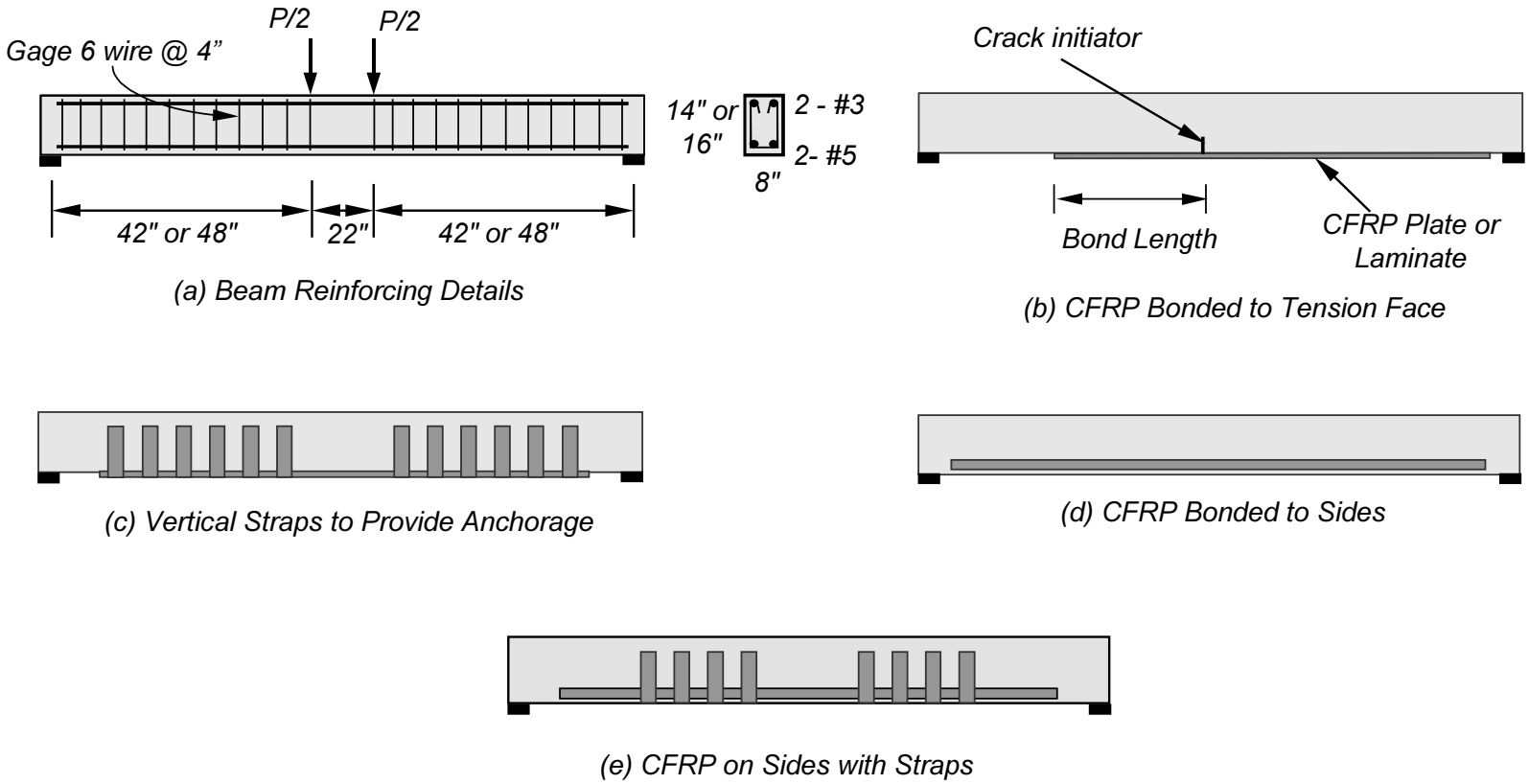

Figure 1.1 Summary of CFRP Configurations Used in Phase

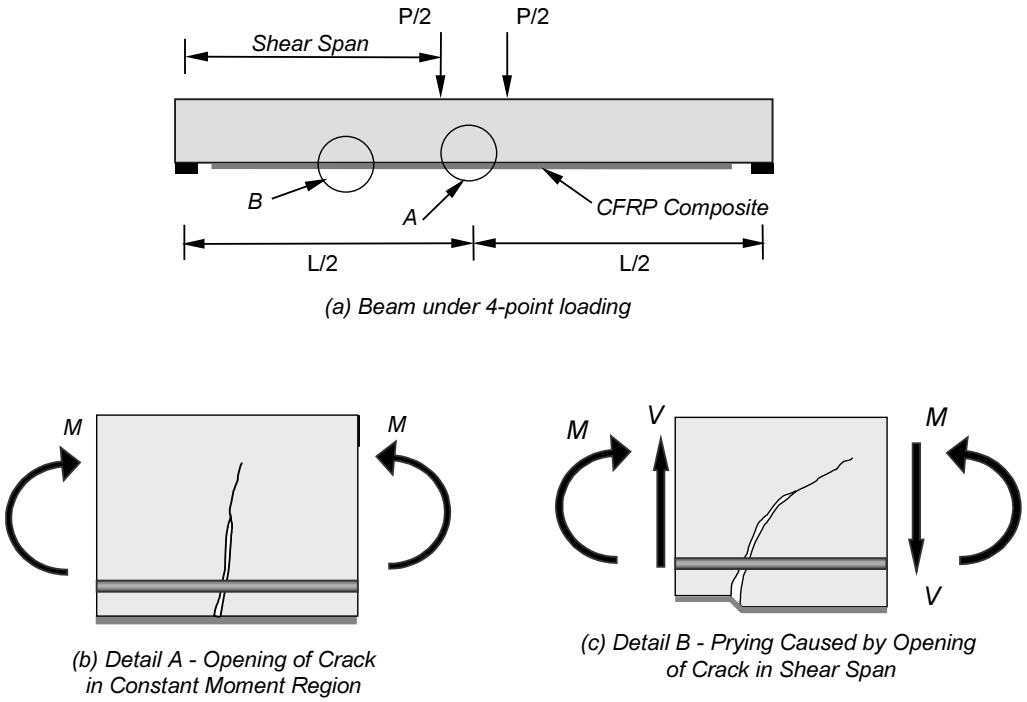

Figure 1.2 Prying Action Observed on CFRP Composite Attached to the Bottom Surface of the Beams

Attaching the composites to the sides of the beams was also effective in delaying total debonding. One beam was strengthened using a CFRP wet-layup system, and two beams were strengthened using a CFRP pultruded system using this technique. The beam strengthened with the wet-layup system failed by rupture of the CFRP laminate at the critical section. Both beams strengthened using the pultruded system failed by debonding of the composite from the surface of the concrete. However, these beams failed after significant deformations had occurred, and local debonding was observable at several locations along the CFRP plates.

The largest measured CFRP strains corresponded to beams where one of the techniques devised to delay debonding was used. A summary of the maximum measured CFRP strains on the beams tested in phase 1 is presented in Table 1.1. The beams where debonding was delayed by one of the methods described in this section achieved a more ductile and repeatable response.

Two beams were tested statically to failure after being exposed to cycles of wet and dry conditions. These beams were strengthened using an identical strengthening scheme as used for beam B4. A sustained load equal to 20% of the yield load was also applied in one of the beams. The results of these tests indicate that the bond between the composite and the surface of the concrete was not affected by exposure to moisture or sustained load. Both beams failed by CFRP rupture, and the maximum measured CFRP strains were comparable to beam B4.

Table 1.1 Summary of Test Results from Beams in Phase 1

Specimen	CFRP Strengthening Scheme	Failure Mode	Maximum Measured Strain in CFRP
Control A & B	None	Crushing	NA
A1	Bottom	Debonding	0.0079
A2	Bottom	Debonding	0.0061
A3	Bottom	Debonding	0.0120
A4	Bottom	Debonding	0.0078
B1	Bottom	Debonding	0.0072
B2	Bottom w/Straps	CFRP Rupture	0.0113
B3	Sides	CFRP Rupture	0.0107
B4	Bottom w/Straps	CFRP Rupture	0.0119
B5	Bottom w/Straps	CFRP Rupture	0.0132
Control C & D	None	Crushing	NA
C1	Bottom	Debonding	0.0076
C2	Bottom	Debonding	0.0070
C3	Bottom w/Straps	CFRP Rupture	0.0075
C4	Sides	Debonding	Unavailable
D1	Bottom	Debonding	0.0035
D2	Bottom	Debonding	0.0048
D3	Sides	Debonding	0.0044
D4	Sides w/Straps	Debonding	0.0065
D5	Sides w/Straps	Debonding	0.0062
A-LT1	Bottom w/Straps	CFRP Rupture	0.0111
A-LT2	Bottom w/Straps	CFRP Rupture	0.0118

Results from this phase indicate that all four of the commercially available CFRP systems could be used to strengthen undamaged reinforced concrete beams. Two were selected for study in phase 3 because they are representative of the different composite systems that were used in phase 1. Therefore these techniques were used in the strengthening schemes for the large scale specimens. A conservative value of the maximum measured CFRP strains in the beams where these schemes were implemented was obtained from the tests in phase 1 and used for design of the strengthening schemes in phase 3. The maximum strain that could be reliably developed in the CFRP composites was assumed to be 0.007.

1.3.2 Summary of Results from Beams Subjected to Fatigue Loads

Bridge elements are subjected to live loads that are applied repeatedly throughout their design life. Therefore, it was considered important to investigate the effects of repeated loads on the behavior of the reinforced concrete beams strengthened using CFRP composites.

Eight rectangular beams strengthened using two different composite systems were subjected to load cycles using different load amplitudes to investigate the effect of cycling on the response of the beams in phase 2. The beams were divided in two groups; four beams were strengthened using an identical strengthening scheme as beam B4, and four were strengthened using a strengthening scheme identical to beam D5. Therefore, it was possible to directly compare the beam response after load cycling to the companion specimens tested during phase 1. The experimental setup was identical to the one used for phase 1, but the load was controlled using a closed-loop system in this case. The load was applied cyclically from a load approximately equal to zero to the load that generated the desired stress in the steel reinforcement.

The load amplitude was selected initially to represent service-load conditions in an existing bridge. Therefore, the beams were subjected to repeated loads that generated stresses equal to 30% or 50% of the yield stress on the longitudinal steel reinforcement. These beams were subjected to either 10,000 or 1,000,000 cycles of load and then tested statically to failure. Results from these tests indicated that the bond between the composites and the surface of the concrete did not deteriorate with service-level loading cycles because all the beams failed at approximately the same load as the companion beams tested in phase 1 (Figure 1.3).

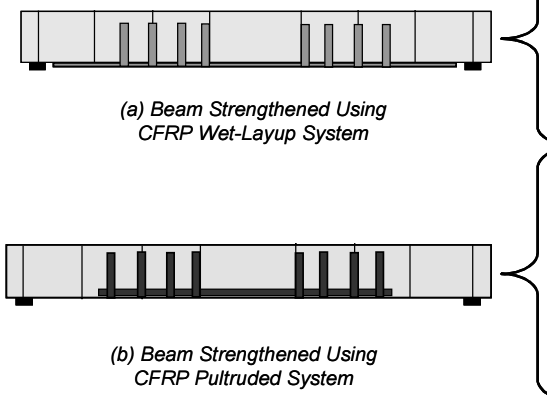

Beam	No. of Cycles	Stress Range	Failure
A-F1	10,000	0.3 fy	Static Test
A-F2	1,000,000	0.3 fy	Static Test
A-F3	1,000,000	0.5 fy	Static Test
A-F4	156,000	0.9 fy	Fracture of Reinforcing Bars
D-F1	1,000,000	0.3 fy	Static Test
D-F2	1,000,000	0.5 fy	Static Test
D-F3	55,000	0.9 fy	Bond Fatigue
D-F4	8,990	1.1 fy	Bond Fatigue

Figure 1.3 Summary of Results from Phase 2

Subsequently, the remaining beams were subjected to higher stress ranges to cause either fatigue failure between the composite and surface of the concrete or of the reinforcing steel. One beam strengthened using a wet-layup composite system failed by fatigue of the steel reinforcement after the application of 156,000 load cycles at a reinforcing bar stress amplitude equal to 90% of the yield stress (Figure 1.3a). Two beams strengthened with a pultruded composite system failed by fatigue of the bond between the composite and the surface of the concrete at stress ranges equal to 90% and 110% of the yield stress (Figure 1.3b).

The results from these tests indicate that cycling under stresses representative of service-load conditions does not deteriorate the bond between the composite and the surface of the concrete. Beams subjected to service-load level stress ranges failed at approximately the same load as the companion specimens tested in phase 1. Fatigue failures were only generated after cycling to very high stress ranges.

1.3.3 Description of Full-Scale Tests and Organization of Project Report

Four full-scale laboratory specimens representative of reinforced concrete bridges in Texas were constructed and tested in phase 3. For this phase of the research project, candidate bridges were first identified in conjunction with TxDOT engineers. The behavior of strengthened reinforced concrete bridge elements using CFRP composites was investigated in the laboratory. A detailed presentation of the design, construction and laboratory tests for phase 3 is included in this report.

To meet the objectives of this investigation, it was considered essential to be able to calculate the capacity and reproduce the behavior of the laboratory specimens representing the strengthened bridge elements that were selected for this project. The analytical model developed in the first phase of this research project [Breña, et al., 2001] was modified to reproduce the key features of the behavior of the full-scale strengthened elements. The refinements implemented into the analytical model are presented in Chapter 2. The refined analytical model was also used as the basis for the design procedure presented in Chapter 9.

Pan-girder bridges were one of the two types selected for detailed investigation in this project. The prototype bridge selected for this study is presented in Chapter 3. The design of the laboratory specimens is also discussed in this chapter. The measured response of two pan-girder specimens is presented in Chapter 4, and the analytical model is verified using measured response of the pan-girder specimens in Chapter 5.

Flat-slab bridges were also selected for investigation in the research project. The prototype bridge that was selected to represent this type of construction is presented in Chapter 6. Particular aspects of this form of construction and the criteria adopted to design the strengthening schemes are also discussed. The measured response and observed behavior of the two flat-slab specimens are discussed in Chapter 7. The analytical model is verified using the measured response of the flat-slab specimens in Chapter 8.

The primary goal of the research project was to develop design guidelines that would produce safe designs of strengthening schemes for the reinforced concrete bridges studied throughout the project. The design recommendations presented in Chapter 9 are based on the experience gained from the laboratory tests of the strengthened specimens. Finally, the conclusions that can be drawn from the results of this investigation are summarized in Chapter 10. Areas requiring further research are also identified.

Chapter 2: Refinement of Analytical Model

2.1 INTRODUCTION

This chapter describes some refinements that were implemented in the analytical model that was described in a companion report of this research project [Breña et al., 2001]. Procedures to calculate the moment-curvature response of strengthened sections were presented in detail in that report. Some of the assumptions that were used in the model are refined in this chapter based on the observed response of the rectangular beams tested under monotically increasing loads.

The mechanical properties of the reinforcing steel that was used to fabricate the large-scale specimens were different from those used in the rectangular beams. Therefore, a material model suitable to the measured properties of the reinforcing steel was incorporated into the model to calculate the moment-curvature response of the large-scale specimens accurately. The uniaxial material model for reinforcing steel that was added to calculate the moment-curvature response is presented in Section 2.2.

The model initially assumed that the CFRP composites remained attached to the concrete surface. Using this assumption, the maximum stress that can be developed in the CFRP is equal to the rupture stress, f_{pu}. The contribution of the CFRP composite to the total tensile force became zero once the rupture stress was reached. However, experimental testing showed that debonding usually occurred before reaching the CFRP rupture stress, and the model was subsequently modified to account for this failure mode (Section 2.3.1).

The procedure to calculate moments and their associated curvatures assumes that the CFRP composites are attached to the reinforced concrete section before any load is applied. However, dead loads are always on a structure before strengthening, and this needs to be considered particularly for field applications. A modification to the procedure presented in this section is described in Section 2.3.2 to account for the presence of dead loads on the section before bonding the CFRP composites.

2.2 STRESS-STRAIN MATERIAL MODELS USED FOR SECTIONAL ANALYSIS

Three material models were used to calculate the response of the strengthened reinforced concrete sections as described in Chapter 3 of the companion report [Breña et al., 2001]. The parameters that are needed to define each material model were based on the measured material properties for concrete and steel, and data obtained from the manufacturers' data for the CFRP composites (Appendix A). Tests on the reinforcing bars used to fabricate the large-scale joist specimens revealed that the steel did not exhibit a well-defined yield point. Therefore, a material model for the uniaxial behavior of reinforcing steel was added to the analytical model to incorporate this effect. This material model was used in addition to the other models defined in the previous report. The details of this model are discussed below.

Reinforcing steel that did not exhibit a well-defined yield point was approximated using the model proposed by Menegotto and Pinto [1973]. In this model the stress-strain relationship of steel is described by an equation that represents a curved transition between initial and final asymptotes to the measured stress-strain curve (Figure 2.1). The nonlinear stress-strain response of steel can be approximated using the following equation:

$$\frac{f}{f_0} = b\frac{\varepsilon}{\varepsilon_0} + \frac{(1-b)\frac{\varepsilon}{\varepsilon_0}}{\left[1+\left(\frac{\varepsilon}{\varepsilon_0}\right)^n\right]^{\frac{1}{n}}} \tag{2.1}$$

where:

f_0 = Stress at intersection of initial and final asymptotes to the stress-strain curve.

ε_0 = Strain at intersection of initial and final asymptotes to the stress-strain curve.

b = Ratio of the slopes of the final to initial asymptotes to the stress-strain curve, $b = \frac{E_\infty}{E_0}$.

n = Parameter that defines the curvature of the transition from the initial asymptotic line to the final asymptotic line.

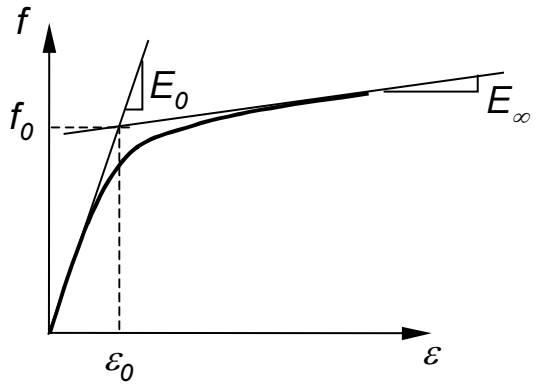

Figure 2.1 Idealized Stress-Strain Relationships for Steel

The parameters in the Menegotto-Pinto model can be determined using the following steps [Stanton and McNiven, 1979]:

- Obtain initial and final asymptotic lines to the stress-strain curve.
- Compute the ratio of initial to final asymptotic lines, b. Find coordinates at the intersection of asymptotes (f_0 and ε_0).
- Normalize stress-strain curve by f_0 and ε_0.
- Compute d^*, where $d^* = \frac{f}{f_0} - b$ at $\frac{\varepsilon}{\varepsilon_0} = 1$.
- Calculate $n = \frac{\log 2}{\log(1-b) - \log d^*}$.

After calculating the Menegotto-Pinto parameters using this procedure, the exponential factor n was modified to better fit the measured stress-strain relationship. Appropriate values of these parameters are reported in Appendix A.

2.3 REFINEMENT OF ANALYTICAL MODEL

2.3.1 Limiting Debonding Strain of CFRP Composites

The analytical model described in the companion report of this research project [Breña et al., 2001] was modified based on the results obtained in the rectangular beam tests. Evaluation of previous experimental research indicated that the maximum measured strains developed in the CFRP composites varied significantly depending on the strengthening scheme. This strain clearly depends on the ability of the CFRP to deform without debonding from the surface of the concrete.

Anchoring the CFRP composites was required to develop the maximum rupture strain reliably. Otherwise, the bond properties between the composite and the concrete surface are highly dependent on the concrete surface conditions at the time of strengthening. In many cases, anchoring was not sufficient to develop the rupture strain of the CFRP material, but a more stable response was achieved.

The model was therefore modified to permit debonding before rupture of the CFRP. This was accomplished by limiting the maximum strain that can be developed in the CFRP. A unique value for the limiting strain could not be defined at this stage in the research project because of the sparse test data. For the design of the large-scale test specimens, however, a limiting strain was selected based on the measured strains in the rectangular beam tests [Breña et al., 2001]. In some of these tests, transverse composite straps were provided to control debonding of the longitudinal CFRP composites that were designed to increase the flexural strength. The CFRP systems used in these tests were similar to those selected for strengthening the large-scale tests in this phase of the research program.

Maximum CFRP strains were measured on two types of carbon composites: a pultruded CFRP system and a wet-layup CFRP system. The average maximum measured strains in the CFRP systems attached to the rectangular beams that also contained transverse straps were 0.0065 and 0.011 for the pultruded and the wet-layup systems, respectively. The average strains were calculated based on two beams for the pultruded system and four beams for the wet-layup system. A limiting CFRP strain value within this range was selected for the design of the large-scale specimens ($\varepsilon_{CFRP} = 0.007$). The maximum measured strains will be compared with the value assumed for design in Chapter 5 for the pan-girder specimens and Chapter 8 for the flat-slab specimens.

2.3.2 Initial Strains Caused by Dead Loads

The analytical model was initially developed based on the assumption that the CFRP composites were attached to the surface of the concrete when the reinforced concrete element was in an undeformed state. This assumption may be valid for elements tested in the laboratory where the CFRP composites are bonded to the concrete before the beam is subjected to dead loads. However, existing bridges and the full-scale specimens tested in this part of the experimental program must continue to carry dead load while the CFRP composites are being applied. Therefore, the reinforcing bars and concrete must carry the total strains induced by the combined live and dead load, but the CFRP composites carry only the strains induced by the live load.

The analytical model was modified to accommodate an initial strain profile. The computational procedure followed the same steps as those described in Section 3.2.3 of the companion report, except that the dead load strains in the concrete and steel were calculated first. These strains were added to the live-load strains at each step in the analysis, and the internal stresses and forces in the materials were calculated using the total strains (Figure 2.2). Only the live load strains contributed to the response of the

CFRP composites. The live-load strains were assumed to vary linearly with depth. However, a discontinuity existed in the total strain profile due to the dead-load strains.

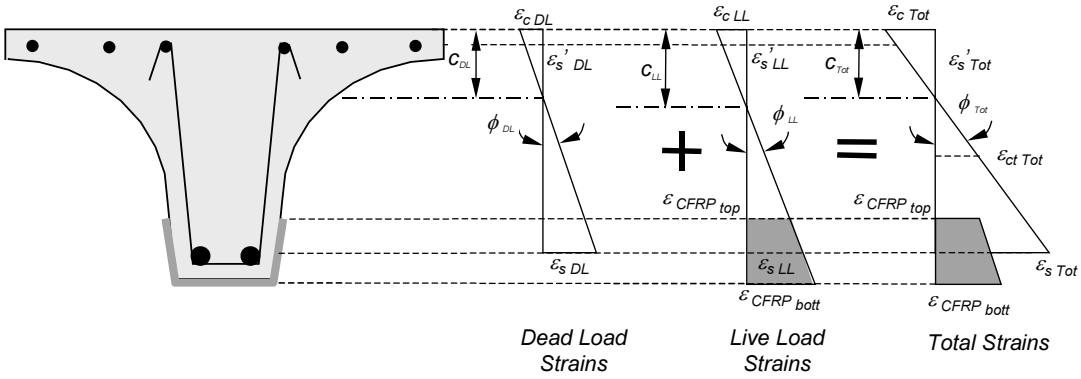

Figure 2.2 Effect of Initial Dead Load Strains on Calculation of Moment-Curvature Response

2.4 SUMMARY

The refinement to the analytical model presented in the companion report of this research project to calculate the moment-curvature response of reinforced concrete sections strengthened using CFRP composites was presented in this chapter. Most beams tested under static loads failed after the CFRP composite debonded from the surface of the concrete, and the original model was not capable of reproducing this mode of failure. The model was therefore refined by adding a limiting composite strain before debonding. The model was also modified to include the strains caused by dead loads on the structure before the composites are bonded to the surface of the concrete.

The analytical method presented in this chapter was used to design the composite systems to strengthen the large-scale specimens for this experimental program. The measured response of these specimens is compared with the calculated response in Chapters 5 and 8.

Chapter 3: Description of Pan-Girder Specimens

3.1 INTRODUCTION

Pan-girder construction was a very popular type of construction in Texas in the 1950s for reinforced concrete bridges spanning 30 to 40 feet. Even today, some bridges with spans up to 40 feet are built using this form of construction. The name given to this type of bridge comes from the formwork used to construct them. Pan-girder bridges are cast using self-supporting metal forms that span from one bent-cap to the next. The forms have a cross-section consisting of an upper semi-circular portion with straight ends at the bottom on each side (Figure 3.1). Two pans are placed next to each other to form one concrete web. Adjoining pans are connected using bolts that pass through holes on the sides of the forms.

Because the pans are not perfectly straight, concrete can flow through gaps between adjacent forms during the casting operation leaving an irregular bottom surface on the bridge webs (Figure 3.2). Although this surface irregularity does not affect the bridge capacity, it does influence the placement of composites used to strengthen the bridges. The composites that were used to strengthen this type of bridge could not be placed along the middle of the web soffit without significant surface preparation. This constraint was considered when designing the strengthening method for pan-girder bridges in order to minimize the labor involved in preparing the concrete surface.

Figure 3.1 View of Metal Pan-Forms inside the Laboratory

The prototype bridge that was selected to examine the effectiveness of the composite strengthening procedures is described in this chapter. The inventory rating for the prototype bridge was calculated to estimate the percent increase in capacity that would be required to upgrade it to a higher design load. Calculated capacities of both prototype and laboratory specimens are compared.

Two strengthening schemes used to meet the desired increase in capacity are presented in this chapter. The physical characteristics of the two different composite systems are highlighted. Finally, the calculated capacities of the strengthened specimens are compared with the flexural strength required to increase the load rating of the prototype bridge to an HS-20 design standard.

Figure 3.2 Photograph of Pan-Girder Bridge in Buda, Texas Indicating Uneven Surfaces on Bottom of Joists

3.2 PROTOTYPE BRIDGE

Most pan-girder bridges constructed in Texas during the 1950s were designed to carry two H-10 or two H-15 design vehicles. Modern bridges are designed to carry two HS-20 design vehicles.

Drawings were obtained from TxDOT for a standard, two-lane, pan-girder bridge designed in 1951 for two H-10 trucks. This bridge was used as the prototype for the laboratory tests and was considered to represent the worst case scenario for existing bridges.

3.2.1 Physical Characteristics of Prototype Bridge

The prototype bridge was designed for a 30-ft span. The drawings included options for roadway widths ranging from 14'-4½" to 23'-4½". The narrowest bridge had eight joists and the widest had eleven. The bridge cross section and reinforcement details are shown in Figure 3.3. The total depth of the bridge is 24 in. and girder webs are 8¼ in. wide. The slab has a minimum thickness of 3½ in. There are structural curbs on each side of the bridge that extend 1'-6" above the bridge deck.

The longitudinal reinforcement consists of 2 - #11 bars, and the shear reinforcement consists of #3 stirrups spaced at 15 in. throughout the span. Slab reinforcement consists of #4 bars at 12 in. longitudinally, and #5 bars at 10 in. transversely.

The joists in the prototype bridge are supported directly on bent caps. One layer of roofing felt is placed between the end diaphragms and the bent cap. Although these types of bridges were designed as simply-supported spans, measured response during diagnostic load tests of an existing pan-girder bridge indicates that significant end-restraint is provided by adjacent bridge spans [Velázquez, 1998].

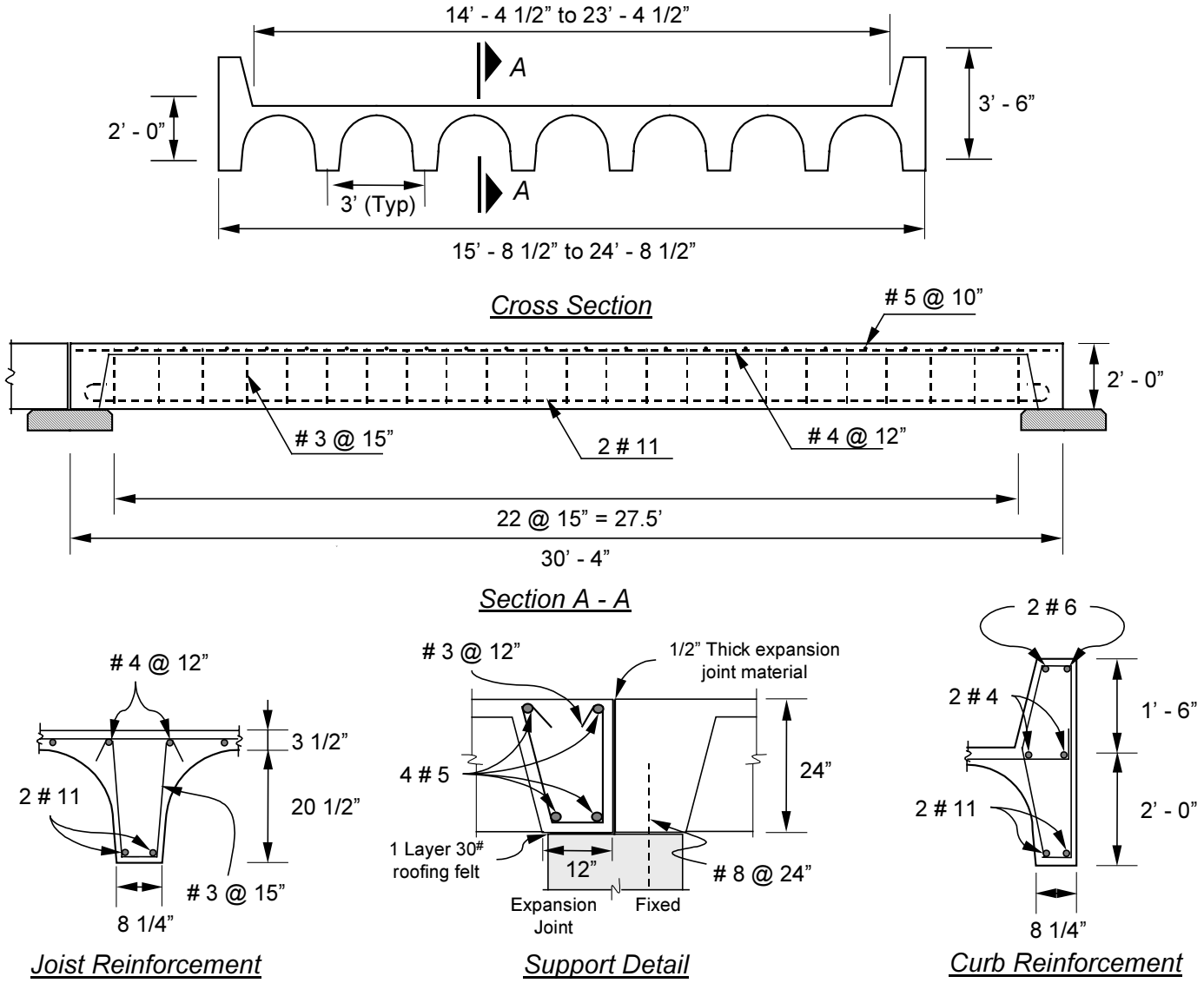

Figure 3.3 Reinforcement Details for Prototype Bridge

3.2.2 Calculated Capacity of Prototype Bridge

Nominal flexural and shear capacities of the prototype bridge were calculated in accordance with the current AASHTO *Design Specifications* [AASHTO, 1996]. Because the actual material strengths were unknown and the nominal design values were not reported on the structural drawings, values recommended in the *AASHTO Manual for Condition Evaluation of Bridges* [AASHTO, 1994] for concrete and reinforcing bar strengths were used. Concrete was assumed to have a compressive strength of 3,000 psi, and reinforcing steel was assumed to have a yield stress of 33,000 psi.

Although the selected prototype bridge was designed with integral structural curbs on each side of the road, the curbs must be removed to widen the bridge. In addition, many pan-girder bridges in Texas were constructed without the concrete curbs, so the joists must carry all the bridge loads longitudinally into the bent caps. For these two reasons, the contribution of the curbs to the flexural capacity of the bridge was neglected in this analysis.

Design flexural strength for each joist was computed using standard design procedures [AASHTO, 1996]:

$$\phi M_n = A_s f_y \left(d - \frac{a}{2} \right) \qquad \text{with} \qquad a = \frac{A_s f_y}{b\left(0.85 f'_c\right)} \tag{3.1}$$

Similarly, the design shear strength was calculated as [AASHTO, 1996]:

$$\phi V_n = \phi \left(V_c + V_s \right) \tag{3.2}$$

where

M_n = Nominal flexural strength, lb-in.

V_n = Nominal shear strength of member, lb.

V_c = $2\sqrt{f'_c}\, b_w\, d$ = concrete contribution to shear strength of member, lb.

V_s = $\frac{A_v f_y d}{s}$ = steel shear reinforcement contribution to nominal shear strength of member, lb.

ϕ = Strength reduction factor, equal to 0.9 for flexural effects and 0.85 for shear effects.

A_s = Area of flexural reinforcement, in^2.

A_v = Area of shear reinforcement within a distance s, in^2.

d = Distance from extreme compression fiber to centroid of flexural reinforcement, in.

b = Width of compression face of member, in.

b_w = Web width used to compute V_c, in.

s = Spacing of shear reinforcement, in.

f_y = Yield strength of flexural or shear reinforcement, psi.

f'_c = Concrete compressive strength, psi.

The concrete contribution to the shear strength was calculated using the web width increase allowed for members with tapered sections [AASHTO, 1996]. Therefore, the web width for concrete shear strength, b_w, was calculated as 1.2 times the minimum joist width. The calculated nominal flexural and shear capacities for a single joist in the prototype bridge are listed in Table 3.1 along with the parameters used in the calculations.

Table 3.1 Calculated Flexural and Shear Capacities of a Single Joist in the Prototype Bridge

Parameter	Value
f'_c, psi	3,000
f_y, psi	33,000
A_s, in.^{2}	3.12
b, in.	36
b_w^*, in.	9.9
A_v, in.^{2}	0.22
d, in.	21.625
ϕ flexure	0.9
ϕ shear	0.85
ϕM_n, kip-ft	162.6
V_c, kip	23.5
V_s, kip	10.5
ϕV_n, kip	28.9

* $b_w = 1.2\ b_{min} = 1.2(8.25) = 9.9$ in. [AASHTO, 1996]

3.2.3 Load Rating for Prototype Bridge

The load factor method given in the AASHTO *Manual for Condition Evaluation of Bridges* [AASHTO, 1994] was used to rate the prototype bridge. Details of the load rating procedure are given in Appendix B. Two load-rating levels are described in the AASHTO *Manual* [AASHTO, 1994]: inventory rating and operating rating. The difference between the two is the load factors used for live load effects in the rating equation (see Appendix B).

A 28-ft clear span was used in all calculations. Live load effects were calculated following the procedures outlined in the *AASHTO Design Specifications.* Maximum moments and shears were determined using the tables contained in Appendix A of the AASHTO *Specifications*. The values reported in these tables are the same as the maximum values that would be calculated for moving loads representing a single H-20 or HS-20 truck (two wheel loads in the transverse direction). Therefore, these values were divided by two to get effects for H-10 or HS-10 trucks, and divided by two again to get effects due to a single wheel loading. Finally, to calculate the live load design effects for a single joist, the moments and shears were distributed transversely using a lateral distribution factor equal to S/6.0 [AASHTO, 1996], where S is the joist spacing in feet. The moments and shears obtained using this procedure are listed in Table 3.2, where each step in the calculations is presented in a separate row.

Table 3.2 Maximum Live Load Moments and Shears Per Joist for the Prototype Bridge

H-truck loading		HS-truck loading		Notes
Moment, kip-ft	Shear, kips	Moment, kip-ft	Shear, kips	
226.8	36.0	252.0	48.0	Maxima for one lane of H-20 or HS-20 loading
113.4	18.0	126.0	24.0	Maxima for one lane of H-10 or HS-10 loading
56.7	9.0	63.0	12.0	Maxima for H-10 or HS-10 wheel loads
28.4	4.5	31.5	6.0	Maxima for one joist of prototype bridge
36.9	5.9	40.9	7.8	Maxima per joist including impact factor

Note: Span is 28.0 ft.

The controlling shear and moment diagrams that produced the maximum live load effects are shown in Figure 3.4 for H-10 loading and in Figure 3.5 for HS-10 loading. The diagrams shown in these figures correspond to one loading lane. For flexure, the critical sections depended on the design truck. The critical sections for an H-truck and an HS-truck were located at 12.6 ft and at 10.5 ft, respectively, from the face of the end diaphragms. The critical section for shear effects was taken at the face of the end diaphragms.

Maximum moments and shears for dead and live load forces for the prototype bridge are listed in Table 3.3. The corresponding load-rating results for H and HS-truck loadings are given in Table 3.4 for both flexure and shear. Although the HS-10 loading vehicle is not included in the AASHTO Design Specifications [AASHTO, 1996], this idealized truck was used to facilitate comparison between the two types of truck loading. The HS-10 truck effects were determined using the magnitudes of the axle loads from the H-10 truck but distributed according to an HS-design vehicle.

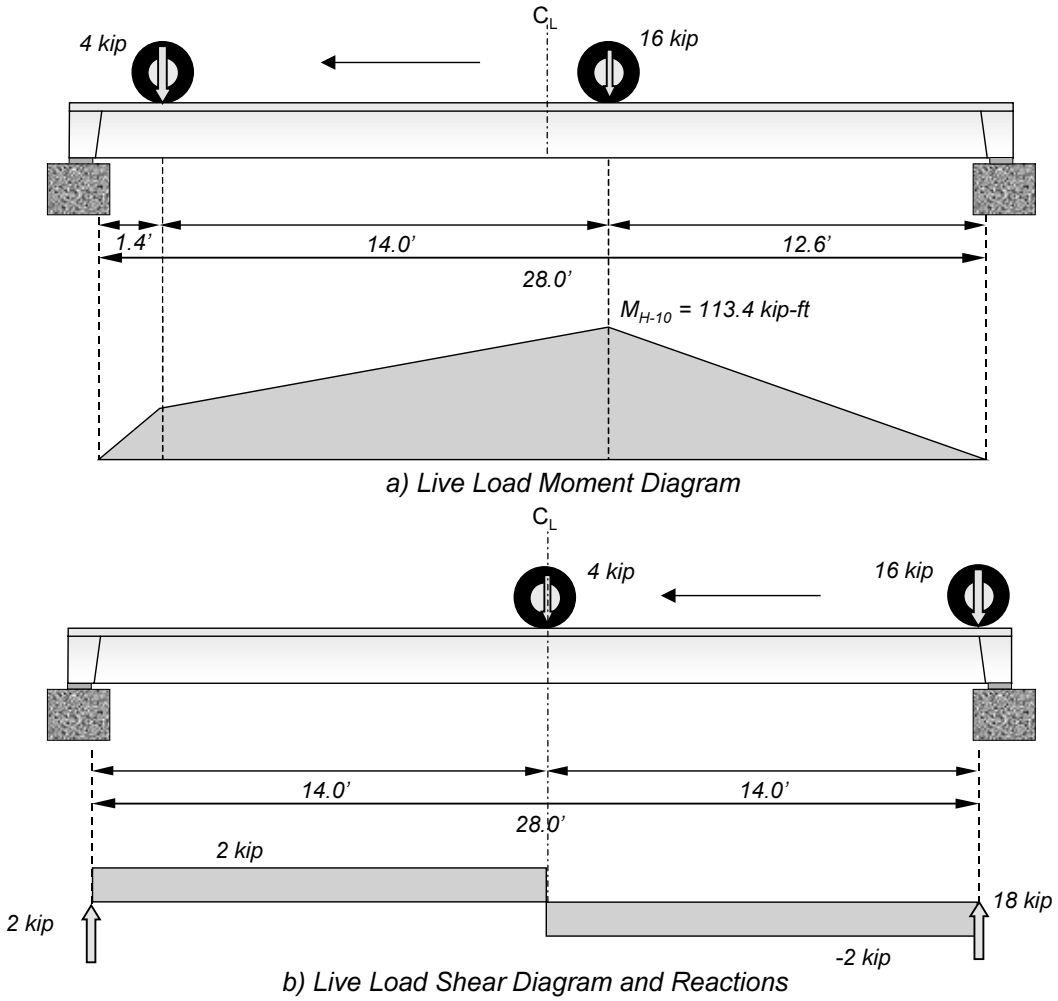

Note: Moment and shear diagrams correspond to a single lane loading

Figure 3.4 H-10 Truck Positions Corresponding to Critical Moments and Shears

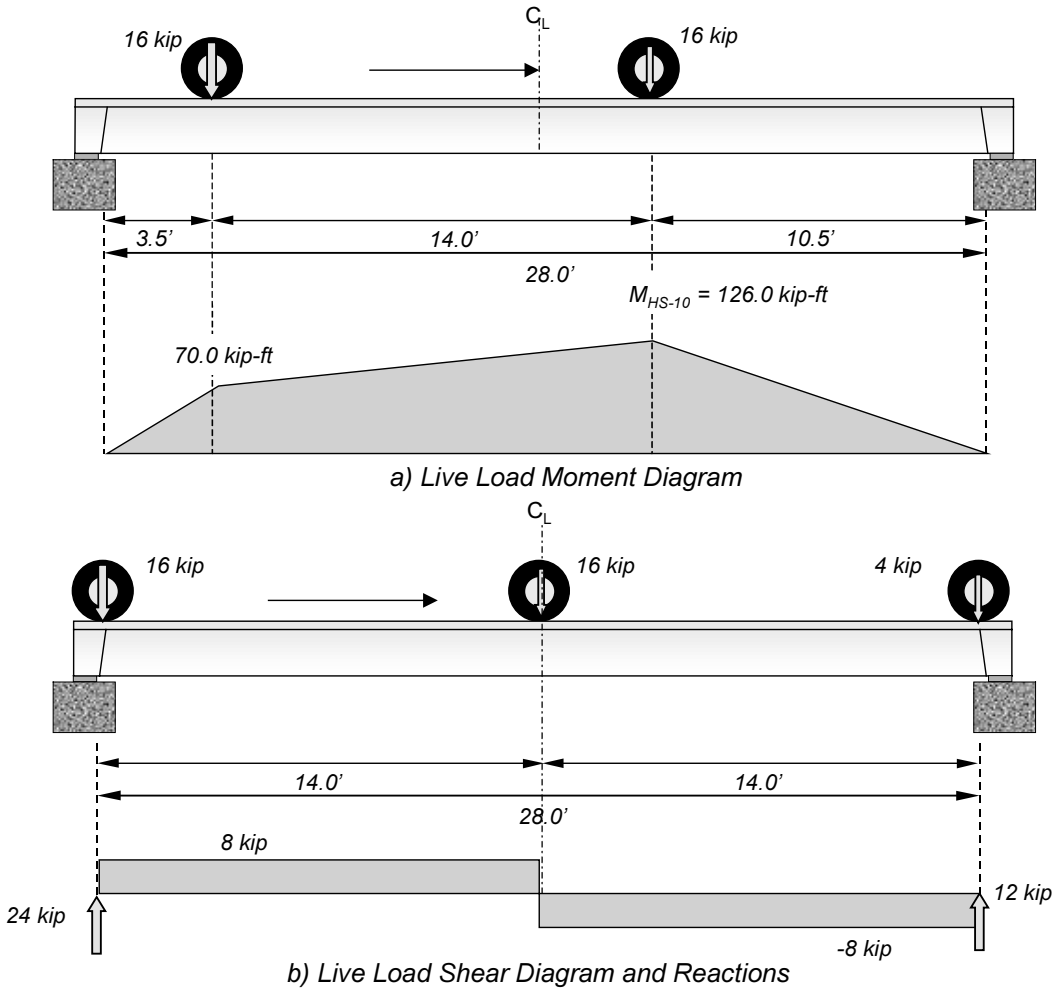

Note: Moment and shear diagrams correspond to a single lane loading

Figure 3.5 HS-10 Truck Positions Corresponding to Critical Moments and Shears

Table 3.3 Unfactored Load Effects Per Joist Used to Rate Prototype Bridge

Unfactored Load Effect	Value
H – 10 truck axle loads, kips	4, front;16, rear (14 ft from front)
M_{DL}, kip-ft	41.7
(1 + I) M_{LL}, kip-ft	36.9
V_{DL}, kip	6.0
(1 + I) V_{LL}, kip	5.9
HS – 10 truck axle loads, kip	4, front; 16, middle (14 ft from front); 16, rear (14 ft from middle)
M_{DL}, kip-ft	41.7
(1 + I) M_{LL}, kip-ft	40.9
V_{DL}, kip	6.0
(1 + I) V_{LL}, kip	7.8

Notes: Live load effects include a 0.3 impact factor (I).
The weight of a ½" overlay is included in dead load.

Table 3.4 Load Rating Results for Prototype Pan-Girder Bridge Originally Designed for an H-10 Truck Loading

Load Effect	**Rating Level**	**Design truck**	
		H – truck loading	**HS – truck loading**
Flexure	Inventory	H-13.6	HS-12.2
	Operating	H-22.6	HS-20.4
Shear	Inventory	H-16.5	HS-12.5
	Operating	H-27.5	HS-20.8

The rating for the prototype bridge was higher than the design H-10 truck loading (Table 3.4). Also, the flexural rating results for the H-truck are very close to those for the HS-truck because one of the truck axles must be located close to midspan to produce maximum live load moments in short span bridges. Therefore, the rear axle lies close to the support for the HS vehicle, and has little influence on the moment (10% difference). On the other hand, there is about a 32% difference in ratings based on shear for the two standard vehicles. If an HS-truck is used, the two 16-kip axles contribute to the maximum live-load shear, while the 4-kip and 16- kip axles contribute to the maximum shear if rating is based on an H-truck.

To comply with current TxDOT requirements, bridges must have an inventory rating of at least HS-20 to be able to qualify for widening and also to qualify for the two-year inspection frequency. If the operating rating is at least HS-20, load posting is not required. Therefore, the prototype bridge requires strengthening to meet the inventory-rating criteria.

3.3 DESIGN AND CONSTRUCTION OF LABORATORY SPECIMENS

The laboratory specimens were selected to reproduce key features of the expected behavior of a portion of the prototype bridge. An interior section of the prototype bridge was chosen for the test specimens because the structural curbs are not present in all bridges and will be removed before an existing bridge is widened. Two identical joist specimens were constructed and tested. Different types of composite materials were used to strengthen the two specimens. The response of each specimen is summarized in Chapter 4 and compared with the calculated response in Chapter 5.

Each test specimen consisted of two interior joists. The specimens were constructed at full scale to avoid scaling effects on the behavior. Concrete diaphragms were cast at both ends of the specimen to replicate field conditions.

The end diaphragms were supported on elastomeric pads to simulate a simply-supported span. The amount of end restraint provided in actual bridges is difficult to predict and can vary from span-to-span as demonstrated in previous research [Velázquez, 1998]. Therefore, simply-supported boundary conditions were chosen in order to evaluate specimen behavior without the influence of end restraint. Also, the most critical condition that could be encountered in the field was replicated by choosing a simply-supported span, because positive moments at midspan are the largest in this case.

Specimens were cast using the same metal forms that are used for pan-girder bridge construction in the field. Therefore, the joist cross sections represent actual field conditions. Wood forms were assembled in the lab to cast the diaphragms at each end of the specimen integrally with the joists. A picture illustrating the reinforcement and formwork prior to casting one of the specimens is shown in Figure 3.6.

Figure 3.6 Specimen Reinforcement and Formwork

Specimen dimensions and reinforcement details are shown in Figure 3.7. The specified yield stress for all reinforcing steel used for the fabrication of the specimens was 60,000 psi. The design 28-day concrete compressive strength was 3,500 psi, and the measured concrete properties are reported in Table 3.5. Details of the material tests for each of the specimens are given in Appendix A.

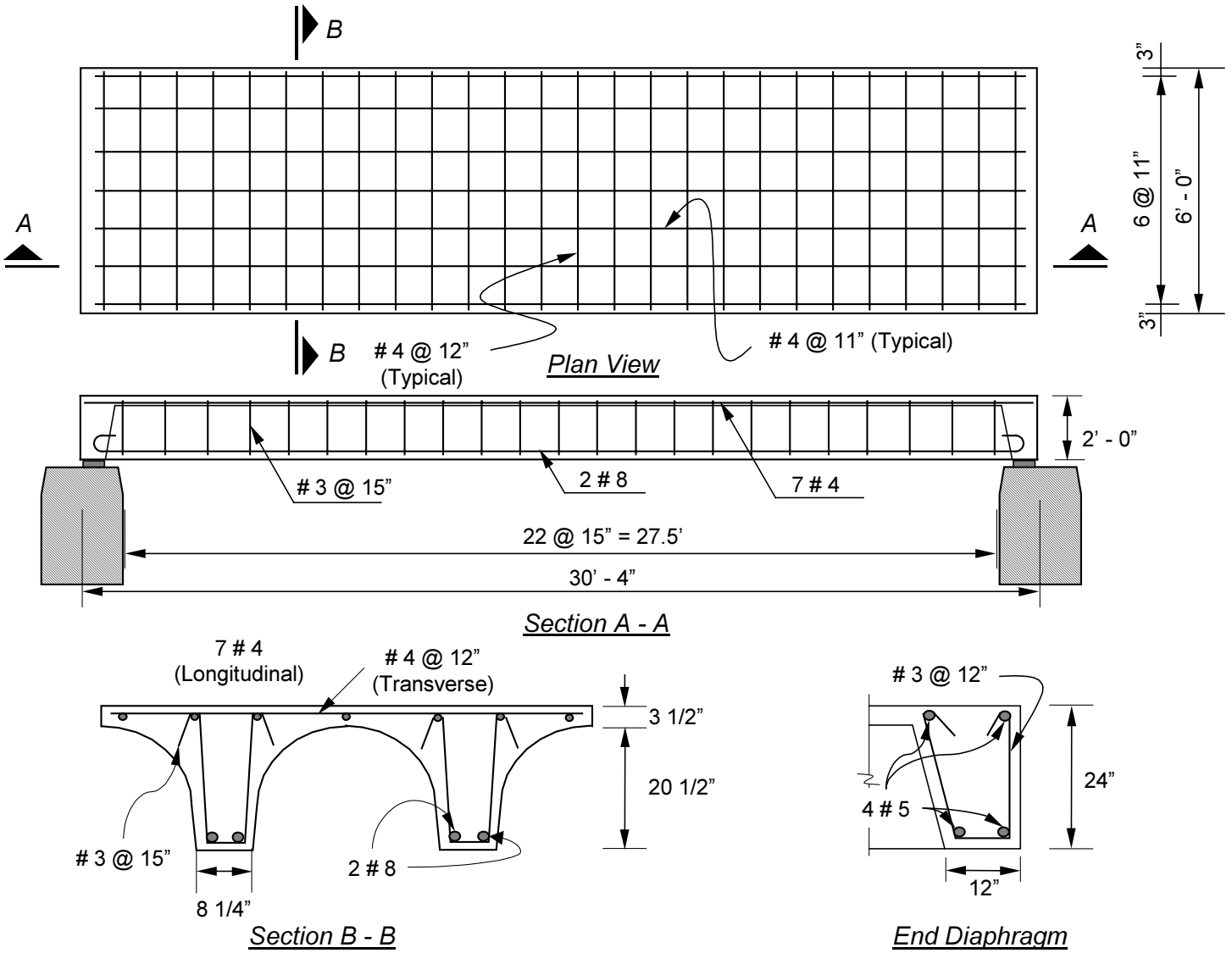

Figure 3.7 Joist Specimen Geometry and Reinforcement

Table 3.5 Average Measured Material Strengths for Joist Specimens

Specimen	Concrete			Reinforcing Bars			
				(#8)		(#3)	
	Age, days	f'_c, psi	f_t, psi	f_y, ksi	f_u, ksi	f_y, ksi	f_u, ksi
J-1	79	3,900	410	71.7	114.0	65.4	106.4
J-2	62	3,500	370				

The main longitudinal reinforcement in the specimens consisted of 2 - #8 bars. The area of the main flexural reinforcement was adjusted for the difference in the nominal yield stresses in the prototype and specimen. Only grade 60 steel was available to construct the test specimens, while it was assumed that 33-ksi steel was used in the prototype bridge. The area was adjusted by multiplying the reinforcement area in the prototype bridge by the ratio of reinforcement yield stress in the prototype to nominal yield stress of the reinforcement in the specimens.

Slab reinforcement consisted of #4 bars at 12" in the transverse direction and #4 bars at 11" in the longitudinal direction. The area of the longitudinal slab reinforcement in the specimens was not adjusted by the ratio of the yield stresses because the additional negative moment strength was required to lift the specimens in the laboratory.

Joist stirrups were #3 bars at 15" spacing throughout the entire span. The stirrup area was not adjusted by the ratio of the yield stresses either. It was considered that using the same bar size in the laboratory specimens as in the prototype bridge replicates field conditions more closely. Also, to have the same number of stirrups crossing a potential diagonal crack, the stirrup spacing in the specimens was the same as in the prototype bridge.

Flexural and shear capacities of the test specimens were determined using Eq. (3.1) and (3.2) respectively [AASHTO, 1996]. The average measured material strengths listed in Table 3.5 were used in these calculations. The specimen capacities are listed in Table 3.6 and are compared with the capacities of two joists from the prototype bridge.

Table 3.6 Nominal Flexural and Shear Capacities of Pan-Girder Specimens

Capacity	**Specimen J-1**	**Specimen J-2**	**Prototype Bridge**
M_n, kip-ft	399.4	398.4	361.4
V_c, kip	44.6	42.2	47.0
V_s, kip	41.4	41.4	21.0
$V_n = V_c + V_s$, kip	86.0	83.6	68.0

As seen in Table 3.6, the flexural strength of both specimens was approximately 10% higher than the calculated flexural capacity of the two joists from the prototype bridge. Shear strengths were approximately 25% higher in the laboratory specimens compared with the prototype. The percentages are higher in this case because the area of shear reinforcement was the same in the test specimens and the prototype, but the yield stress of the reinforcement was higher in the test specimens.

3.4 DESIGN AND CONSTRUCTION OF STRENGTHENING SCHEMES FOR LABORATORY SPECIMENS

The design of the strengthening schemes for each specimen was based on the load-rating procedure described in Section 3.2.3. The required increase in flexural capacity for the prototype bridge to achieve an inventory rating of an HS-20 truck was determined using the rating equation, cast in terms of the capacity, C (Appendix B):

$$C = RF\left[A_2\, L\,(1 + I)\right] + A_1\, D \tag{3.3}$$

where L is the live load effect, D is the dead load effect, I is the impact factor equal to 0.3, A_1 = 1.3, A_2 = 2.17, and RF = 2.0 to reach an HS-20 inventory rating. The load effects used in Eq. (3.3) were those listed in Table 3.3 for flexure.

Equation (3.3) gives a required nominal flexural capacity, $C = \phi\, M_n$, of 232 kip-ft per joist in the prototype. As shown in Table 3.1, the original flexural strength per joist in the prototype is 163 kip-ft. Therefore, the nominal flexural capacity must be increased by 42% to raise the inventory rating of the prototype bridge from HS-12.2 to HS-20.

Both joist specimens were strengthened using CFRP composite systems to increase their flexural capacity. The required nominal strength of the specimens was obtained by multiplying the required capacity of one joist in the prototype, C, by two and dividing by the strength reduction factor, ϕ. The strength reduction factor was assumed to be 0.85. This factor was chosen because failure of the specimens was expected to occur suddenly when the composite systems debonded from the surface of the concrete. This assumption is evaluated using the observed response of the test specimens in Chapter 10.

Two commercially available CFRP systems were chosen to strengthen the laboratory specimens: a pultruded system and a wet-layup system. The pultruded system consisted of CFRP plates that were fabricated in a manufacturing facility through the process of pultrusion and subsequently attached to the concrete surface using an epoxy paste. This system was designated "D" in the first phase of this investigation [Breña et al., 2001]. The wet-layup system consisted of dry unidirectional carbon fibers that were formed into a composite by impregnation using an epoxy resin. The wet-layup system was designated "A" in the first phase of this investigation [Breña et al., 2001]. Details of the application procedure for each system are described in Appendix C.

The required area of composite material to reach the target flexural strength was determined using the analysis procedure described in Chapter 3 of the report by Breña, et al. (2001) and modified per Chapter 2. The expected strength of the strengthened member depends on the strain in the CFRP at which debonding occurs. For design of the test specimens, this strain was determined using results of previous testing on rectangular concrete beams strengthened using similar CFRP systems. In those tests, the strains were measured on the surface of the CFRP composites. For design of the strengthening schemes, a strain of 0.007 was assumed to be the strain at debonding.

The parameters used for the design of the strengthening schemes are summarized in Table 3.7. The factored design moments in Table 3.3 were multiplied by two, because each test specimen comprised two joists.

Table 3.7 Parameters Used to Design the Strengthening Schemes

Parameter	Value	Notes
$A_1 M_D$, kip-ft	108	Factored dead load moment
$A_2 M_L (1 + I)$, kip-ft	355	Factored live load moment + impact
M_u, kip-ft	463	Required ultimate strength (2-joists)
ϕ	0.85	Strength reduction factor
$M_n = M_u/\phi$, kip-ft	545	Required nominal capacity (2-joists)
ε_{CFRP}	0.007	Max. attainable CFRP strain for design

Notes: Moments calculated using HS-20 loading on 2 joists of prototype bridge

A_1 and A_2 = Load factors for dead and live load effects equal to 1.3 and 2.17, respectively, for inventory rating

I = Impact factor for live load effects equal to 0.3

An iterative approach was used to determine the area and placement of the CFRP plates and sheets. The areas of CFRP plates or sheets were adjusted using commercially available dimensions until the desired capacity of the strengthened specimens was achieved within a reasonable tolerance. The calculated moment-curvature curves for two strengthened sections are shown in Figure 3.8. For comparison, the calculated moment-curvature response of the unstrengthened prototype is also shown. The nominal material properties were used in these calculations.

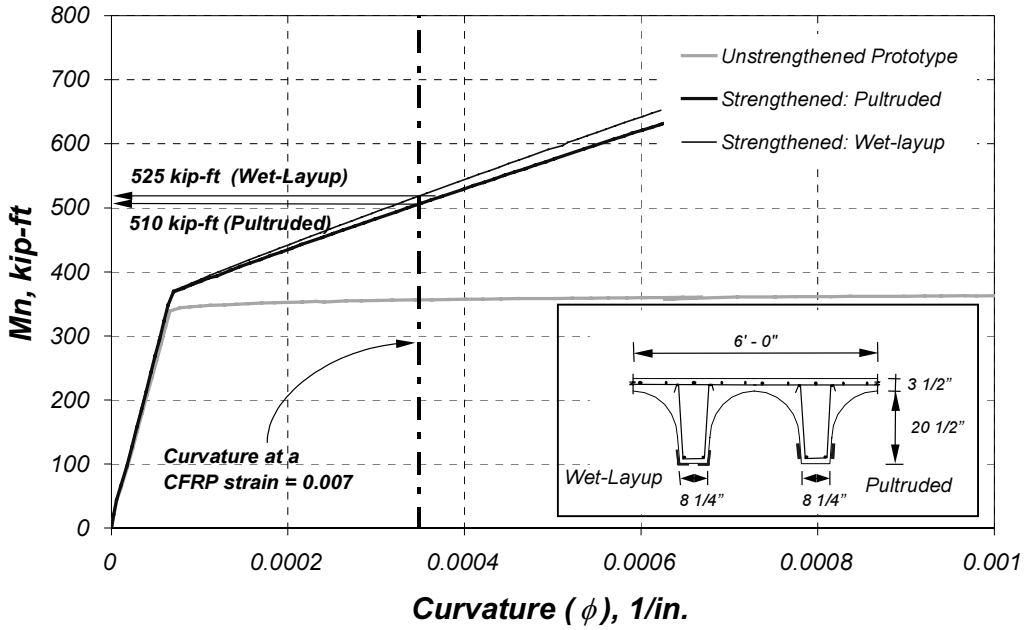

Figure 3.8 Calculated Moment-Curvature Response of Two Joists of Prototype Bridge Strengthened Using Different Composite Systems

The required specimen flexural strength was 545 kip-ft (Table 3.7) in order to achieve an inventory rating of HS-20. The calculated flexural capacity of the strengthened prototype consisting of two joists was slightly lower than the target strength because commercially available CFRP systems were used.

The strengthened prototype bridge was first designed using the CFRP pultruded system because only specific plate widths are available commercially. Then the wet-layup system was designed to develop the same strength as the pultruded system design in order to facilitate comparisons of the performance during the laboratory tests.

Details of the final CFRP configuration for each of the specimens are presented in Sections 3.4.1 and 3.4.2 for Specimens J-1 and J-2 respectively. All calculations were based on the measured material properties for concrete and steel and the material properties provided by the manufacturers for the CFRP systems.

3.4.1 Strengthening Scheme for Specimen J-1

Specimen J-1 was strengthened using pultruded carbon fiber reinforced polymer (CFRP) plates bonded to the sides of each joist. The composite plates were bonded to the concrete specimen following the procedures specified by the manufacturer. Details of this procedure are presented in Appendix C.

Previous tests on strengthened rectangular beams showed that bonding these types of composite plates to the sides of flexural members instead of adhering them to the tension face delayed debonding and increased the deformation capacity of the members. Therefore, the composite plates were bonded to the side of the joists. An epoxy-based adhesive paste supplied by the plate manufacturer was used to bond the pultruded plates to the concrete surface. The procedures recommended by the manufacturers were followed to prepare the concrete surface before bonding the composites (Appendix C).

The CFRP plates used for this specimen were fabricated with continuous unidirectional carbon fibers (fiber roving) using the pultrusion process (see Appendix C). The volumetric content of carbon fibers in the plates is 68% and the cross-sectional dimensions are 3 1/8 in. wide by 0.047 in. thick. Mechanical properties of the CFRP plates and epoxy paste are listed in Appendix A.

CFRP composite straps were placed at 12-in. spacing around the pultruded plates throughout the shear span of the specimen using a wet lay-up procedure. A unidirectional carbon fiber woven fabric supplied by the same manufacturer as the pultruded plates was used to form these straps. The composite straps were intended to delay debonding of the pultruded plates from the concrete surface as demonstrated in previous tests [Breña et al., 2001]. Straps were fabricated using a 3-in. wide ply of carbon fiber fabric. The straps extended 11 in. above the bottom of the specimen. The length of the straps was selected so that they would end before the curved portion of the joist cross section. No attempt was made to determine the strap length based on calculations. However, longer straps are advised in the future based on results from the experimental testing.

Epoxy paste was built up next to the pultruded plates where CFRP straps intersected the plates to avoid wrapping the straps around sharp bends at the edges of the pultruded plates. Both the epoxy paste used to bond the pultruded plates and the composite straps were allowed to cure at ambient temperature for 7 days before testing. The locations of CFRP pultruded plates and anchoring straps on Specimen J-1 are shown in Figure 3.9.

The required length of the plates was determined using the loading configuration and the maximum moment expected to be applied during the test. The plates were extended beyond the theoretical cut-off points to prevent premature debonding.

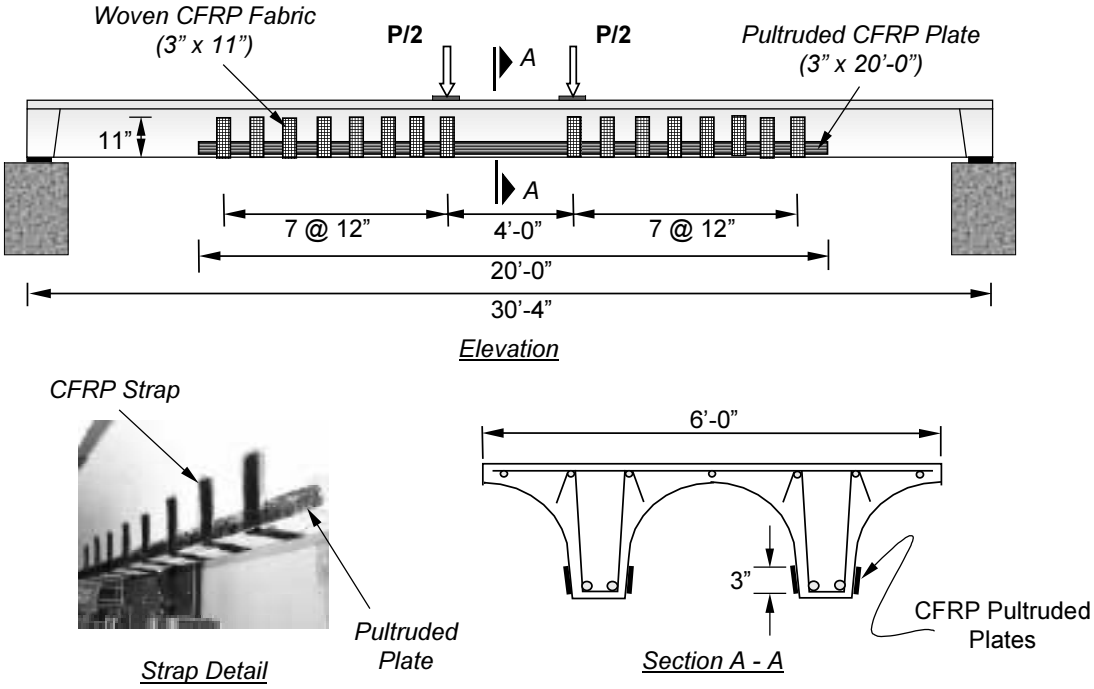

Figure 3.9 CFRP Strengthening Details for Specimen J-1

The procedure used to determine the plate length is illustrated graphically in Figure 3.10. The maximum moment indicated in the figure was calculated by subtracting the service dead load moment from the required nominal capacity listed in Table 3.7. Dead load moments were acting on the specimen before the composite system was bonded. The theoretical cut-off points were situated where a moment equal to the prototype nominal capacity minus the service dead load moment intersects the applied moment diagram.

The calculated flexural capacity of Specimen J-1 with the CFRP plates was determined using a maximum strain in the CFRP plates of 0.007 and the measured material properties for steel and concrete. The calculated moment-curvature response is shown in Figure 3.11. Also shown is the calculated response of the bare, reinforced concrete specimen. The difference in the calculated capacity of the strengthened joists from the prototype bridge, 510 kip-ft, and the calculated capacity of the laboratory specimen, 570 kip-ft, may be attributed to two factors: (a) Strain hardening of the reinforcement was considered for Specimen J-1, but was ignored for the prototype and (b) the measured yield stress in the longitudinal reinforcement exceeded the nominal yield stress.

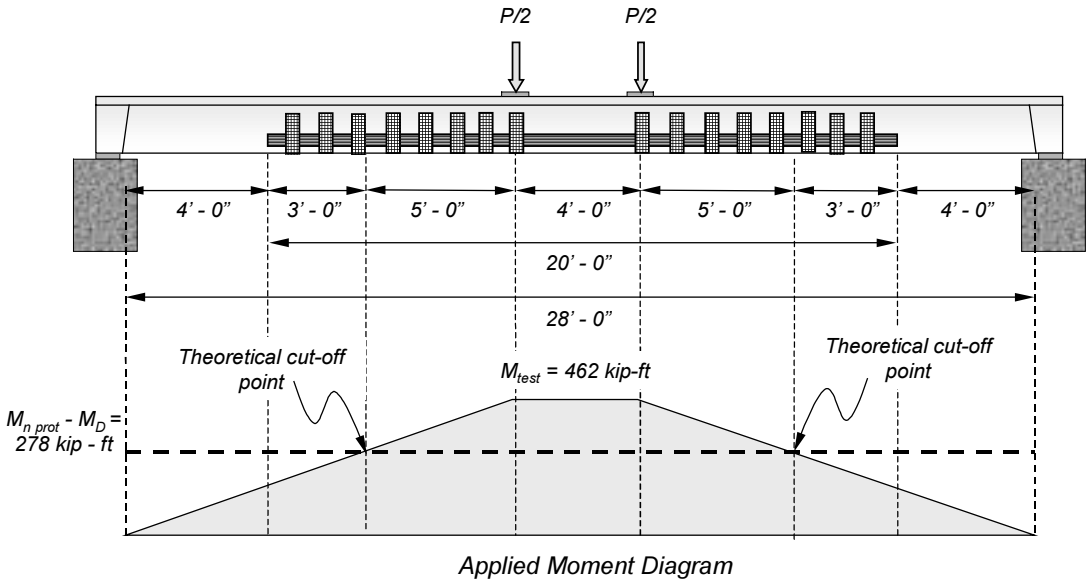

Nomenclature: $M_{n\ prot}$ = Prototype moment capacity
M_{test} = Maximum expected moment in test
M_D = Dead load moment

Figure 3.10 Required CFRP Plate Length for HS-20 Truck Loading on 28 ft Clear Span for the Design of Specimen J-1 (2-Joists)

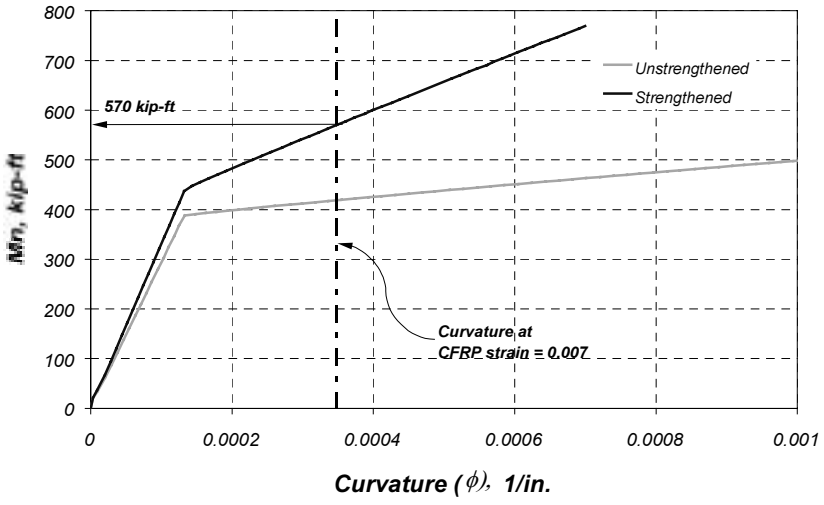

Figure 3.11 Calculated Moment-Curvature Response of Specimen J-1 Using Measured Material Properties

3.4.2 Strengthening Scheme for Specimen J-2

Specimen J-2 was strengthened using CFRP sheets that were applied using a wet lay-up procedure (see Appendix C). These sheets were fabricated with continuous unidirectional carbon fibers. A two-component epoxy resin was used to impregnate the carbon fibers to form and bond the composite to the concrete surface. A detailed description of the fabrication procedure for this type of system is presented in Appendix C.

Two layers of carbon fiber sheets (plies) were formed on Specimen J-2 to be able to reach the required target strength. The carbon fiber sheets were cut to 8-in. widths and placed around the bottom corners of each joist, leaving 3 in. on the bottom and 5 in. on the sides. Partially wrapping the bottom surface was necessary to avoid the concrete surface irregularity that was generated during casting (Figure 3.12). The length of these sheets was determined as for Specimen J-1 (see Section 3.4.1). Details showing the location and geometry of the CFRP composite on Specimen J-2 are shown in Figure 3.13.

Figure 3.12 Partial Wrapping of Joists in Specimen J-2 to Avoid Concrete Surface Irregularities

Straps were placed to anchor the longitudinal composites at 1-ft spaces along the shear span. The straps were fabricated using one ply of 3-in. wide strips with the same carbon fiber sheets used for the longitudinal direction. In this case, the straps extended into the curved part of the cross section (16-in. from the bottom). The composite fabrication was done on the same day and left to cure for 7 days at ambient temperature before testing.

The calculated moment-curvature response of Specimen J-2 is shown in Figure 3.14. The measured strengths of steel and concrete were used in the calculations. The flexural capacity of the specimen was estimated at a curvature corresponding to an expected maximum CFRP composite strain equal to 0.007.

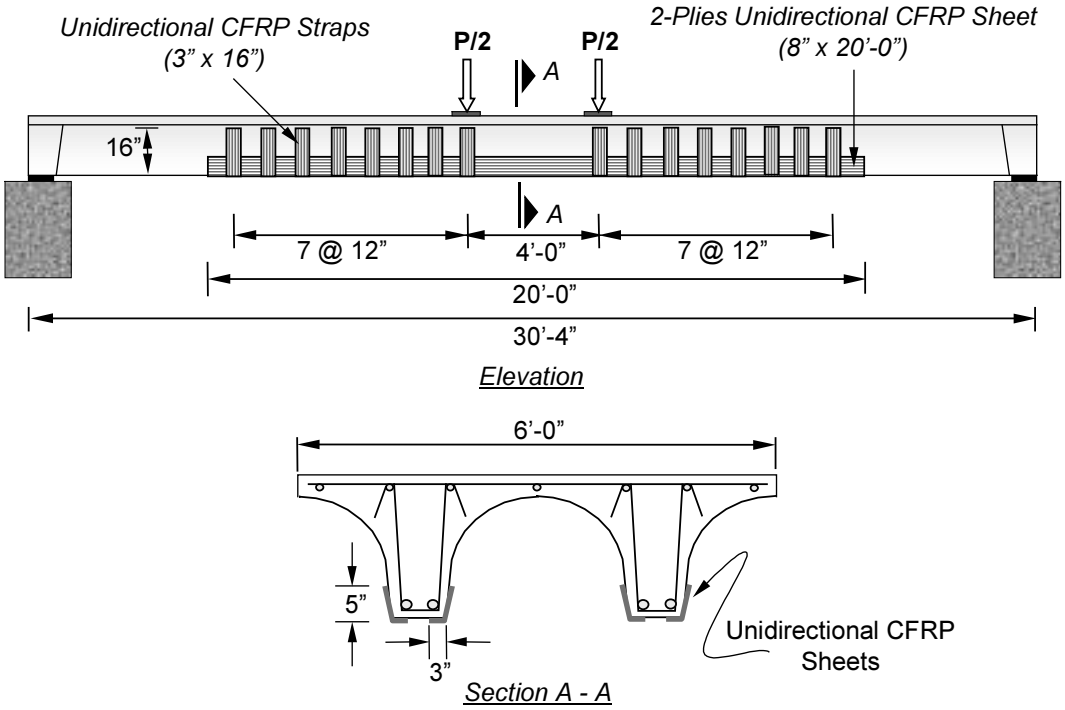

Figure 3.13 CFRP Strengthening Details for Specimen J-2

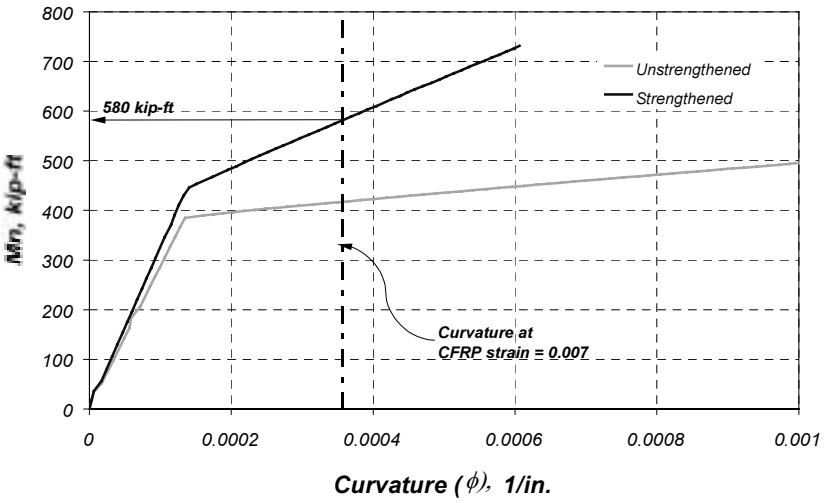

Figure 3.14 Calculated Moment-Curvature Response of Specimen J-2 Using Measured Material Properties

As shown in Figure 3.14, the calculated specimen capacity, 580 kip-ft, exceeds the required flexural capacity, 510 kip-ft, determined during design of the strengthening scheme. The same explanation can be given for the difference in calculated prototype capacity and calculated capacity of the laboratory specimen as for Specimen J-1.

3.5 LOAD LEVELS FOR PROTOTYPE BRIDGE

As discussed in Section 3.2, the prototype bridge must be strengthened to meet the inventory rating criteria for widening and reduced inspection frequency. The strengthening scheme for the prototype bridge was designed such that the strengthened bridge would have an inventory rating of at least HS-20. Maximum moments and shears corresponding to service and design levels for the original and strengthened bridge are summarized in Table 3.8.

The service-level moments due to dead and live load in a single joist in the as-built prototype bridge are 41.7 and 36.9 kip-ft, respectively (Table 3.8). If the design vehicle is changed from an H-10 truck to an HS-20 truck, the service-level live load moment increases to 81.8 kip-ft. Design-level moments due to dead and live loads increase to 54.2 kip-ft and 177.5 kip-ft, respectively. Moments corresponding to the four load levels listed in Table 3.8 were used to define the stages of loading used during the experimental tests.

Table 3.8 Moments Associated to Different Design Levels for One Joist in Prototype Bridge

Design Truck	Load Level	Design Condition	M_{DL}, kip-ft	$M_{LL(1+I)}$, kip-ft	Load Factor	
H-10	1	Service loads (Unstrengthened)	41.7	36.9	D	1.0
					L	1.0
HS-20	2	Service loads (Strengthened)	41.7	81.8	D	1.0
					L	1.0
HS-20	3	Service dead load + Factored live load	41.7	177.5	D	1.0
					L	2.17
HS-20	4	(Factored dead load + Factored live load)/ϕ	63.8	208.8	D	1.3
					L	2.17

Notes: Impact factor, I = 0.3.

Load levels were used during laboratory tests to evaluate performance of strengthened joists.

3.6 SUMMARY

Typical pan-girder bridge construction in Texas was presented in this chapter. This form of construction was common 50 years ago, and many existing bridges were designed for lower loads than are now required, typically H-10 or H-15 truck loading. Therefore, a two-lane prototype bridge, which was designed for an H-10 truck loading, was selected to represent the case where maximum strengthening is required.

The calculated inventory load ratings for the prototype bridge were H-13.6 and HS-12.2 for the different types of design trucks used currently. Because TxDOT requires that a bridge have an inventory rating of at least HS-20 to qualify for widening, an increase in flexural capacity of the prototype bridge was required. A 42% increase in flexural capacity is required to meet this design objective.

The design, construction, and strengthening procedures used in two full-scale laboratory specimens were presented in this chapter. These specimens represent a 6-ft wide section of the prototype bridge consisting of two joists. The design of these specimens in the laboratory was aimed at capturing the general behavior of the prototype bridge after strengthening.

The procedures used for design and construction of two strengthening schemes that are appropriate for joist specimens were presented. Two different composite systems were used to increase the capacity of the prototype bridge from an HS-12.2 inventory rating to an HS-20 rating. These systems were constructed and applied to the laboratory specimens. The measured response of the laboratory tests of the pan-girder specimens is presented in Chapter 4.

Chapter 4: Measured Response of Pan-Girder Specimens

4.1 INTRODUCTION

The measured response of Specimens J-1 and J-2 are presented in this chapter. The experimental setup, loading history, and specimen instrumentation are also described. The instrumentation was designed to provide information about the internal forces at specified sections, as well as global response of the specimens. Recorded outputs from the instruments are presented and discussed.

4.2 TEST SETUP AND INSTRUMENTATION

4.2.1 Description of Experimental Setup

The strengthened joist specimens (J-1 and J-2) were subjected to static loads to evaluate their behavior under service and ultimate loads. The test specimens were idealized as being simply supported. Each end diaphragm rested on two steel-rubber elastomeric pads on top of concrete blocks.

Loads were applied statically using a 200-kip hydraulic ram reacting against a steel frame that was anchored to the laboratory strong floor. The total load was distributed to four points on the slab to simulate wheel loads. The loading points were located symmetrically about the specimen centerline with a 4-ft spacing in the longitudinal direction and a 3-ft spacing in the transverse direction. Loading point spacing in the transverse direction was selected to load each joist directly. In the longitudinal direction, the load spacing was selected to simulate the tandem rear axle of a typical truck. AASHTO design vehicles have a longer axle spacing, but real trucks have an axle spacing that resembles the tandem configuration more closely.

Elastomeric pads were used under each load point to avoid crushing of the concrete due to stress concentrations. Details of the test setup are shown in Figures 4.1 and 4.2.

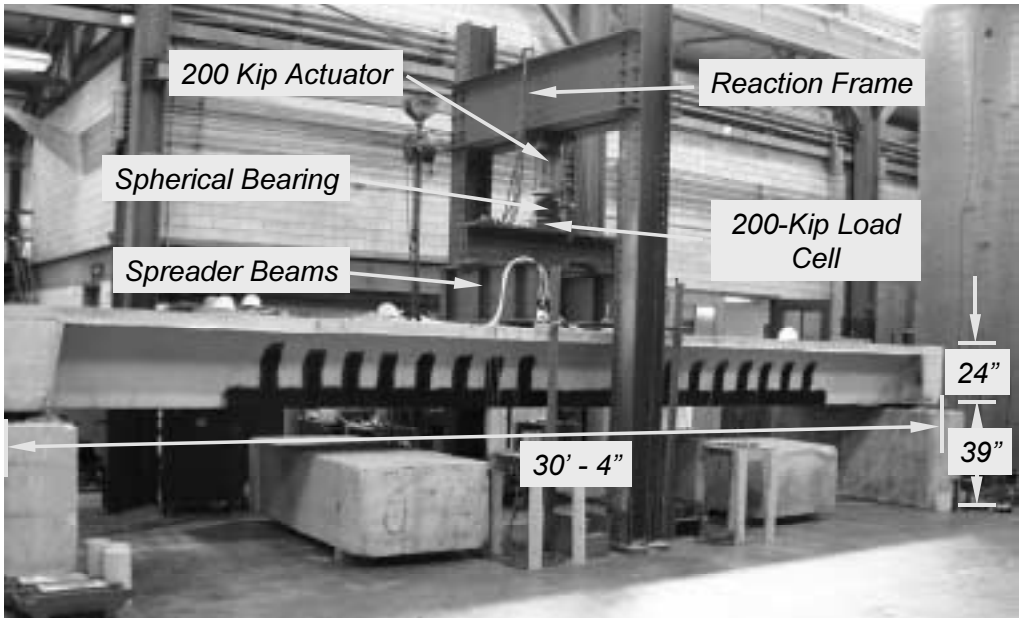

Figure 4.1 Side View of Pan-Girder Specimen in Laboratory Test Setup

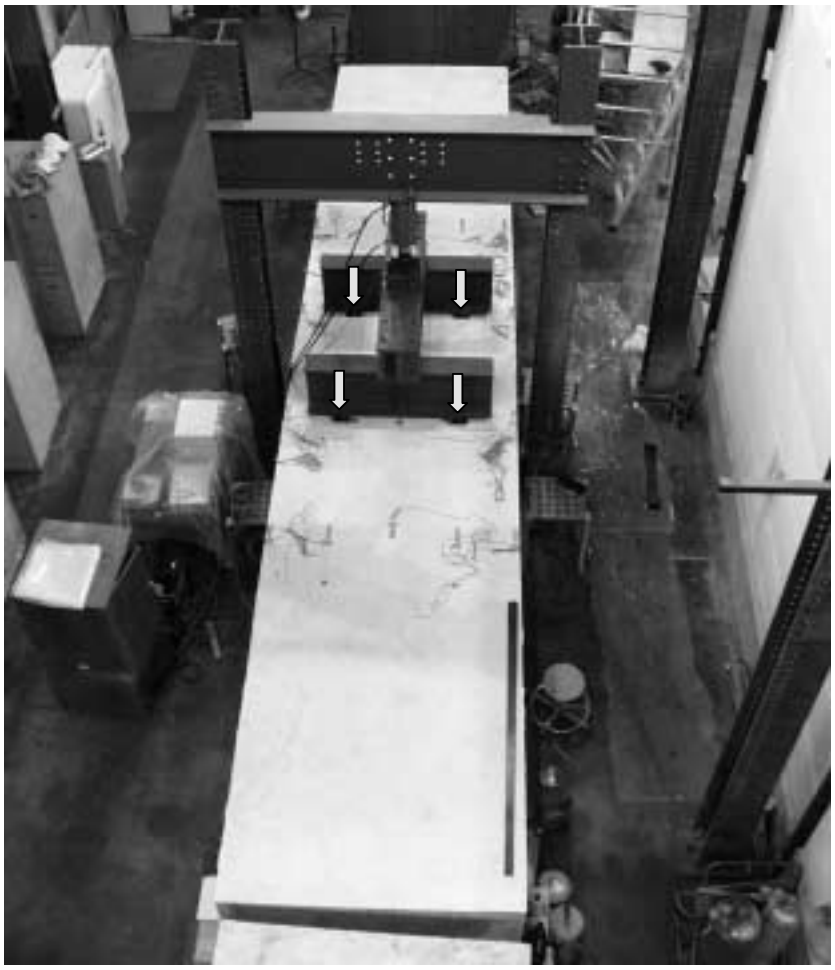

Figure 4.2 Overhead View of Pan-Girder Specimen Showing the Location of Loading Points

4.2.2 Loading Sequence

The loading sequence was selected to evaluate the behavior of the joists under moments equivalent to service and factored load conditions in the prototype bridge. Before bonding the CFRP composites to the reinforced concrete joists, the specimens were subjected to the load corresponding to service load moments for the original design (78.6 kip-ft). The objective of this step was to induce cracking in the test specimens before the CFRP systems were applied. Flexural cracking has been observed in existing pan-girder bridges [Velázquez, 1998]. The specimens were subjected to two cycles at this load level after which they were unloaded and strengthened using the composite systems described in Chapter 3.

The second stage of loading began after the composite systems had undergone a seven-day curing period at ambient temperature. During this stage, the specimens were subjected to moments corresponding to different design levels: service live load before strengthening, service live load after strengthening, factored live load, and required ultimate load. After reaching each of the predetermined load levels, the specimens were unloaded and then reloaded to the same load. This repeated loading scheme was adopted to evaluate changes in specimen stiffness, and to observe deterioration of the composite-concrete interface.

The different load levels and the number of cycles at each load that were imposed on both pan-girder specimens are listed in Table 4.1. These loads correspond to service and design loads for the prototype bridge (Table 3.8). Because the specimens were constructed at full scale, it was assumed that the service-level dead loads were acting at the time of the test. Therefore, the applied load level was selected such that the total moment at midspan of the test specimen matched the total moment in the prototype bridge for two joists.

Table 4.1 Required Moments and Loads During Testing Corresponding to Design Levels in the Prototype Bridge

Load Level	Moments in Prototype Bridge		Moments in Test Specimen		Total Applied Load, kip	# of Cycles
	Dead Load, kip-ft	Live Load, kip-ft	Dead Load, kip-ft	Applied Load, kip-ft		
1	83.4	73.8	83.4	73.8	12.3	2
2	83.4	163.6	83.4	163.6	27.3	2
3	83.4	355.0	83.4	355.0	59.2	2
4	127.5	417.6	83.4	461.7	77.0	1

Note: Total moments in two joists are tabulated.
Load Level 1: 1.0D +1.0L (Original Live Load).
Load Level 2: 1.0D + 1.0L (Increased Live Load).
Load Level 3: 1.0D + 2.17L (Increased Live Load).
Load Level 4: (1.3D+2.17L)/0.85 (Increased Live Load).

After the last design-level load was applied, the specimens were unloaded and reloaded until the composite systems debonded from the concrete surface. Failure of the composite system was defined when there was a sudden reduction in the strength of the specimen.

After debonding of the CFRP composites, the reinforced concrete elements were still able to carry load, although at a reduced level. Therefore, the loading was continued until the onset of concrete crushing to determine the capacity of the bare reinforced concrete joists.

4.2.3 Instrumentation

Three types of instruments were used in the tests: linear potentiometers, strain gages, and load cells. Linear potentiometers were used to monitor global specimen response. A total of 10 potentiometers were attached to Specimen J-1 and 12 were attached to Specimen J-2. Four sections in each specimen were instrumented with strain gages bonded to the reinforcement, CFRP composites, and concrete slab. A total of 13 gages were attached in each section for Specimen J-1 and 11 were attached in each section for Specimen J-2. A 200-kip load cell was used to monitor load throughout the tests. The voltage output from the instruments was collected every 4 seconds using a Hewlett Packard-75000 scanner and recorded in a computer.

Linear potentiometers were positioned on the east and west sides of the specimens at midspan and at the points of load application. Because the specimens were supported on flexible bearing pads, the ends were also instrumented with potentiometers to determine the deformation of the supports. The support movement was subtracted from the displacement measured along the span to determine the deformation of the specimen relative to its ends. Potentiometers with a 6-in. stroke were used at midspan and with a 2-in. stroke for the rest of the locations. The location of the linear potentiometers for Specimens J-1 and J-2 are summarized in Table 4.2.

Strain gages were used to calculate internal forces and the neutral axis depth at four sections along the span. The moment-curvature response at the instrumented sections was calculated from these values.

Table 4.2 Displacement Limits of Linear Potentiometers

Test Specimen	Joist	North Load Point	Midspan	South Load Point	End Diaphragms*
J-1	East	2 in.	6 in.	2 in.	2 in.
	West	2 in.	6 in.	2 in.	2 in.
J-2	East	2 in.	6 in.	2 in.	2 in.
	West	2 in.	6 in.	2 in.	2 in.

*See Figures 4.3 and 4.4 for the location of potentiometers at the end diaphragms

Each instrumented section had strain gages placed on the bottom longitudinal reinforcement in both joists, on the concrete slab, and on the CFRP composite bonded to each joist. Characteristics of the strain gages are listed in Table 4.3.

Table 4.3 Characteristics of Strain Gages

Material	Strain Gage Type	Gage Length, mm
Steel	Foil	6
CFRP	Foil	6
Concrete	Wire	60

The locations of the strain gages are shown in Figure 4.3 for Specimen J-1 and Figure 4.4 for Specimen J-2. These sections were selected to be able to determine the moment-curvature response at the maximum moment section in the specimen and at a section within the shear span.

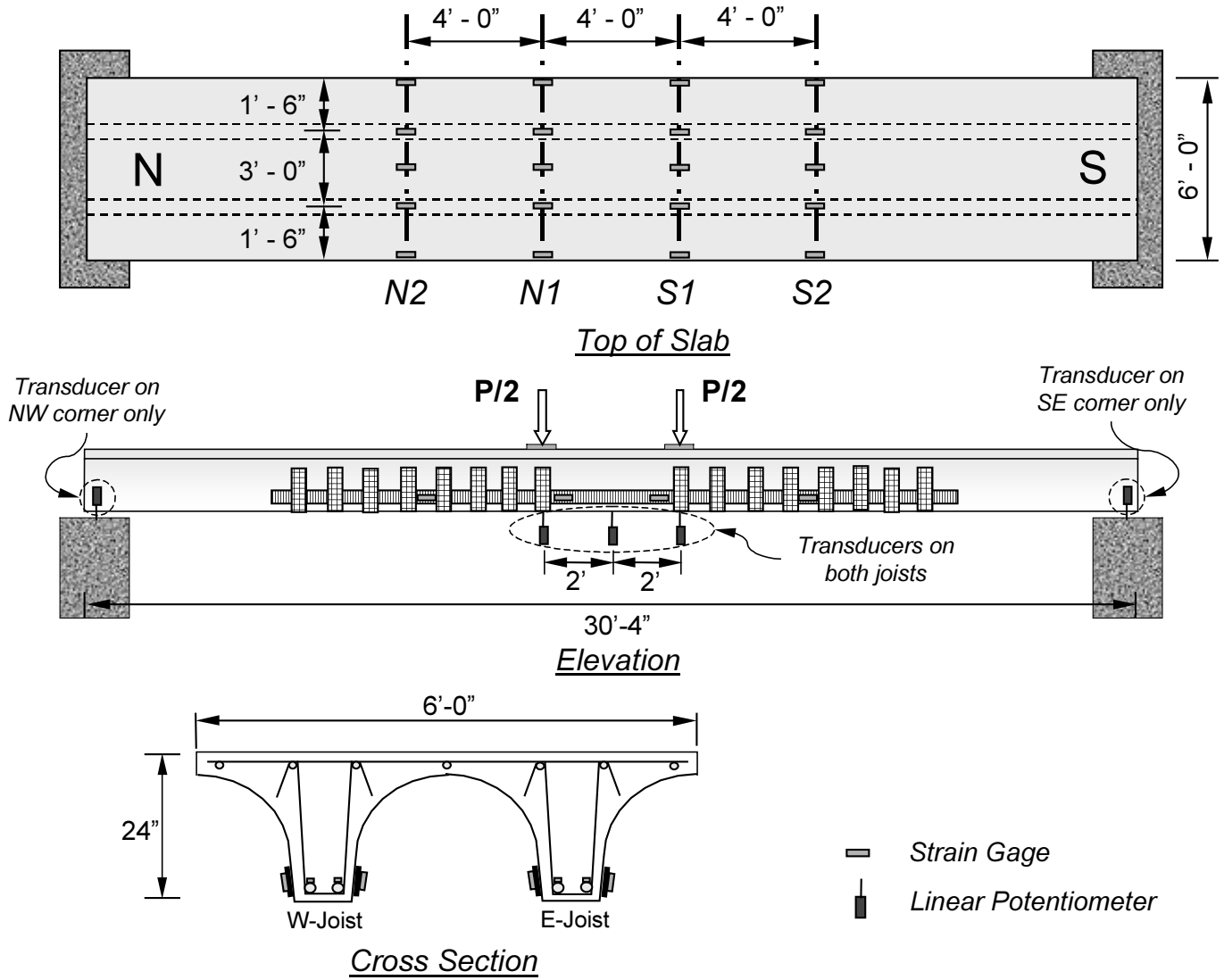

Figure 4.3 Location of Instrumented Sections Showing Position of Potentiometers and Strain Gages in Specimen J-1

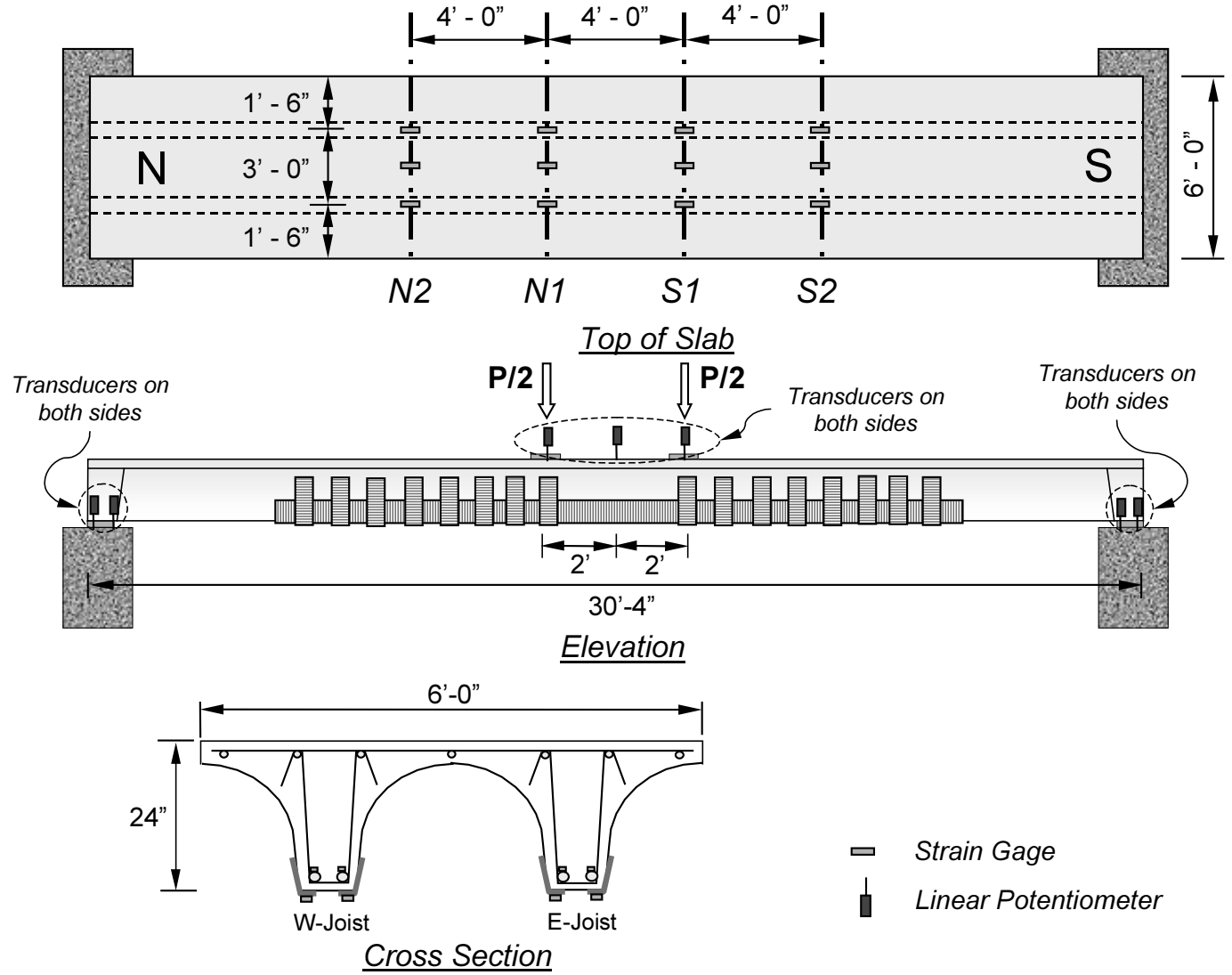

Figure 4.4 Location of Instrumented Sections Showing Position of Potentiometers and Strain Gages in Specimen J-2

4.3 OBSERVED BEHAVIOR DURING TESTS

The observed behavior of the specimens during the tests is described in this section. Visible damage in the concrete-CFRP composite interface due to debonding is summarized in Section 4.3.1. Cracking patterns that were observed at two of the design levels are also presented. Representative measured response from the instruments is discussed in Section 4.4.

4.3.1 Description of Failure Sequence and Cracking Distribution

(a) Specimen J-1

The bare reinforced concrete specimen was subjected to two cycles at the original service load level. Flexural cracks formed uniformly at about 12-in. spacing. The last observed crack was located approximately 4 ft from the face of the end diaphragms. All the cracks that formed within the shear span were less than 0.002 in. wide. The maximum crack width inside the constant moment region was 0.007 in. The specimen was strengthened without repairing the cracks that formed after these loading cycles.

After strengthening, Specimen J-1 did not show signs of distress during the first load cycle to the original service loads. Cracks were documented at load levels 2 and 3. The longitudinal reinforcement was observed to yield at load level 3. Crack patterns for the west joist are shown in Figure 4.5 for both of these loading stages. Diagonal cracks propagated from existing flexural cracks as the specimen was loaded to 60 kip. This behavior gave an indication of stresses being transferred into the CFRP plates after the longitudinal reinforcement yielded. Also, crack widths increased considerably, especially inside the constant moment region.

Initial debonding of the CFRP plate was observed on the east joist after the first excursion to yield. Debonding initiated at midspan and was only observed on the top of the plate (Figure 4.6). However, no other signs of bond deterioration were seen along other plates or transverse straps. The specimen was then unloaded and reloaded past the observed yield point. The first transverse strap debonding occurred at an applied load of approximately 77 kip (load level 4). Strap debonding was characterized by a sudden release from the concrete surface (Figure 4.7). Debonding of straps took place after a flexural crack propagated behind the strap leaving only the upper portion of the strap bonded to the concrete surface.

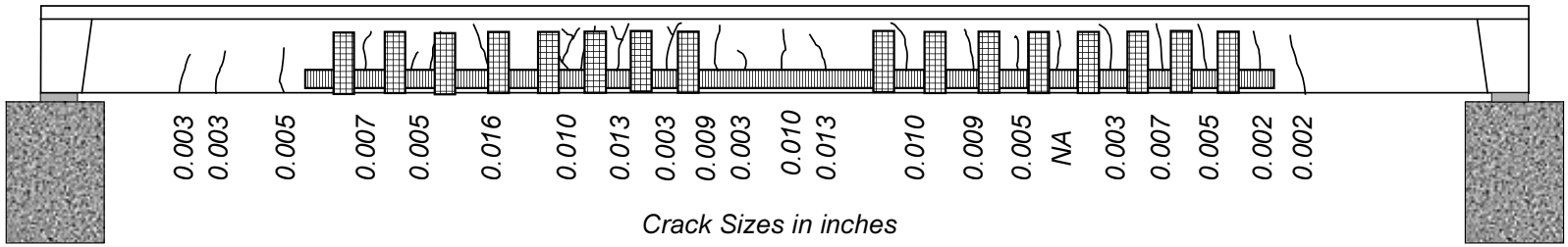

Load Level 2 (Applied Load = 27 kip)

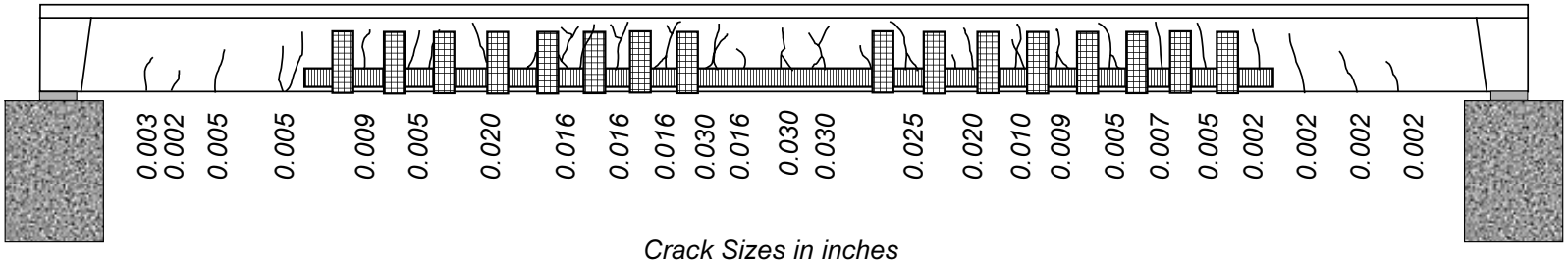

Load Level 3 (Applied Load = 60 kip)

Figure 4.5 Typical Crack Patterns for Specimen J-1 (West Joist)

Figure 4.6 Observed Initial Debonding of CFRP Plate on East Joist

Figure 4.7 Transverse Strap Debonding at Ultimate Design Load

As the load was increased, the ends of the CFRP plates detached from both joists. Also, cracks propagated horizontally along the top of the CFRP plates, mainly at strap locations. Finally, the CFRP plate debonded from the east joist at an applied load of 97.3 kip. As the CFRP plates pulled-off from the concrete surface, they sheared the anchoring straps and pulled off a significant amount of surface concrete. The debonding sequence is illustrated in Figures 4.8 and 4.9.

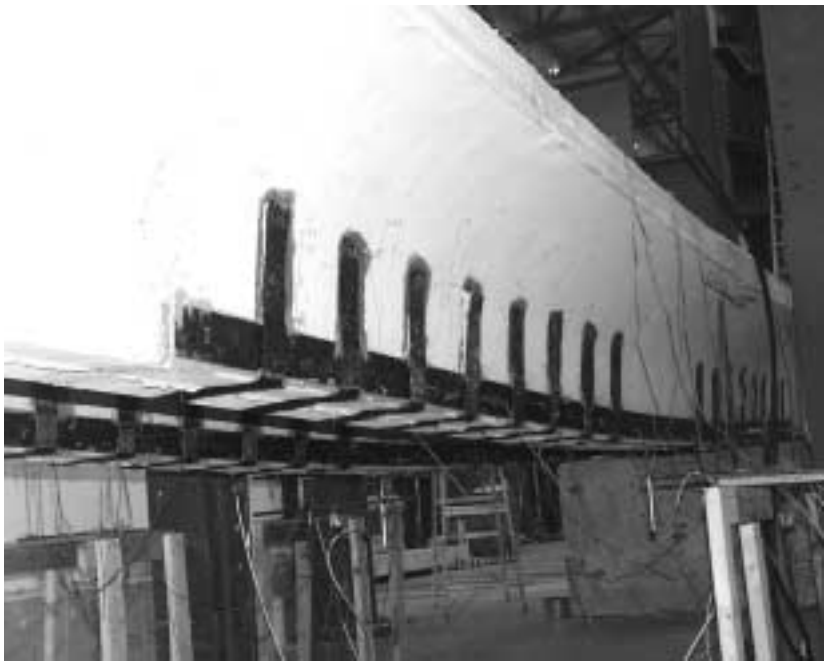

Figure 4.8 East Joist of Specimen J-1 Before CFRP Debonding

Figure 4.9 East Joist of Specimen J-1 at Failure

Immediately after debonding, the specimen was unloaded to insert steel shims between the actuator and the loading beams in order to accommodate the permanent deformation of the specimen and permit further testing. Upon reloading to 78.5 kip, the plates on the west joist debonded from the surface and the load dropped to 61.8 kip. Finally, the specimen was unloaded and reloaded until concrete crushing was observed on the top surface of the slab at an applied load of approximately 70 kip.

(b) Specimen J-2

The bare reinforced concrete specimen was subjected to the original design service loads. Crack distribution and widths were similar to those observed for Specimen J-1 at this load stage. Crack spacing was fairly uniform (approximately 12 in.) throughout the 20-ft center portion of the specimen. The maximum observed crack width after this load stage was 0.007 in. within the constant moment region. Cracks that formed in the shear span had a maximum width of 0.002 in. The composite system was applied without repairing the cracks that formed after subjecting the bare specimen to this load level.

The global behavior of Specimen J-2 after strengthening was similar to that of Specimen J-1. Typical crack patterns at load levels 2 and 3 are shown in Figure 4.10. Cracking along the top of the CFRP sheet was observed during the load hold at yield on some areas between strap locations and gave an indication of initiation of debonding (Figure 4.11). Debonding of the CFRP sheet at midspan was observed at a load of 78 kip (load level 4). At this stage, flexural cracks started crossing the top portion of some of the anchoring straps located on the south shear span of the specimen (east joist). It is important to note, however, that strap debonding was delayed because the straps on Specimen J-2 were extended farther toward the top of the specimen (Figure 4.12).

As loads were increased, debonding of the longitudinal CFRP sheets propagated towards the ends of the specimen. The portion of CFRP sheet bonded to the bottom of the joists experienced localized fiber rupture at approximately 83 kip within the maximum moment region. However, only a minor drop in load was observed and the specimen was able to carry higher loads. Failure of Specimen J-2 occurred at a load of 95.4 kip when the CFRP sheets debonded completely. The north end of the east joist debonded first, followed by the south end of the west joist (Figure 4.13).

The concrete surface condition after CFRP debonding is shown in Figure 4.14. This surface appearance was typical of the bottom surface of the joists. A significant amount of concrete was pulled off after the sheets debonded from the surface.

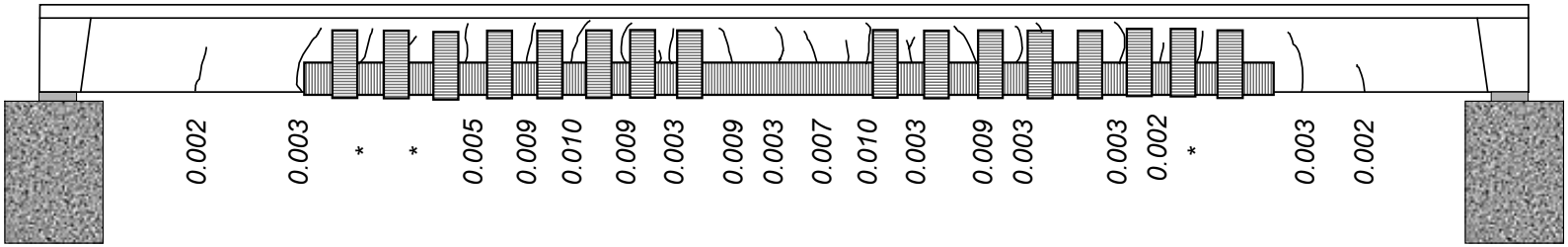

Crack Sizes in inches

Load Level 2 (Applied Load = 27 kip)

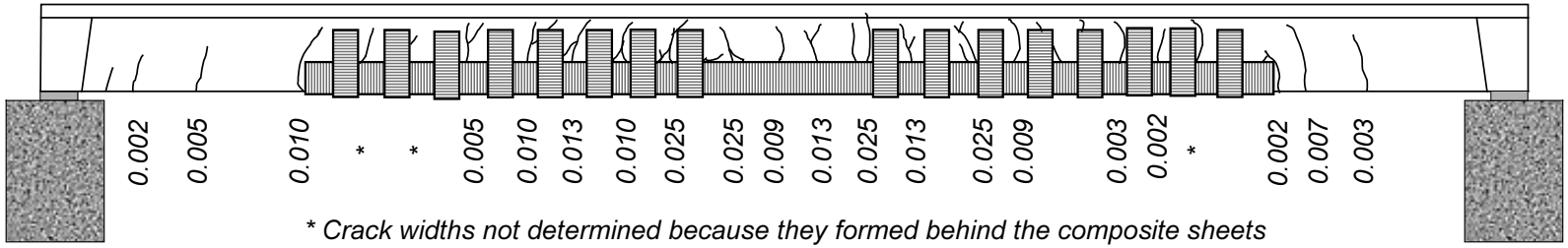

** Crack widths not determined because they formed behind the composite sheets*

Crack Sizes in inches

Load Level 3 (Applied Load = 60 kip)

Figure 4.10 Typical Crack Patterns for Specimen J-2 (West Joist)

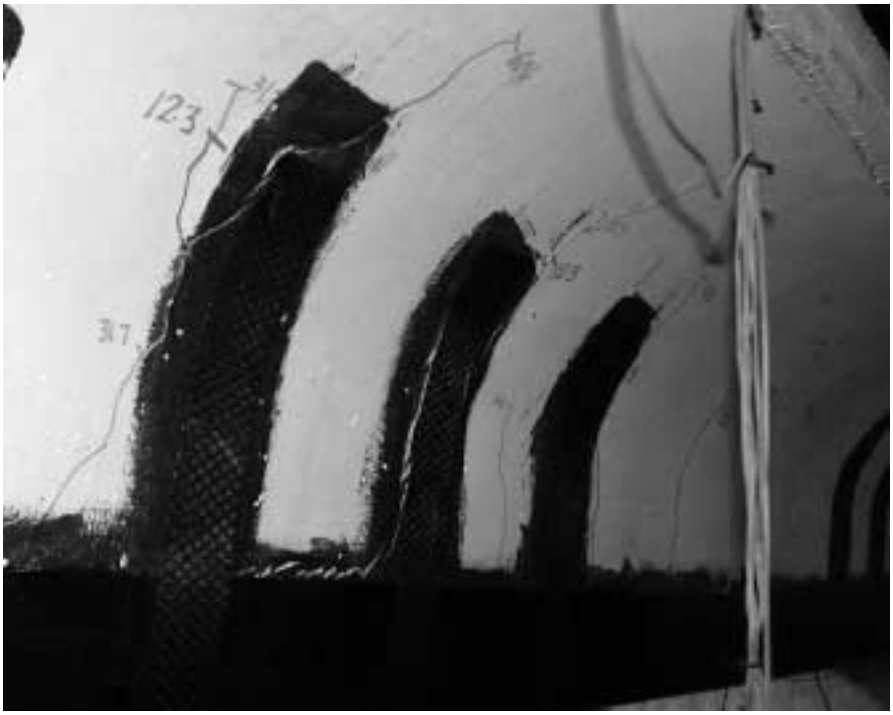

Figure 4.11 Initiation of Debonding Along CFRP Sheet

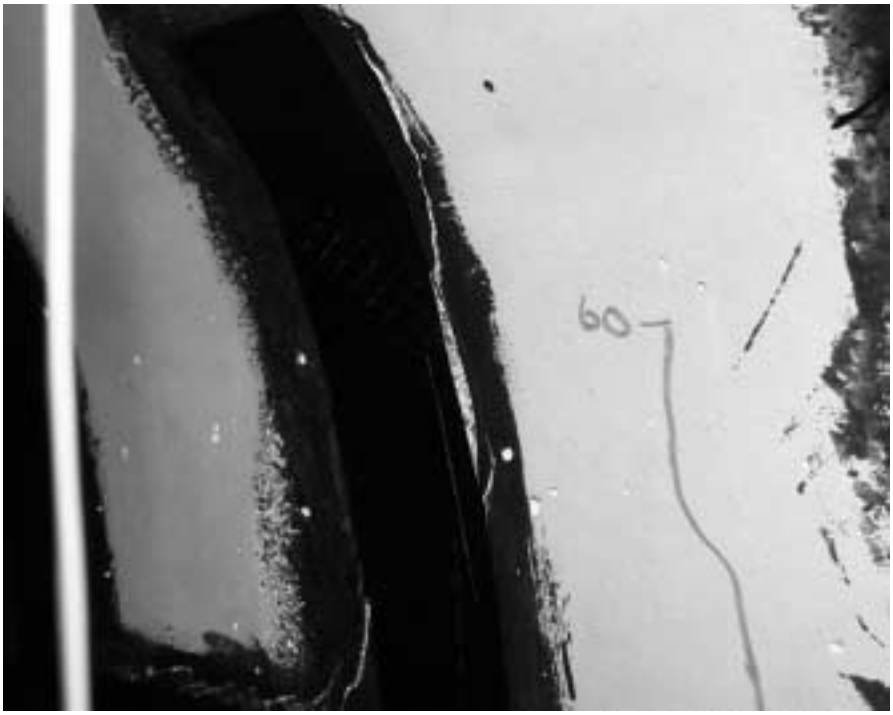

Figure 4.12 Crack Propagation Behind Strap Caused Debonding

Figure 4.13 View of West Joist in Specimen J-2 at Failure

Figure 4.14 Bottom Surface Condition of West Joist after CFRP Debonding

4.4 MEASURED RESPONSE

The measured displacement and strain response are presented in this section. The instrument readings are plotted against the applied load to verify that the instruments were operating properly throughout the tests. Calculations using the instrument readings to compare measured response parameters with calculated specimen response are presented in Chapter 5. Summaries of the measured response parameters corresponding to different load levels are presented in Tables 4.4 and 4.5 for Specimens J-1 and J-2, respectively.

4.4.1 Deflection Measurements

Linear potentiometers were used to monitor deflections at midspan, at sections N1 and S1, and at the supports. The instruments at sections N1 and S1 were removed before failure. Their stroke capacity was exceeded and it was considered too dangerous for research staff to reposition them. They were removed from Specimen J-1 at load level 3 and from Specimen J-2 at load level 4. Midspan potentiometers were repositioned at load level 3 and left in place until failure of both specimens. More potentiometers were used to monitor movement of the supports for Specimen J-2 than for Specimen J-1, because significant rotation occurred at the supports during testing of Specimen J-1.

Recorded deflections along the span and at the supports are shown in Figures 4.15 to 4.17 for Specimen J-1 and in Figures 4.18 to 4.20 for Specimen J-2.

The deflection readings of instruments at midspan, and sections N1 and S1 were corrected by subtracting the average support deflections shown in Figures 4.15 and 4.18 for Specimens J-1 and J-2, respectively.

The plots show readings taken on the east and west sides of the specimens. The similarity in these plots indicates that the specimens did not twist during the tests. Therefore, the average deflection was used in the comparison to the calculated response presented in Chapter 5.

The load-deflection plots for both specimens exhibit similar characteristics. The slope in the load-deflection diagrams is indicative of the specimen stiffness at different stages of loading. The response of the specimens was characterized by three different regions (Figure 4.21). The initial two regions in the load-deflection diagrams correspond to uncracked and cracked specimen response, respectively. These two regions are typical of the behavior of reinforced concrete members. The third region corresponds to member response after yielding of the longitudinal reinforcement. The post-yield stiffness was larger than would be expected for ordinary reinforced concrete. This difference is the result of the contribution of the CFRP composites to the member stiffness.

Although the specimens were initially cracked, the CFRP composites increased the specimen stiffness at low load levels after strengthening. This can be observed in Figure 4.22. The figure compares the unstrengthened and strengthened load-deflection cycles up to the first two load stages for Specimen J-1. After strengthening, the slope in the load-deflection diagram increased to approximately the slope before cracking the unstrengthened specimen. Points A and B in the figure indicate where the apparent stiffness reduction took place (approximately 5 and 18 kip, respectively). Point A corresponds to specimen cracking before strengthening and point B corresponds to the initial stiffness reduction after strengthening. It can be seen that stiffness reduction takes place at a higher load after the specimen was strengthened although the specimen had already been cracked before strengthening. The broken line in the figure shows that the apparent stiffness after cracking is approximately equal to the strengthened specimen stiffness after point B. Specimen J-2 displayed similar behavior.

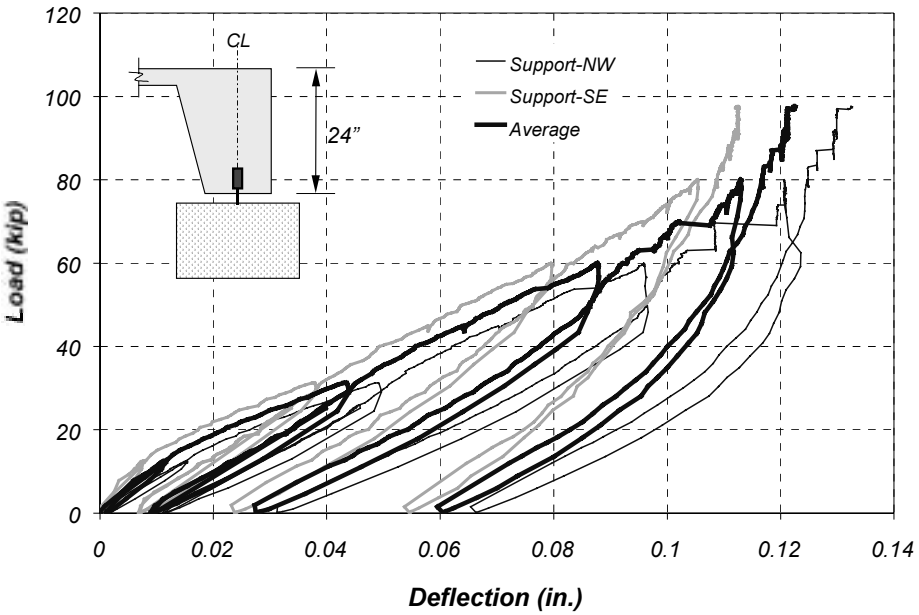

Figure 4.15 Measured Displacements at Supports in Specimen J-1

(a) East Joist

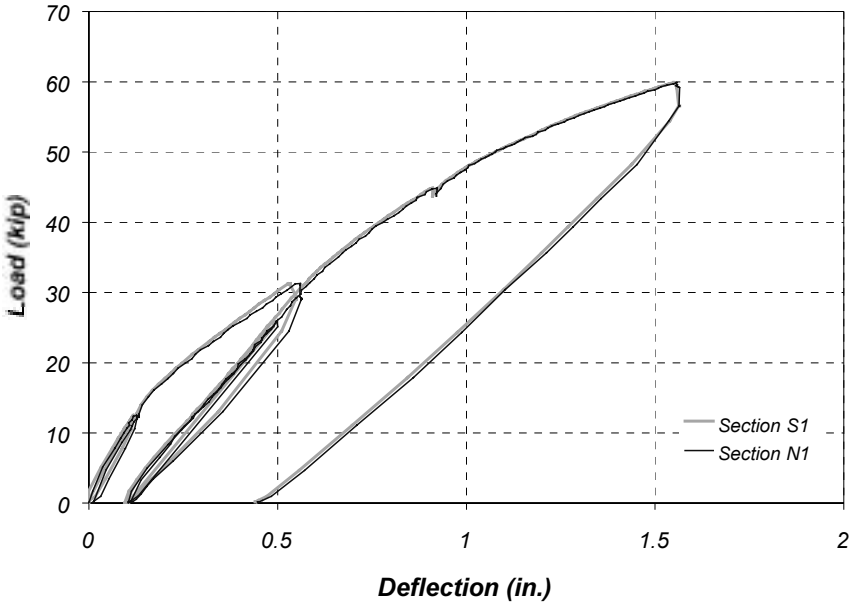

(b) West Joist

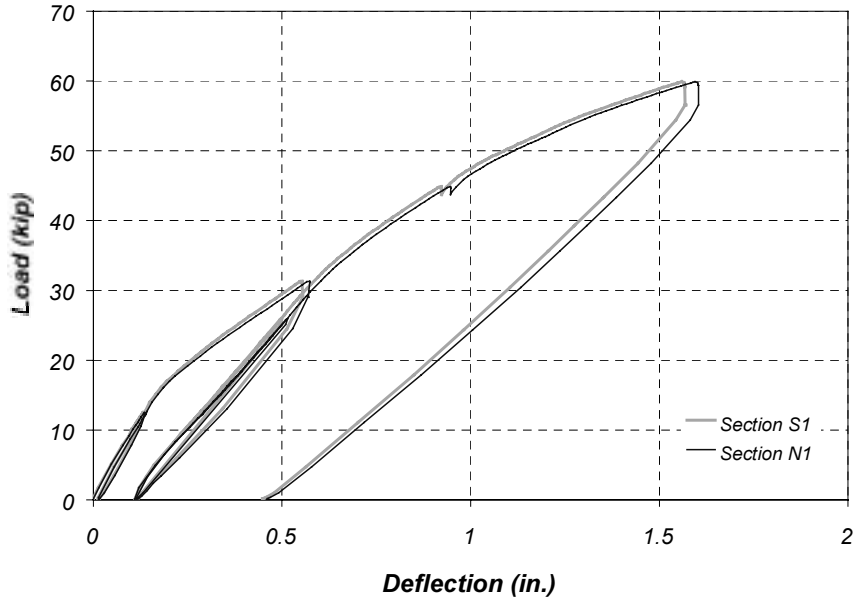

Figure 4.16 Measured Deflections at Sections N1 and S1 in Specimen J-1

(a) East Joist

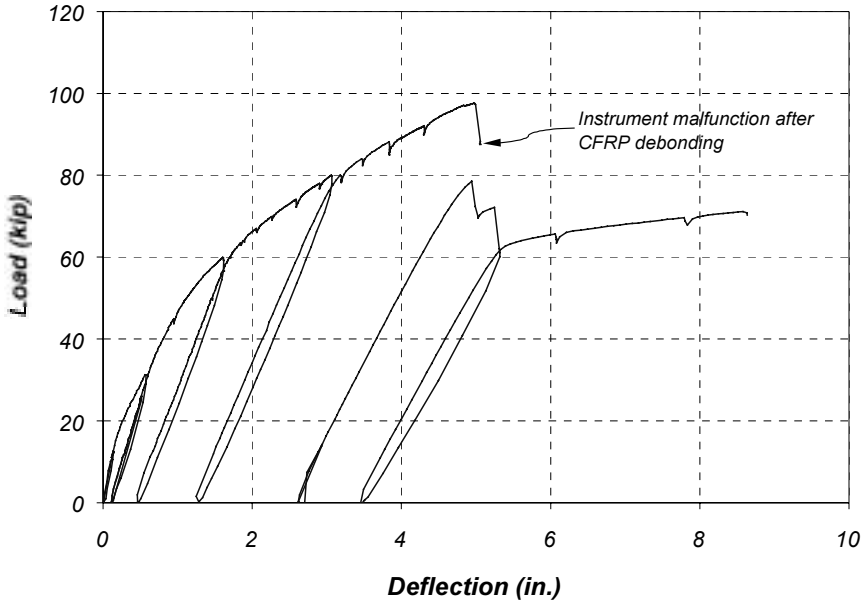

(b) West Joist

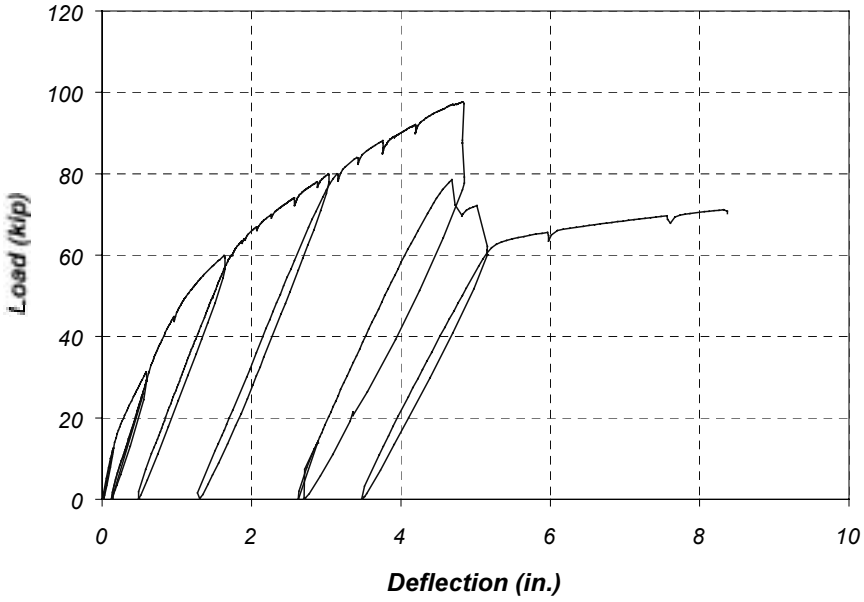

Figure 4.17 Measured Deflections at Midspan in Specimen J-1

(a) North block

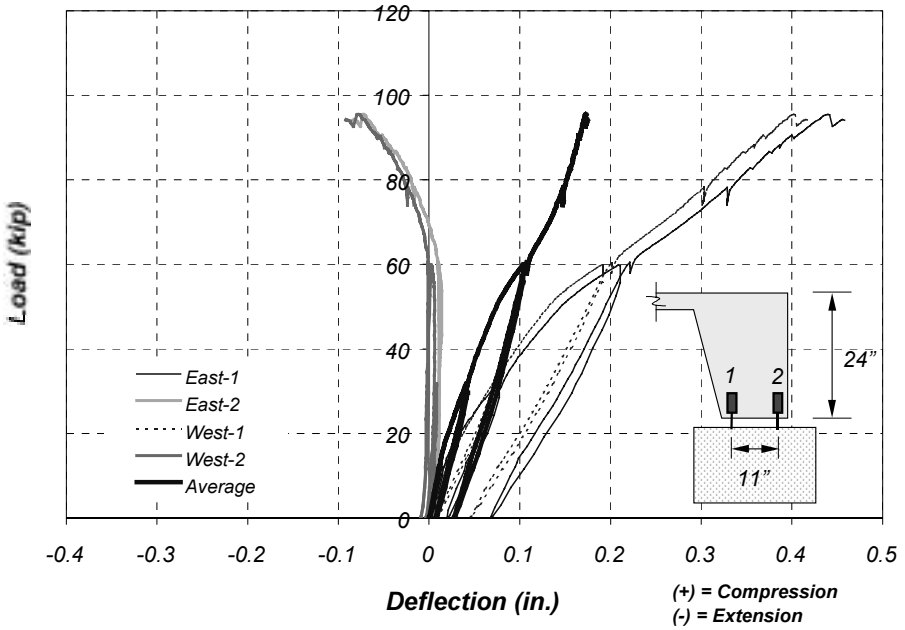

(b) South Block

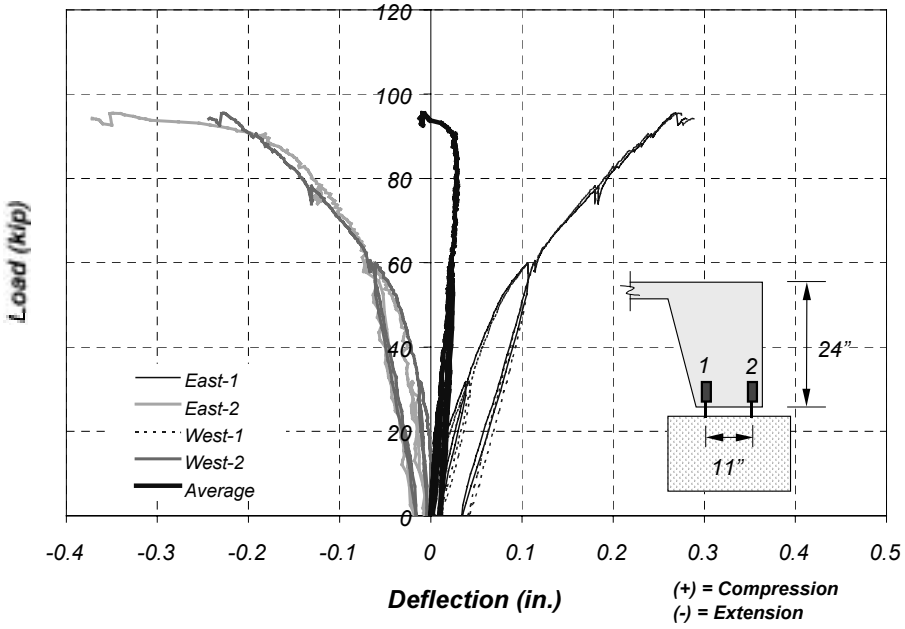

Figure 4.18 Measured Displacements at Supports in Specimen J-2

(a) East Joist

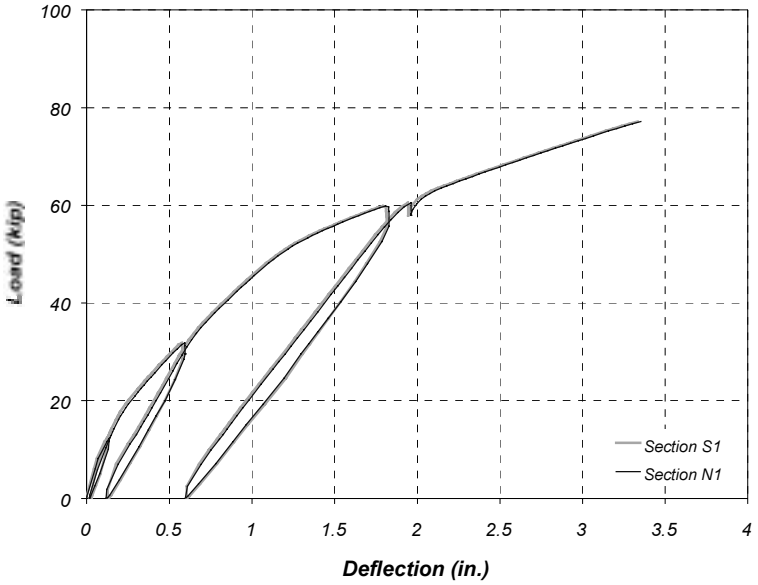

(b) West Joist

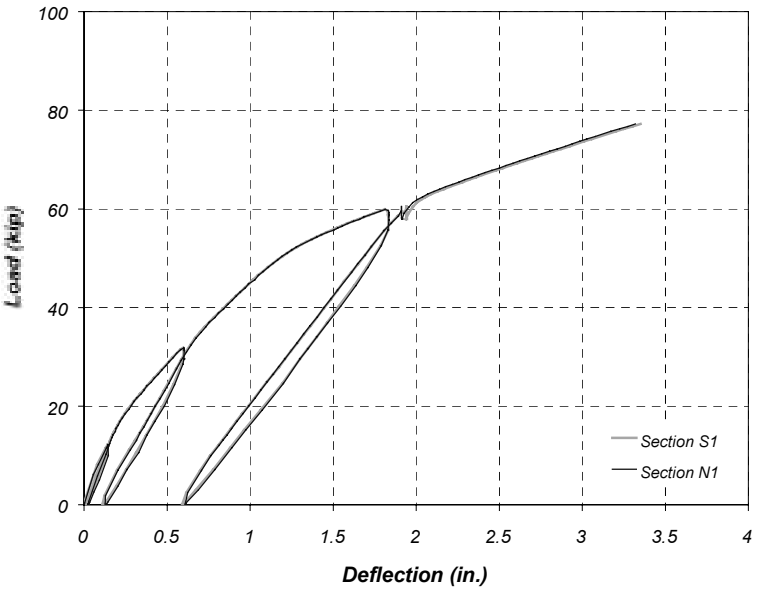

Figure 4.19 Measured Deflections at Sections N1 and S1 in Specimen J-2

(a) East Joist

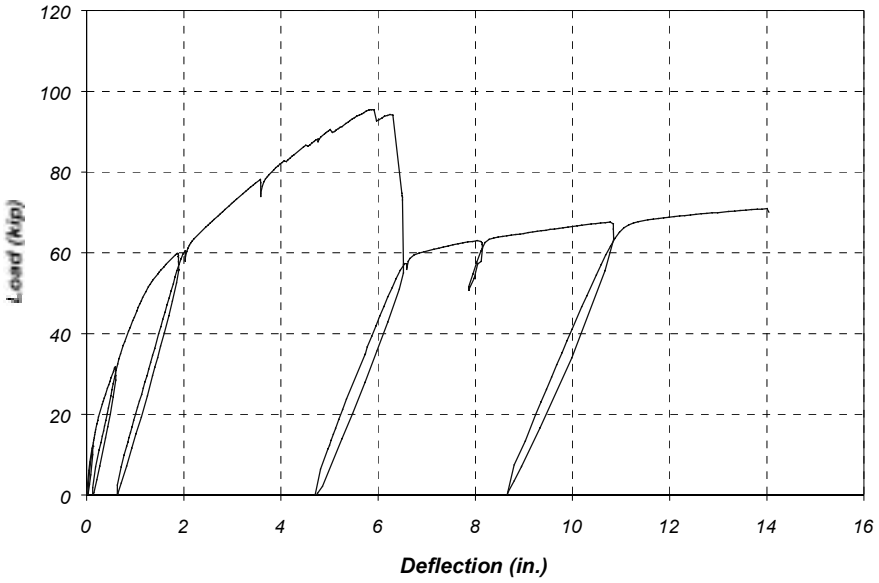

(b) West Joist

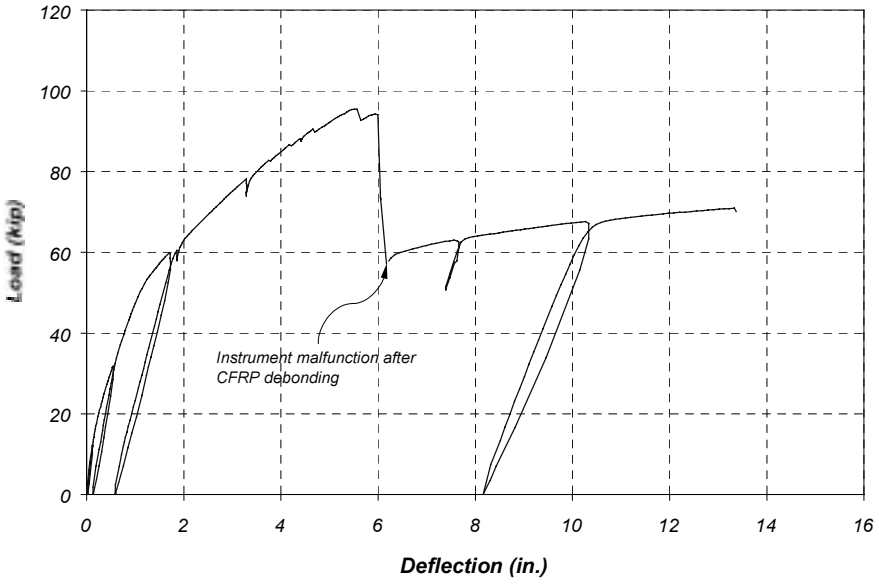

Figure 4.20 Measured Midspan Deflections in Specimen J-2

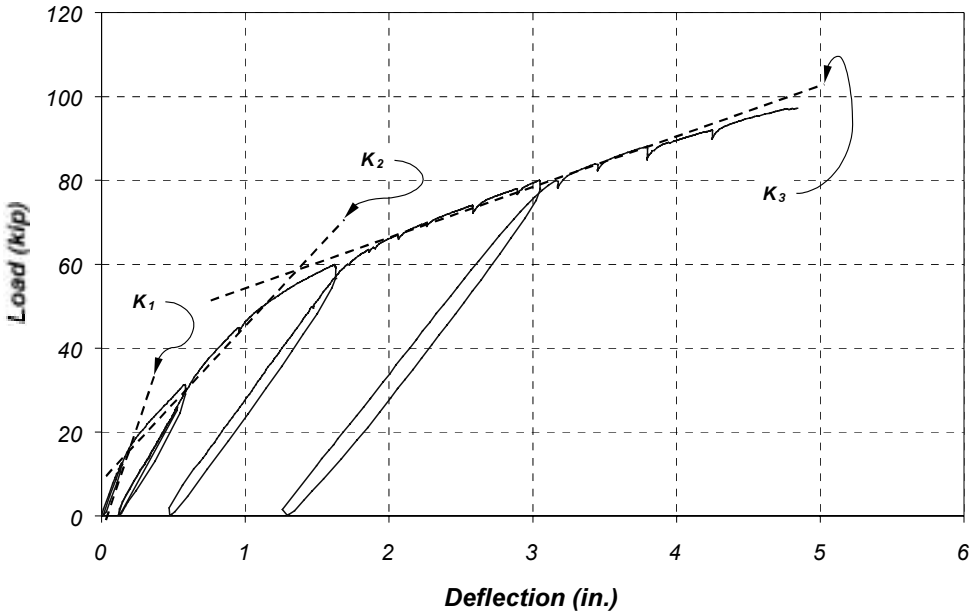

Figure 4.21 Load-Deflection Behavior Characterized by Change in Global Stiffness

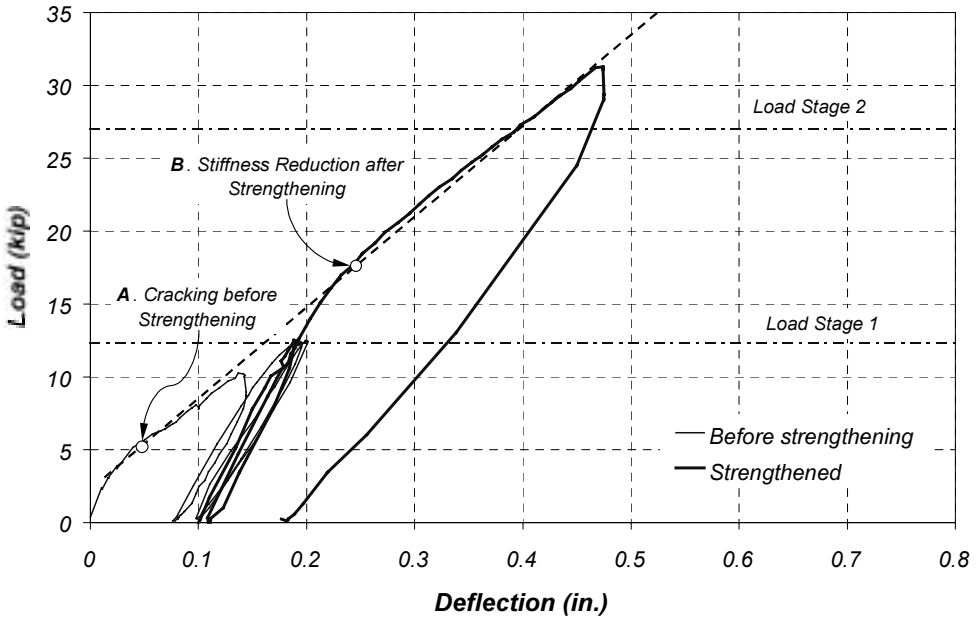

Figure 4.22 Typical Stiffness Increase after CFRP Strengthening (Specimen J-1)

Tables 4.4 and 4.5 give a summary of the measured specimen response at different loading stages for Specimens J-1 and J-2, respectively. The measured midspan deflection in these tables has been corrected by subtracting the support displacements.

Table 4.4 Maximum Response Measured During Testing of Specimen J-1

Load Stage	Maximum Measured Parameters			Maximum Average Strain (Microstrain)			Notes
	Load, kip	Moment, kip-ft	Deflection, in.	Reinforcement	Concrete	CFRP Plates	
1A	12.3	74	0.20	453	110	-	Reinforced concrete specimen before application of CFRP
1B	12.3	74	0.14	200	61	137	Reinforced concrete joists with CFRP plates
2	27.3	164	0.54	737	178	836	Reinforced concrete joists with CFRP plates
3	59.2	355	1.68	2,778	534	2,845	Observed yielding of longitudinal reinforcement
4	75	450	2.66	4,920	878	5,038	Target design load
5	97.3	584	4.92	8,993	1,615	8,441	Debonding of CFRP plate on east joist
6	78.5	471	4.91	*	1,548	*	Debonding of CFRP plate on east joist
7	71	426	8.60	*	2,590	*	Capacity of bare reinforced concrete specimen

* Readings were unavailable because gages were damaged after CFRP debonding

Table 4.5 Maximum Response Measured During Testing of Specimen J-2

Load Stage	Maximum Measured Parameters			Maximum Average Strain (Microstrain)			Notes
	Load, kip	Moment, kip-ft	Deflection, in.	Reinforcement	Concrete	CFRP Sheets	
1A	12.3	74	0.20	495	125	-	Reinforced concrete specimen before application of CFRP
1B	12.3	74	0.12	204	76	68	Reinforced concrete joists with CFRP sheets
2	27.3	164	0.41	602	199	368	Reinforced concrete joists with CFRP sheets
3	59.2	355	1.66	2,726	718	3059	Observed yield of longitudinal reinforcement
4	75	450	3.05	5,122	1,285	4751	Target design load
5	95.4	572	5.66	8,514	2,311	8717	Local rupture of CFRP sheet on east joist
6	73.8	443	6.19	7,828	2,496	*	Debonding of CFRP sheet on east and west joists
7	70	420	13.88	*	4,316	*	Capacity of bare reinforced concrete specimen

* Readings were unavailable because gages were damaged after CFRP debonding

The measured deflections for load stages 1 to 3, corresponding to service load levels, are summarized in Table 4.6. These deflection values were normalized by the span length. It is interesting to note that the deflections measured after the specimens were strengthened were smaller than those measured for the bare reinforced concrete joists. This indicates that the application of the CFRP composites stiffened the specimens at low load levels.

Table 4.6 Measured Deflections during Service Load Stages

Load Stage	Specimen J-1		Specimen J-2	
	Δ, in.	Δ/L_{test}	Δ, in.	Δ/L_{test}
1A	0.195	1/1,720	0.197	1/1,710
1B	0.143	1/2,350	0.120	1/2,800
2	0.490	1/690	0.467	1/720
3	1.858	1/180	1.876	1/180

The global response of the specimens was evaluated also by comparing the displacement ductility (μ_Δ) of the strengthened specimens with the displacement ductility of the bare reinforced concrete section. Displacement ductility was defined as the ratio of maximum displacement measured at failure to the displacement measured at yield. Even though the specimens did not exhibit a well-defined yield point, the measured deflection at the start of load stage 3 was assumed to be the yield deflection. The yield displacement for the bare reinforced concrete section was assumed to be the same as the yield displacement for the strengthened specimens.

Displacement ductility of the strengthened specimens is compared with the displacement ductility of the bare reinforced concrete specimens in Table 4.7. The displacement ductility of the strengthened specimens was lower than the ductility of the unstrengthened specimen. However, considerable deformation capacity was observed after yielding, before failure of the specimens.

Table 4.7 Comparison of Displacement Ductility

Specimen	Strengthened			Unstrengthened		
	Δ_y, in.	Δ_{max}, in.	μ_Δ (Δ_{max}/Δ_y)	Δ_y, in.	Δ_{max}, in.	μ_Δ (Δ_{max}/Δ_y)
J-1	1.66	4.92	3.0	1.66	8.60	5.2
J-2	1.74	5.66	3.3	1.74	13.84	8.0

4.4.2 Strain Gage Measurements

Strain gage readings were used to compute internal stresses and forces and to determine the location of the neutral axis at various stages of loading. The calculated moment-curvature response using the strain gage readings is presented in Chapter 5. Load vs. average strain plots for sections N1 and N2 are presented in this section. The characteristics of these plots were the same for the mirror sections (S1 and

S2) on the south side of the specimens. The recorded output from all the instruments can be found in Appendix D. Further discussion on the measured strain response is presented in Chapter 5.

(a) Strain gage readings in Specimen J-1

Measured strains for instrumented sections N1 and N2 in Specimen J-1 are presented in Figures 4.23 and 4.24. These figures show the average strain readings taken by gages bonded to the main flexural reinforcement (#8 bars), CFRP pultruded plates, and concrete slab surface. The average strain readings were used to determine internal stresses in the reinforcement to calculate the moment-curvature response of the specimen.

Whenever the output from an instrument was considered unreliable, it was eliminated from the average calculations. After this point, only the readings from gages that were still functioning were used to calculate the average readings. Gage readings were considered unreliable whenever there was a sudden change in voltage output caused by gage debonding or wire damage during the test. The curves for the individual gages included in Appendix D indicate whenever readings were considered unreliable.

Curves for instruments located in section N1 show very distinct regions that are bounded by loads corresponding to the loss in specimen stiffness due to cracking (15 – 20 kip) and yielding of the steel reinforcement (55 – 60 kip). These sections are located at the points of load application and correspond to the start of the constant moment region in the specimen (Figure 4.23).

The load-strain curves for instruments located in section N2 also show distinct regions defined by different slopes. However, as expected, the loads that define the change in general slope in the plots for section N2 are higher than for section N1. At a specific load stage, the moment in section N2 was lower than the moment in section N1. The readings of the concrete gages on section N2 exhibit a fairly linear response after the change in slope corresponding to cracking.

(b) Strain gage readings in Specimen J-2

Strain vs. load plots for sections N1 and N2 in Specimen J-2 are presented in Figures 4.25 and 4.26, respectively. The location of these instrumented sections was shown in Figure 4.4. These figures show readings taken with gages bonded to the main flexural reinforcement (#8 bars), CFRP pultruded plates, and concrete slab surface.

In this specimen, only three strain gages were bonded to the top concrete slab at each section instead of the five that were used for Specimen J-1. This was decided after observing that the readings across a section in Specimen J-1 were very similar, so the gages at the slab edge were eliminated (see Appendix D).

The same general trends that were observed for the gages in Specimen J-1 can be observed in these figures. Therefore, similar conclusions can be reached about the observed strain response for this specimen.

(a) Average #8 reinforcing bar strains

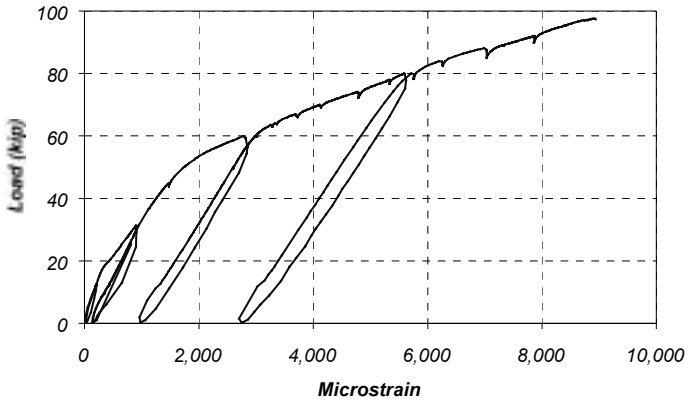

(c) Average concrete strains

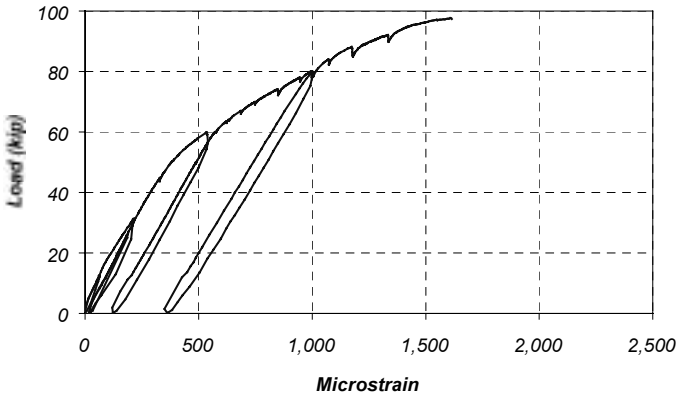

(b) Average CFRP strains

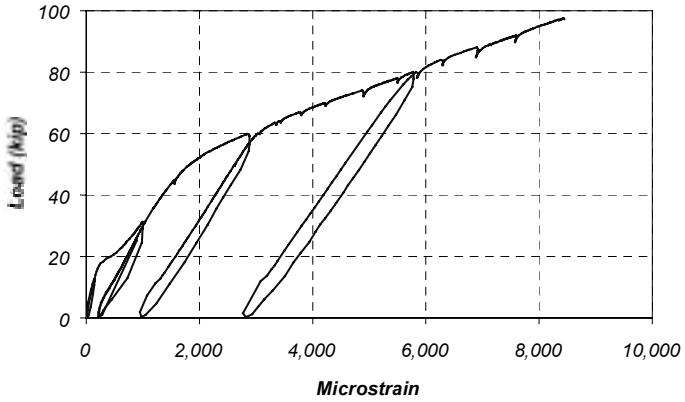

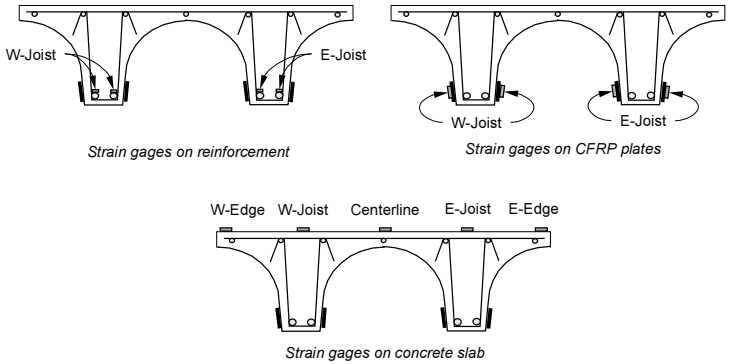

Figure 4.23 Average Strains Measured at Section N1 (Specimen J-1)

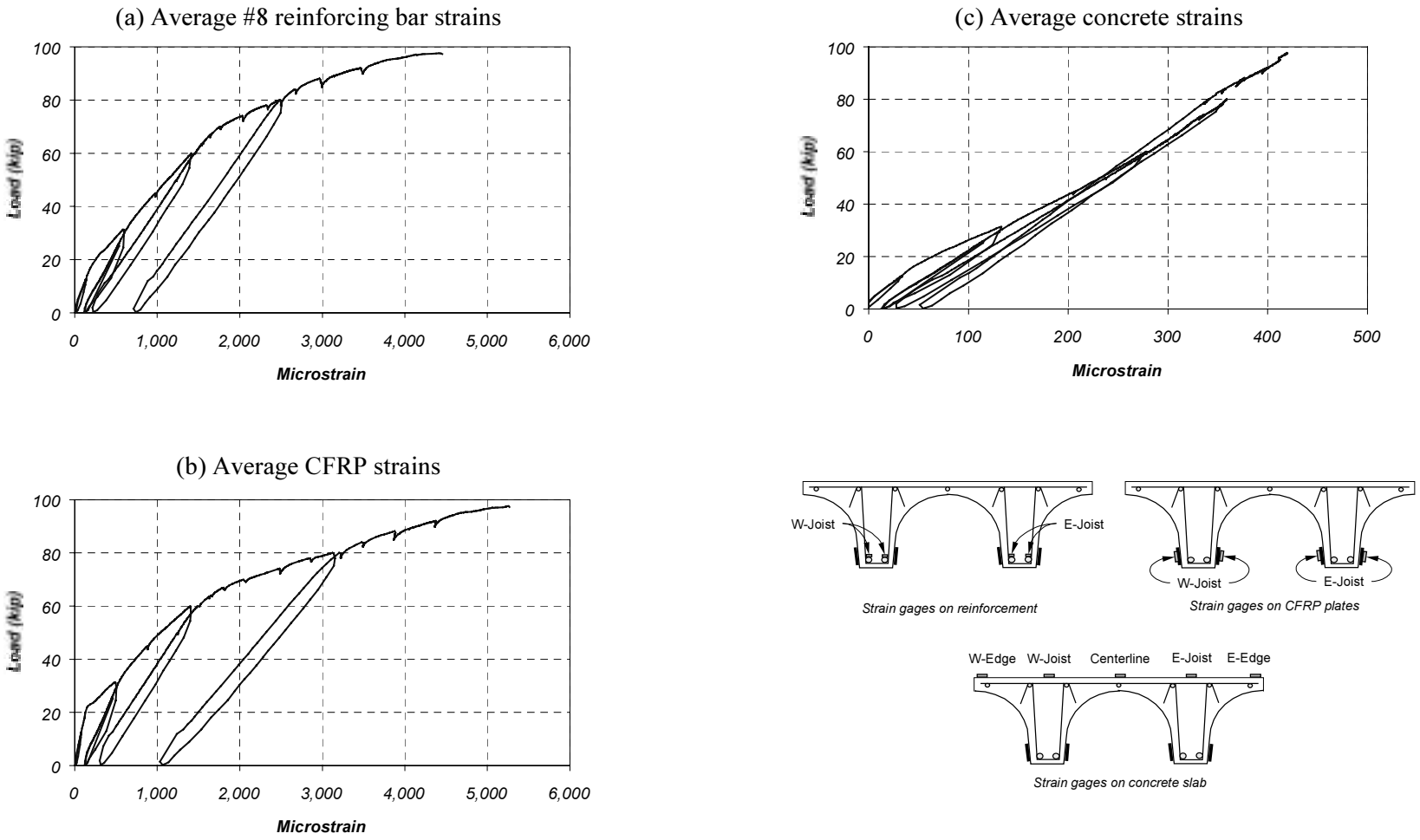

Figure 4.24 Average Strains Measured at Section N2 (Specimen J-1)

(a) Average #8 reinforcing bar strains

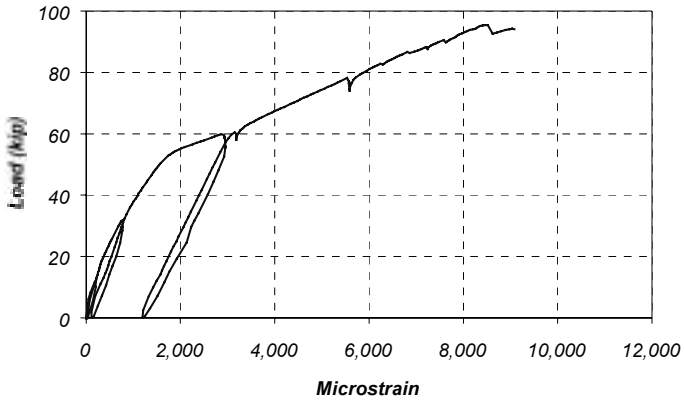

(b) Average CFRP strains

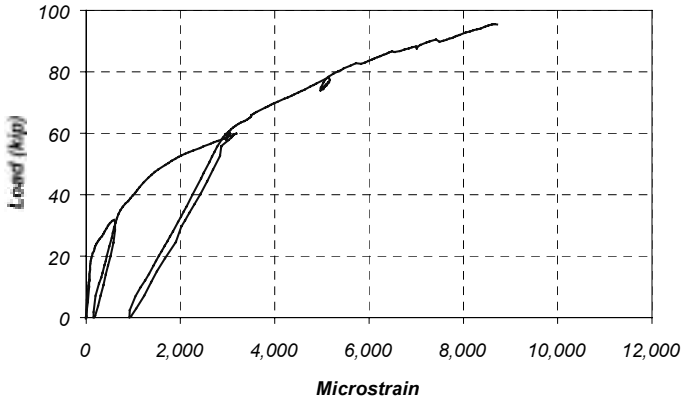

(c) Average concrete strains

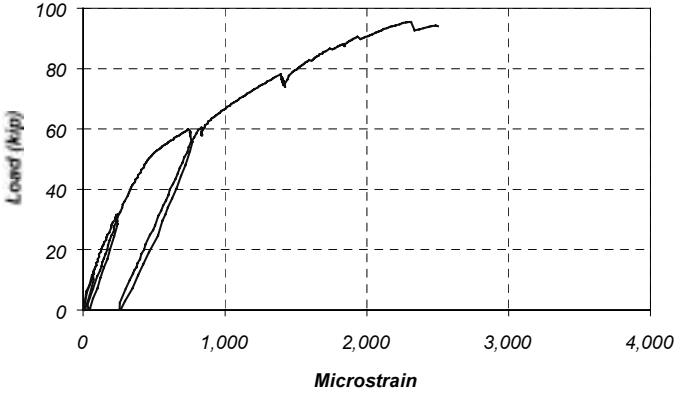

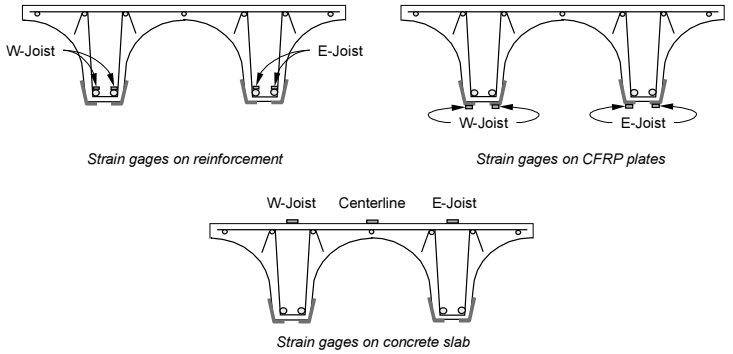

Figure 4.25 Average Strains Measured at Section N1 (Specimen J-2)

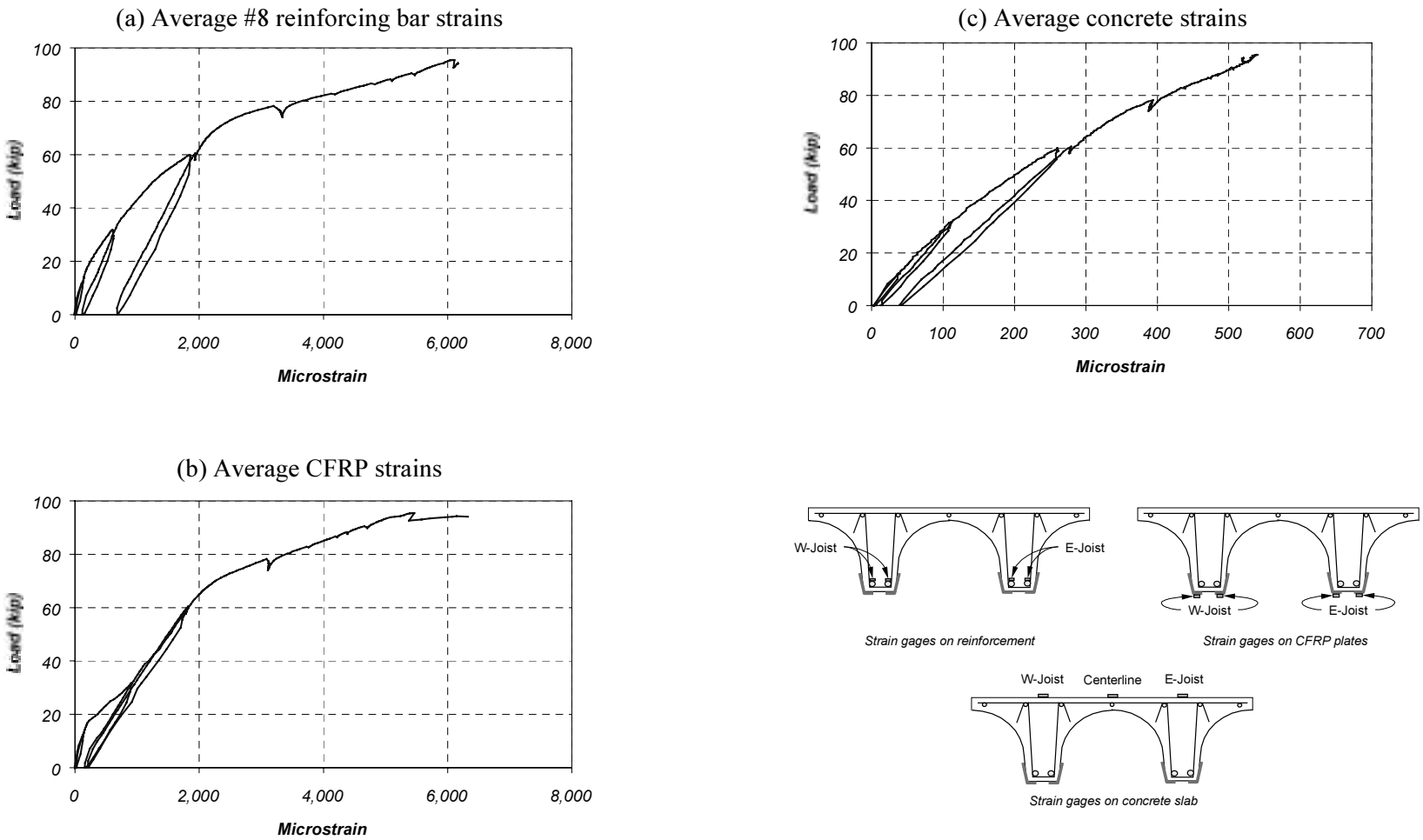

Figure 4.26 Average Strains Measured at Section N2 (Specimen J-2)

4.5 SUMMARY

The laboratory tests of the two pan-girder specimens are described in this chapter. The loading sequence, testing apparatus, and instrumentation were also presented.

Selected results of recorded instrument readings during the tests were shown as load-deflection or load-strain plots. The average strain readings from two sections in each specimen were shown to illustrate the general behavior observed during the tests. These figures illustrate the general characteristics of the observed response and are representative of the behavior at the other sections symmetrically located about midspan. The average strains were used to compute the specimen moment-curvature response presented in Chapter 5.

Chapter 5: Verification of the Analytical Model Using the Measured Response of the Girder-Joist Specimens

5.1 INTRODUCTION

The analytical model developed in Chapter 3 of the report documenting the first two phases of this research project [Breña et al., 2001], including the refinements presented in Chapter 2 of this report, is verified in this chapter by comparing the strains, curvatures, and displacements with the measured response of Specimens J-1 and J-2. Strains are discussed in Section 5.2, and moment-curvature response is presented in Section 5.3. Data from both these sections may be used to evaluate the strain at which the CFRP composites debond from the surface of the concrete. This information is needed to calculate the capacity of reinforced concrete members strengthened using CFRP composites. Displacement response is evaluated in Section 5.4. In general, the analytical models are able to represent the measured global response quite well; however, some aspects of the local behavior were not well represented.

5.2 EVALUATION OF STRAIN RESPONSE

The analytical procedures were based on a number of assumptions about the distribution of strain within the cross section. Therefore, the first step in evaluating the applicability of the computational models must be a detailed comparison of the calculated and measured strains. If the measured strains follow the same trends that form the basis of the analytical model, then it is likely that the analytical model will be successful in representing the response of the specimens. However, if the measured strains differ significantly from these assumptions, then the analytical model will be of limited use for understanding the response of reinforced concrete elements strengthened using CFRP composites.

Strains were measured on the reinforcing bars, on the top surface of the concrete, and on the surface of the CFRP composites during testing of Specimens J-1 and J-2. Measured data were presented in Chapter 4 and Appendix C, and those data are compared with the calculated response of the test specimens in this section. Strains due to dead loads are evaluated in Section 5.2.1, and the variations of strain with distance from the neutral axis are discussed in Section 5.2.2. Calculated and measured strains in each of the three materials are compared in Section 5.2.3, and the strains at which the CFRP composites debonded from the surface of the concrete are evaluated in Section 5.2.4.

5.2.1 Strains Due to Dead Loads

Strains due to dead loads are typically ignored in laboratory tests of reinforced concrete members because test specimens are often constructed at a reduced scale, and the resulting strains are small. However, Specimens J-1 and J-2 were the same size as the prototype bridge, and the dead loads in the laboratory were nearly the same as the dead loads in the field. Therefore, the strains due to dead loads could not be ignored when evaluating the response of the test specimens.

The construction process precluded direct measurement of dead-load strains. Although the strain gages were attached to the reinforcing bars before the concrete was cast, the gages were not connected to the data acquisition system until the beam was positioned on the support blocks. The strain gages were attached to the top surface of the concrete after the test specimens were in their final position in order to avoid damaging the gages as the specimens were moved. The CFRP composites were bonded to the

surface of the concrete while the full dead load was acting on the system. Therefore, the measured strains in the CFRP during the tests corresponded to the strains induced by the applied loads.

The strains in the reinforcing steel and concrete under dead load were estimated using the analytical procedure discussed in Chapter 3 of the companion report (Breña, et al., 2001) for the bare cross section. The dead-load moment was calculated by assuming a unit weight of concrete equal to 150 pcf and a span of 28 ft. The measured material properties (Appendix A) were used in these calculations. Calculated dead-load strains for sections N1 and S1 are reported in Table 5.1.

Table 5.1 Calculated Dead-Load Strains

M_{DL}, kip-ft	Strains, Microstrain		Curvature, 1/in.	NA Depth, in.
	Concrete	Steel		
Specimen J-1				
81.6	116	514	2.9×10^{-5}	4.00
Specimen J-2				
81.6	117	528	3.0×10^{-5}	3.92

5.2.2 Measured Strain Profiles Due to Live Loads

During the development of the analytical model, prefect bond was assumed between the CFRP laminates and the surface of the concrete. If this assumption is true, then the measured live-load strains would vary linearly with depth within the cross section at all levels of applied load.

Measured strain profiles at sections N1 and S1 are shown in Figure 5.1 for Specimen J-1. Similar data are shown in Figure 5.2 for Specimen J-2. The average strain in each material at each stage of loading is plotted as a function of the distance from the top of the specimen to the gage.

The strains in the two specimens were similar at the sections directly beneath the applied loads. The strain profiles were approximately linear up to yielding of the reinforcement (load stage 3). At the higher load levels, the strains in the CFRP composites tended to be lower than those expected using a linear distribution of strain. Debonding of the CFRP composites from the surface of the concrete would tend to reduce the measured strains, because the CFRP composite deformations are distributed over a longer length. Therefore, the measured response is not surprising.

It is clear from the measured strain profiles that debonding of the CFRP composites and cracking of the concrete have a significant influence on the distribution of strain within the cross section. The strains in the CFRP composites were typically lower than those expected using a linear variation of strain with depth.

(a) Section N1

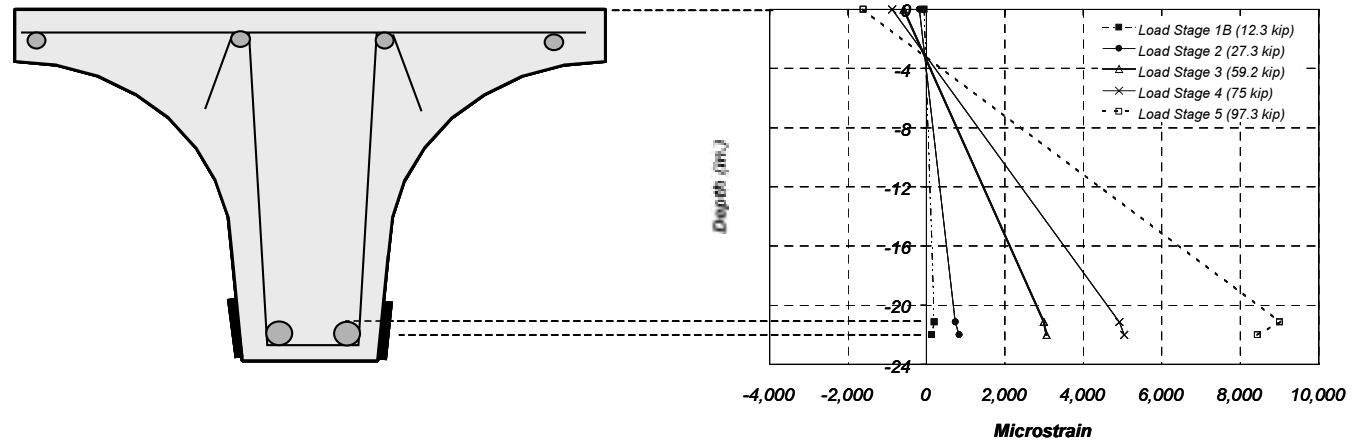

(b) Section S1

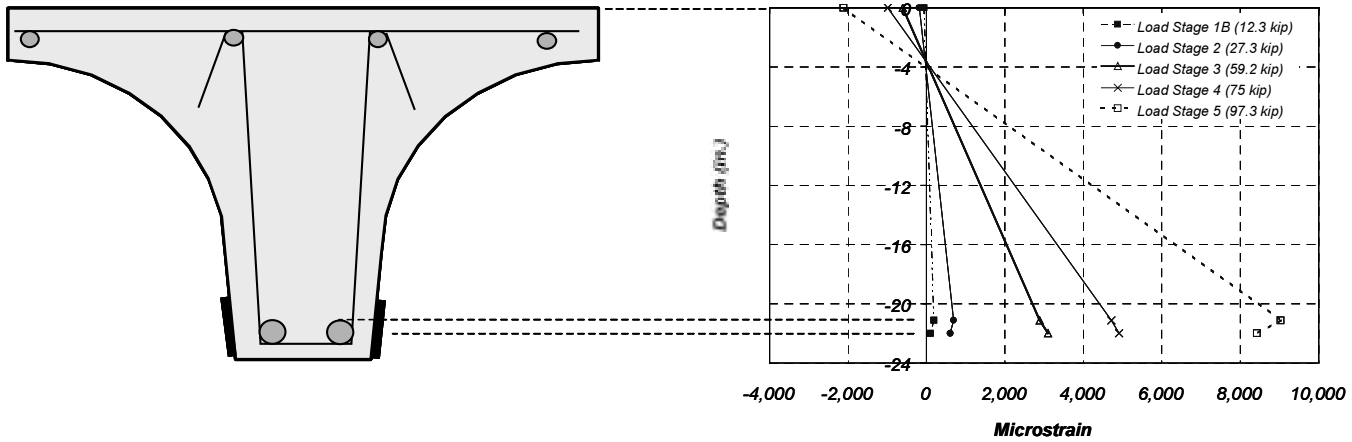

Figure 5.1 Measured Live-Load Strain Profiles in Sections N1 and S1 for Specimen J-1

(a) Section N1

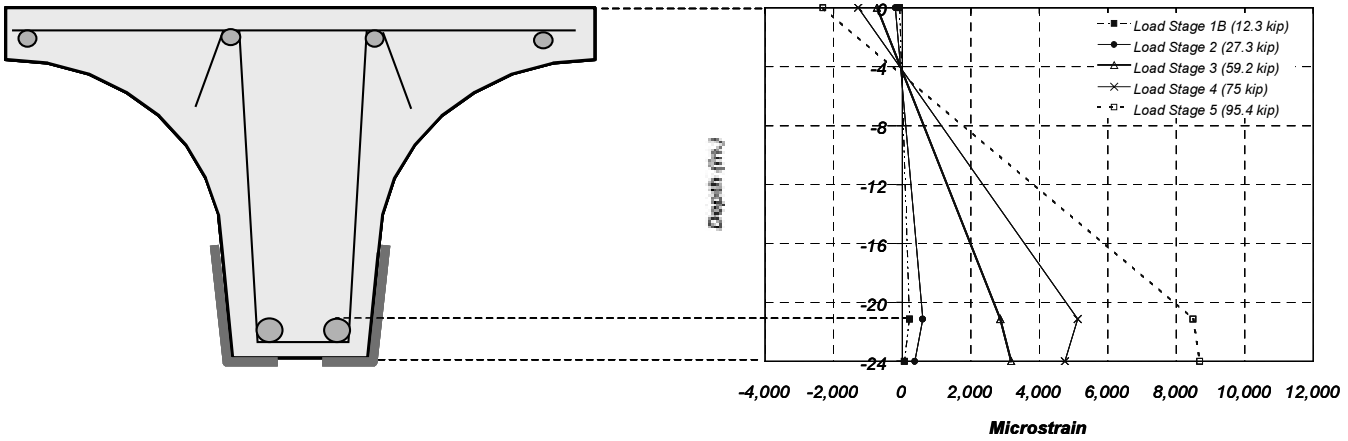

(b) Section S1

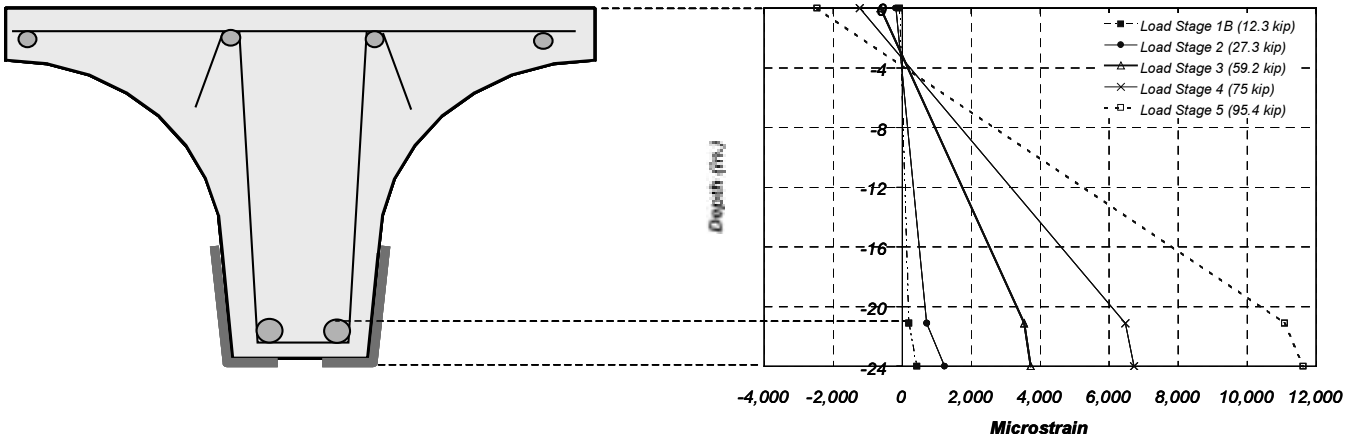

Figure 5.2 Measured Live-Load Strain Profiles in Sections N1 and S1 for Specimen J-2

5.2.3 Comparison of Measured and Calculated Strains Due to Live Loads

The live-load strains in each of the materials were calculated to provide a direct comparison with the measured strain response. The analytical procedures described by Breña et al. [2001] in Chapter 3 were used to relate the calculated total strains in the materials to the internal moment in the cross section using the measured material properties (Appendix A). The internal moment was then related to the applied load using the clear span of the beam, 28 ft, and the dead loads described in Section 5.2.1. The calculated strains corresponding to dead loads were then subtracted from the calculated total strains in the reinforcement and concrete. No attempt was made to model debonding of the CFRP laminates from the surface of the concrete in this phase of the analysis. Therefore, the failure condition for all calculations corresponds to rupture of the CFRP composites or crushing of the concrete.

Calculated and measured live-load strains are compared in Figure 5.3 through Figure 5.6 for locations under the loading points (sections N1 and S1). The measured steel and CFRP strains represent the average of readings from four gages, while the measured concrete strains represent the average of readings from five gages for Specimen J-1 and the average of readings from three gages for Specimen J-2.

The calculated strain curves approximate the measured response very closely. The primary difference between the measured and calculated strain response is the magnitude of the strain at failure. Because the CFRP composites debonded from the concrete during the tests, the measured failure strains were less than the calculated failure strains in the reinforcement and CFRP composites. The strains corresponding to debonding of the CFRP are quantified later in this section; therefore, discussion of failure conditions is deferred until later.

Above the yield load (approximately 60 kip), the calculated strains in the reinforcing bars and the CFRP were nearly the same as the measured strains. The calculated strains were approximately 1,000 microstrain less than the measured strains at section S1 in Specimen J-2, but the calculated strains were within 100 microstrain at the other three sections. The cause of this difference is likely due to the location of cracks near section S1 in Specimen J-2. In contrast, the calculated strains in the concrete were less than the measured strains at all four sections. At load levels above 80 kip, the differences exceeded 500 microstrain at three of the sections.

At applied loads below 60 kip, the calculated strains in all three materials tended to be greater than the measured strains. In most cases, these differences were less than 50 microstrain. It appears that bonding the CFRP laminates to the surface of the concrete stiffened the test specimens, even through the specimens had been cracked previously. No attempt was made to incorporate the influence of stiffening into the analytical model. A comparison of the strains measured at the critical load stages with the calculated strains for Specimens J-1 and J-2 is presented in Table 5.2 and Table 5.3, respectively.

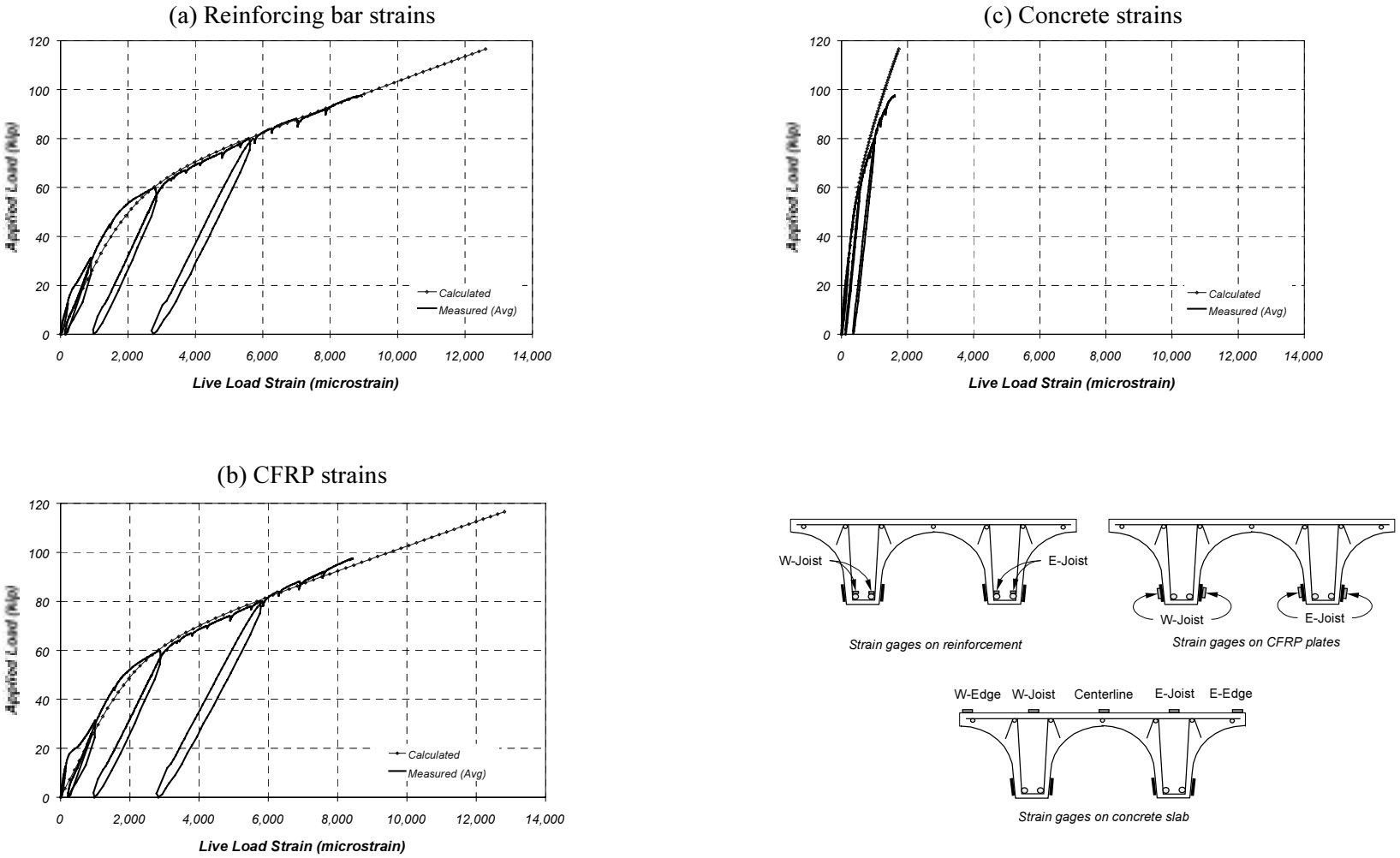

Figure 5.3 Comparison of Measured and Calculated Live-Load Strains at Section N1 (Specimen J-1)

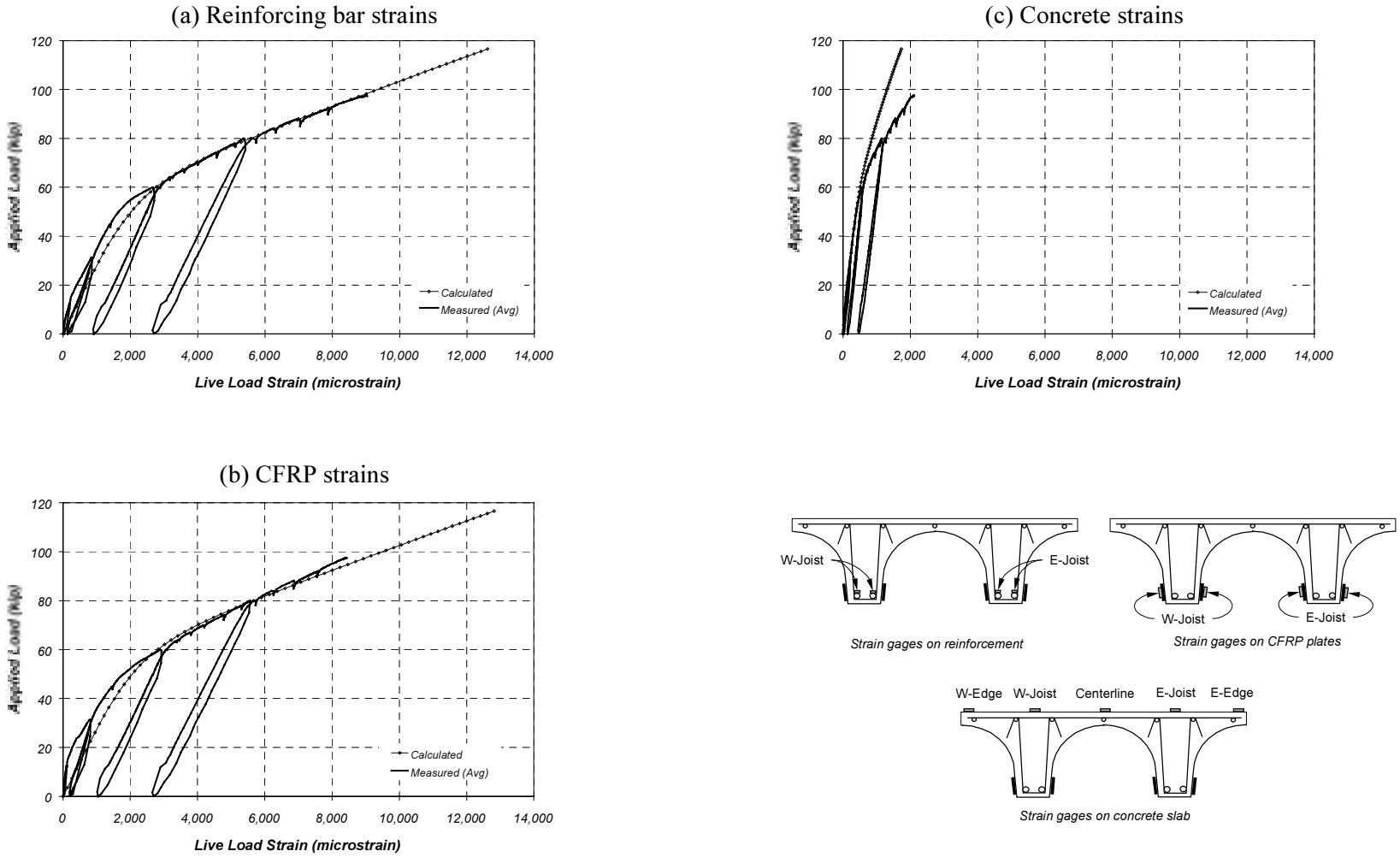

Figure 5.4 Comparison of Measured and Calculated Live-Load Strains at Section S1 (Specimen J-1)

(a) Reinforcing bar strains

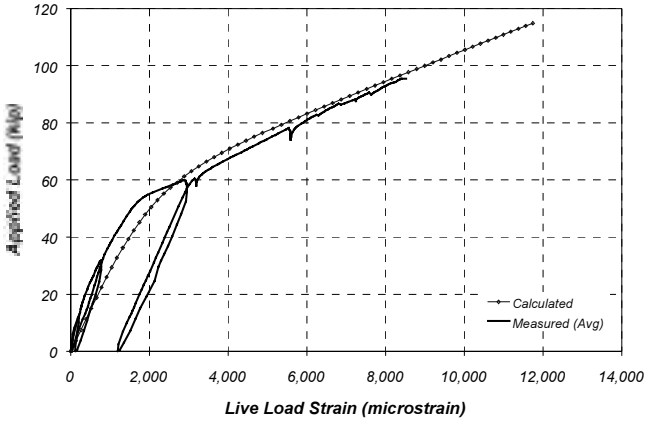

(c) Concrete strains

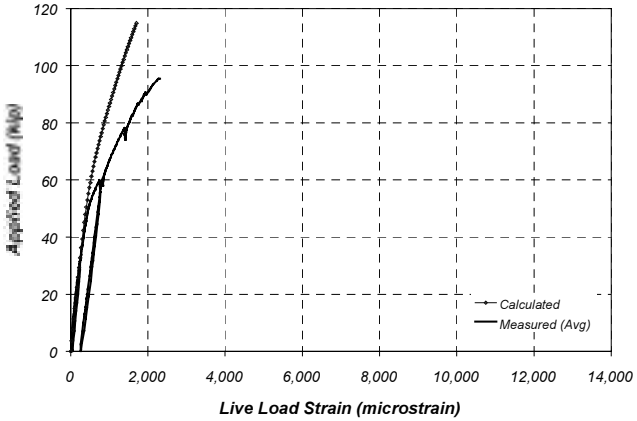

(b) CFRP strains

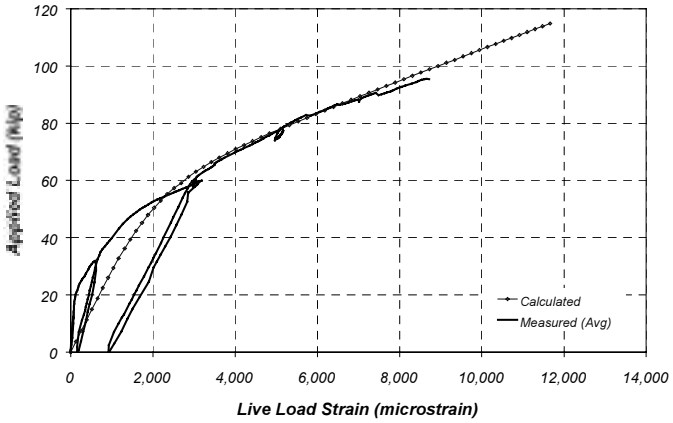

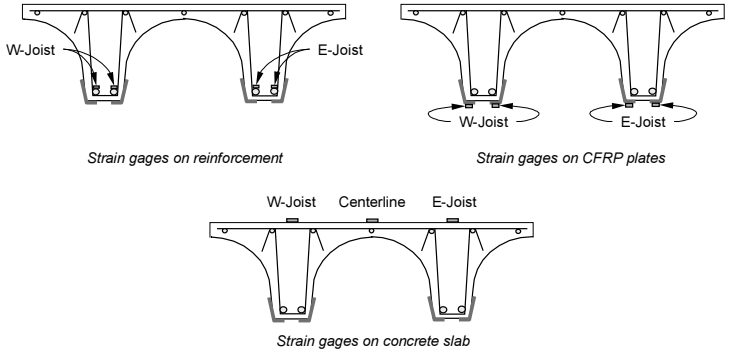

Figure 5.5 Comparison of Measured and Calculated Live-Load Strains at Section N1 (Specimen J-2)

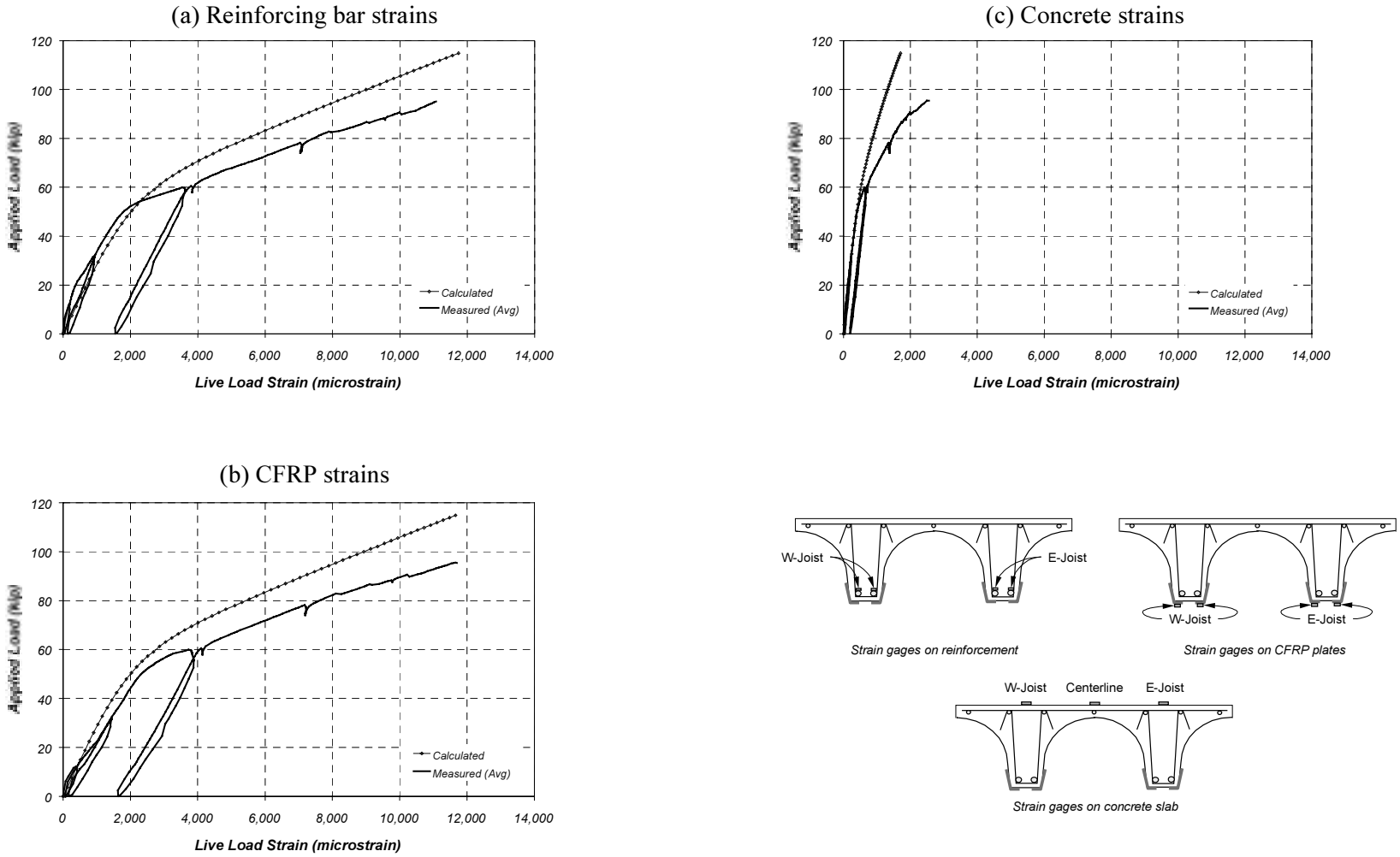

Figure 5.6 Comparison of Measured and Calculated Live-Load Strains at Section S1 (Specimen J-2)

Table 5.2 Measured and Calculated Live-Load Strains for Specimen J-1

Load Stage	Load, kip	Steel Strain, microstrain			CFRP Strain, microstrain			Concrete Strain, microstrain		
		Measured		Calculated	Measured		Calculated	Measured		Calculated
		N1	S1		N1	S1		N1	S1	
1B	12.3	200	189	399	137	102	406	61	64	75
2	27.3	737	692	934	836	607	951	178	182	186
3	59.2	2,693	2,558	2,783	2,766	2,817	2,831	522	543	511
4	75.0	4,920	4,683	4,839	5,038	4,909	4,921	878	983	778
5	97.3	8,938	9,035	8,781	8,442	8,428	8,927	1,615	2,110	1,239

Table 5.3 Measured and Calculated Live-Load Strains for Specimen J-2

Load Stage	Load, kip	Steel Strain, microstrain			CFRP Strain, microstrain			Concrete Strain, microstrain		
		Measured		Calculated	Measured		Calculated	Measured		Calculated
		N1	S1		N1	S1		N1	S1	
1B	12.3	204	188	391	68	386	388	76	70	78
2	27.3	602	711	914	368	1,226	908	199	185	189
3	59.2	2,726	3,367	2,706	3,059	3,524	2,688	718	613	512
4	75.0	5,122	6,470	4,660	4,751	6,621	4,629	1,285	1,233	777
5	95.4	8,514	11,068	8,155	8,717	11,697	8,101	2,312	2,558	1,209

5.2.4 Measured Strains at which the CFRP Composites Debonded from the Surface of the Concrete

As noted in the previous section, the failure strains in the materials were not well represented by the analytical model, because failure was defined in the analytical model as rupture of the CFRP composites. Both strengthened specimens failed after the CFRP composites debonded from the surface of the concrete, and crushing of the concrete was not observed until later stages of the test when the bare specimen was loaded to failure. The strain at which the composites debonded from the concrete was estimated by comparing the measured and calculated strains.

Figures 5.7 and 5.8 show a comparison between measured and calculated CFRP strains assuming no slip of the CFRP composites from the surface of the concrete. The calculated CFRP strains were determined using the measured concrete and steel strains and extrapolating the strain diagram to the centroid of the CFRP composites. In addition to the curves representing the measured and calculated live-load strains, the difference between the strains is also shown. For Specimen J-1, a sudden increase in the difference between the calculated and measured strains may be seen at an applied load of approximately 80 kip. As the applied load increased, the difference in strain increased, reaching a maximum of nearly 1,000 microstrain immediately before the composites debonded completely from the surface of the concrete. Local debonding was observed at a measured strain of approximately 6,000 microstrain, and failure was observed at a measured strain of approximately 8,500 microstrain.

These limits agree with the observed behavior of Specimen J-1 during the test. Local debonding was observed along the top of the CFRP plate at midspan at a load of approximately 60 kip. At approximately 80 kip, the first transverse strap debonded, which indicated that larger regions of the CFRP plates were debonding from the surface of the concrete (Chapter 4).

The trends were similar for Specimen J-2, although the calculated strains in the CFRP did not match the measured strains as well at the lower load levels. Local debonding was observed to occur at an applied load of approximately 60 kip, corresponding to a strain of less than 4,000 microstrain, and failure was observed at a strain between 8,500 and 11,500 microstrain. The CFRP laminates were observed to debond along the top edge at midspan at a load of approximately 80 kip. It can be assumed that laminates on the bottom surface began to debond at a lower load.

The maximum measured strains in the CFRP composites for both specimens were larger than the assumed value used to represent debonding (7,000 microstrain) for the design of the composite systems. At three locations, the average strain in the CFRP composites at debonding was approximately 8,500 microstrain. The failure strain exceeded 11,500 microstrain at location S1 in Specimen J-2. This variation in the maximum measured strains in the CFRP composites can be attributed to the formation of cracks in the immediate vicinity of the strain gages. Higher failure strains were recorded at locations where the cracks crossed the instrumented section.

Because the measured strains in the CFRP were so sensitive to the distance between the strain gage and cracks in the concrete, it is recommended that more than one gage be used in future tests in order to evaluate the influence of local effects in more detail. In addition, positioning strain gages along the height of the composite will provide information about the distribution of strains in the CFRP.

(a) Section N1

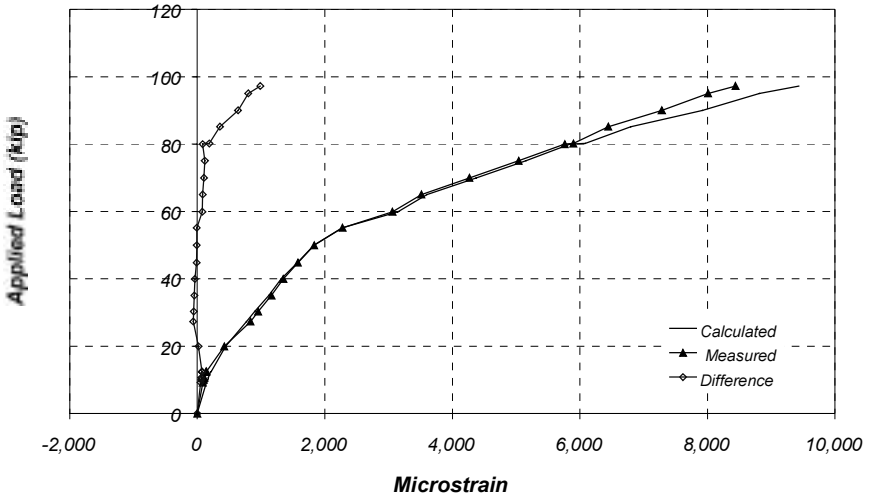

(b) Section S1

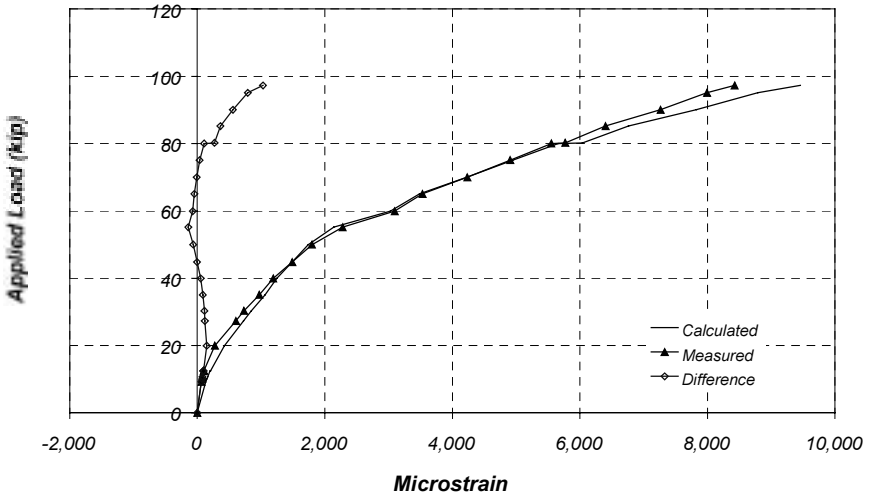

Figure 5.7 Comparison of Measured and Calculated CFRP Strains for Specimen J-1

(a) Section N1

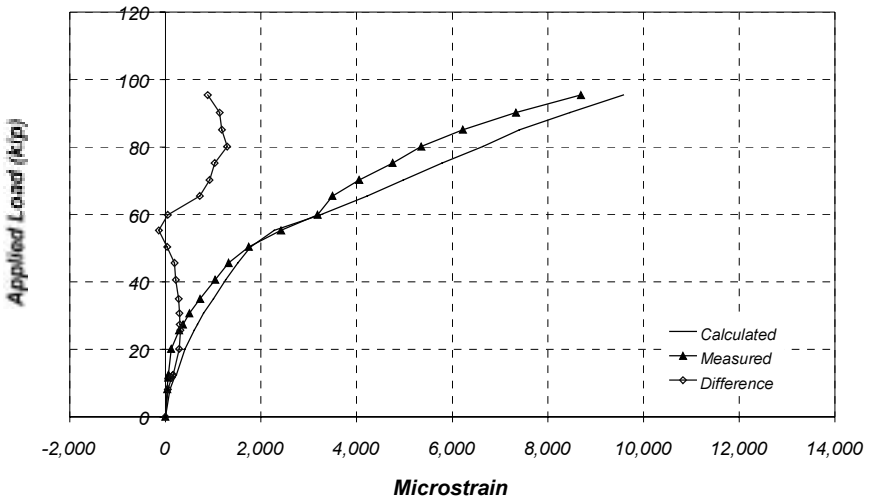

(b) Section S1

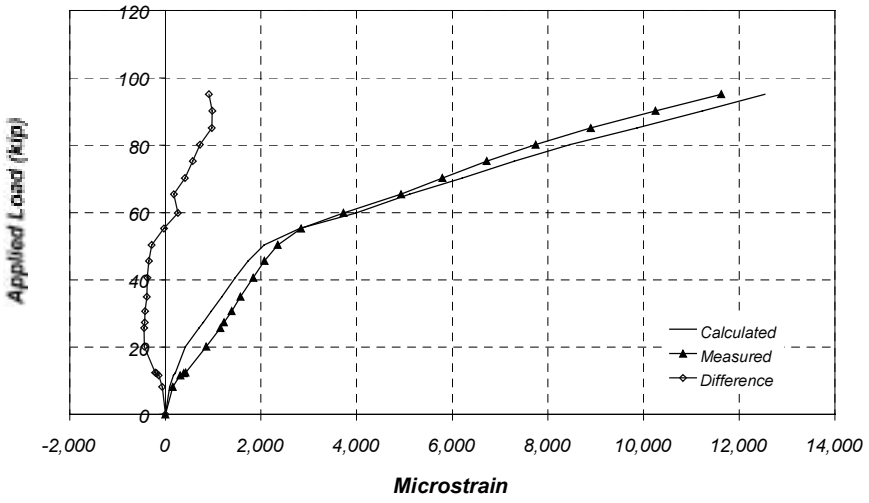

Figure 5.8 Comparison of Measured and Calculated CFRP Strains for Specimen J-2

5.3 EVALUATION OF MOMENT-CURVATURE RESPONSE

The measured strains were used to calculate the relationship between moment and curvature for the test specimens. Moment-curvature response derived from the measured strains is compared with the results of the analytical model in Section 5.3.3.

The procedures used to calculate internal forces and moments from the measured strains were similar to those used in the analytical model. The basic steps are outlined in Section 5.3.1 for Specimen J-1, where the strains were measured at the centroid of the CFRP plates. Modifications were required to calculate the internal forces in Specimen J-2, because strains were measured on the bottom surface of the specimen, and the CFRP sheets were wrapped around the bottom and side faces of the specimens. Therefore, the distribution of strains with depth within the CFRP sheets was assumed in the analysis. The procedures used to determine internal forces in Specimen J-2 are described in Section 5.3.2.

5.3.1 Calculating Internal Forces from Measured Strains for Specimen J-1

A typical profile of average live-load strains for Specimen J-1 is shown in Figure 5.9(a). The measured strain in the CFRP is less than the expected value corresponding to a linear variation of strain with depth in the cross section, as discussed in Section 5.2.2. The dead-load strains calculated in Section 5.2.1 were added to the measured live-load strains in the concrete and tension steel to obtain the total strain, as shown in Figure 5.9(b).

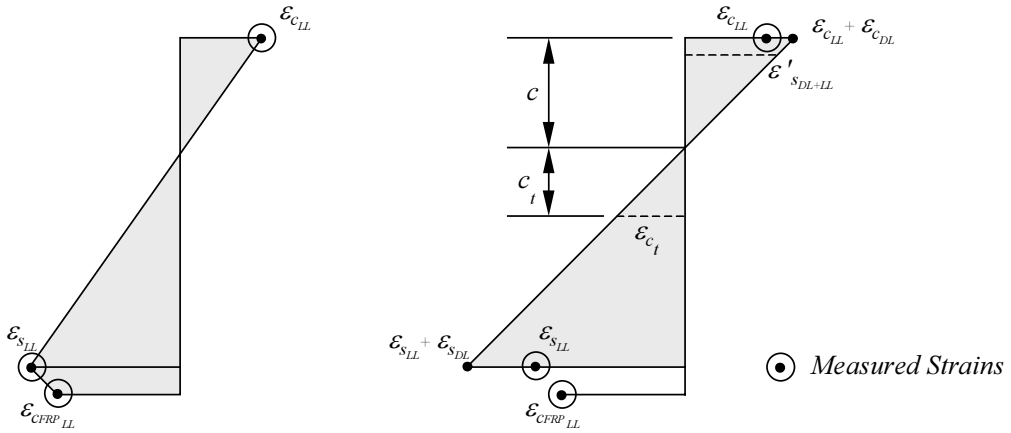

a) Measured Live-Load Strains b) Total Strains

Figure 5.9 Typical Strain Profile for Specimen J-1

Total strains in the concrete and steel were assumed to vary linearly with depth between the maximum compressive strain in the concrete, $\varepsilon_{c_{LL}} + \varepsilon_{c_{DL}}$, and the maximum tensile strain in the steel, $\varepsilon_{s_{LL}} + \varepsilon_{s_{DL}}$. The neutral axis depth, c, and the strain in the compression steel, $\varepsilon'_{s_{DL+LL}}$, were then determined from the assumed distribution of total strain. The depth of the concrete capable of resisting tension, c_t, was also determined using the tensile strain capacity of the concrete, which was estimated as the modulus of rupture divided by the initial tangent modulus of the concrete.

Stresses were calculated in each of the materials using the idealized stress-strain curves. Internal forces in the steel and CFRP were calculated by multiplying the stress at the centroid of the bar or plate by the cross-sectional area of the material. Internal forces in the concrete were calculated by dividing the tension and compression zones into ten segments, and multiplying the average stress in each segment by the cross-sectional area.

The sum of the internal forces inferred from the measured strains in compression is plotted as a function of the sum of the internal forces in tension in Figure 5.10. These forces should be equal at all levels of applied load to satisfy equilibrium. However, the sum of the internal compressive forces consistently exceeded the sum of the internal tensile forces, and the differences between the force levels increased as the applied load increased.

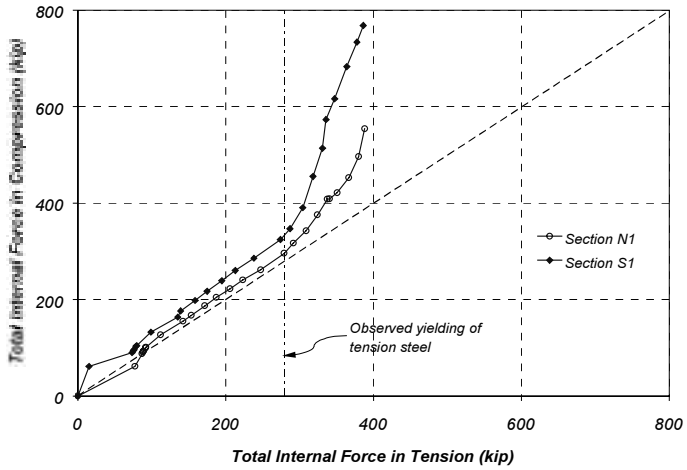

Figure 5.10 Internal Force Resultants for Specimen J-1

Several factors could have caused these differences in tensile and compressive forces. At low load levels, where the application of the theory of elasticity is still reasonable, a local perturbation of stress is generated at the sections of applied load. The tensile stresses can be expected to be lower than those calculated from a linear distribution of strain with depth [Timoshenko and Goodier, 1970]. After the concrete cracks, the strain readings in the reinforcement are largely dependent on the distance from the gage location to the section where the bar is crossed by a crack. If the gage happens to be offset from a crack, the strain readings on the reinforcement are lower than anticipated using a cracked section analysis because the concrete can still develop significant tensile stresses between cracks. At loads above yield, local bending of the reinforcing bars may also influence the measured strains.

It is impossible to identify the actual source of this discrepancy with the measured data. However, it is possible to use some of the measured data combined with the assumed linear distribution of strain to satisfy force equilibrium within the cross section, and then use the revised strain distribution to evaluate the moment-curvature response.

The revised strain distribution is shown in Figure 5.11, where the measured live-load strains in the reinforcement and CFRP plates are the same as those shown in Figure 5.9. However, the revised peak compressive strain in the concrete, $\overline{\varepsilon}_{c_{DL+LL}}$, was selected such that the cross section was in equilibrium. This revised peak compressive strain is plotted as a function of the measured peak compressive strain in Figure 5.12. The differences in strain tended to increase as the applied load increased, and were quite large near the failure load, especially at section S1. However, the corresponding differences in the neutral axis depth were less than 10% for most of the testing sequence (Figure 5.13). Differences of more than 15% in the neutral axis depth were observed only at loads close to failure. These relatively modest changes in the neutral axis depth were considered to be reasonable, and the revised strains in the concrete and compression reinforcement were used in all subsequent calculations involving internal forces.

It is interesting to note that the portion of the total internal tensile force carried by the CFRP plate increased as testing progressed. Each of the tensile force components (tensile force in the concrete, tensile force in the reinforcing bars, and tensile force in the CFRP plates) was normalized by the total tensile force. These data are plotted as a function of the ratio of applied load to yield load in Figure 5.14. The contribution of the tensile force in the concrete was approximately 40% of the total tensile force at low levels of load and decreased rapidly with applied load. The contribution of the reinforcing steel was close to 60% with only dead load acting on the specimen, increased to approximately 85% of the total tensile force near yield, and then decreased steadily to 70% at failure. As expected, the tensile force in

the CFRP plates was zero under dead load only and it increased to approximately 30% of the total tensile force at failure.

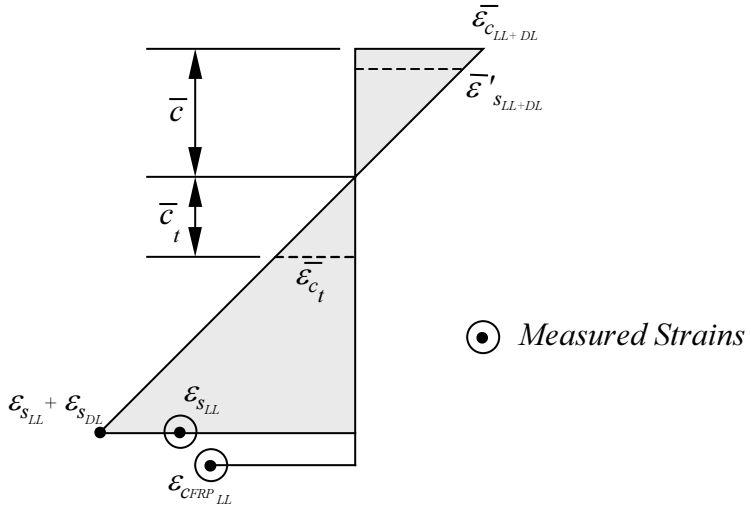

Figure 5.11 Possible Strain Distribution Corresponding to Equilibrium of Internal Forces

(a) Section N1

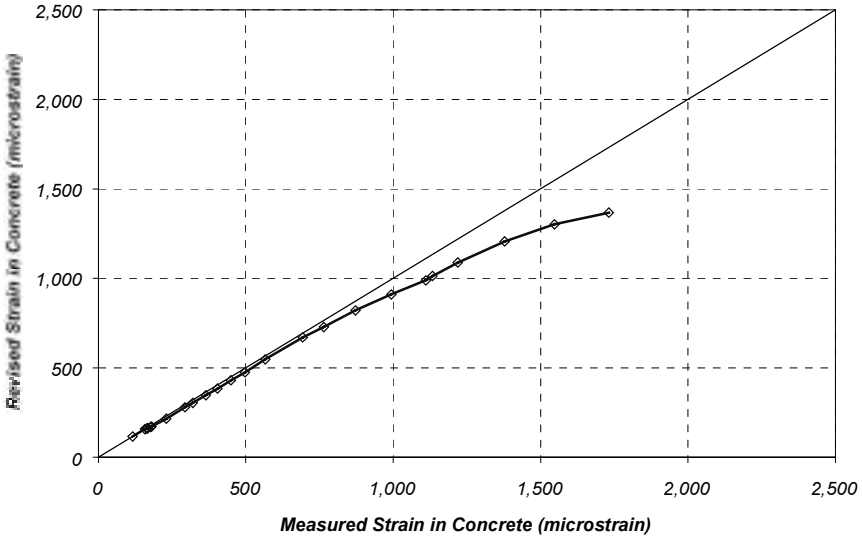

(b) Section S1

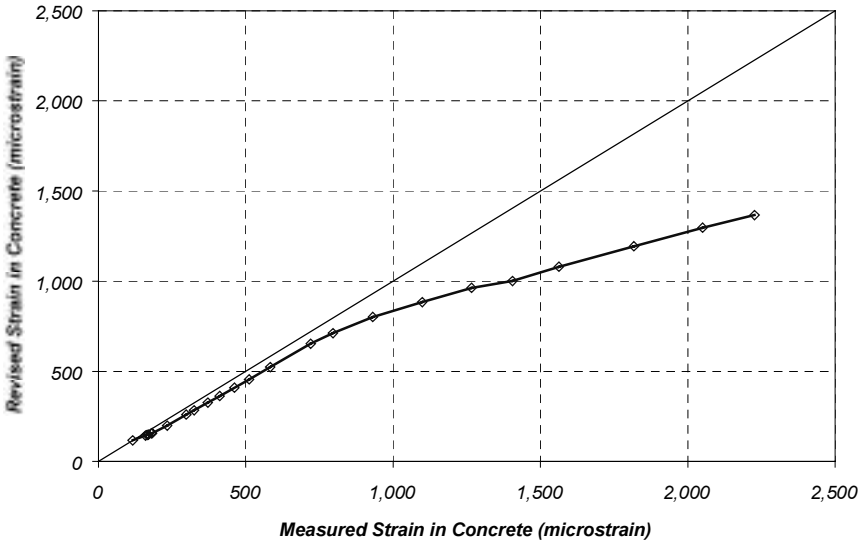

Figure 5.12 Comparison of Revised and Measured Peak Compressive Strains for Specimen J-1

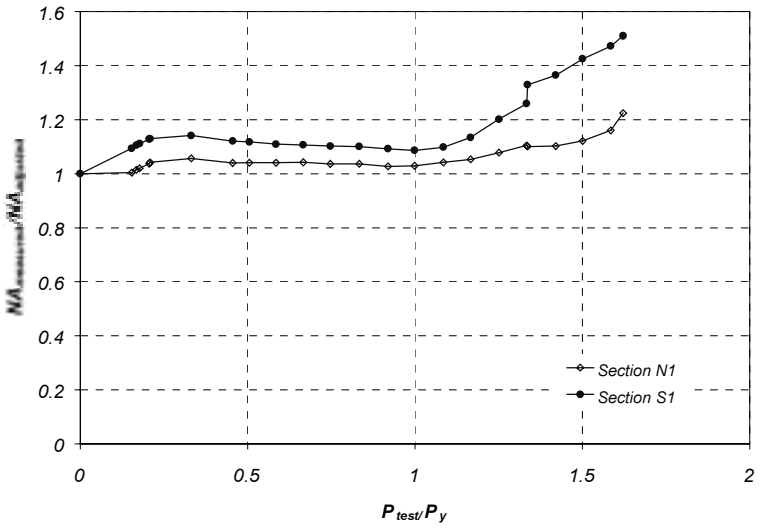

Figure 5.13 Comparison of Neutral Axis Depth from Revised and Measured Strain Profiles

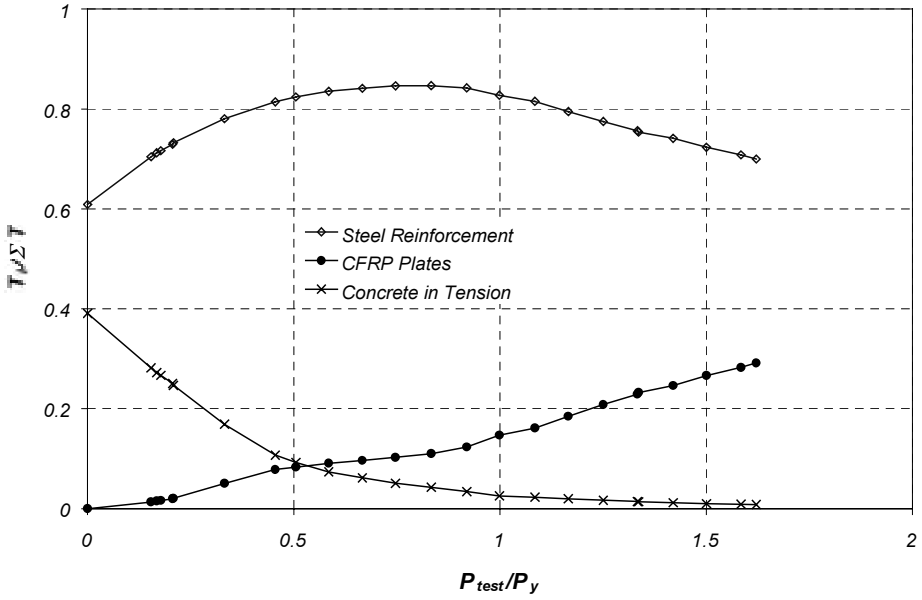

Figure 5.14 Variation of Tensile Force Components at Section N1 for Specimen J-1

5.3.2 Calculating Internal Forces from Measured Strains for Specimen J-2

The primary differences between Specimens J-1 and J-2 were the type and layout of the CFRP composites and the placement of the strain gages used to measure the strain in the CFRP. Pultruded plates were attached to the sides of the joists in Specimen J-1, and the strain gages were attached to the centroid of the plates. In contrast, CFRP sheets were wrapped around the bottom corners of the joists in Specimen J-2, and the strain gages were attached to the bottom surface of the specimen.

The live-load strain distribution shown in Figure 5.15 was used to determine the tensile force in the CFRP laminates. The strain gradient in the CFRP composite was assumed to be the same as the live-load strain gradient in the reinforced concrete section. From this strain distribution, stresses were determined at the top and bottom of the CFRP sheets. The tensile force in the bottom portion of the sheets was calculated by multiplying the bottom stress by the area of the composite material attached to the bottom. The tensile force on the side portion of the sheets was determined by multiplying the average stress on the side by the corresponding area of CFRP sheet. The total tensile force in the CFRP sheet was the sum of the contributions from the bottom and sides. The internal force components from the concrete and reinforcement were calculated following the same procedure as described for Specimen J-1.

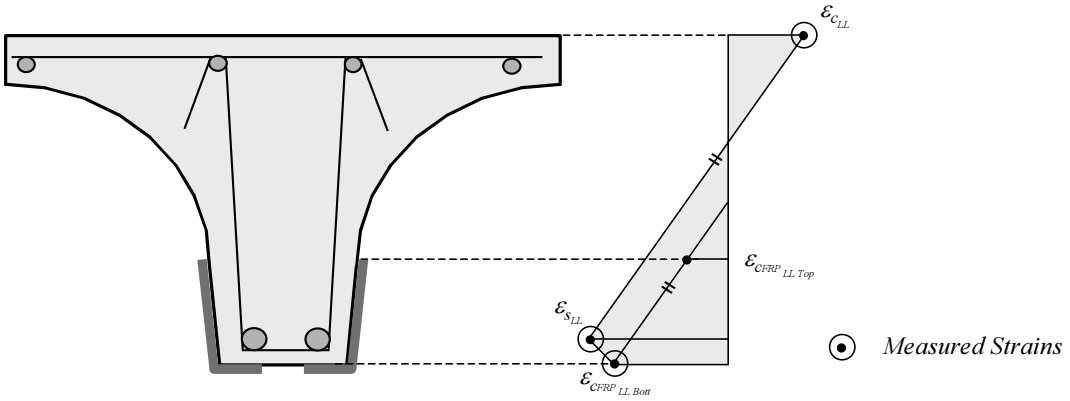

Figure 5.15 Distribution of Live-Load Strains on CFRP Sheets

A comparison of the total internal compressive force and the total tensile force for Specimen J-2 is shown in Figure 5.16. Similarly to Specimen J-1, internal force equilibrium was not satisfied. Therefore, the peak compressive strain in the concrete was also adjusted using the procedure as for Specimen J-1 to satisfy internal force equilibrium.

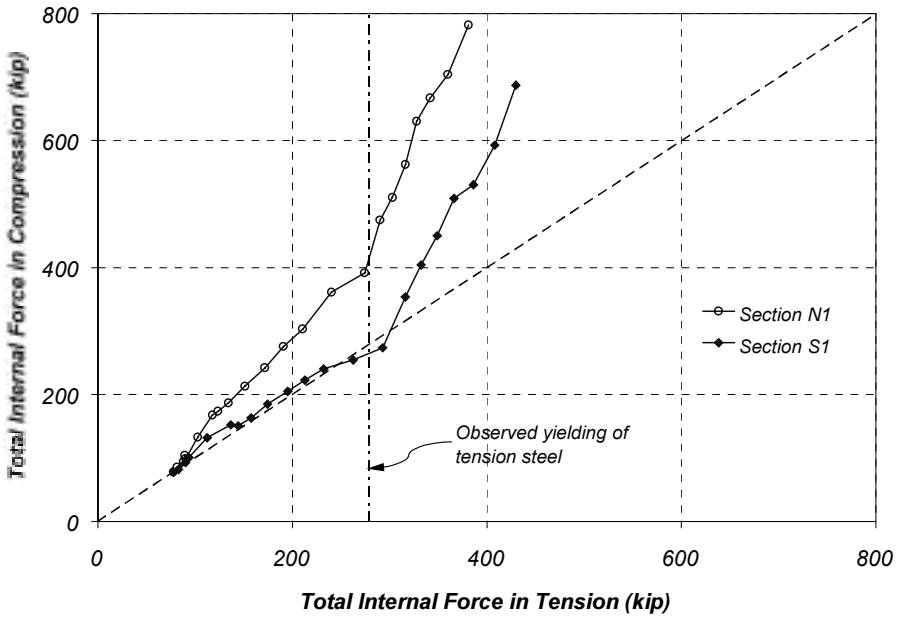

Figure 5.16 Internal Force Resultants for Specimen J-2

Figure 5.17 shows the revised peak compressive strains as a function of measured peak compressive strain in the concrete. The same trend that was observed for Specimen J-1 is evident in this figure. The difference between the measured and revised strains increases with increasing applied load, particularly for load levels above the observed yield.

Although both sections shown in Figure 5.17 were subjected to the same external moment, the amount by which the neutral axis was shifted to satisfy equilibrium of internal forces was different for these two sections. For section N1 a 20% adjustment of the neutral axis depth was required throughout most of the loading sequence, whereas the adjustment needed at section S1 was typically less than 5% and only exceeded 20% during the final stages of loading (Figure 5.18). This variation is consistent with the assumption that the measured strains at a section are greatly influenced by the distance from gages to the nearest crack.

The contribution of the individual tensile force components normalized by the total tensile force at a particular load level is plotted as a function of the applied load divided by the observed yield load in Figure 5.19. The relative contribution of each force component followed the same trends as those observed for Specimen J-1.

(a) Section N1

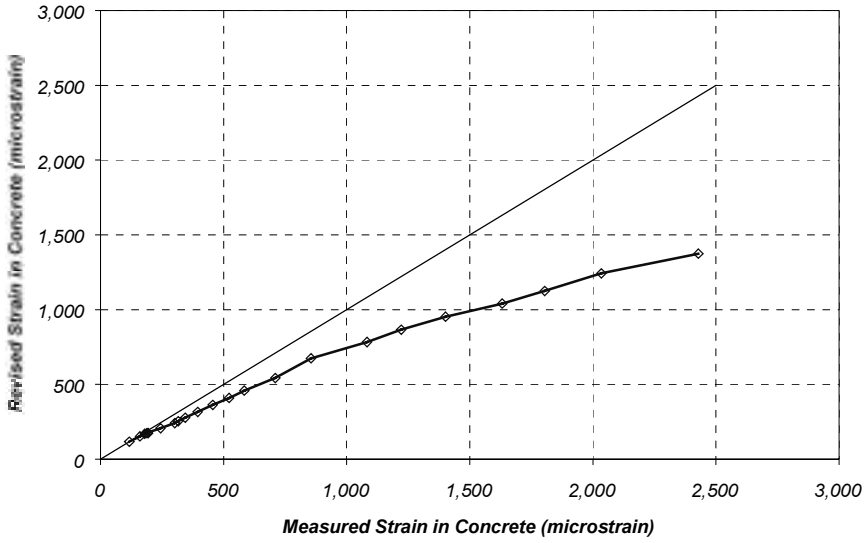

(b) Section S1

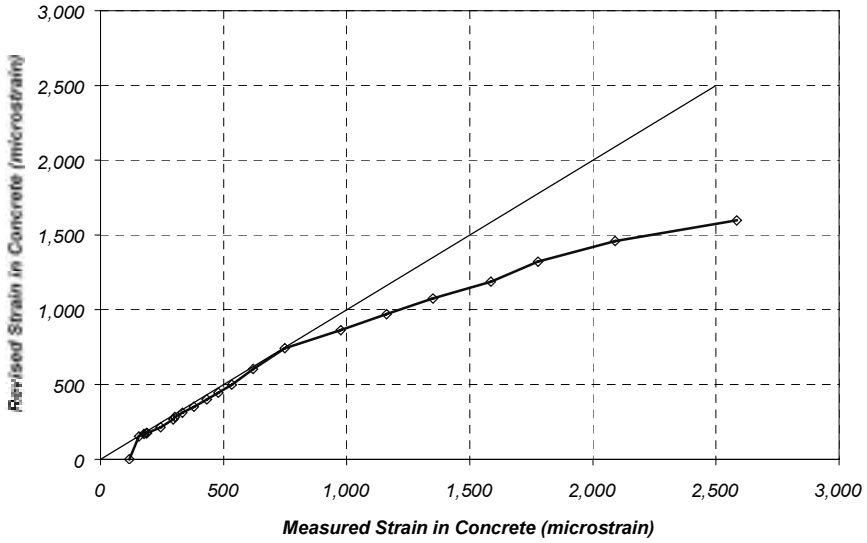

Figure 5.17 Comparison of Revised and Measured Peak Compressive Strains for Specimen J-2

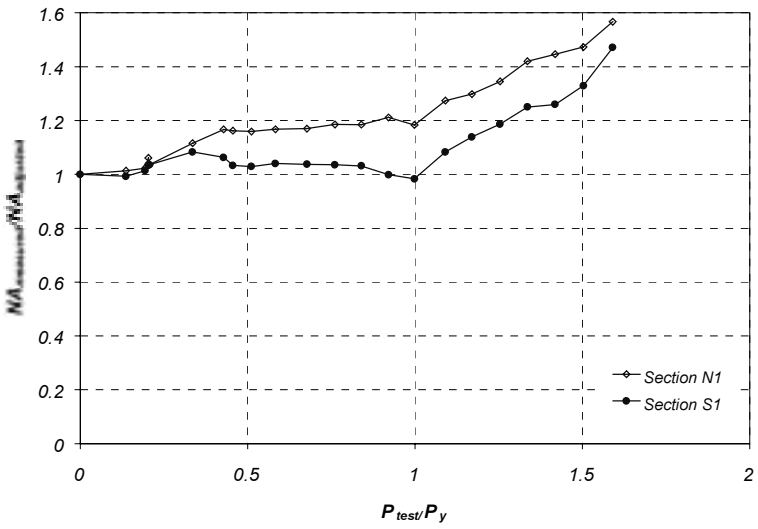

Figure 5.18 Comparison of Neutral Axis Depth from Revised and Measured Strain Profiles

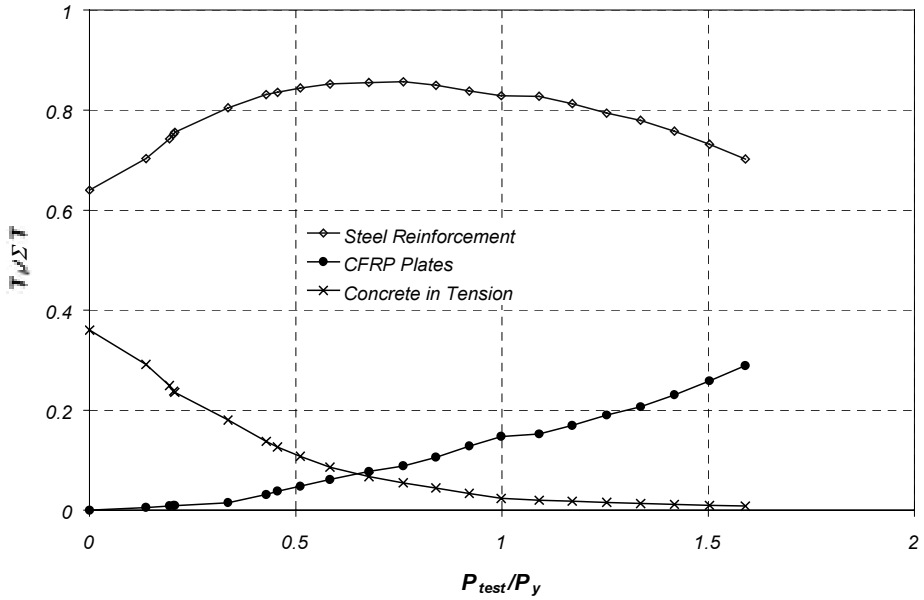

Figure 5.19 Contribution of the CFRP Sheets to the Total Internal Moment at Section N1 for Specimen J-2

5.3.3 Moment-Curvature Response

Internal moments and curvature were calculated in both specimens using the internal forces that satisfied equilibrium. The moment and curvature corresponding to dead loads (Table 5.1) were then subtracted from each of the calculated values to obtain the relationship between moment and curvature for the applied loads. This response is compared with the results from the analytical model in Figure 5.20 and Figure 5.21 for Specimens J-1 and J-2, respectively. No attempt was made to include debonding of the CFRP in these calculations.

The moment-curvature response calculated from the measured strains is well represented by the results of the analytical model. At the same moment, the curvature inferred from the measured strains tended to be slightly less than the calculated curvature, but the differences were small. In most cases, the calculated curvature capacity exceeded the measured curvature at failure of the strengthened specimens.

section S1 of Specimen J-2 was the only exception to these trends. The curvatures inferred from the measured strains exceeded the calculated curvatures above yield, and the curvature capacity was similar for the two curves. The CFRP ruptured near section S1 during the test.

The CFRP composites debonded from the concrete at the other three locations; therefore, the actual curvatures at failure are expected to be less than the calculated curvatures at failure at these locations.

5.3.4 Comparison of Internal and External Moments

The applied load is plotted as a function of the maximum internal moment due to live load obtained from the measured strains in Figure 5.22. Also shown in the figure is the external midspan moment determined from statics using a span equal to 28 ft. Both specimens exhibited the same general response. At low levels of applied load, the internal moment was less than the external moment, and the internal moment was larger than the external moment at applied loads above the yield level (60 kip).

The response below the yield load is consistent with the assumption that the measured steel strains were less than the steel strains at the location of a crack due to concrete transmitting tensile stresses between cracks. Therefore, the internal moment was underestimated at low load levels. At load levels above yield, the span may have increased due to rotation of the bearings, leading to larger internal moments.

(a) Section N1

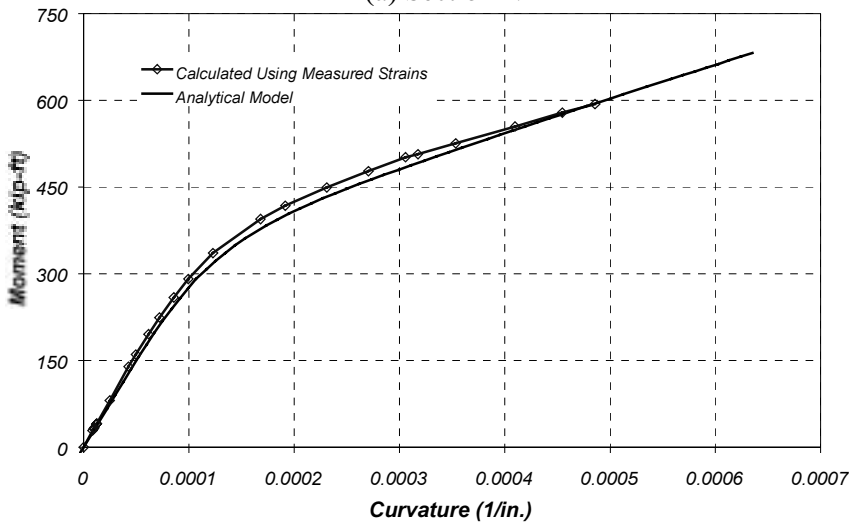

(b) Section S1

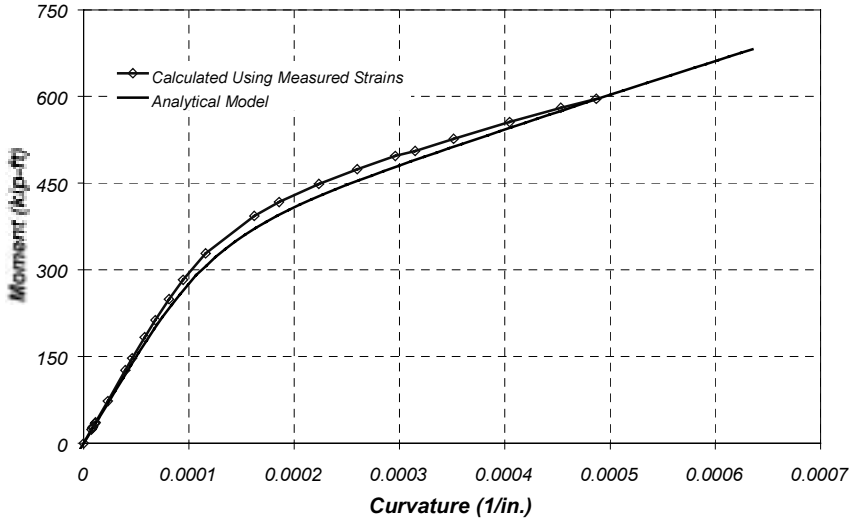

Figure 5.20 Comparison of Measured and Calculated Moment-Curvature Response for Specimen J-1

(a) Section N1

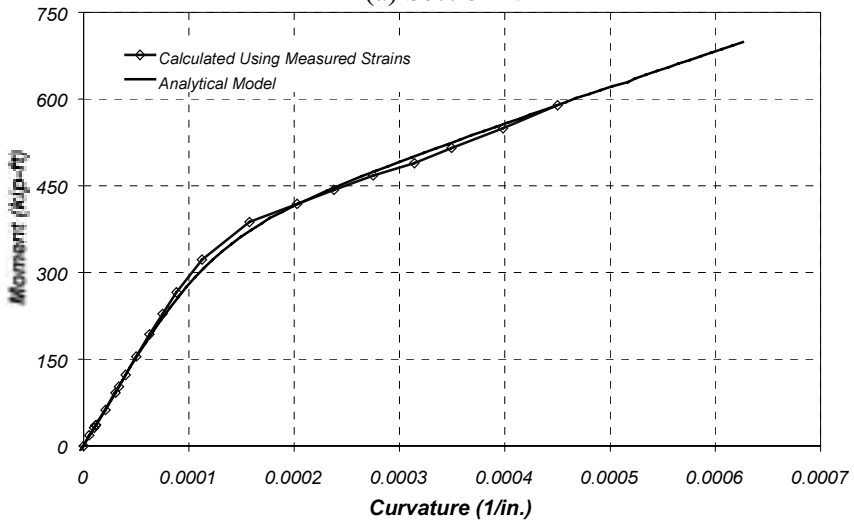

(b) Section S1

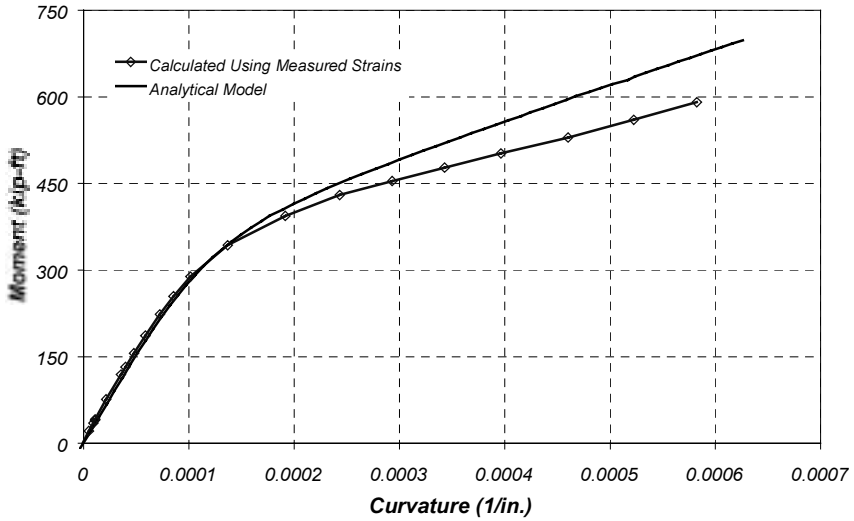

Figure 5.21 Comparison of Measured and Calculated Moment-Curvature Response for Specimen J-2

(a) Specimen J-1

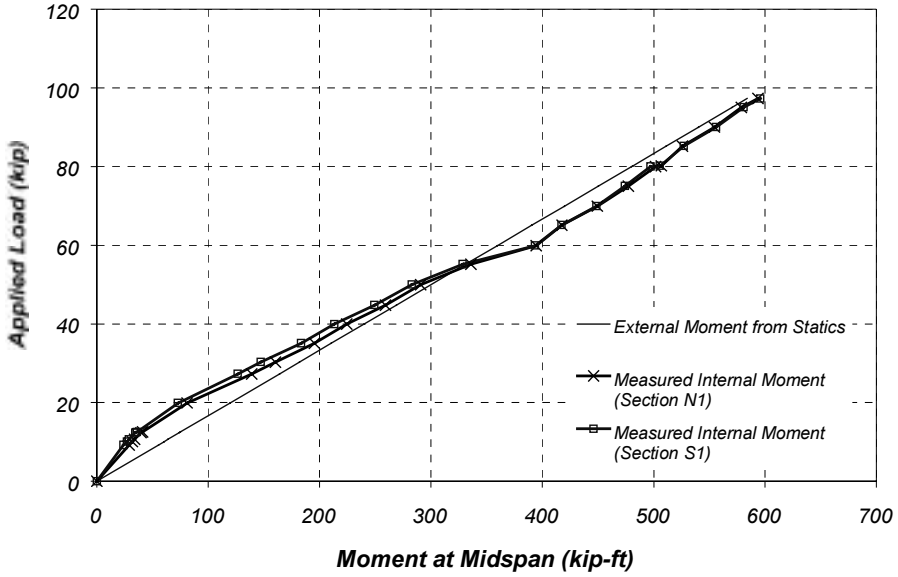

(b) Specimen J-2

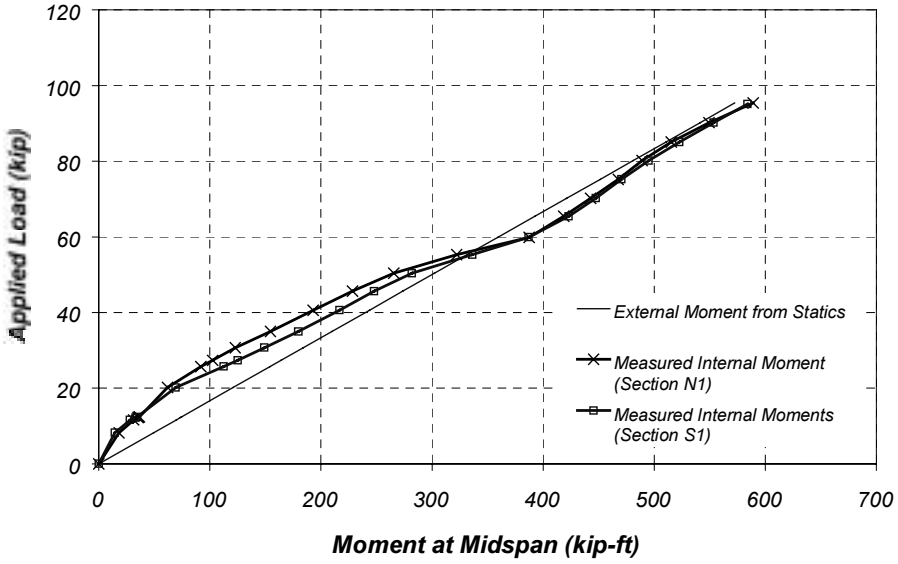

Figure 5.22 Comparison of Internal and External Moments

5.4 EVALUATION OF LOAD-DEFLECTION RESPONSE

The global response of the strengthened specimens was first evaluated by comparing their measured response. The response of each specimen was then compared with the calculated response obtained using the analytical procedure presented in Chapter 3 of the companion research report [Breña et al, 2001]. The model was evaluated for the strengthened and unstrengthened conditions of the specimens. The calculated response was compared with the measured response of the bare reinforced concrete specimens only at large deformation levels, after the composites had debonded from the surface of the concrete.

The average displacement response was obtained by averaging the displacement measurements from midspan of the east and west joists. The measurements were adjusted by subtracting the average vertical displacement at the supports. The load-deflection behavior of specimens J-1 and J-2 is shown in Figure 5.23. It can be seen that the overall behavior of both specimens was similar up to the yield point. After the yield point, Specimen J-1 was stiffer than Specimen J-2. Therefore, although both specimens were designed to reach approximately the same ultimate load, Specimen J-2 reached its failure load at a larger deflection than Specimen J-1. The post-yield stiffness was controlled by the stiffness of the two types of CFRP composites used to strengthen the specimens.

At failure, the load dropped suddenly and the residual load was carried by the bare reinforced concrete elements. The maximum deformation capacity of the bare specimens was also different. Specimen J-2 had a larger deformation capacity than Specimen J-1. The difference in deformation capacities can be attributed to differences in the material properties of the concrete used to fabricate the specimens.

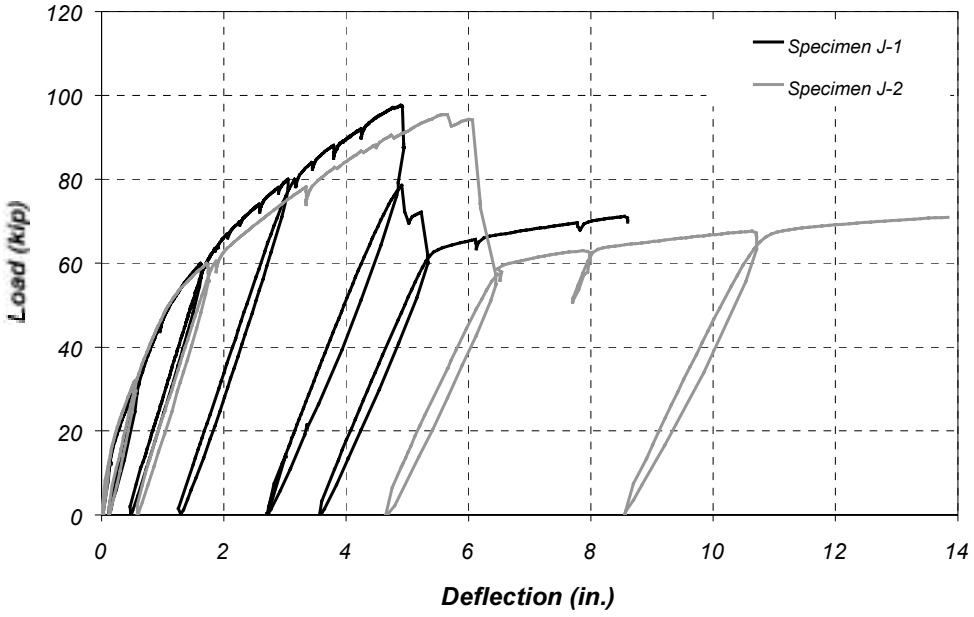

Figure 5.23 Measured Load-Deflection Response of Pan-Girder Specimens

The measured response of the specimens at large deflection levels is compared with the calculated response in Figures 5.24 and 5.25 for Specimens J-1 and J-2, respectively. The comparisons show that the model was capable of reproducing the response of the bare reinforced specimens. This result implies that the material models used for the concrete and steel were appropriate for the comparison with the strengthened specimens. From these plots, the strengthening effect of the CFRP composites on the specimens is also apparent.

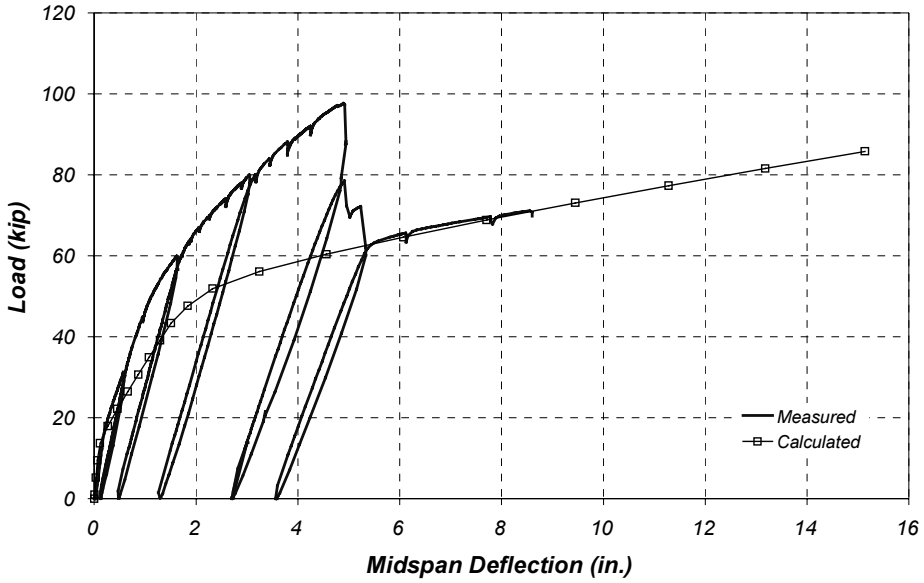

Figure 5.24 Comparison of Measured and Calculated Load-Deflection Response of Specimen J-1 (Unstrengthened)

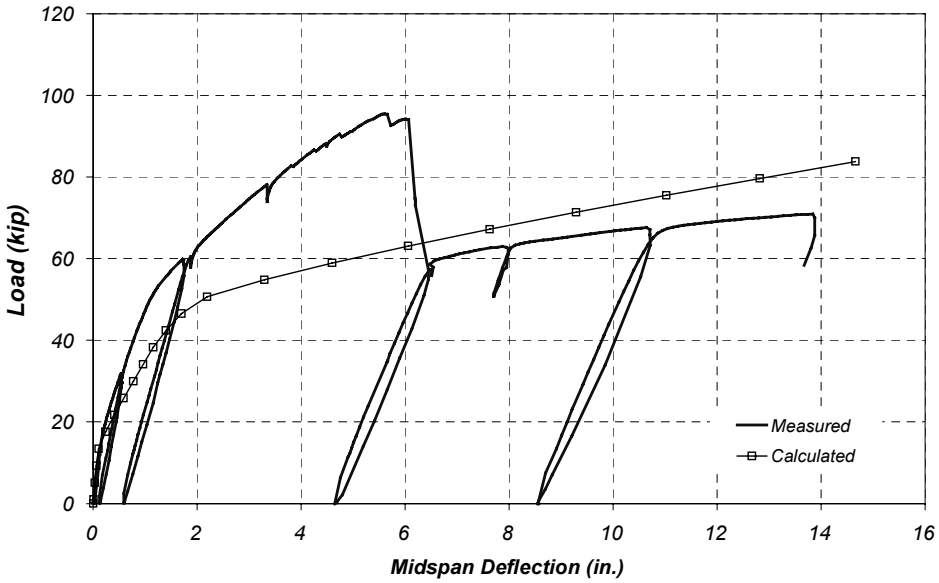

Figure 5.25 Comparison of Measured and Calculated Load-Deflection Response of Specimen J-2 (Unstrengthened)

The measured response of the test specimens is compared with the calculated load-deflection response in Figures 5.26 and 5.27 for Specimens J-1 and J-2, respectively. The results presented show that the analytical model was able to reproduce the displacement response adequately for both specimens.

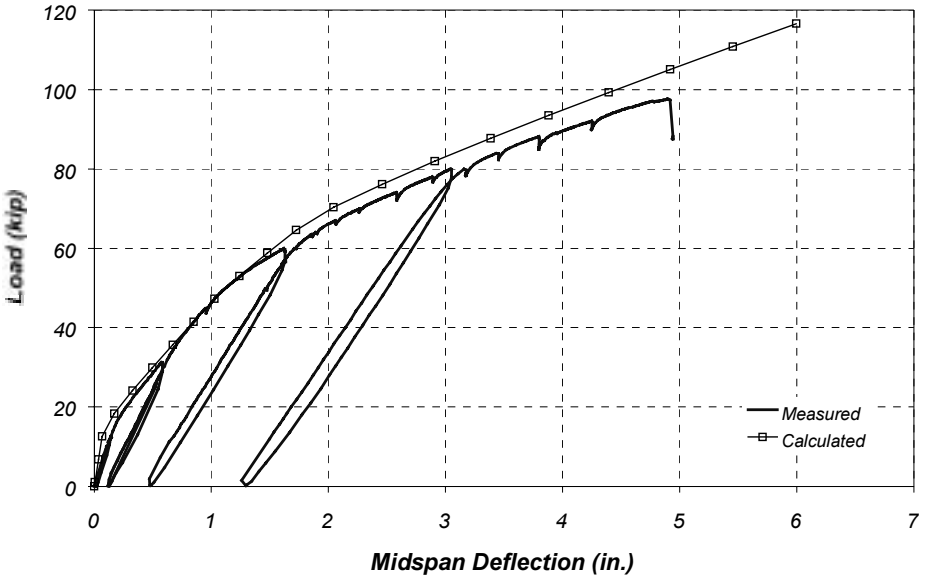

Figure 5.26 Comparison of Measured and Calculated Load-Deflection Response of Specimen J-1 (Strengthened)

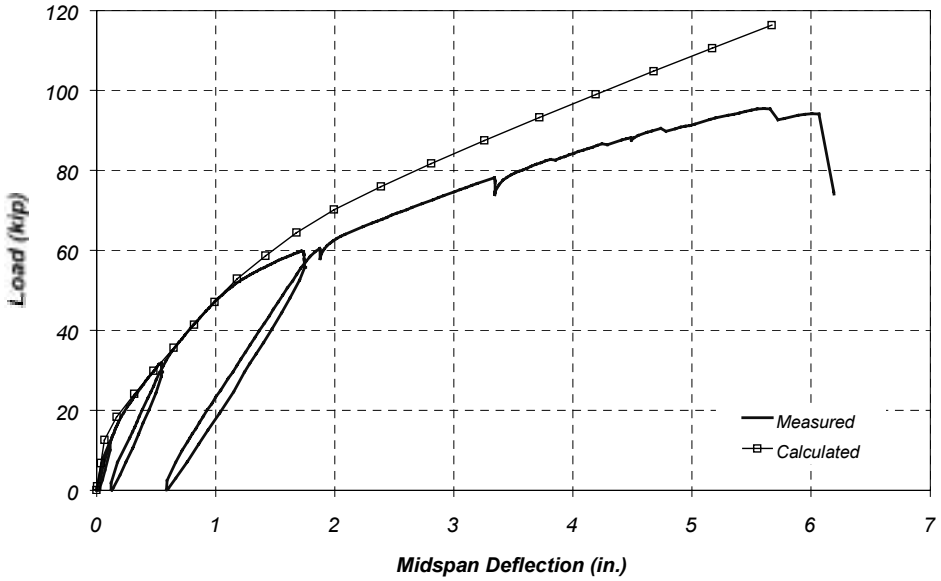

Figure 5.27 Comparison of Measured and Calculated Load-Deflection Response of Specimen J-2

5.5 SUMMARY

The measured response of Specimens J-1 and J-2 was compared to the response calculated using the analytical model developed as part of this investigation. The comparisons show that the model was able to reproduce the measured global response of the test specimens accurately at all levels of loading.

However, it was also clear that local effects such as cracking of the concrete and debonding of the CFRP composites controlled the measured response at a particular location. As expected, the analytical model was not able to reproduce aspects of the response controlled by local effects.

In order to obtain additional information about the local effects and the distribution of strain within the cross section, additional instruments must be used to monitor the response of the test specimens.

Chapter 6: Description of Flat-Slab Specimens

6.1 INTRODUCTION

Flat-slab bridges were commonly used in off-system roads, as well as some on-system roads, in Texas in the 1940s and 1950s [Bussell, 1997]. Their design does not meet the current legal load requirement of HS-20 truck loading. The majority of the flat-slab bridges were designed using H-10 or H-15 design vehicles. These bridges were used for short spans (up to 25 ft) with different roadway widths depending on the number of lanes to be carried (14 ft to 44 ft). However, bridges were typically designed for two lanes. In some cases structural curbs of the bridge were used on both sides to reduce the slab thickness. Bridges without edge curbs were called S-Slab bridges, and bridges with edge curbs were called FS-Slab bridges.

In FS-Slab bridges, most of the load is transferred to the curbs and into the supporting bent caps. When an FS-Slab bridge is widened, the curbs need to be removed and the load-carrying capacity of the bridge is reduced significantly. Therefore, temporary shoring needs to be placed under the bridge to avoid compromising the structural integrity of the bridge during the widening operation. This procedure can be very time-consuming and in some cases difficult to implement.

An alternative to bridge shoring is to strengthen the slab using carbon fiber reinforced polymer (CFRP) composites before the structural curbs are removed. The objective of this technique is to replace the capacity that was originally provided by the curbs, and to strengthen the existing slab once the bridge is widened to meet the current legal load (HS-20 vehicle). Two CFRP systems were used to strengthen laboratory specimens consisting of a section of a flat-slab bridge.

The description and load rating of a prototype FS-Slab bridge is presented in this chapter. The design of the laboratory specimens and key characteristics used to simulate the response of the prototype slab are also presented. The CFRP composite configurations that were used to meet the strengthening criterion described above are discussed.

6.2 PROTOTYPE BRIDGE

6.2.1 Physical Characteristics of Prototype Bridge

Drawings were obtained for an FS-Slab bridge designed in 1945 to carry two lanes of H-10 truck loading. The prototype bridge was designed for a 25-ft span and 20'-0" roadway width. The bridge cross section and reinforcement details are shown in Figure 6.1.

The structural curbs on both sides of the prototype bridge have a trapezoidal cross section. The curbs extend 1'-6" above the bridge deck. The slab has a constant thickness of 11 in. across the prototype bridge.

The bottom reinforcement consists of #7 bars spaced at 6 ½ in. longitudinally and #5 bars spaced at 7 ½ in. transversely throughout the bridge span. The concrete cover to the centroid of the main longitudinal reinforcement is 1 ¾ in. Top reinforcement consists of #4 bars placed longitudinally and transversely at 36 and 18 in., respectively. Curbs are reinforced with 2 - #11 bars top and bottom longitudinally, and shear reinforcement consisting of #4 stirrups spaced at 12 in. along the span.

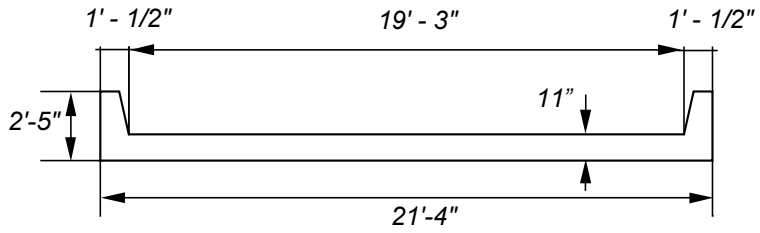

Bridge Cross Section

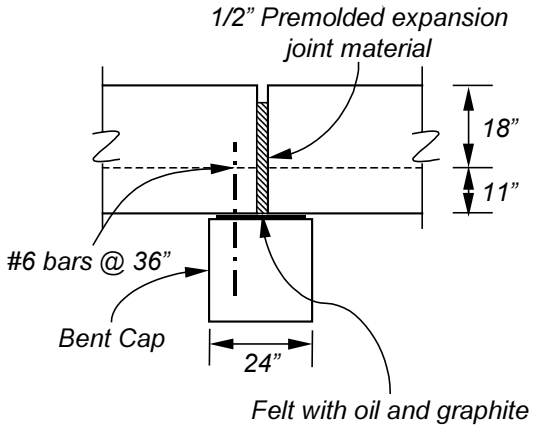

Typical Support Detail

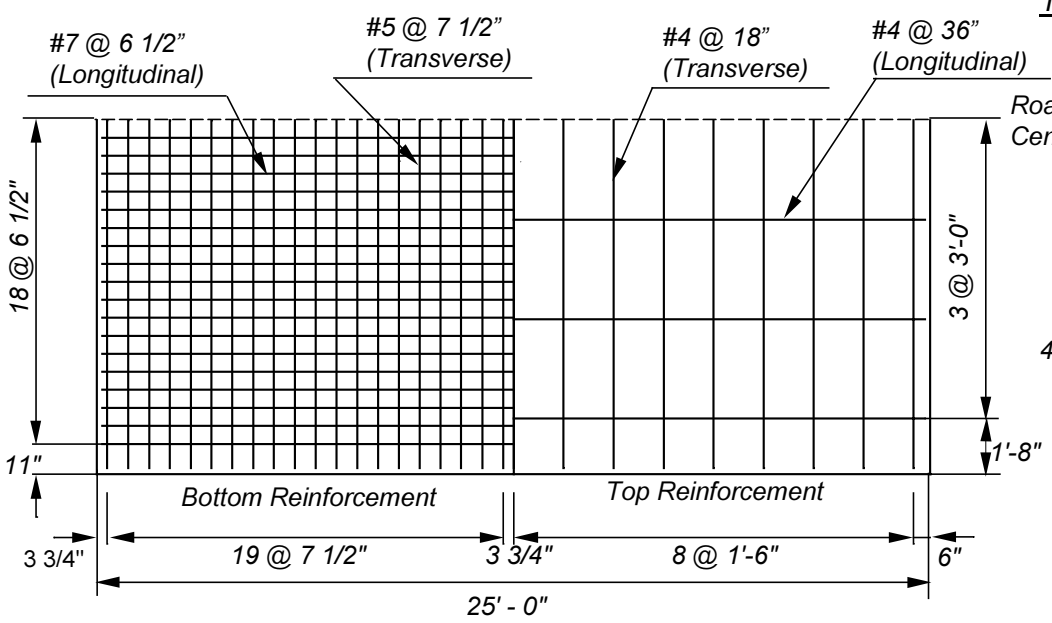

Slab Reinforcement (Half Plan)

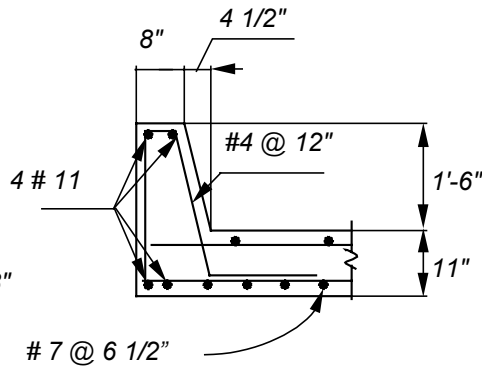

Detail of Curb Reinforcement

Figure 6.1 Reinforcement Details for FS-Slab Prototype Bridge

During construction, the flat-slab bridges are cast directly on top of 2-ft wide bent caps. At a typical expansion joint, one end of the slab is anchored to the supporting bent cap using dowels made from #6 bars spaced at 36 in. The bent caps are oiled with 60-grade oil and covered with powdered graphite to allow the slabs to expand and contract due to temperature effects. One layer of 30-lb felt is placed on top of the graphite layer before casting the slab on the bent cap (Figure 6.1). Even though this detail intended to avoid end restraint, the conditions encountered in the field show that there could be some rotational restraint provided by adjacent spans and by deterioration of the felt with time. Evaluation of the results of the diagnostic testing of a flat-slab bridge supports this observation [Bussell, 1997].

6.2.2 Calculated Capacity of Prototype Bridge

The nominal flexural strength of the slab and curbs of the prototype bridge were calculated in accordance with the AASHTO *Design Specifications* [AASHTO, 1996]. Concrete was assumed to have a compressive strength of 3,000 psi, and reinforcing steel was assumed to have a specified yield stress of 40,000 psi. Determining the capacity of prototype bridge components that contribute to the flexural strength was required for the prototype bridge load rating.

The nominal flexural strength, per ft of slab, was computed using,

$$M_n = A_s\, f_y \left(d - \frac{a}{2} \right) \qquad \text{with} \qquad a = \frac{A_s\, f_y}{b\,(0.85\, f'_c)} \tag{6.1}$$

and the nominal flexural strength of the curbs was calculated including the contribution of steel in the compression area using the following expression:

$$M_n = A_s'\, f_y\,(d - d') + C_{C1}\,(d - \frac{a}{2}) \;+\; C_{C2}\,(d - \frac{2a}{3}) \tag{6.2}$$

where a is the depth of the stress block and may be calculated as:

$$a^2 + 8b\,a \;=\; \frac{8\,(A_s - A_s')\,f_y}{(0.85\, f'_c)} \tag{6.3}$$

where

- M_n = Nominal flexural strength, lb-in.
- ϕ = Strength reduction factor equal to 0.9
- A_s = Area of tensile reinforcement including portion of slab steel considered to be effective in the curb, in^2.
- A_s' = Area of steel in the compression zone, in^2.
- C_{C1} = Fraction of the total compressive force in the concrete calculated based on the rectangular portion of the compressed area, kips.
- C_{C2} = Fraction of the total compressive force in the concrete calculated based on the triangular portion of the compressed area, kips.
- d = Distance from extreme compression fiber to centroid of tensile reinforcement, in.
- d' = Distance from extreme compression fiber to centroid of A_s', in.
- b = Width of the top face of member, in.

f_y = Yield strength of flexural or shear reinforcement, psi.

f'_c = Concrete compressive strength, psi.

The reinforcement within a 44-in. width of slab (4 times the slab thickness) was considered as part of the tensile reinforcement area for the curbs, Figure 6.2 [Jensen et al., 1943]. The calculated nominal flexural capacity of the slab and curbs in the prototype bridge are listed in Table 6.1 along with the parameters used in the calculations.

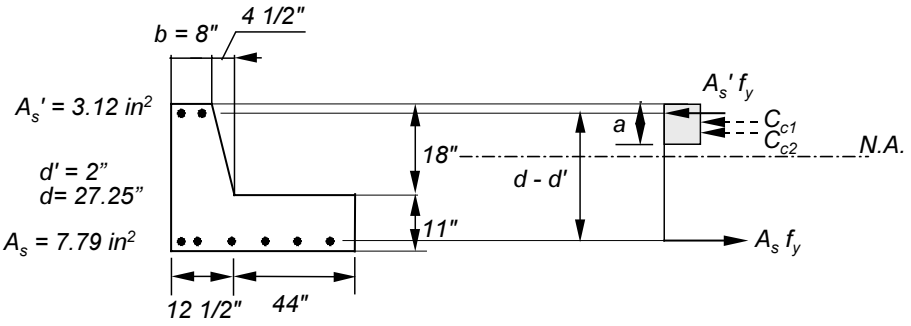

Figure 6.2 Geometric Properties of the Curbs to Compute Flexural Strength

Table 6.1 Design Flexural Strength of Slab (per ft) and Curbs for Prototype Bridge

Parameter	Value
f'_c, psi	3,000
f_y, psi	40,000
ϕ	0.9
Slab (per ft)	
d, in.	9.25
b, in.	12
A_s, in.^{2}	1.11
$M_{n\ slab}$, kip-ft/ft	31.54
$\phi M_{n\ slab}$, kip-ft/ft	28.39
One Curb (Figure 6.2)	
A_s', in.^{2}	3.12
A_s, in.^{2}	7.70
b_{top}, in.	8
b_{bott}, in.	44
d', in.	2
d, in.	27.25
h_{slab}, in.	11
$M_{n\ curb}$, kip-ft	621.2
$\phi M_{n\ curb}$, kip-ft	559.1

6.2.3 Prototype Bridge Load Rating

The load factor method given in the AASHTO *Manual for Condition Evaluation of Bridges* [AASHTO, 1994] was used to rate the prototype bridge. TxDOT distributes moments to the curbs and slab in accordance with *Bulletin 346* from the University of Illinois [Jensen et al., 1943]. Therefore, this approach was also used for load rating the prototype FS-Slab bridge. A summary of the details of the load rating procedure are given in Appendix B and are described in greater detail elsewhere [Bussell, 1997]. The prototype bridge was first rated considering the contribution of the curbs to the flexural strength. The bridge was then rated considering only the contribution of the flat slab to the strength to examine the effect of removing the curbs on the rating.

The two load-rating levels (inventory and operating) described in the AASHTO *Manual* [AASHTO, 1994] were used to rate the prototype bridge. In the case of FS-Slabs, the difference between the two rating levels depends, not only on the load factors used for live load effects in the rating equation, but also on the way that the critical element is identified (Appendix B). For the inventory rating level, the element having the lowest rating factor controls the overall bridge rating. For the operating rating level, a weighted average of the ratings between slab and curbs is used to calculate the overall bridge rating. The weighting factor for each element is obtained using the ratio of its tributary width to the total bridge width. These factors are multiplied by the individual component rating to calculate the overall bridge rating.

The total moment across the bridge was distributed to the curbs and the slab using the empirical coefficients contained in *Bulletin 346* from the [Jensen et al, 1943]. The total moment included dead and live-load effects. Dead-load effects were generated by the self weight of the slab and curbs. The live-load effects were calculated using the weight of the rear wheels of the design vehicles positioned at midspan. The total live-load effect was obtained by multiplying the load from the individual wheels on the design truck by the number of wheels that can fit across the prototype bridge. A summary of this procedure is presented in Appendix B.

The dead and live load moments used in the prototype bridge rating are listed in Table 6.2 and the load-rating results for H-truck and HS-truck loading are presented in Table 6.3. The HS-truck effects were determined using the axle weights from the H-10 truck but distributed according to an HS-design vehicle. A 24-ft span was used in all calculations after subtracting half the bearing length on each end of the prototype bridge.

The effective widths of the slab and curbs were determined to calculate the weighting factors for the operating rating of the prototype bridge. The same width of the slab that was considered to act compositely with the curbs for the flexural strength calculations was used in the effective width calculation (Figure 6.2). The effective widths of slab and curbs used for the operating rating level are also presented in Table 6.3.

The prototype bridge had an inventory rating of H-12.5 (Table 6.3). Also, the rating results for the prototype bridge from H-truck loading are very close to those for HS-truck loading because the bridge has a total length of 25 ft. For the H-truck loading, the maximum positive total moment on the bridge is caused by positioning the rear axle at midspan for this span. The rear axle of the HS-truck needs to be positioned at 3'-6" from midspan to generate the maximum positive total moment on the bridge. However, the difference in maximum positive moments generated by each truck is less than 1% for this span.

Table 6.2 Unfactored Load Effects Used in Prototype Bridge Rating

Unfactored Load Effect	Value
H – 10 truck axle loads, kip	4, front;16, rear (14 ft from front)
Slab	
M_{DL}, kip-ft/ft	5.2
(1 + I) M_{LL}, kip-ft/ft	8.0
One Curb	
M_{DL}, kip-ft	92.7
(1 + I) M_{LL}, kip-ft	93.2
HS – 10 truck axle loads, kip	4, front; 16, middle (14 ft from front); 16, rear (14 ft from middle)
Slab	
M_{DL}, kip-ft/ft	5.2
(1+ I) M_{LL}, kip-ft/ft	8.0
One Curb	
M_{DL}, kip-ft	92.7
(1+ I) M_{LL}, kip-ft	93.5

Notes: Live load effects include a 0.3 impact factor (I).
The weight of a ½ in. overlay is included in dead load effects.
Slab effects determined for a 1-ft wide section.

Table 6.3 Load Rating Results for Flat-Slab Prototype Bridge

Bridge Element	Effective Width, ft	Rating Level	Design truck	
			H – truck	HS – truck
Individual Component Rating				
Slab	11.91	Inventory	H – 12.5	HS – 12.4
		Operating	H – 20.8	HS – 20.8
One Curb	4.71	Inventory	H – 21.7	HS – 21.6
		Operating	H – 36.2	HS – 36.1
Overall Prototype Bridge Rating				
Bridge	21.33	Inventory	H – 12.5	HS – 12.4
		Operating	H – 27.6	HS – 27.5

As mentioned earlier, the curb strength represents a significant portion of the total bridge strength. Once the curbs are removed when the bridge undergoes widening, the bridge rating drops significantly. Therefore, the prototype bridge was also rated without considering the contribution of the curbs.

Results of the prototype bridge slab rating without the contribution of the curbs are presented in Table 6.5. The unfactored moments used for the slab rating are presented in Table 6.4. The dead and live-load effects listed in this table were calculated per unit width of slab. The live-load effects were determined by distributing the wheel loads from the design vehicles over a slab width equal to [AASHTO, 1996]:

$$E = 4 + 0.06\,S \leq 7\,ft \tag{6.4}$$

where

E = Effective slab width over which wheel loads are distributed, ft.

S = Span length = Distance from center to center of supports, ft.

Table 6.4 Unfactored Load Effects Used to Rate the Slab in the Prototype Bridge

Unfactored Load Effect	Value
H – 10 truck axle loads, kip	4, front;16, rear (14 ft from front)
Slab	
M_{DL}, kip-ft/ft	10.3
(1 + I) M_{LL}, kip-ft/ft	11.5
HS – 10 truck axle loads, kip	4, front; 16, middle (14 ft from front); 16, rear (14 ft from middle)
Slab	
M_{DL}, kip-ft/ft	10.3
(1+ I) M_{LL}, kip-ft/ft	11.5

Notes: Live load effects include a 0.3 impact factor (I).
The weight of a ½ in. overlay is included in dead load effects.
Span, S = 24 ft.
Effective slab width, E = 5.44 ft.
Slab effects were determined for a 1-ft wide section.

Table 6.5 Prototype Bride Load Rating after Curb Removal

Bridge Element	Rating Level	Design truck	
		H – truck loading	HS – truck loading
Slab	Inventory	H – 6.0	HS – 6.0
	Operating	H – 10.0	HS – 10.0

It can be observed by comparing Tables 6.2 and 6.4 that the dead load moment on the slab is higher after the curbs are removed from the bridge. This difference arises from the method that was used to rate the bridge. In the method used to design the bridge, a portion of the total moment on the bridge (dead and live-load moment) is distributed to the curbs depending on the bridge width and the relative stiffness of the slab and curbs. Because dead and live-load effects have to be considered separately to rate the bridge, the total moment is then divided into the dead and live-load components using empirical coefficients obtained from analyses of elastic plate theory [Jensen et al., 1943]. Therefore, a portion of the dead load moment acting on the slab is effectively distributed to the curbs. Although it was recognized that some inconsistencies arose from using this method, it was selected to be consistent with the current practice used by TxDOT to rate slab-bridges.

Because the slab in the prototype bridge had an H-6.0 inventory rating after removing the curbs, strengthening of the slab was proposed as an alternative to the current construction practice of using temporary shoring during roadway widening. The criterion that was selected for the design of the strengthening schemes was to restore the bridge strength that was lost after curb removal. Therefore, the slab strength had to be increased to raise the inventory rating of the slab acting alone to the original design rating of H-10.

6.3 DESIGN AND CONSTRUCTION OF LABORATORY SPECIMENS

Two full-scale laboratory specimens (FS-1 and FS-2) were built and tested to compare the behavior of two different slab strengthening methods using CFRP composites. The specimens represent a 6-ft wide section of the slab in the prototype bridge. Only the slab was modeled in the laboratory to study the behavior of the strengthened specimens without the contribution from the structural curbs. This represents the condition of the prototype bridge after the curbs have been removed to widen the roadway.

The flat-slab specimens were assumed to be simply-supported. As has been demonstrated in previous research, the calculated moments during diagnostic testing of an actual FS-Slab bridge indicate that there is rotational restraint at the supports [Bussell, 1997]. The source of end restraint can vary considerably from span to span in a typical bridge and is therefore difficult to quantify. The moments generated during testing of the specimens using a simply-supported condition represent an upper bound of the positive moments that are developed at midspan. This support condition was also chosen to facilitate the calculations to determine internal stresses and forces at the instrumented sections of the test specimens.

Reinforcement consisted of two mats of uniformly spaced reinforcement. The bottom reinforcement mat consisted of #6 bars at 8 ½ in. in the longitudinal direction and #4 bars at 8 ½ in. in the transverse direction. The top steel mat consisted of #3 bars at 18 in. in both directions. The areas of steel reinforcement were adjusted to develop the same force as in the prototype bridge because Grade 60 steel was used in the specimens and Grade 40 steel was assumed for the prototype bridge construction. The total area of the top reinforcement in the longitudinal direction in the laboratory specimens does not represent the prototype design. The longitudinal top reinforcement was increased in the laboratory specimens to avoid failure during lifting. Figure 6.3 shows a photograph of the reinforcement in one of the flat-slab specimens inside the formwork before the concrete was placed. Specimen dimensions and reinforcement details of the specimens are illustrated in Figure 6.4.

Figure 6.3 Reinforcement in a Typical Flat-Slab Specimen

The specified yield stress for all reinforcing steel used for the fabrication of the specimens was 60,000 psi. The design 28-day concrete compressive strength was 4,000 psi. Table 6.6 lists the average measured material properties for the Flat- Slab Specimens at the time of testing. The values shown for the yield stress of the bottom bars correspond to the static yield measurements. Full details of the material tests for both specimens are presented in Appendix A.

The nominal flexural capacity for each of the flat-slab specimens was calculated using the material strengths listed in Table 6.6. Equation 6.1 was used to compute the flexural strength per foot of slab of each specimen. The specimen capacities are listed and compared with the slab capacity of the prototype bridge in Table 6.7.

The flexural strength for both specimens was lower than the calculated flexural capacity of the prototype bridge with a maximum difference between the specimens and prototype of approximately 10%.

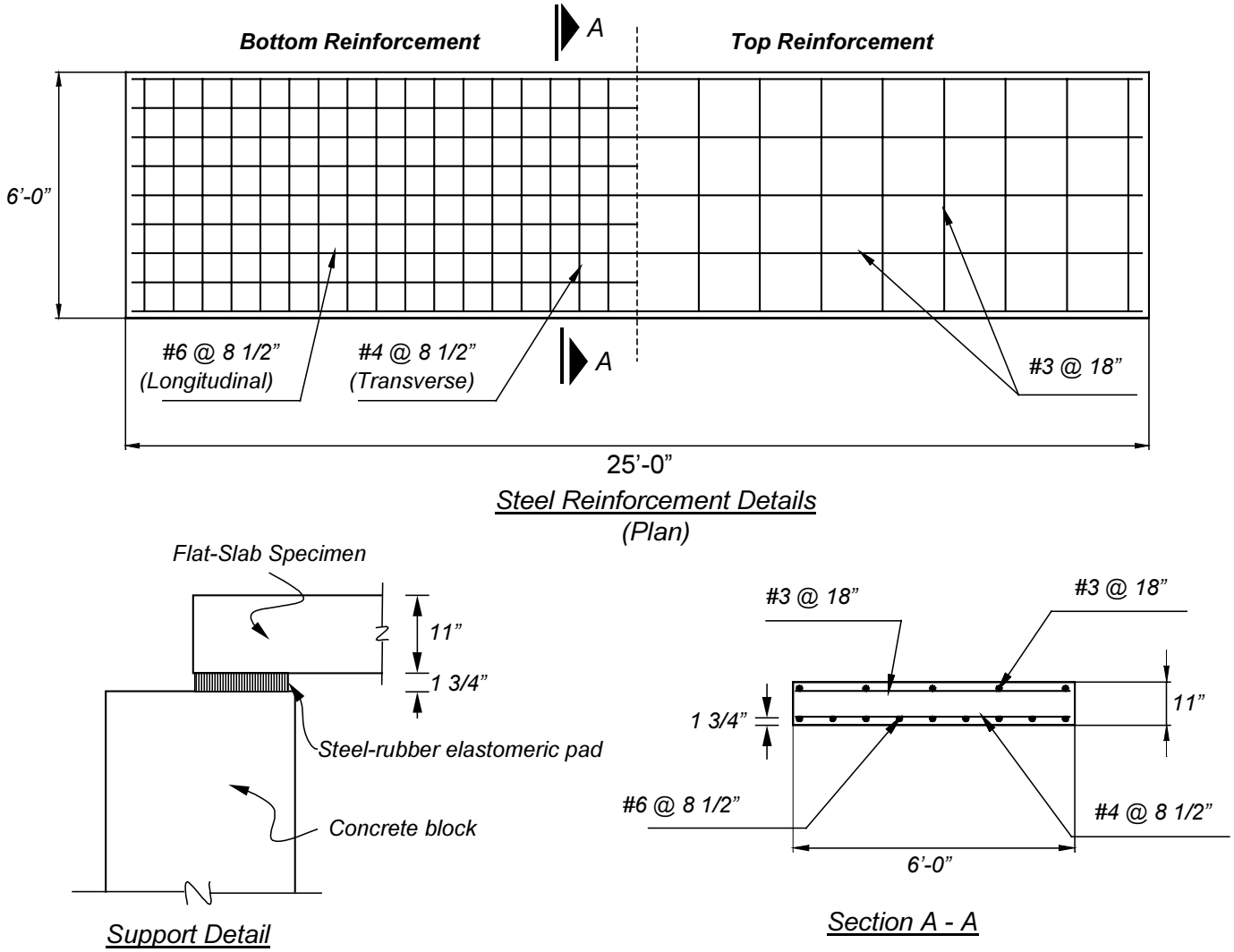

Figure 6.4 Geometry and Reinforcement Details of Flat-Slab Specimens FS-1 and FS-2

Table 6.6 Average Measured Material Strengths for Flat-Slab Specimens

Specimen	Concrete			Longitudinal Bars (#6)		Transverse Bars (#4)	
	Age, days	f '$_c$, psi	f_t, psi	f_y, ksi	f_u, ksi	f_y, ksi	f_u, ksi
FS-1	33	4,800	400	63.5	106.1	65.8	107.4
FS-2	22	3,900	400				

Table 6.7 Flexural Capacity of Flat-Slab Specimens (per unit width of slab)

Specimen	M_n Prototype, kip-ft/ft	M_n Specimen, kip-ft/ft	$M_{n\ spec}/M_{n\ prot}$
FS-1	31.5	29.0	0.92
FS-2	31.5	28.7	0.91

6.4 DESIGN AND CONSTRUCTION OF STRENGTHENING SCHEMES FOR LABORATORY SPECIMENS

Two full-scale laboratory specimens were constructed to evaluate the behavior of the strengthened slab using different CFRP composite systems (Specimens FS-1 and FS-2). As discussed in Section 6.2.3, strengthening of the prototype bridge slab was required to raise the inventory rating. The slab capacity required to reach the target inventory rating of an H-10 design vehicle was determined using Eq. 6.5. The moments per unit width of slab generated by an H-10 design vehicle (Table 6.4) were used in this equation so the rating factor was set to 1.00. The bridge rating is obtained by multiplying the rating factor by the weight in tons of the two front axles of the design vehicle (Appendix B). Equation 6.5 yielded a required capacity, *C*, equal to 38.4 kip-ft/ft. The calculated flexural strength of the slab in the prototype bridge was 28.4 kip-ft/ft (Table 6.1). The values that were used for the variables in Eq. 6.4 to determine the required increase in the flexural capacity of the slab are shown below.

$$C = \phi M_n = RF\left[A_2\ L\ (1 + I)\right] + A_1\ D \tag{6.5}$$

where:

$RF = 1.00$
$A_1 = 1.3$
$D = 10.3$ kip-ft/ft
$A_2 = 2.17$
$L = 8.8$ kip-ft/ft
$I = 0.3$

The strength reduction factor (ϕ) used in the strengthening design was assumed equal to 0.85. Therefore, the target nominal flexural capacity for the strengthened slab was 45.2 kip-ft/ft, which is more than 40% larger than the nominal capacity of the slab in the prototype bridge (Table 6.1).

The required area of composite material to develop the target flexural strength was determined by calculating the moment-curvature response of the slab in the prototype bridge strengthened using the two different types of CFRP composites (Chapter 3). An assumed limiting strain before debonding of the composite systems equal to 0.007 was used for design, as discussed in Chapter 2.

The moment-curvature response of a 6-ft section of the strengthened slab in the prototype bridge was compared with the unstrengthened section. Two different CFRP composite systems were used to increase the flexural capacity to the required strength of the prototype bridge slab. The area of CFRP composites was adjusted until the target strength was reached. The CFRP material properties published by each of the composite system manufacturers (Appendix A) and the nominal material strengths of the prototype bridge were used in these calculations. Table 6.8 lists the required flexural strength and the calculated capacities of the strengthened prototype based on a 6-ft slab section and using the two different CFRP composite systems.

Table 6.8 Flexural Strength Parameters and Calculated Capacity of a 6-ft Section of Strengthened Slab in the Prototype Bridge

Parameter	Value	Notes
$A_1 M_D$, kip-ft	80.3	Factored dead load moment
$A_2 M_L (1+I)$, kip-ft	149	Factored live load moment + impact
M_u, kip-ft	229.3	Required ultimate strength (6-ft slab)
ϕ	0.85	Strength reduction factor
$M_n = M_u/\phi$	270	Required nominal capacity (6-ft slab)
$M_{n\ wet\text{-}layup}$	282	Calculated strength of laboratory specimen
$M_{n\ pultruded}$	265	Calculated strength of laboratory specimen
ε_{CFRP}	0.007	Maximum CFRP strain used for design

Notes: A_1 and A_2 = Load factors for dead and live load effects equal to 1.3 and 2.17 respectively.
I = Impact factor for live load effects equal to 0.3.
Slab width equal to 6-ft.

The CFRP configuration that was used in the construction of the curves shown in Figure 6.5 for each system is presented in Sections 6.4.1 and 6.4.2 for Specimens FS-1 and FS-2, respectively. The calculated moment-curvature response of each specimen is also presented in each of these sections. The measured material properties for concrete and steel, and the properties contained in the manufacturers' literature for the CFRP systems were used in these calculations.

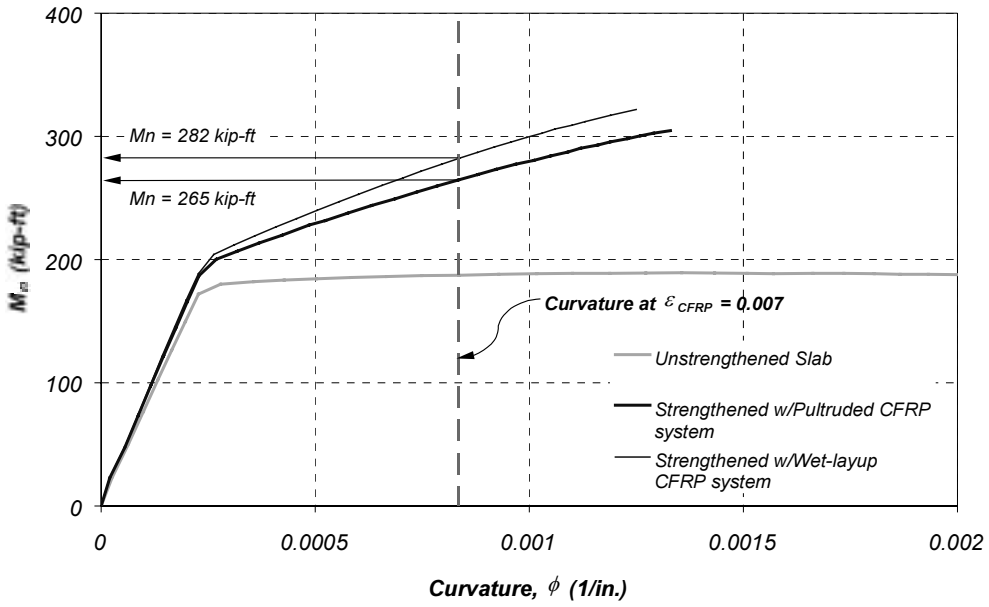

Figure 6.5 Calculated Moment-Curvature Response of a Strengthened and Unstrengthened 6-ft Wide Section of the Slab in the Prototype Bridge

6.4.1 Strengthening Scheme for Specimen FS-1

Specimen FS-1 was strengthened using CFRP pultruded plates bonded to the slab bottom surface. This composite system was designated "D" in the first phase of this investigation [Breña et al., 2001]. The techniques used to bond this type of system to the test specimen are described in Appendix C. The plates were bonded to the concrete surface using an epoxy-based adhesive supplied by the plate manufacturer.

The CFRP plates had a 68% volumetric fiber content. The plate dimensions were 20 ft long by 3.17 in. wide and 0.047 in. thick. The cross sectional dimensions were obtained from the manufacturer's literature. Mechanical properties of the CFRP plates and the epoxy adhesive are listed in Appendix C. The plates were uniformly spaced at 18 in. across the bottom surface (Figure 6.7).

The longest practical CFRP plate length was used to strengthen the laboratory specimen. However, the shape of the moment diagram developed during testing was used to ensure that the plate length would extend beyond the required theoretical cut-off point. The theoretical cut-off point was determined by superimposing the nominal prototype flexural strength on the test moment diagram. The unfactored moment caused by dead loads was subtracted from all calculations because the specimens were constructed at full-scale. The maximum moment applied during the test had to be equal to the required flexural strength of a 6-ft section of the slab in the prototype bridge minus the dead-load moment. In this case, the plates extended 3'-2" beyond the theoretical cut-off points. This procedure is illustrated graphically in Figure 6.6.

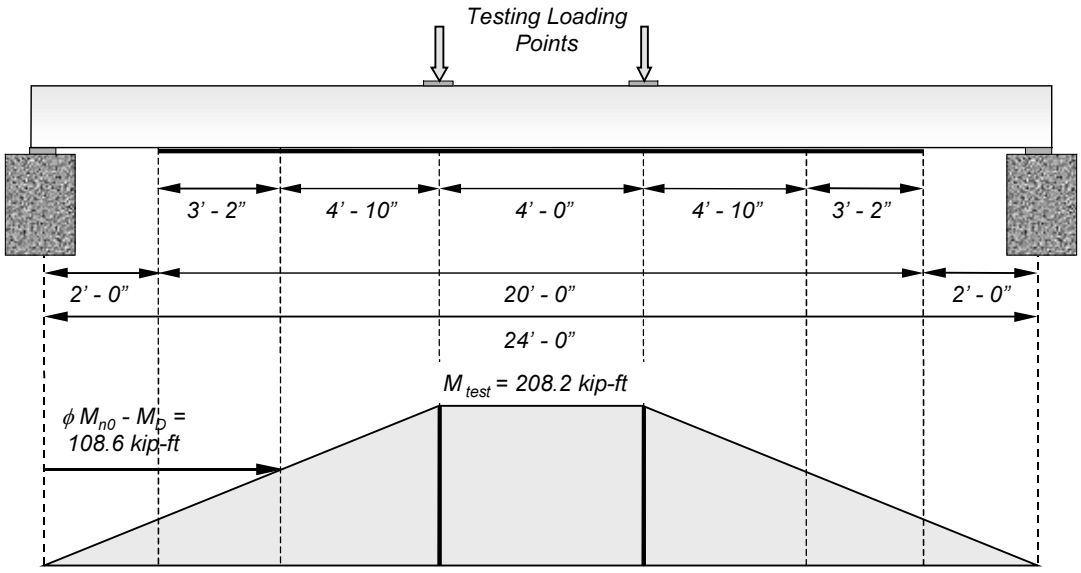

Moment Diagram (6-ft wide slab)

Nomenclature: ϕM_{n0} = Original moment capacity = 170.4 kip-ft
M_D = Service dead load moment = 61.8 kip-ft
M_{test} = Applied moment = $M_U/\phi - M_D$

Figure 6.6 Required CFRP Plate Length on Specimen FS-1 Based on Moments Generated During Laboratory Testing

Six CFRP composite woven fabric sheets were placed transversely along the pultruded plates at 3 ft. on center (Figure 6.7). The sheets were 12-in. wide and were bonded using a two-component epoxy resin. Details of the bonding procedure are presented in Appendix C. The sheets were placed only on the bottom surface without continuing them on the sides of the slab specimen because the specimen represents an interior section of the slab in the prototype bridge. Attaching these sheets transversely to the CFRP plates was expected to delay debonding of the pultruded plates from the concrete surface.

Both the epoxy adhesive used to bond the pultruded plates, and the composite straps were cured at ambient temperature for 7 days to develop their design strength. Details showing the location of CFRP pultruded plates and woven fabric sheets on Specimen FS-1 are shown in Figure 6.7. A picture showing the bottom surface of the slab specimen after strengthening can be seen in Figure 6.8.

The calculated capacity of Specimen FS-1 was determined to compare with the required capacity computed for the prototype bridge. The measured concrete compressive strength and steel yield stress were used in these calculations.

The calculated moment-curvature response of Specimen FS-1 is shown in Figure 6.9. The calculated response of the unstrengthened specimen is also shown for comparison. The calculated test specimen capacity was determined at a CFRP strain equal to 0.007 to compare with the prototype design strength. The difference in the calculated capacity of the strengthened prototype bridge (265 kip–ft) and the calculated capacity of the laboratory specimen (274 kip–ft) can be attributed to the higher measured yield stress of the reinforcement and the higher concrete strength at the time of testing.

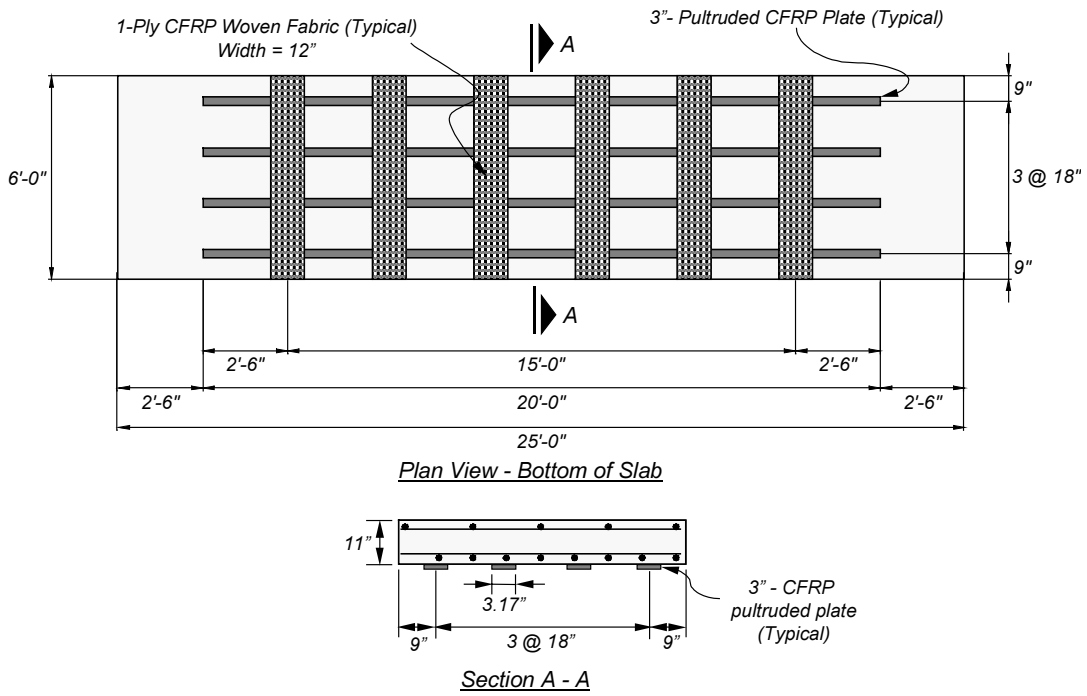

Figure 6.7 Strengthening Details for Specimen FS-1

Figure 6.8 Bottom Surface of Specimen FS-1 after Strengthening with the CFRP Pultruded System

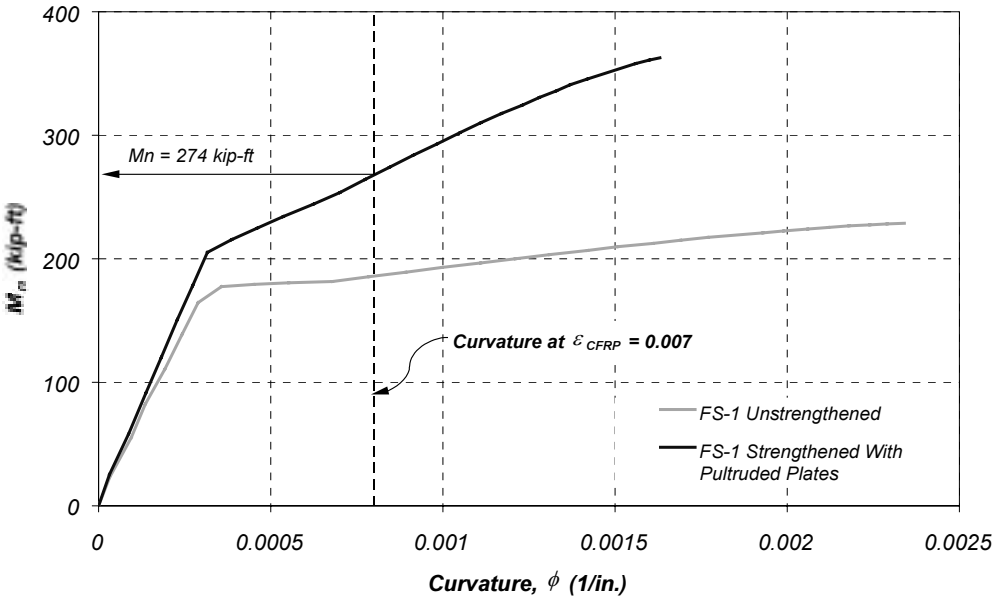

Figure 6.9 Calculated Moment-Curvature Response of Specimen FS-1 Using the Measured Material Properties

6.4.2 Strengthening Scheme for Specimen FS-2

Specimen FS-2 was strengthened using a CFRP composite system applied using a wet lay-up procedure (Appendix C). This composite system was designated "A" in the first phase of this investigation [Breña et al., 2001]. The system consisted of unidirectional carbon fiber sheets that had not been impregnated in epoxy prior to installation. A two-component epoxy resin was used to impregnate the carbon fibers and bond them to the concrete surface. A detailed description of the fabrication procedure for this type of system is presented in Appendix C.

Two 20-in.-wide layers (plies) of carbon fiber sheets were bonded to Specimen FS-2 at a spacing of 36 in.. The length of the sheets was determined based on the moment generated during testing as for Specimen FS-1 (Figure 6.6). Details showing the location and geometry of the CFRP composite on Specimen FS-2 are illustrated in Figure 6.10.

CFRP sheets were also placed transversely at a 26-in. spacing along the total length of the longitudinal sheets. They were fabricated using one ply of 10-in. wide carbon fiber sheets. The objective of the transverse sheets was to increase the contact surface area and delay debonding of the longitudinal CFRP sheets that were used to increase the flexural capacity of the test specimen.

The calculated moment-curvature response of Specimen FS-2 is shown in Figure 6.12. The measured material properties of steel and concrete were used in the calculations. The flexural capacity of the specimen at CFRP debonding was estimated at a curvature corresponding to an expected maximum CFRP composite strain equal to 0.007.

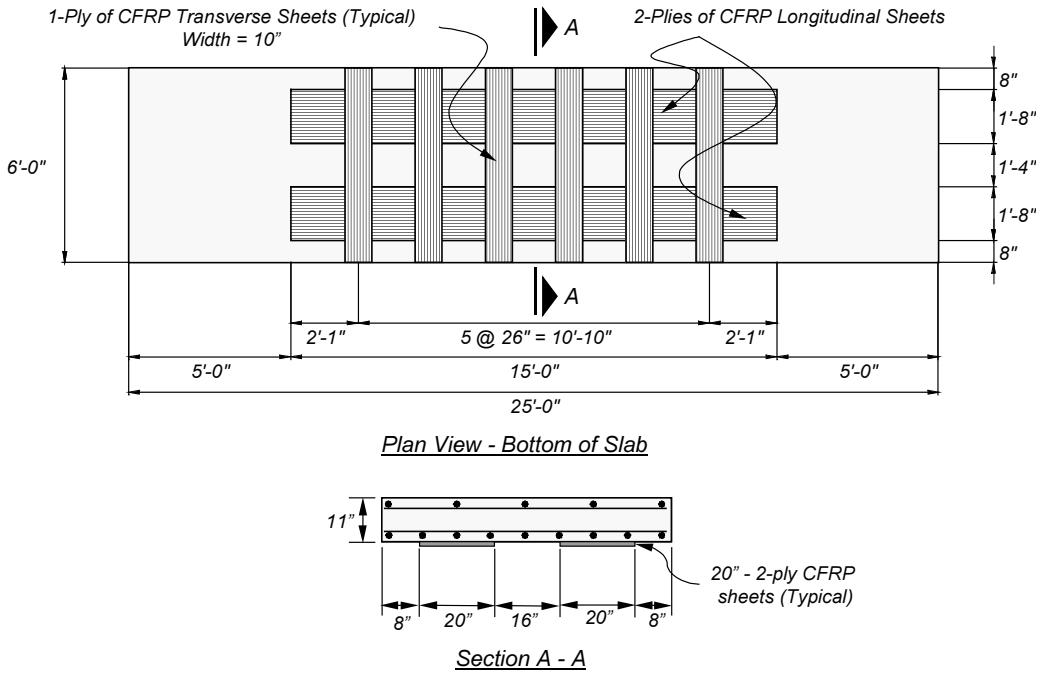

Figure 6.10 Strengthening Details for Specimen FS-2

Figure 6.11 Bottom Surface of Specimen FS-2 after Strengthening with the CFRP Wet-Layup System

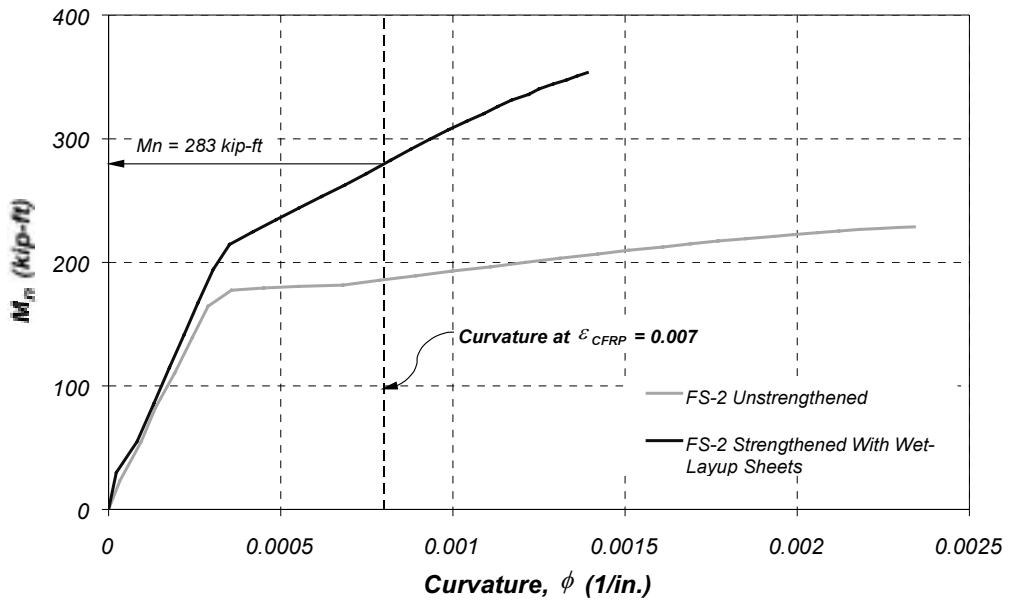

Figure 6.12 Calculated Moment-Curvature Response of Specimen FS-2 Using the Measured Material Properties

The calculated capacity of Specimen FS-2 exceeded the required flexural strength of 270 kip-ft. Therefore, the strengthened specimen was expected to meet the design goal. A comparison between the calculated and measured moment-curvature response of this specimen is presented in Chapter 8.

6.5 SUMMARY

A description of flat-slab bridge construction in Texas is presented in this chapter. Bridges in this category were designed using older load standards and therefore strengthening is required to meet current legal loads. The load rating deficiencies associated with this type of construction were discussed and the criterion used to justify strengthening this type of bridges was described.

The design, construction, and strengthening procedures used in two full-scale laboratory specimens were presented in this chapter. These specimens represent a 6-ft wide section of the slab in the prototype bridge. The laboratory specimens were designed to replicate the behavior of a strengthened slab after curbs have been removed from the bridge for widening purposes.

Two commercially available composite systems were used to restore the capacity of the bridge after the curbs are removed. The calculated moment-curvature response of the strengthened specimens was compared with the calculated response of the prototype bridge used in the design of the composite strengthening systems.

Chapter 7: Measured Response of Flat-Slab Specimens

7.1 INTRODUCTION

The measured response of Specimens FS-1 and FS-2 are presented in this chapter. The experimental setup, loading history, and specimen instrumentation are also described. Representative deflection and strain responses that were measured during the tests are presented and discussed.

7.2 TEST SETUP AND INSTRUMENTATION

7.2.1 Description of Experimental Setup

The flat-slab specimens were tested under loads that were applied statically. The test setup was the same as for the pan-girder specimens. The flat-slab specimens were supported on two steel-rubber elastomeric pads at each support simulating a simply-supported condition. The elastomeric pads rested on concrete blocks on both ends of the specimens.

Loads were applied using a 200-kip hydraulic ram reacting against a steel frame that was anchored to the laboratory strong floor. The total load was distributed to 4 points on the specimen slab surface using longitudinal and transverse spreader beams. The loads were applied symmetrically about the center of the specimen, spaced at 4 ft. longitudinally and 3 ft. transversely. The spreader beams were supported on 10-in. by 5-in. steel-rubber elastomeric pads to avoid concrete crushing under the load points. A view of the experimental setup is shown in Figure 7.1.

Figure 7.1 Experimental Setup Used for the Laboratory Tests of the Flat-Slab Specimens

7.2.2 Loading Sequence

The flat-slab specimens were initially loaded to form cracks before the CFRP composite systems were bonded. A load equal to 7 kip was applied to the specimens. This load approximated the service-load moments in the slab for the prototype bridge. Therefore, the strains in the reinforcing bars were assumed to be equal in the test specimens and the prototype bridge under service conditions. In this way, cracks in the laboratory specimens were assumed to have approximately the same widths as cracks present in the prototype bridge

The composite systems were bonded to the specimens after the initial cracking test. The composite systems were cured for seven days at ambient temperature. After curing, the flat-slab specimens were tested to failure.

The test to failure was conducted applying two cycles to predetermined load stages. The load that was used during the cracking test (7 kip) was initially applied to compare the strengthened specimen response (stiffness and reinforcement strains) with the unstrengthened behavior. The load was then increased until first yielding of the longitudinal reinforcement was observed. The load at yield was defined as the point on the load-deflection curve where an apparent reduction in stiffness was observed. This load was approximately equal to 34 kip in both specimens. Finally, the load was increased until failure of the specimens by CFRP composite debonding. Table 7.1 summarizes the load-levels and number of cycles used during testing of the Flat-Slab Specimens.

Table 7.1 Applied Moments and Loads During Testing

Load Stage	Moments in Test Specimen		Total Applied Load, kip	# of Cycles
	Dead Load, kip-ft	Applied Load, kip-ft		
1	59.4	35	7	2
2	59.4	170	34	2
3 (FS-1)	59.4	270	54	1
3 (FS-2)	59.4	285	57	1
4 (FS-1)	59.4	201	40.2	1
4 (FS-2)	59.4	184	36.7	1

Note: Load Stage 1: Service Live Load
Load Stage 2: Yield Load
Load Stage 3: Ultimate Load
Load Stage 4: Maximum Load in Bare Specimen

Failure of the flat-slab specimens was defined by debonding of the CFRP composite systems. After failure, both specimens retained the strength of the bare reinforced concrete slab because the maximum usable concrete strain, ε_{cu}, had not been reached. At this point, the specimens were unloaded to zero and reloaded until initiation of concrete crushing on the slab top was observed to measure the strength of the bare reinforced concrete section.

7.2.3 Instrumentation

The flat-slab specimens were instrumented to measure deflections, strains in different materials, and the total load applied during the tests. The voltage outputs from all the instruments were collected and recorded every 4 seconds using a Hewlett Packard (HP-75,000) data acquisition unit.

The instrumentation used in the flat-slab specimen tests was similar to the one employed for the pan-girder specimens. The total load was measured using a 200-kip Interface load cell. Deflections were measured using either 2-in. or 6-in. linear potentiometers at different locations on the specimens. Strains were monitored at four instrumented sections on the steel reinforcement, concrete surface, and CFRP composites.

Linear potentiometers were attached at midspan and at sections under the points of load application on the east and west sides of the specimens. The ends of the specimens were also instrumented with potentiometers to determine the end rotation during the tests. All instruments had a resolution of 0.001 in. Table 7.2 summarizes the location of linear potentiometers on the Flat-Slab Specimens.

Table 7.2 Displacement Limits of Linear Potentiometers

Test Specimen	Side	North Load Point	Midspan	South Load Point	End Diaphragms
FS-1 and FS-2	East	2 in.	6 in.	2 in.	2 in.
	West	2 in.	6 in.	2 in.	2 in.

Four sections along the span were instrumented using electric resistance strain gages. Each instrumented section had strain gages attached to 3 bars on the bottom longitudinal reinforcement, to 3 points on the concrete slab, and to 4 points on the CFRP composite plates or sheets. Table 7.3 lists the characteristics of the strain gages used for the flat-slab specimen tests. Additional technical specifications are contained in Appendix A.

Table 7.3 Characteristics of Strain Gages

Material	Strain Gage Type	Gage Length, mm
Steel	Foil	6
CFRP	Foil	6
Concrete	Wire	60

The position of linear potentiometers and the location of the sections instrumented with strain gages are presented in Figure 7.2. Figure 7.3 shows the position of strain gages bonded to the steel reinforcement (#6 bars) and concrete surface for Specimens FS-1 and FS-2. The position of strain gages on the CFRP composite systems for each flat-slab specimen is illustrated in Figure 7.4.

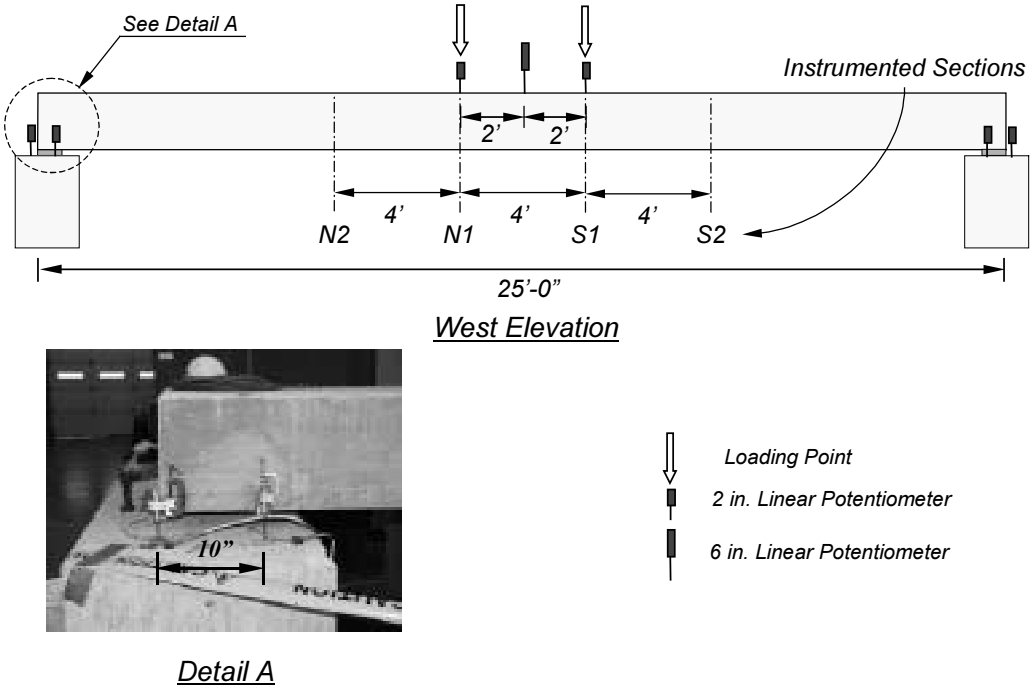

Figure 7.2 Position of Linear Potentiometers on East and West Sides and Location of Instrumented Sections in Flat-Slab Specimens

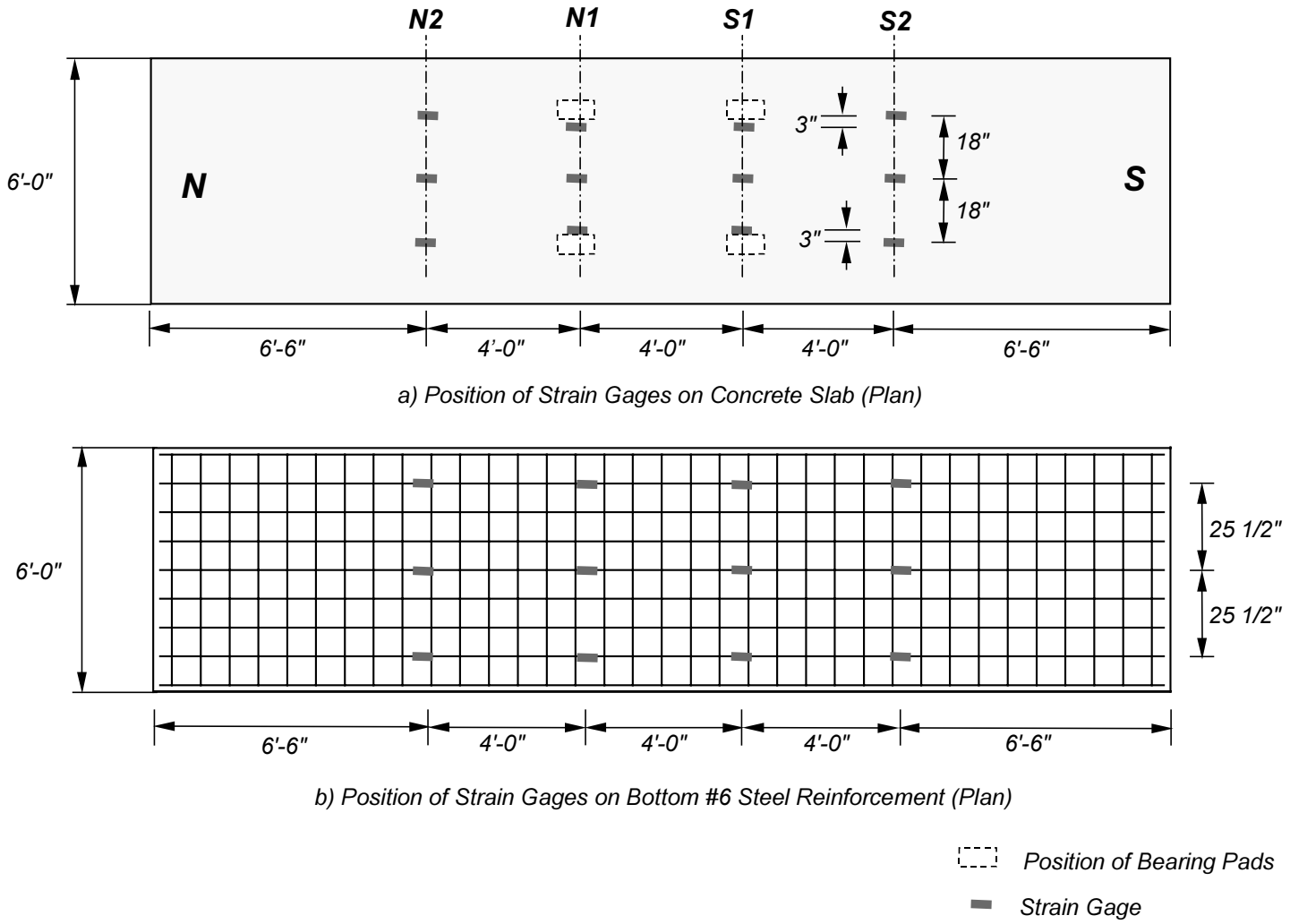

Figure 7.3 Position of Strain Gages on the Reinforcement and Concrete Surface in Specimens FS-1 and FS-2

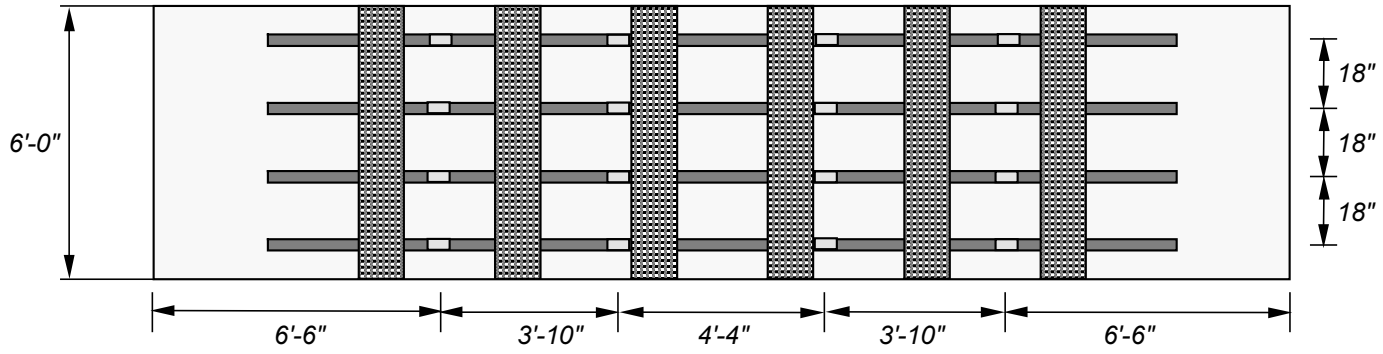

a) Position of Strain Gages on CFRP Plates in Specimen FS-1 (Bottom View)

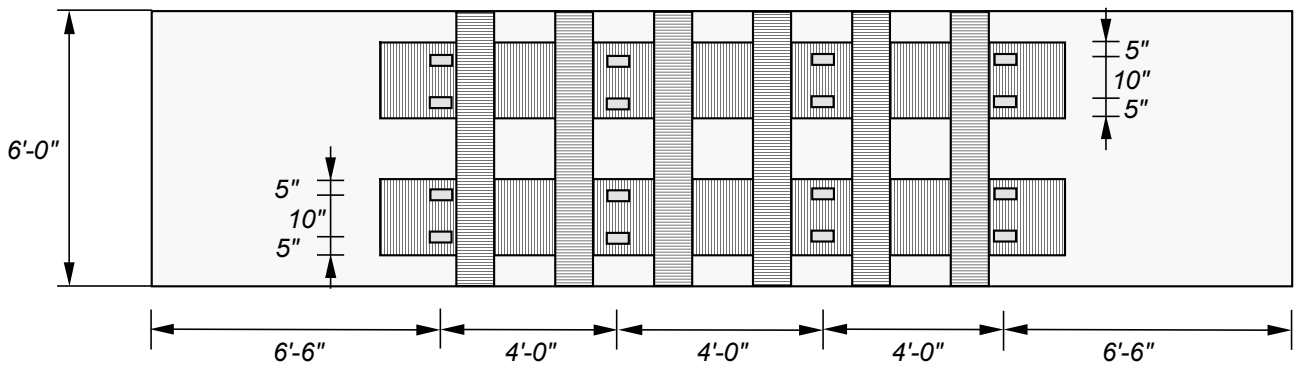

b) Position of Strain Gages on CFRP Sheets in Specimen FS-2 (Bottom View)

Strain Gage

Figure 7.4 Position of Strain Gages Bonded to the CFRP Composite Systems in Specimens FS-1 and FS-2

7.3 OBSERVED BEHAVIOR DURING TESTS

The observed behavior of the specimens during testing is described in this section. The concrete cracks that were observed on the side faces of the specimens at different load levels are presented. Representative outputs from the instruments are also discussed.

7.3.1 Description of Failure Sequence and Cracking Distribution

(a) Specimen FS-1

Cracks were marked and measured on the sides of the specimen after the application of 2 cycles to load-stage 1 (7 kip) on the unstrengthened specimen. The cracks formed across the bottom surface of the specimen and extended 6 in. towards the top surface on both sides. Cracking was visible on the sides in a region extending to sections N2 and S2. Cracks were spaced at approximately 6 to 8 in. throughout this region (Figure 7.5).

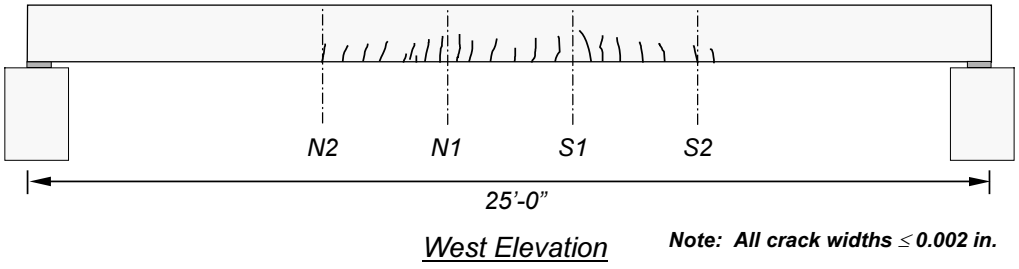

Figure 7.5 Typical Crack Pattern after Load Cycles to 7 kip on Specimen FS-1 before CFRP Strengthening

After strengthening, cracks on Specimen FS-1 were marked and measured on the sides at load-stage 2 (34 kip). The cracking pattern on the west side is shown in Figure 7.6. CFRP debonding was not observed along the CFRP plates up to this load stage.

Initial debonding of the CFRP plate could not be determined by visual inspection because the plates were bonded to the bottom surface of the specimen. However, cracking sounds indicating initial debonding were heard at a load equal to 47 kip. Debonding initiated at midspan and proceeded toward the north end of the plates.

At a load of 54 kip, there was a sudden reduction of load to 53 kip accompanied by a cracking sound. The peak load was never reached again and debonding of the two east plates took place on the north end of the specimen. The load was maintained at approximately 44 kip for several minutes and finally the two west plates debonded from the bottom, at the north end of the specimen.

A photograph illustrating the bottom of the test specimen after CFRP debonding is shown in Figure 7.7. As the plates debonded, the woven CFRP-transverse sheets were pulled off the concrete surface along almost the entire width of the slab. Approximately two-thirds of the plates debonded longitudinally from the surface leaving only the plates attached on the south side of the specimen (Figure 7.8).

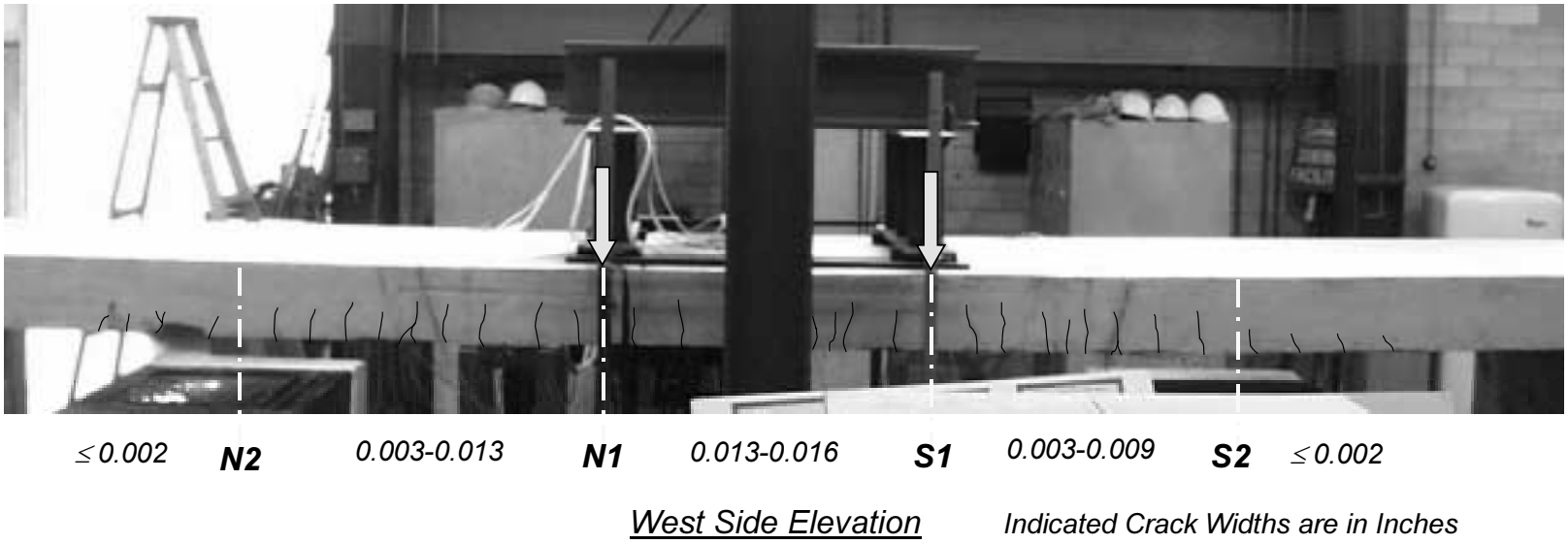

Figure 7.6 Crack Pattern for Specimen FS-1 at Load Stage 2 (34 kip)

Figure 7.7 Bottom View Toward North End of Specimen FS-1 after CFRP-Plate Debonding

Figure 7.8 South End of the CFRP Plates Still Attached After Failure of Specimen FS-1

Some areas of the plates delaminated leaving pieces of carbon fibers attached to the concrete surface, particularly near the ends of the plates. A detail showing plate delamination and the concrete surface where the CFRP plate was bonded is presented in Figure 7.9. A drawing illustrating the areas on the slab bottom surface where the plates debonded is shown in Figure 7.10.

Figure 7.9 Evidence of Plate Delamination of the East CFRP Plate at the North End of Specimen FS-1

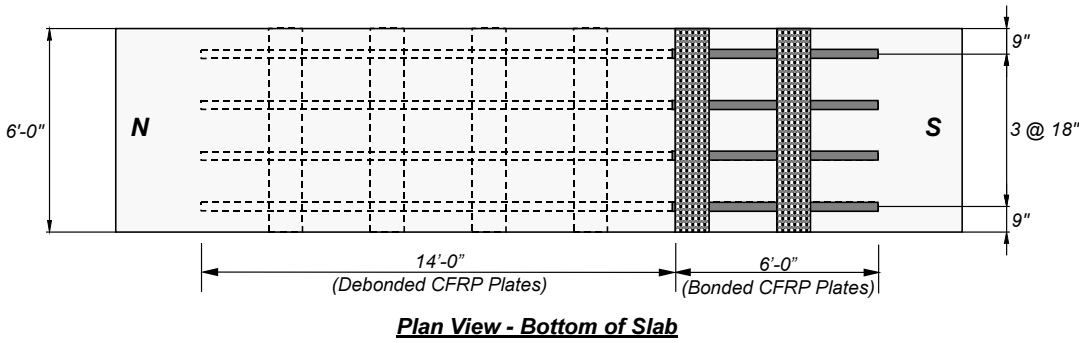

Figure 7.10 Extent of Debonding of CFRP Plates on Specimen FS-1

The load dropped to approximately 33 kip after CFRP debonding occurred. However, the specimen still retained its unstrengthened load-carrying capacity because the maximum usable concrete strain had not been reached. Loading was stopped when concrete crushing was observed at sections N1 and S1.

(b) Specimen FS-2

The response and cracking pattern of Specimen FS-2 during the initial cracking cycles was similar to Specimen FS-1 (Figure 7.5) except that cracks did not form at sections N2 and S2 in this specimen. After the load was increased to the observed specimen yield, cracks were marked and measured. A photograph illustrating the crack pattern and widths is shown in Figure 7.11. The widths of the cracks shown in this figure have been increased for clarity.

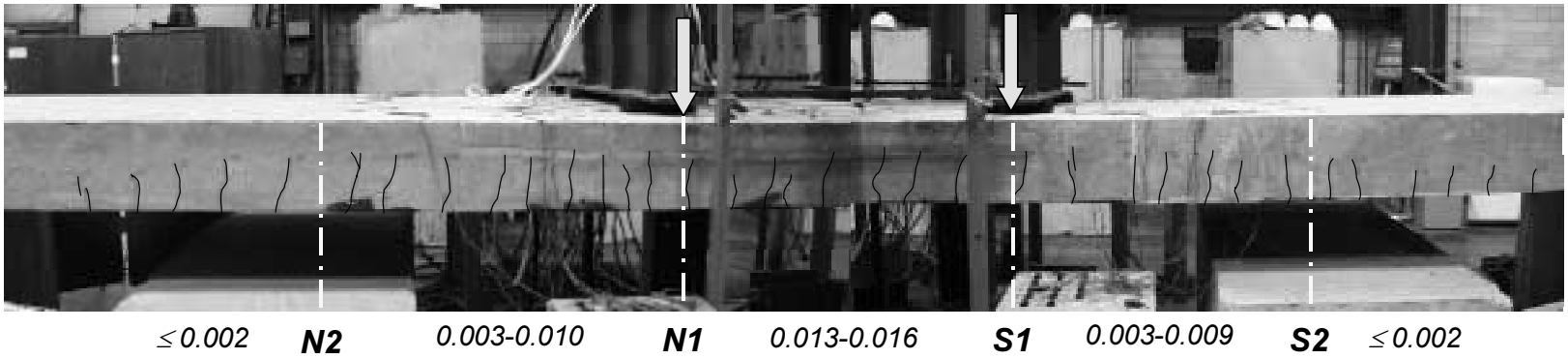

Figure 7.11 Cracking Pattern of Specimen FS-2 at Load Stage 2 (34 kip)

Initial debonding along the sides of the west CFRP sheet was observed at load stage 2 in a localized area near section N1 where the concrete surface had a small indentation (Figure 7.12). The formation of white lines along the carbon fiber direction in the sheets that were oriented transversely was also apparent at this load level. These lines gave an indication of epoxy cracking on the transverse sheets as the longitudinal laminates began to pull-off from the concrete surface.

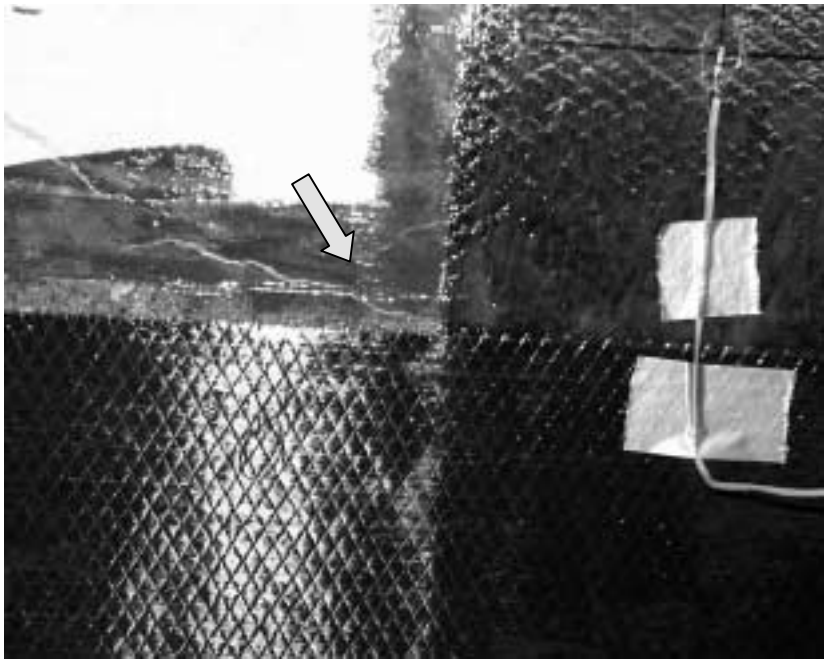

Figure 7.12 Initiation of Debonding Along CFRP Sheet

As the applied load was increased to 57 kip, debonding of the CFRP sheet progressed toward the north end until the sheet detached completely from the concrete surface. A bottom view of the west CFRP sheet is seen in Figure 7.13. The deformation and splitting experienced by the transverse sheets after debonding can be observed in Figure 7.14. Similarly, the east sheet debonded toward the south end of Specimen FS-2. Only a portion on the north end of CFRP sheet remained attached to the concrete surface. The extent of CFRP sheet debonding at failure is indicated in Figure 7.15.

After debonding the load dropped to 32 kip. The specimen was unloaded and reloaded until concrete crushing initiated on top of the slab. Figure 7.16 illustrates the deformation typical of both flat-slab specimens at initiation of concrete crushing.

Figure 7.13 View of West CFRP Sheet after Debonding from Specimen FS-2

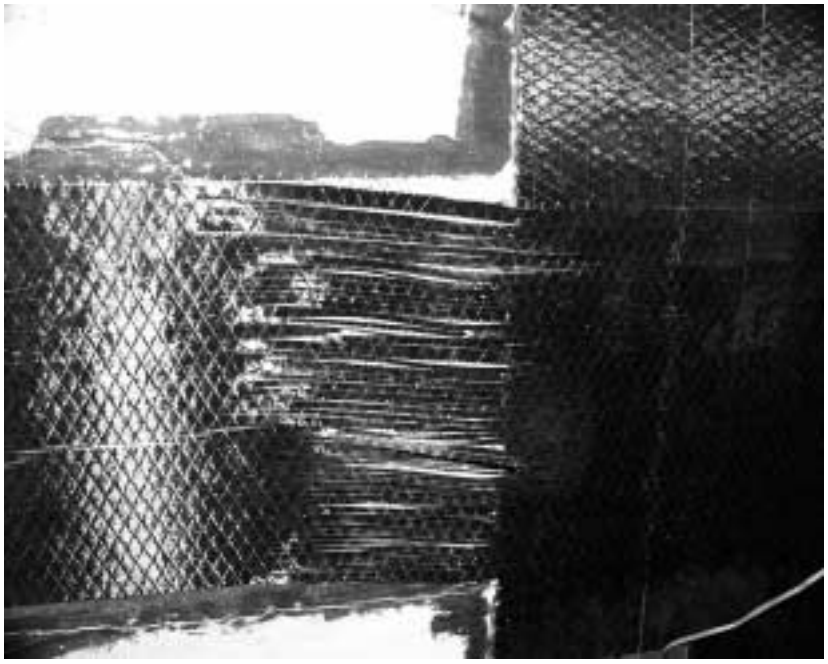

Figure 7.14 Deformation and Splitting of Transverse Sheet Caused by Movement of the Longitudinal Sheet

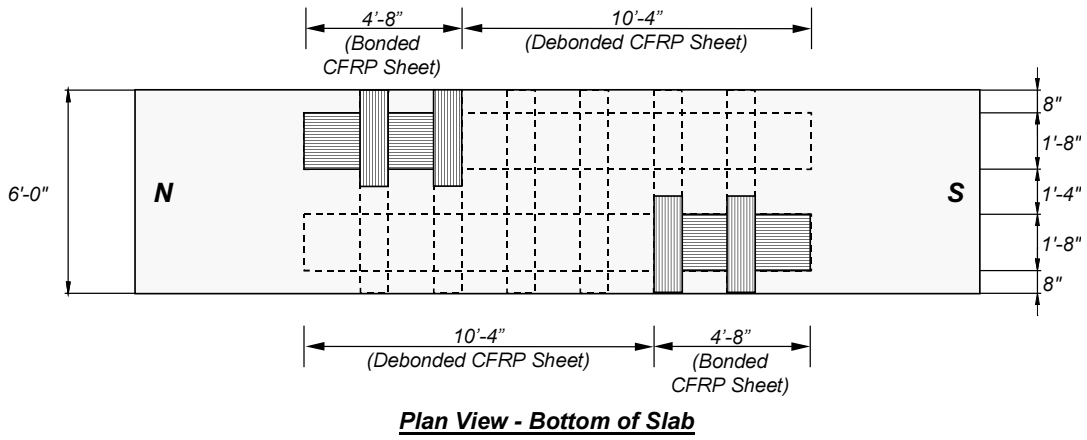

Figure 7.15 Bottom View of Specimen FS-2 Indicating the Extent of Debonding of CFRP Sheets

Figure 7.16 West Side of Specimen FS-2 at Deformation Corresponding to Initiation of Concrete Crushing

7.4 MEASURED RESPONSE

The recorded readings of representative instruments during the flat-slab specimen tests are presented in this section. These readings were plotted against the applied load to verify that the instruments were operating properly throughout the tests.

7.4.1 Deflection Measurements

Plots showing the deflection response are illustrated in Figures 7.17 to 7.19 for Specimen FS-1 and in Figures 7.20 to 7.22 for Specimen FS-2. The instruments on sections N1 and S1 were removed at a load of approximately 47 kip. Their stroke capacity was exceeded and it was considered too dangerous for research staff to reposition them. Midspan potentiometers were repositioned at yield and left in place until failure.

(a) North block

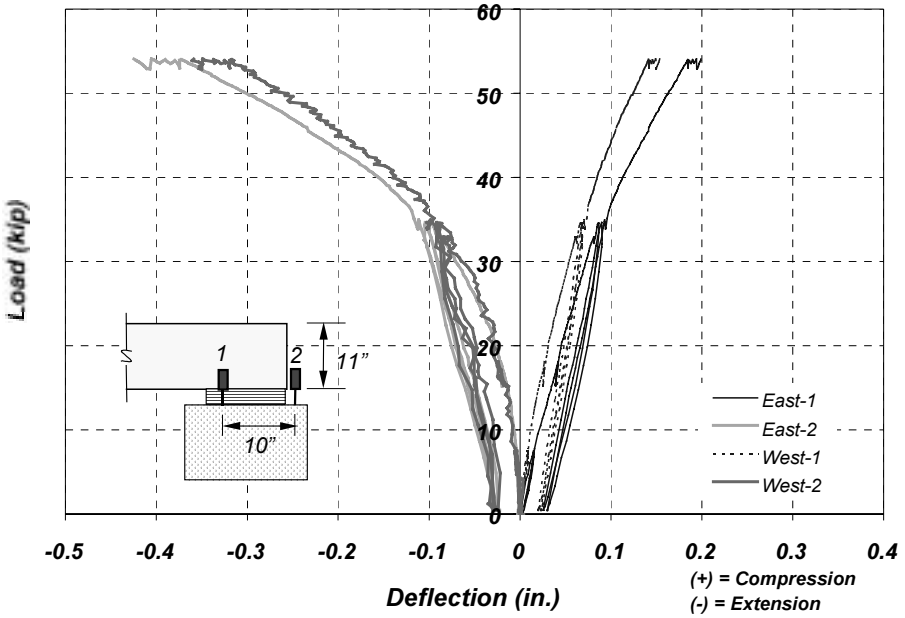

(b) South Block

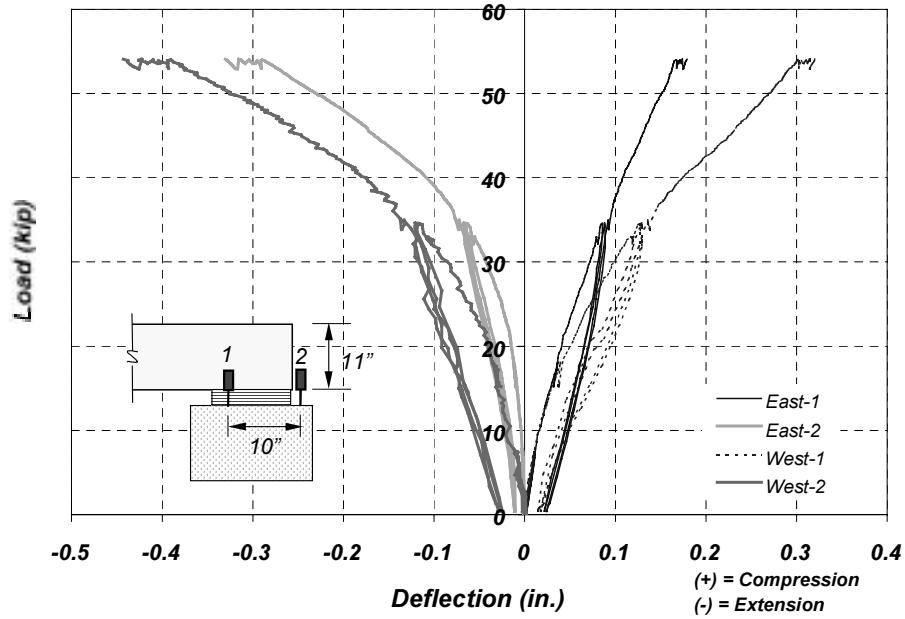

Figure 7.17 Measured Displacements at Supports in Specimen FS-1

(a) East Side

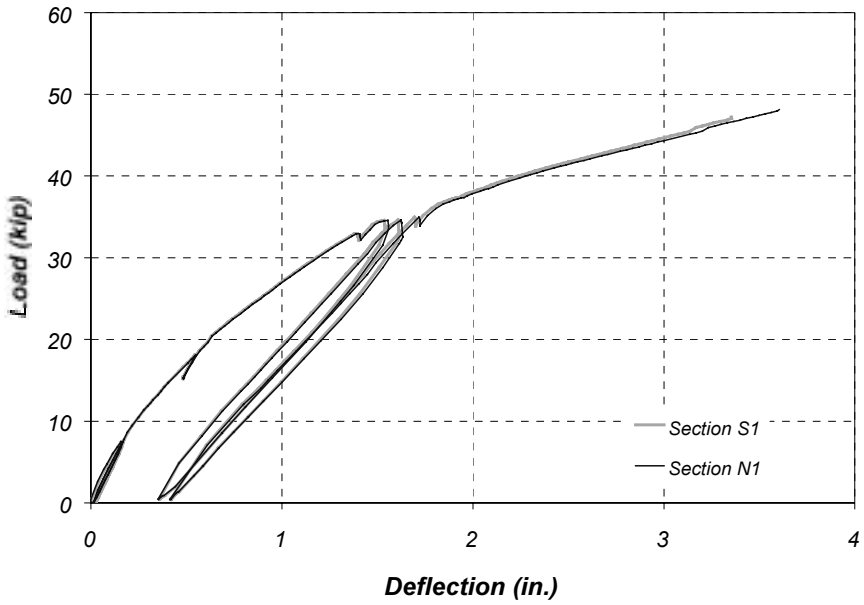

(b) West Side

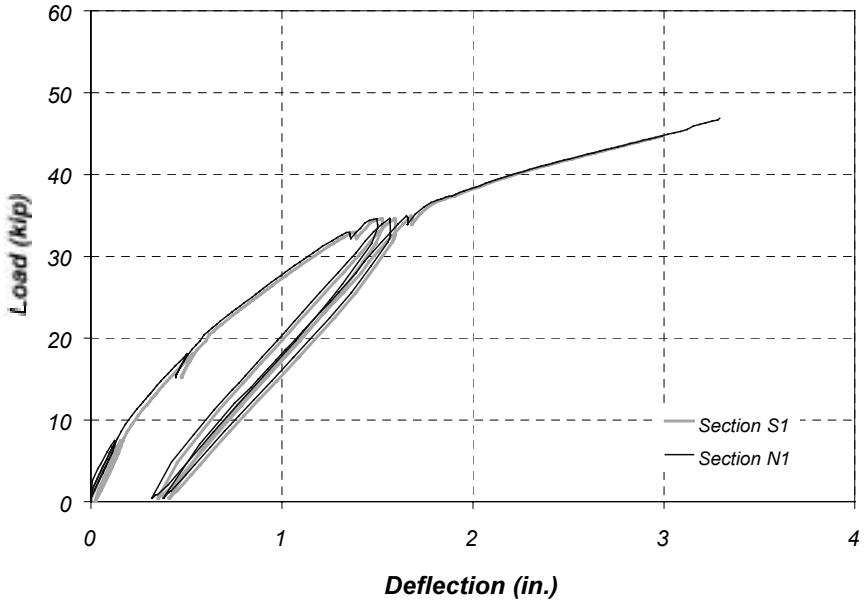

Figure 7.18 Measured Deflections at Sections N1 and S1 in Specimen FS-1

(a) East Side

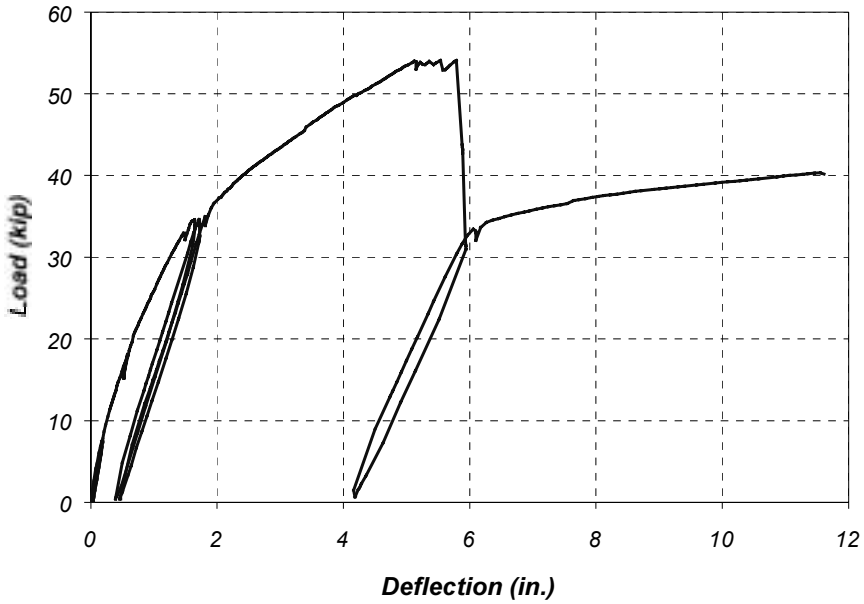

(b) West Side

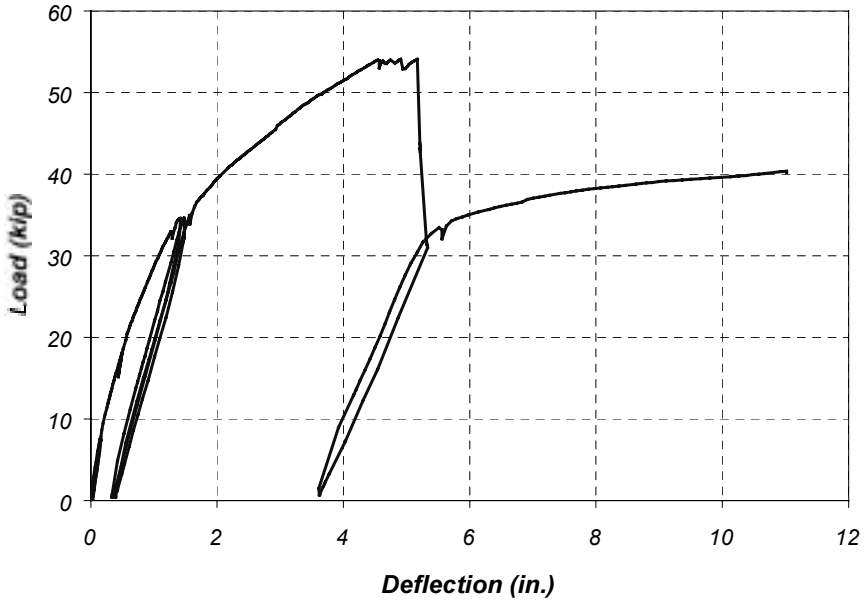

Figure 7.19 Measured Deflections at Midspan in Specimen FS-1

(a) North block

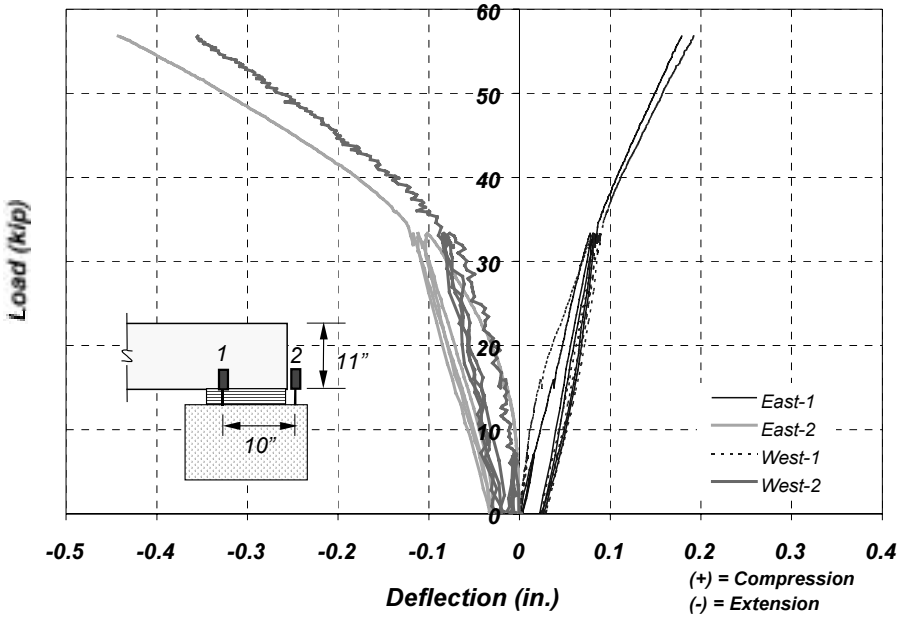

(b) South Block

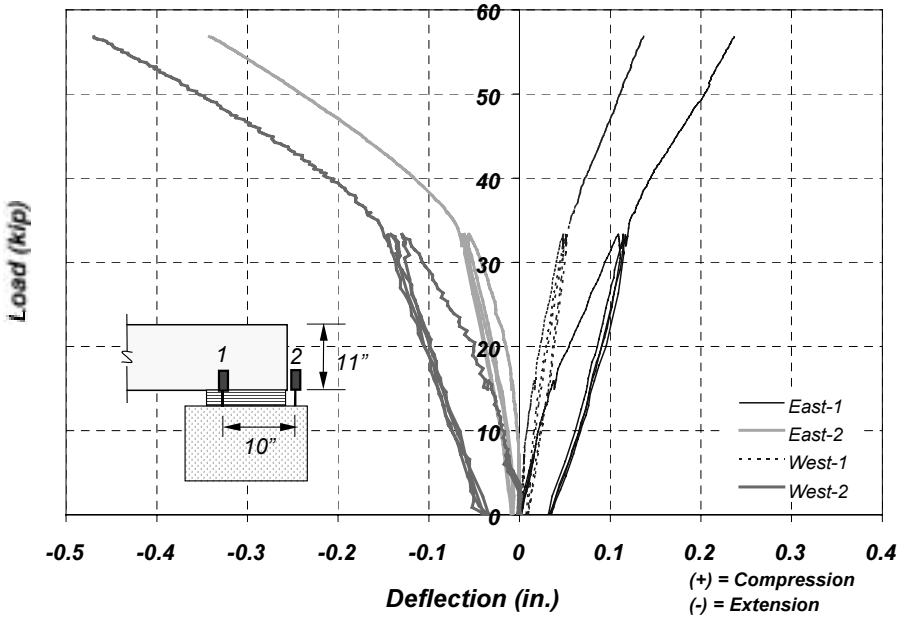

Figure 7.20 Measured Displacements at Supports in Specimen FS-2

(a) East Side

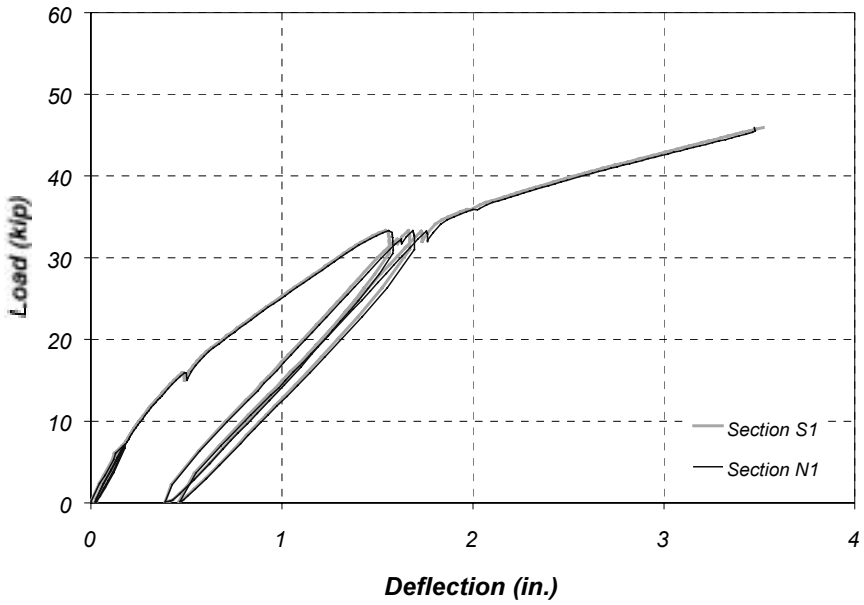

(b) West Side

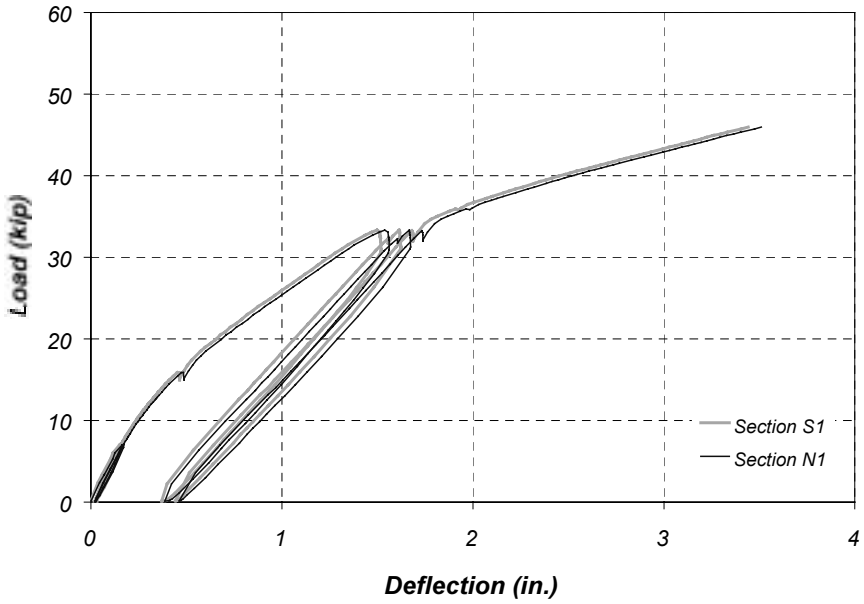

Figure 7.21 Measured Deflections at Sections N1 and S1 in Specimen FS-2

(a) East Side

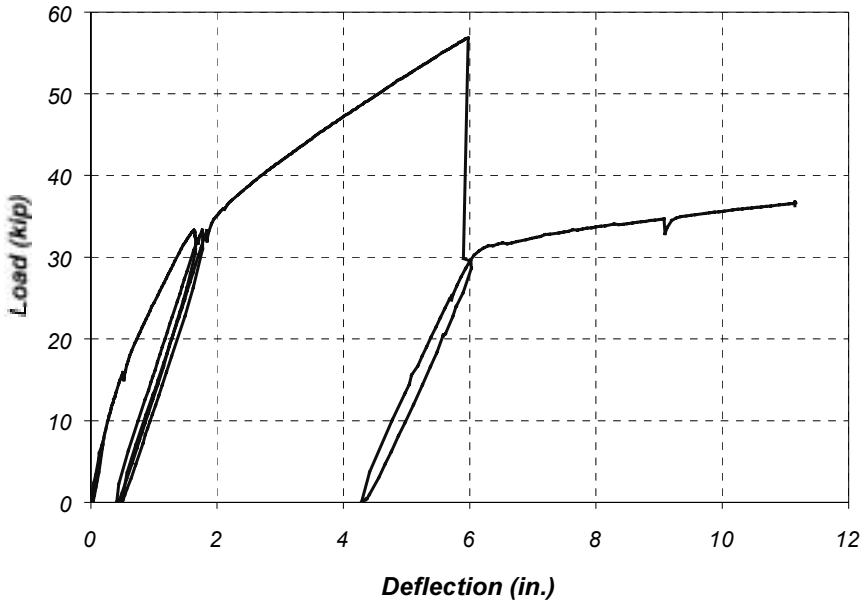

(b) West Side

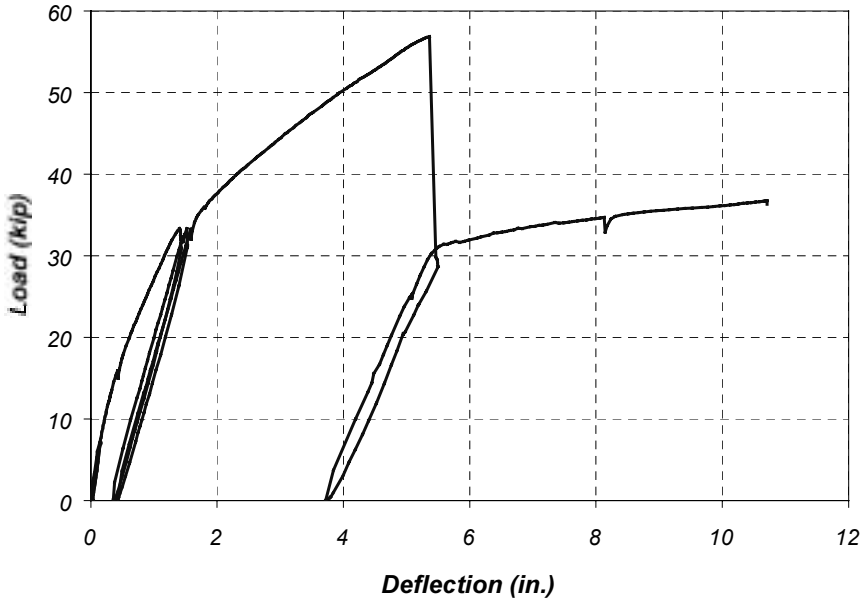

Figure 7.22 Measured Deflections at Midspan in Specimen FS-2

The deformations at the supports are presented in Figure 7.17 for Specimen FS-1 and Figure 7.20 for Specimen FS-2. With these measurements the average bearing deformation was subtracted from the specimen deflections. The deflection readings of instruments at midspan, and sections N1 and S1 were corrected by subtracting the average support deflections for Specimens FS-1 and FS-2, respectively.

The plots show readings taken on the east and west sides of the specimens. The similarity in these plots indicates that the specimens did not twist during the tests. Also, the deflection measurements taken at symmetric sections (sections N1 and S1) about the specimen centerlines are comparable (Figures 7.18 and 7.21). Therefore, the average deflection was used in the comparison with the calculated response presented in Chapter 8.

The measured deflection response of both specimens shows three distinct regions defined by the slope of lines tangent to the load-deflection curves. Although the specimens were previously cracked before running the test to failure, the curves show an initial steep slope. This is due to a stiffening effect from the CFRP composites. The global stiffness reduced to the fully cracked section stiffness at approximately 15 kip. The final change in slope observed in the load-deflection diagrams took place at load-stage 2, when the specimens reached yield of the main longitudinal reinforcement.

The post-yield slope observed in the load-deflection diagrams is steeper than expected for a conventionally reinforced concrete element. Instead of having an almost constant load after load-step 2, Specimens FS-1 and FS-2 exhibited a significant increase in load with increasing deflection. This behavior is attributable to the tensile stresses that were developed by the CFRP composites after yielding of the steel reinforcement.

Tables 7.4 and 7.5 show measured response parameters at different load stages for Specimens FS-1 and FS-2, respectively. The deflections listed in these tables were measured at midspan and were corrected by subtracting the average support displacements. The strains were calculated averaging the measured values at sections N1 and S1 (maximum moment sections).

Table 7.4 Maximum Response Measured During Testing of Specimen FS-1

Load Stage	Maximum Measured Parameters			Maximum Average Strain (Microstrain)			Notes
	Load, kip	Moment, kip-ft	Deflection, in.	Reinforcement	Concrete	CFRP Plates	
1A	7	35	0.36	418	166	-	Reinforced concrete specimen before application of CFRP
1B	7	35	0.16	155	80	233	Reinforced concrete slab with CFRP plates
2	34	170	1.53	2,062	640	2,152	Observed yielding of longitudinal reinforcement
3	54	270	5.48	5,390	2,055	6,392	Debonding of CFRP plates
4	40.2	200	11.31	*	3,204	*	Capacity of bare reinforced concrete slab

* Readings were unavailable because gages were damaged after CFRP debonding

Table 7.5 Maximum Response Measured During Testing of Specimen FS-2

Load Stage	Maximum Measured Parameters			Maximum Average Strain (Microstrain)			Notes
	Load, kip	Moment, kip-ft	Deflection, in.	Reinforcement	Concrete	CFRP Sheets	
1A	7	35	0.36	383	127	-	Reinforced concrete specimen before application of CFRP
1B	7	35	0.16	184	87	254	Reinforced concrete slab with CFRP sheets
2	34	170	1.52	3,198	703	1,892	Observed yield of longitudinal reinforcement
3	57	285	5.67	8,154	2,222	7,473	Debonding of CFRP sheets
4	36.7	184	10.93	6,011	3,171	*	Capacity of bare reinforced concrete specimen

* Readings were unavailable because gages were damaged after CFRP debonding

7.4.2 Strain Gage Measurements

The strains measured on the steel reinforcement, CFRP composites and concrete surface were used to compute internal stresses and forces and to determine the location of the neutral axis at various load stages. The procedures to determine the moment-curvature response are presented in Chapter 8. Load vs. average strain plots for sections N1 and N2 are presented in this section. The characteristics of these plots were the similar for the mirror sections (S1 and S2) on the south side of the specimens. The recorded output from all the instruments can be found in Appendix D. Further discussion on the measured strain response is presented in Chapter 8.

The average measured strains were calculated using the readings from gages that were giving reliable outputs up to a specific load during the test. In some cases, the strain gages registered readings that were no longer reliable during the test so the outputs from these instruments were eliminated in the calculations. Strain gage debonding or wires being damaged during the test typically caused malfunction of strain gages.

(a) Strain Gage Readings in Specimen FS-1

Load vs. strain plots for sections N1 and N2 are presented in Figures 7.23 and 7.24, respectively. These figures show the average measured strains on the reinforcing steel (#6 bars), on the CFRP pultruded plates, and on the concrete slab.

Figure 7.23(a) shows an increase in strain under constant load during cycling at load stage 2 (34 kip). This is due to the accumulation of plastic strains after reinforcement yielding. On the other hand, the average measured strains on the CFRP plates and concrete slab (parts (b) and (c)) remain approximately constant during cycling to 34 kip. Examination of Figure 7.24 indicates that the reinforcement did not yield at section N2. The measured strain on the reinforcement exhibits linear behavior until failure of the specimen.

The average measured strains on the CFRP plates are shown in part (b) of Figures 7.23 and 7.24 for sections N1 and N2, respectively. A comparison among the strains at sections N1 and N2 shows an interesting aspect of the behavior at the load corresponding to CFRP-plate debonding. It can be observed that as the plates began debonding at section N1 (Figure 7.23), the measured strains started to decrease. During CFRP-plate debonding, the measured strains decreased because deformations were distributed over a longer length of the plate. At the same time, measured strains in section N2 increased significantly without an increase in load as debonding approached this section. The average CFRP measured strains at both sections are similar just prior to total debonding of the composite plates.

The maximum average strain measured at section N1 on the concrete slab was approximately 0.0025 at debonding of the CFRP plates. This strain is below the value usually assumed as the maximum usable strain associated with concrete crushing (ε_{cu} = 0.003). Because of this, Specimen FS-1 was able to maintain its bare reinforced concrete strength after CFRP-plate debonding without collapsing.

(b) Strain Gage Readings in Specimen FS-2

The average measured strains on the reinforcing bars, CFRP sheets, and concrete surface are presented in Figures 7.25 and 7.26 for sections N1 and N2, respectively. The measured strains on the reinforcement at section N1 show a very large accumulation of plastic strains after cycling to 34 kip. This can be the consequence of a crack forming close to the instrument location. The reinforcing bar strains at section N2

remain fairly constant during cycling to 34 kip indicating that yielding did not reach this section (Figure 7.26).

Strains on the CFRP sheets are presented in part (b) of Figures 7.25 and 7.26. The large reduction in slope at a load of approximately 25 kip at section N2 is attributable to specimen cracking. This change in slope is also observed in the reinforcing bar strain curve.

The maximum average strain measured on the concrete slab at section N1 before CFRP-sheet debonding was approximately 0.0024. As for Specimen FS-1, this strain is below the assumed maximum usable concrete strain of 0.003.

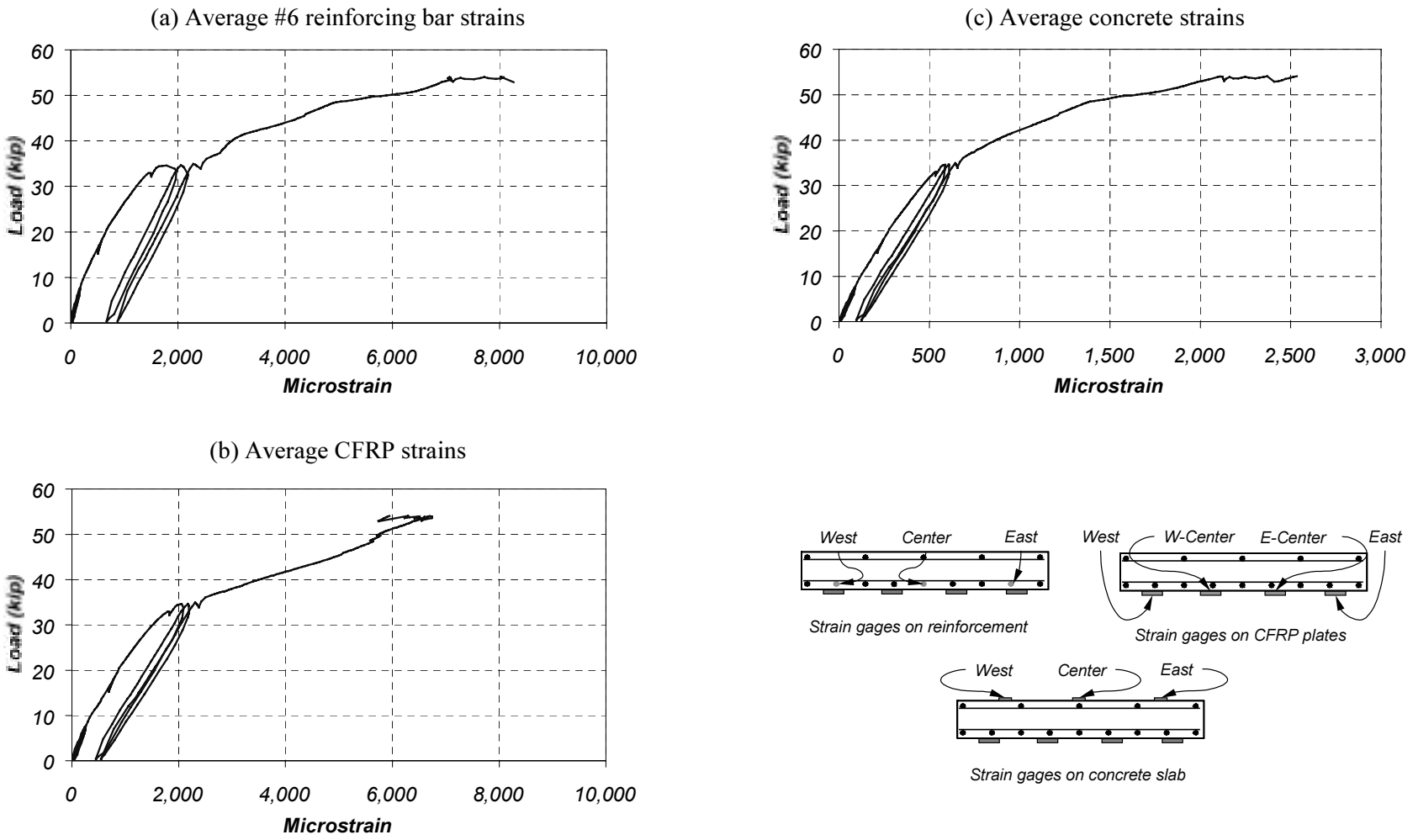

Figure 7.23 Average Strains Measured at Section N1 (Specimen FS-1)

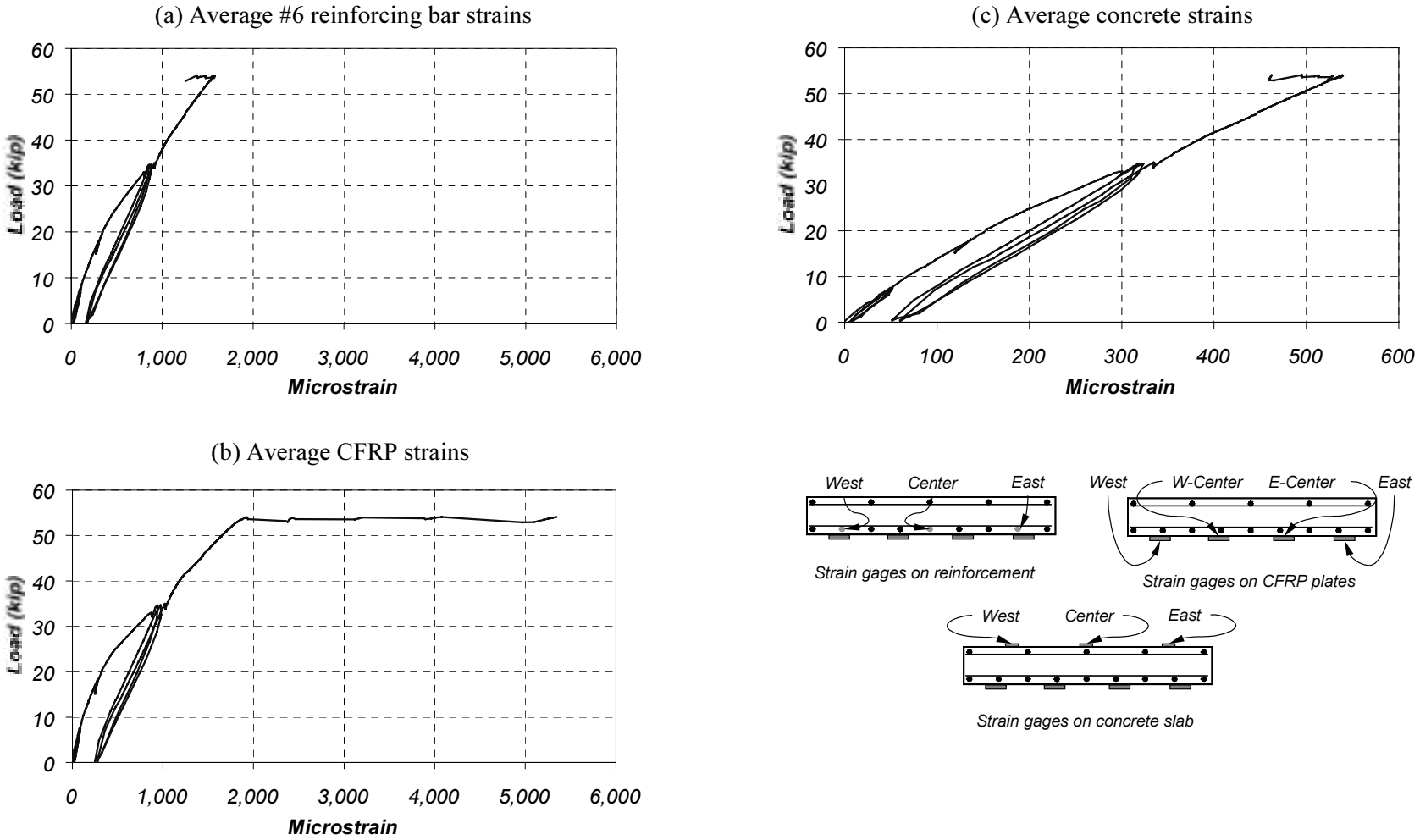

Figure 7.24 Average Strains Measured at Section N2 (Specimen FS-1)

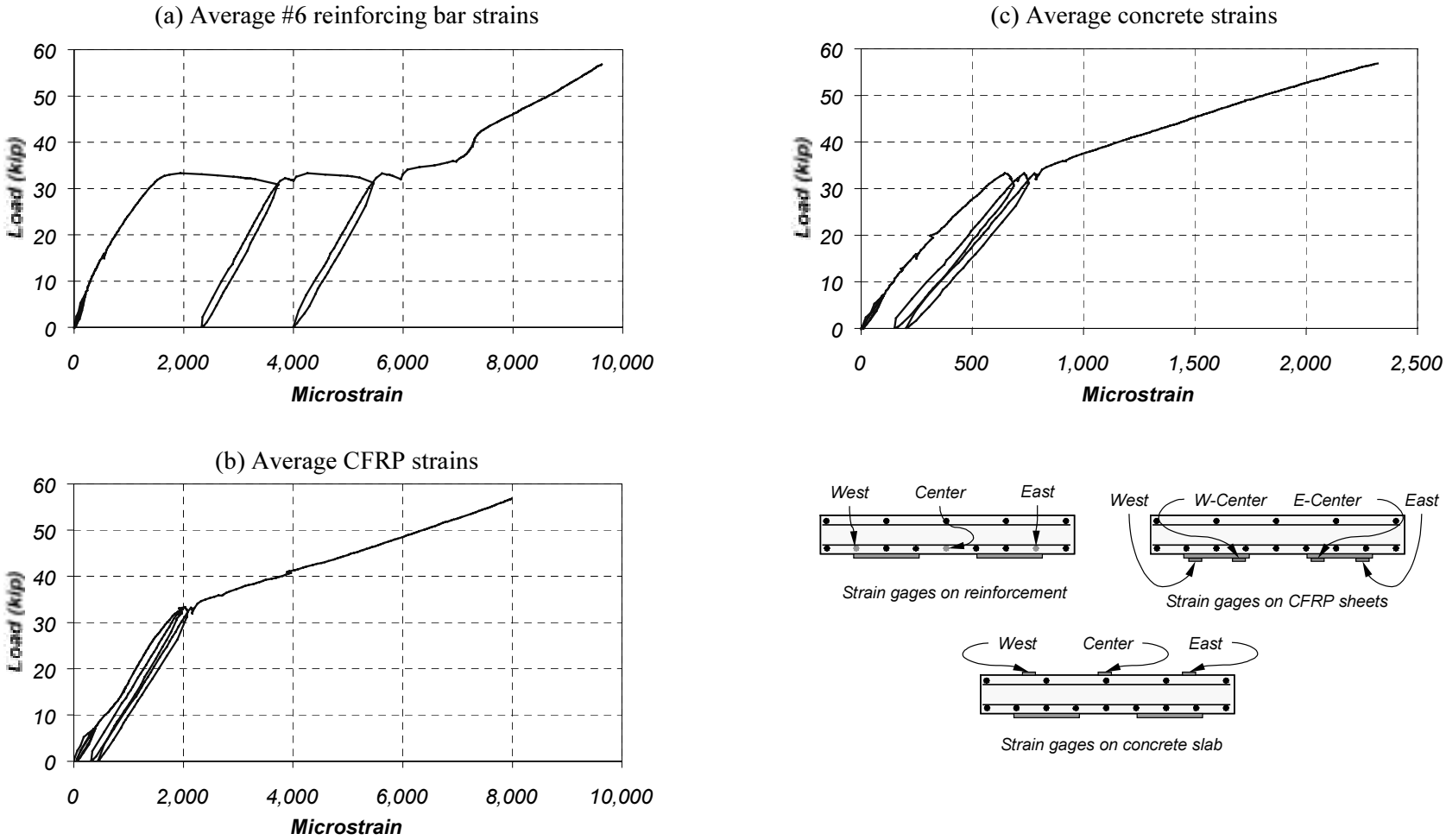

Figure 7.25 Average Strains Measured at Section N1 (Specimen FS-2)

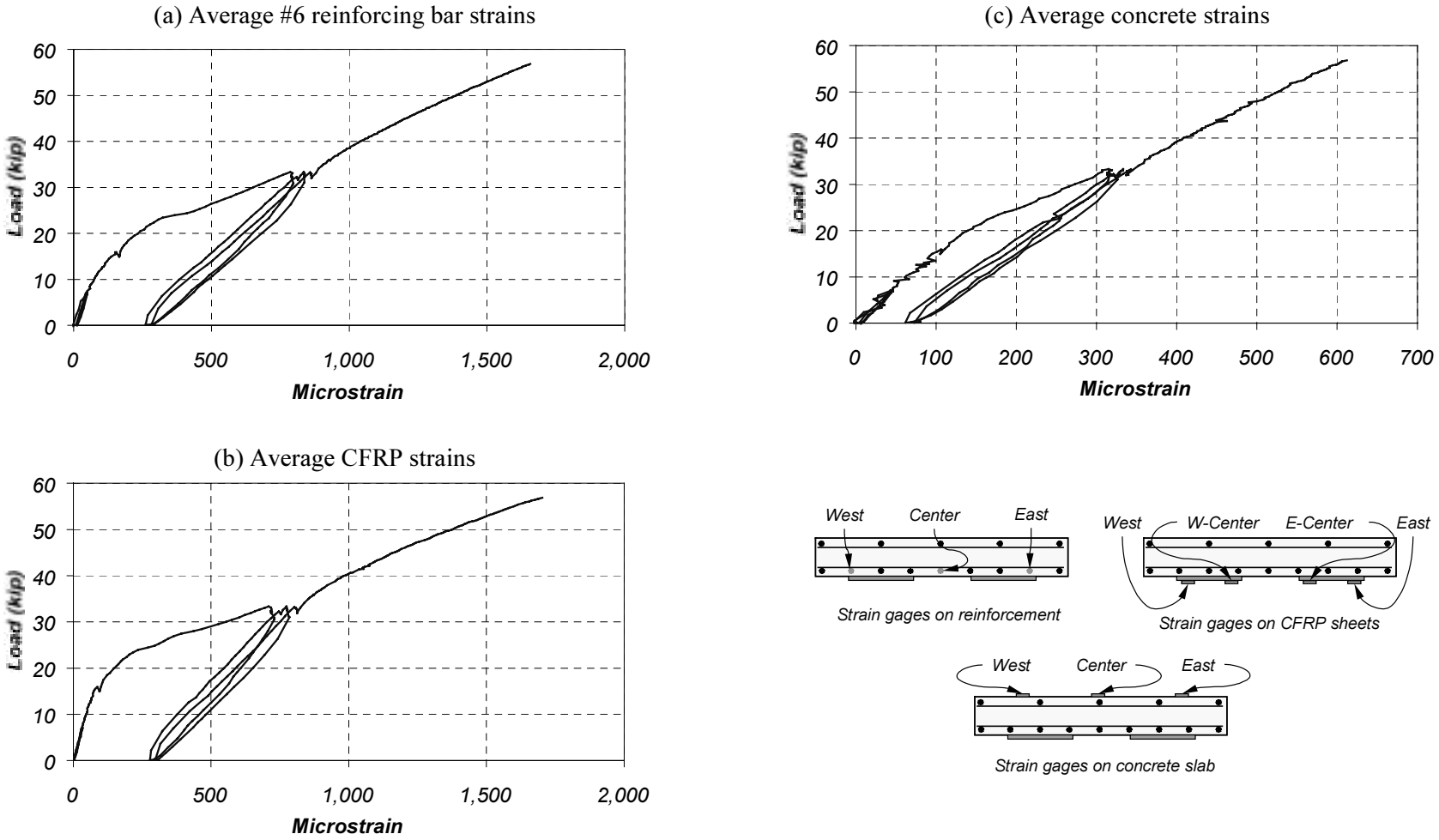

Figure 7.26 Average Strains Measured at Section N2 (Specimen FS-2)

7.5 SUMMARY

A description of the laboratory tests of two full-scale flat-slab specimens strengthened using different CFRP composite systems was presented in this chapter. The experimental setup, loading sequence, and test specimen instrumentation were also described. The specimen behavior and the failure sequence that were observed during the tests were discussed.

Representative outputs from instruments attached to the laboratory specimens were presented and discussed. These included the displacement and strain response of the specimens during testing. An evaluation of the measured response parameters of the flat-slab specimens is presented in Chapter 8.

Chapter 8: Verification of the Analytical Model Using the Measured Response of the Flat-Slab Specimens

8.1 INTRODUCTION

The analytical model described by Breña et al. [2001] in Chapter 3, including the refinements presented in Chapter 2, is verified in this chapter by comparing the strains, curvatures, and displacements with the measured response of specimens FS-1 and FS-2. Strains are discussed in Section 8.2, and moment-curvature response is presented in Section 8.3. Data from both of these sections may be used to evaluate the strain at which the CFRP composites debond from the surface of the concrete. This information is needed to calculate the capacity of reinforced concrete members strengthened using CFRP composites. Displacement response is evaluated in Section 8.4. In general, the analytical models are able to represent the measured global response quite well; however, some aspects of the local behavior were not well represented.

8.2 EVALUATION OF STRAIN RESPONSE

The same approach that was used for the pan-girder specimens was used for the flat-slab specimens to validate the analytical procedures developed in this research project. Therefore, a detailed comparison of the calculated and measured strains was also conducted as a first step for these specimens.

Strains were measured on the reinforcing bars, on the top surface of the concrete, and on the surface of the CFRP composites during testing of specimens FS-1 and FS-2. Measured data were presented in Chapter 7 and Appendix C, and those data are compared with the calculated response of the test specimens in this section. Strains due to dead loads are evaluated in Section 8.2.1, and the variations of strain with distance from the neutral axis are discussed in Section 8.2.2. Calculated and measured strains in each of the three materials are compared in Section 8.2.3, and the strains at which the CFRP composites debonded from the surface of the concrete are evaluated in Section 8.2.4.

8.2.1 Strains Due to Dead Loads

As for the pan-girder specimens, the strains caused by dead loads were calculated for the flat-slab specimens. Inclusion of dead-load strains was particularly important in this case because their effect was anticipated to have a greater impact on the response of these specimens due to the thinner cross section.

The dead-load moment was calculated by assuming a unit weight of concrete equal to 150 pcf and a span of 24 ft. The measured material properties (Appendix A) were used in these calculations. The calculated dead-load strains are reported in Table 8.1.

Table 8.1 Calculated Dead Load Strains

Specimen	M_{DL}, kip-ft	Strains, Microstrain		Curvature, 1/in.	NA Depth, in.
		Concrete	Steel		
FS-1	57.8	196	538	7.7×10^{-5}	2.55
FS-2	57.8	210	470	6.9×10^{-5}	3.05

8.2.2 Measured Strain Profiles Due to Live Loads

Measured strain profiles at sections N1 and S1 are shown in Figure 8.1 for Specimen FS-1. Similar plots are shown in Figure 8.2 for Specimen FS-2. The average strain in each material at each stage of loading is plotted as a function of the distance from the top of the specimen to the gage. Strain data for two additional load levels (20 and 50 kip) were also included to provide more information for applied load levels between the critical load stages.

The strains in the two specimens were similar at these sections. The strain profiles were approximately linear up to yielding of the reinforcement (load stage 3). At the higher load levels, the strains in the CFRP composites tended to be lower than those expected using a linear distribution of strain. Debonding of the CFRP composites from the surface of the concrete would tend to reduce the measured strains, because the CFRP composite deformations are distributed over a longer length. The measured response is similar to the response observed for the pan-girder specimens.

8.2.3 Comparison of Measured and Calculated Strains Due to Live Loads

The live-load strains in each of the materials were calculated to provide a direct comparison with the measured strain response. These were calculated using the analytical procedures in Chapter 2. The same procedure that was used for the pan-girder specimens was used in the flat-slab specimens to calculate the internal moment from the calculated strains in each of the materials. The internal moment was related to the applied load using the clear span of the beam equal to 24 ft and the dead loads described in Section 8.2.1. The calculations were based on failure of the CFRP composite by rupture or crushing of the concrete. Debonding of the CFRP composites was not incorporated into the calculations.

Calculated and measured live-load strains are compared in Figure 8.3 through Figure 8.6 for locations under the loading points (sections N1 and S1). The measured steel strains represent the average from readings on three bars, the CFRP strains represent the average of readings from four gages, and the measured concrete strains represent the average of readings from three gages.

In general, the largest difference was in the magnitude of the calculated and measured strains at failure. While failure was caused by composite rupture in the calculated curves, it was always triggered by debonding of the CFRP materials in the laboratory tests. However, at specific load levels, the measured and calculated strains are relatively close for both specimens.

a) Section N1

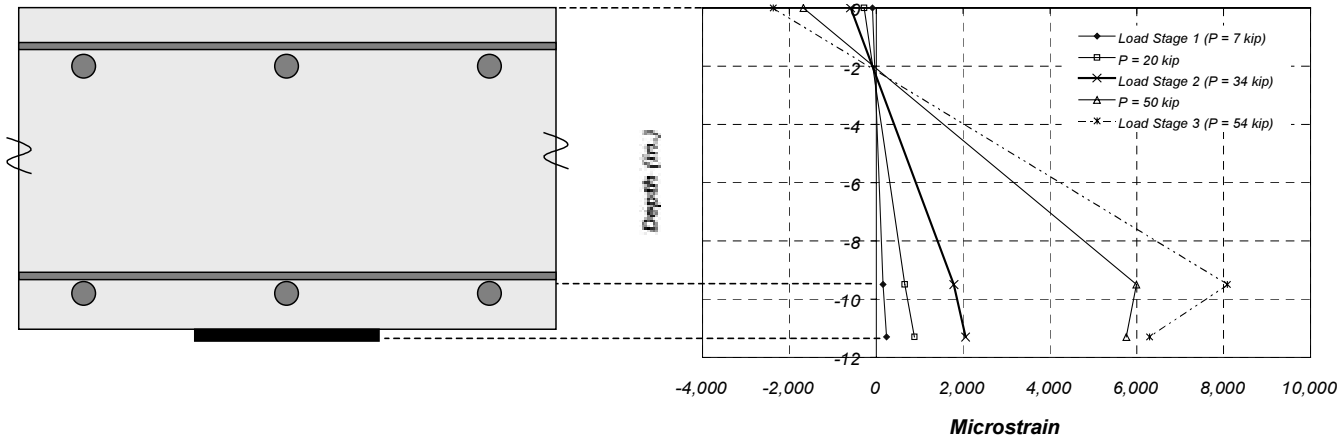

b) Section S1

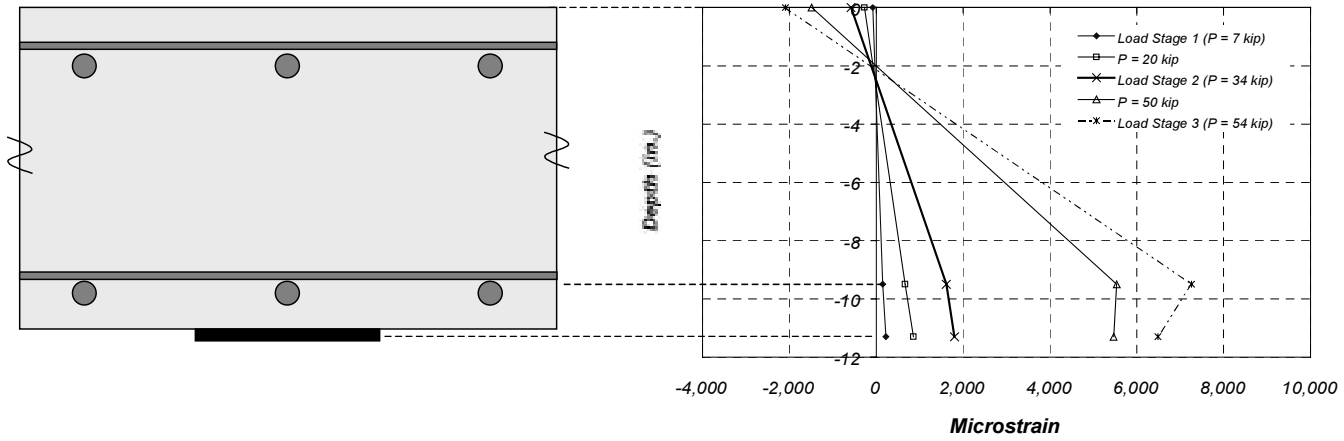

Figure 8.1 Measured Live-Load Strain Profiles in Sections N1 and S1 for Specimen FS-1

a) Section N1

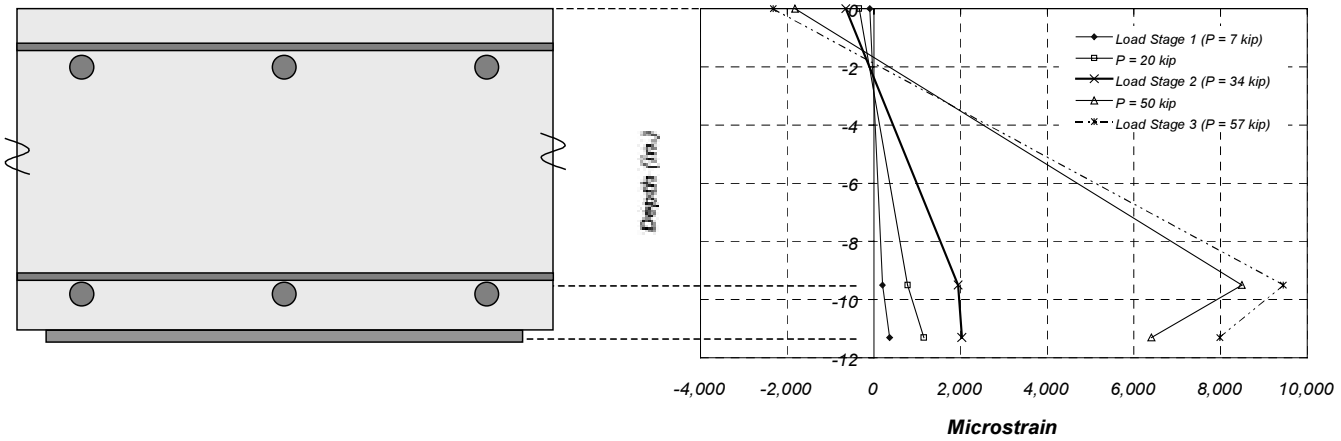

b) Section S1

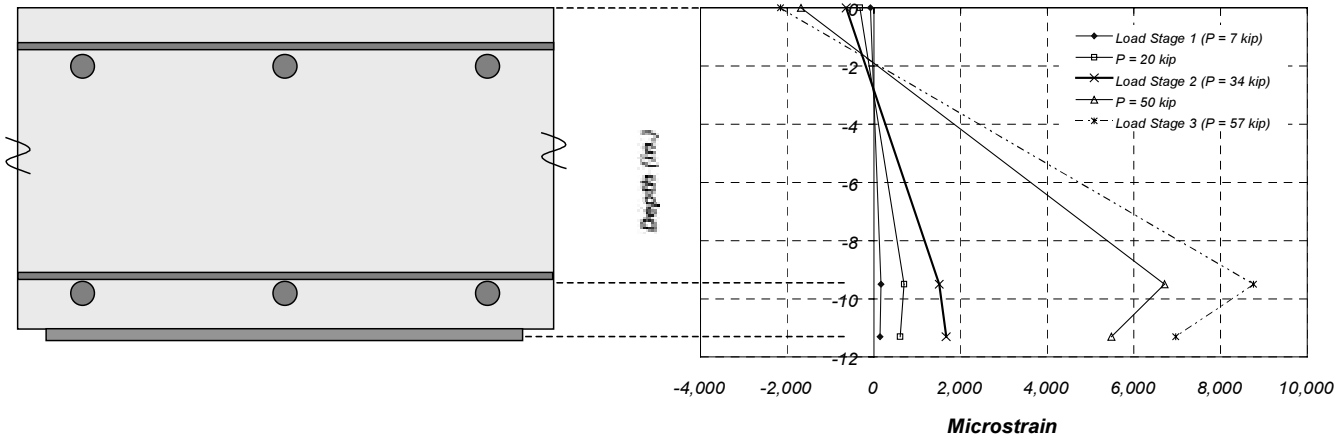

Figure 8.2 Measured Live-Load Strain Profiles in Sections N1 and S1 for Specimen FS-2

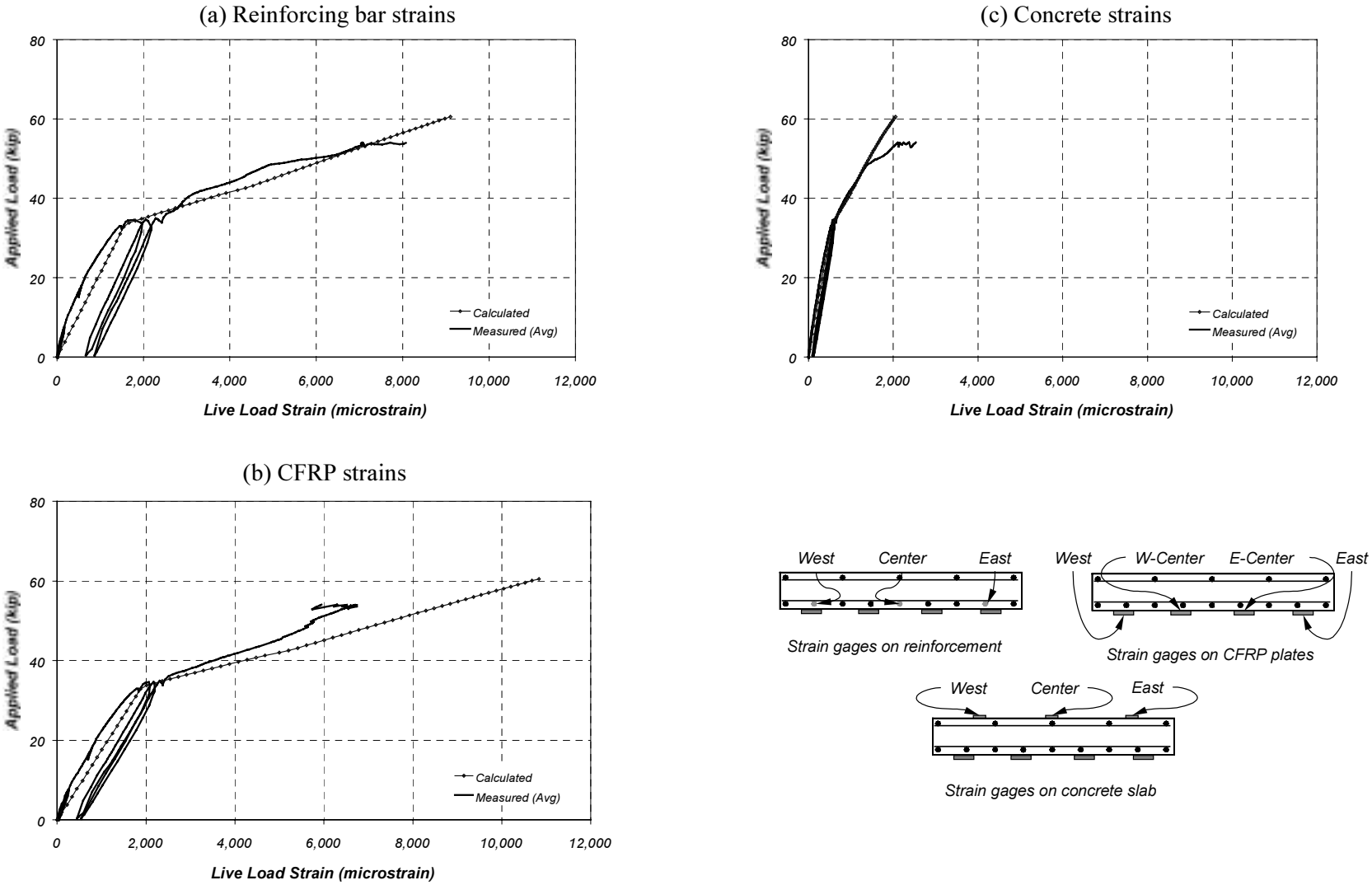

Figure 8.3 Comparison of Measured and Calculated Live-Load Strains at Section N1 (Specimen FS-1)

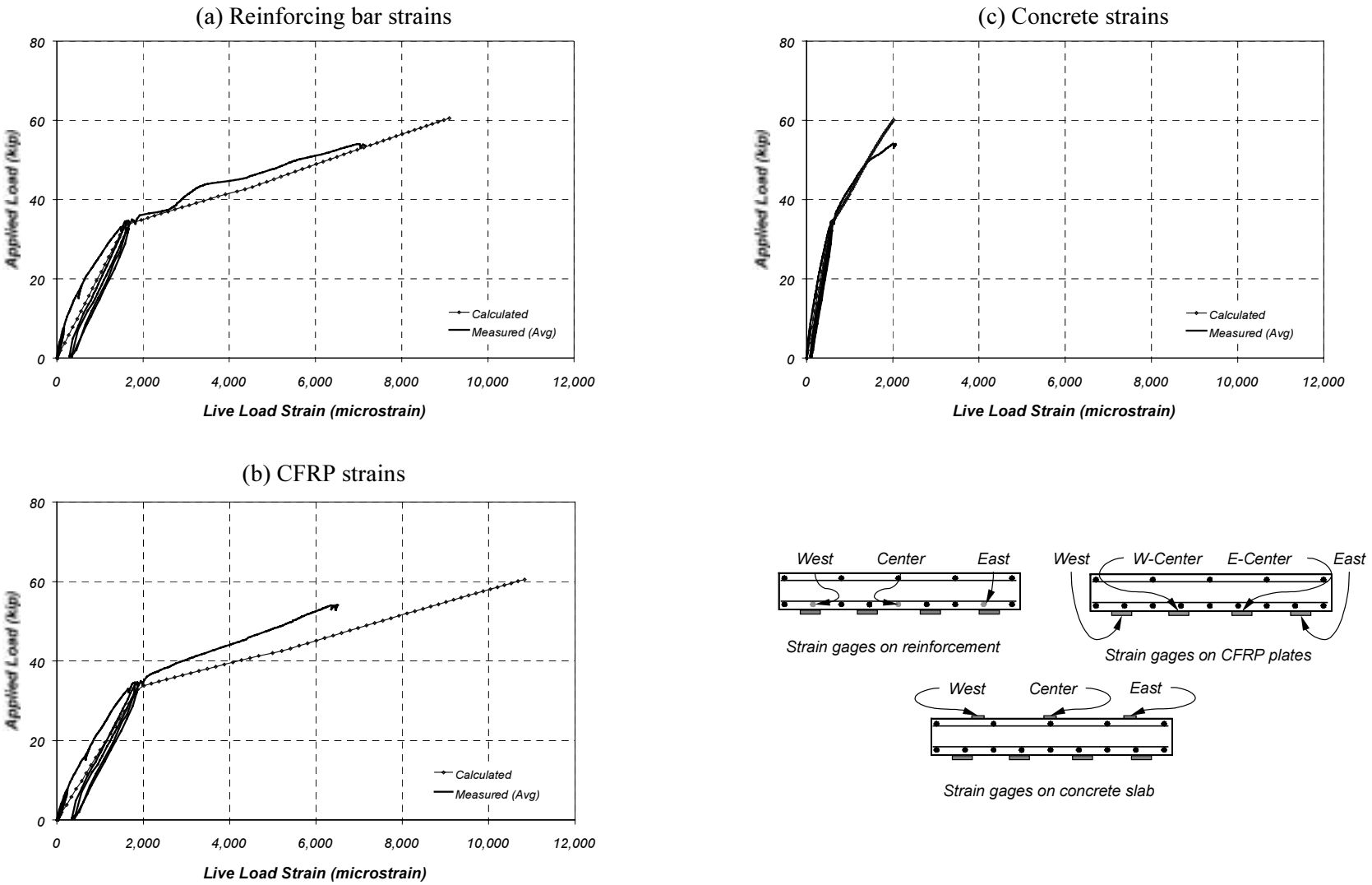

Figure 8.4 Comparison of Measured and Calculated Live-Load Strains at Section S1 (Specimen FS-1)

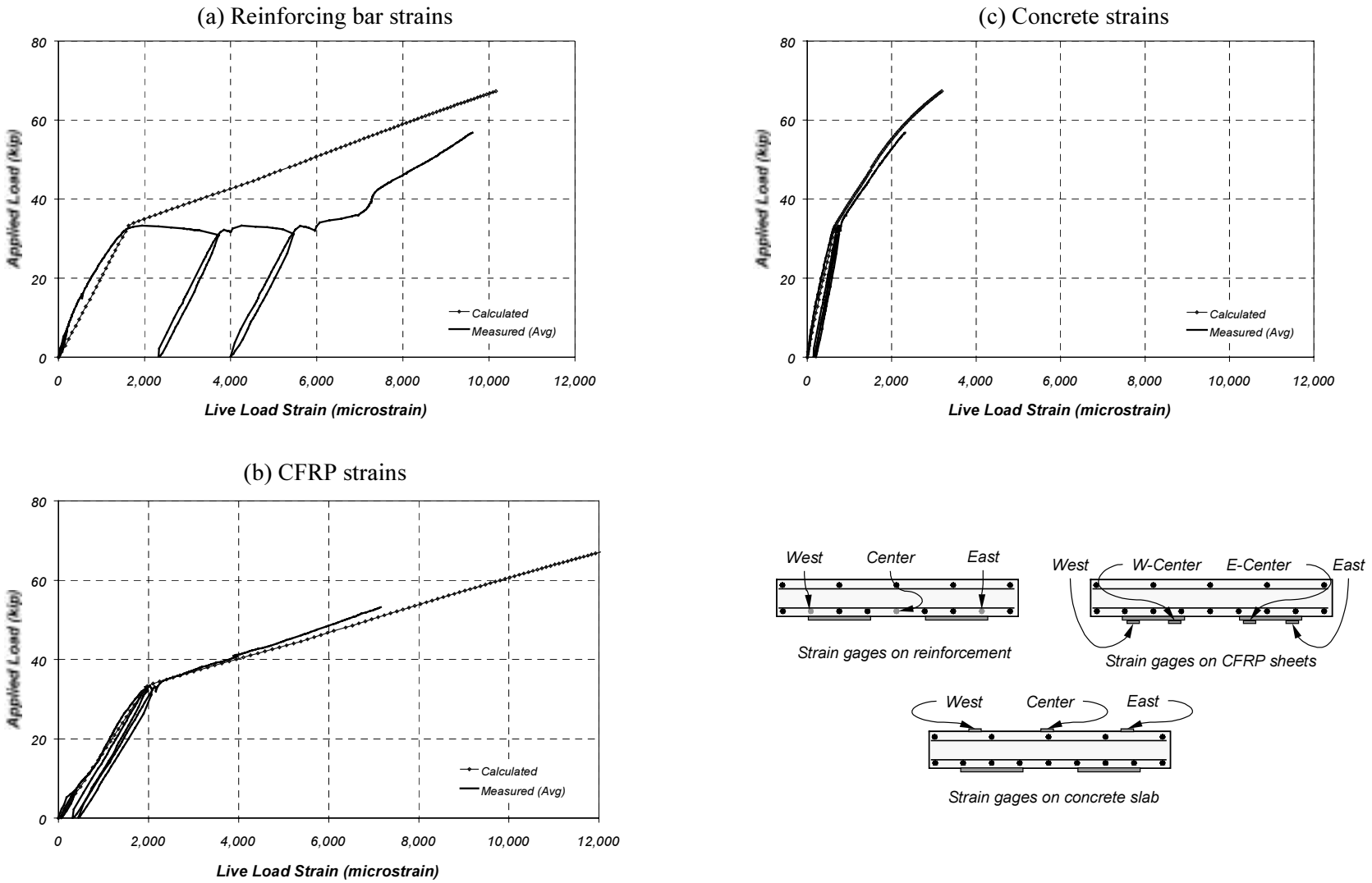

Figure 8.5 Comparison of Measured and Calculated Live-Load Strains at Section N1 (Specimen FS-2)

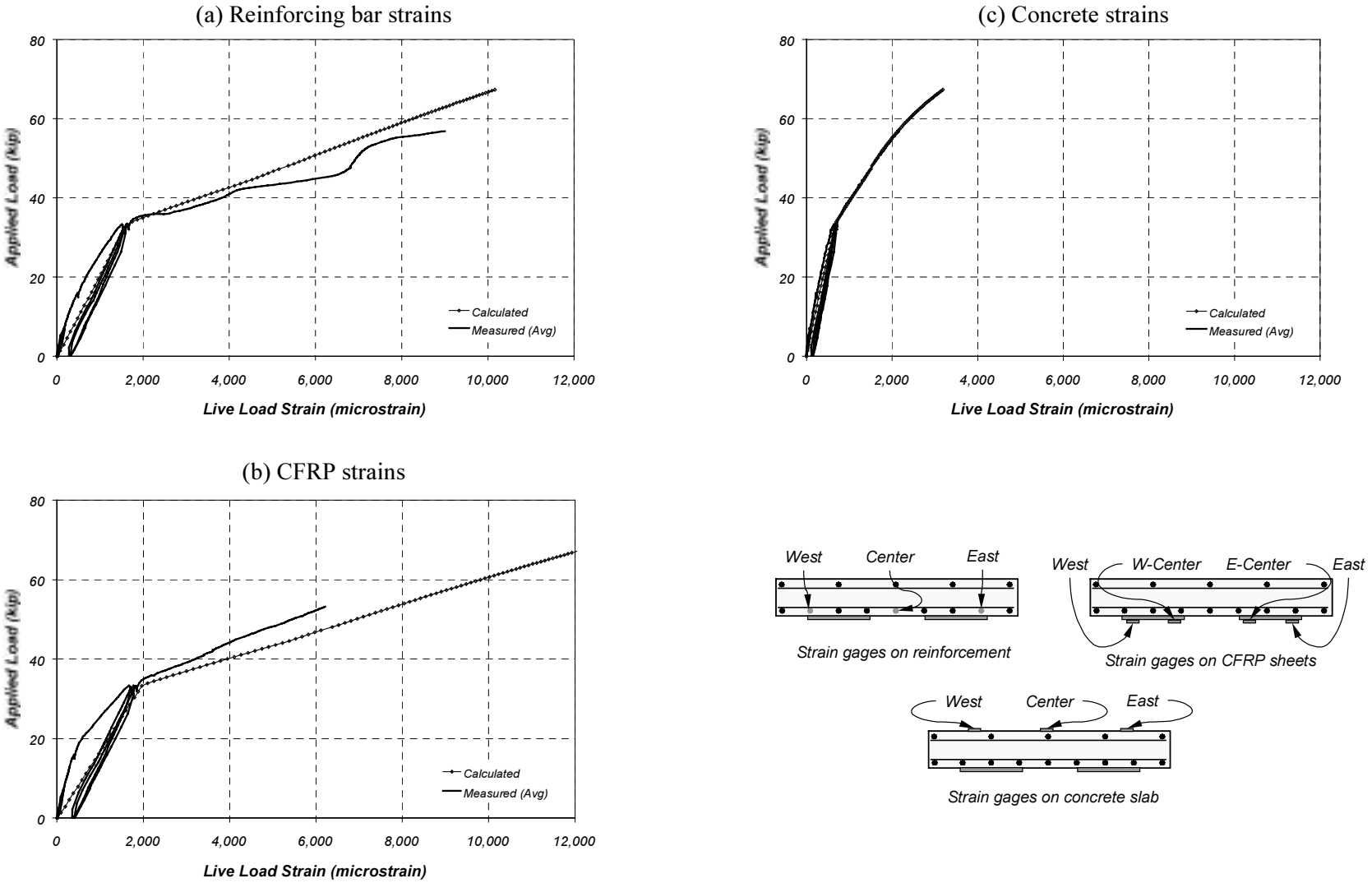

Figure 8.6 Comparison of Measured and Calculated Live-Load Strains at Section S1 (Specimen FS-2)

The trends observed in the comparisons of the calculated strain curves with the measured response are very similar for both sections for specimen FS-1. The calculated and measured steel strains are very close, particularly for low load levels. The general trend of the calculated strains on the steel above the yield load (34 kip) is approximately the same as the measured curves. The irregular shape of the measured curves, especially section N1 in specimen FS-2, is due to the formation of cracks at the location of the gage and concentrated yielding of the reinforcement. These local effects are not well represented by the analytical model, because it is based on a smeared distribution of cracks.

The calculated concrete strains are very close to the measured values for the majority of the response. At load levels above approximately 50 kip, the calculated concrete strains were 1,000 microstrain less than the measured values. At low load levels, the difference is not noticeable in these curves but was less than 50 microstrain for most of the loading sequence.

On the other hand, strains in the CFRP plates were adequately calculated with the analytical model at low load levels, but were overestimated at load levels above yield. The difference in the calculated and measured strains seemed to increase uniformly as loading progressed, reaching a maximum of approximately 1,500 microstrain at failure. Lower measured CFRP strains are consistent with debonding for load levels above yielding. The strains corresponding to debonding of the CFRP are quantified later in this section.

For specimen FS-2, a significant difference is observed for the two sections. The measured CFRP and concrete strains had similar trends as the two sections for specimen FS-1. However, the calculated steel strains are significantly different from the measured values above the yield load for section N1. This difference is clearly due to the accumulation of plastic strains as the specimen was cycled to load stage 3 (yield load). The calculated strains obtained from the analytical model were not able to reproduce this effect because the model is based on a monotonic increase in load to failure. The maximum difference between the measured and calculated strains in this case is about 3,000 microstrain at a load of approximately 40 kip. A comparison of the strains measured at the critical load stages with the calculated strains for specimens FS-1 and FS-2 is presented in Table 8.2 and Table 8.3, respectively.

8.2.4 Measured Strains at which the CFRP Composites Debonded from the Surface of the Concrete

As noted in the previous section, the failure strains in the materials were not well represented by the analytical model, because failure was defined in the analytical model by rupture of the CFRP composites. Both strengthened specimens failed after the CFRP composites debonded from the surface of the concrete, and crushing of the concrete was not observed until later stages of the test when the bare specimens were loaded to failure. The strain at which the composites debonded from the concrete was estimated by comparing the measured strains on the CFRP composites and the strains extrapolated from the measured concrete and reinforcement strains, assuming a linear variation of strain with depth.

Measured envelopes of the CFRP strain curves are shown in Figures 8.7 and 8.8 for specimens FS-1 and FS-2, respectively. The calculated CFRP strain curves depicted in these figures were obtained from the measured concrete and steel strains and projected linearly to the position where the CFRP gages were attached. The difference between the measured and calculated CFRP strain envelopes is also plotted in Figures 8.7 and 8.8.

Table 8.2 Measured and Calculated Live-Load Strains for Specimen FS-1

Load Stage	Load, kip	Steel Strain, microstrain			CFRP Strain, microstrain			Concrete Strain, microstrain		
		Measured		Calculated	Measured		Calculated	Measured		Calculated
		N1	S1		N1	S1		N1	S1	
1B	7	160	152	368	243	224	444	84	77	125
2	34	1,788	1,613	1,960	2,059	1,804	2,363	587	579	636
3	54	4,508	7,433	7,427	5,948	6,510	8,837	2,534	2,117	1,664

Table 8.3 Measured and Calculated Live-Load Strains for Specimen FS-2

Load Stage	Load, kip	Steel Strain, microstrain			CFRP Strain, microstrain			Concrete Strain, microstrain		
		Measured		Calculated	Measured		Calculated	Measured		Calculated
		N1	S1		N1	S1		N1	S1	
1B	7	198	163	407	364	144	488	97	80	144
2	34	1,942	1,509	1,746	2,031	1,669	2,100	647	640	698
3	57	9,620	9,002	7,504	7,982	6,964	8,904	2,321	2,155	2,144

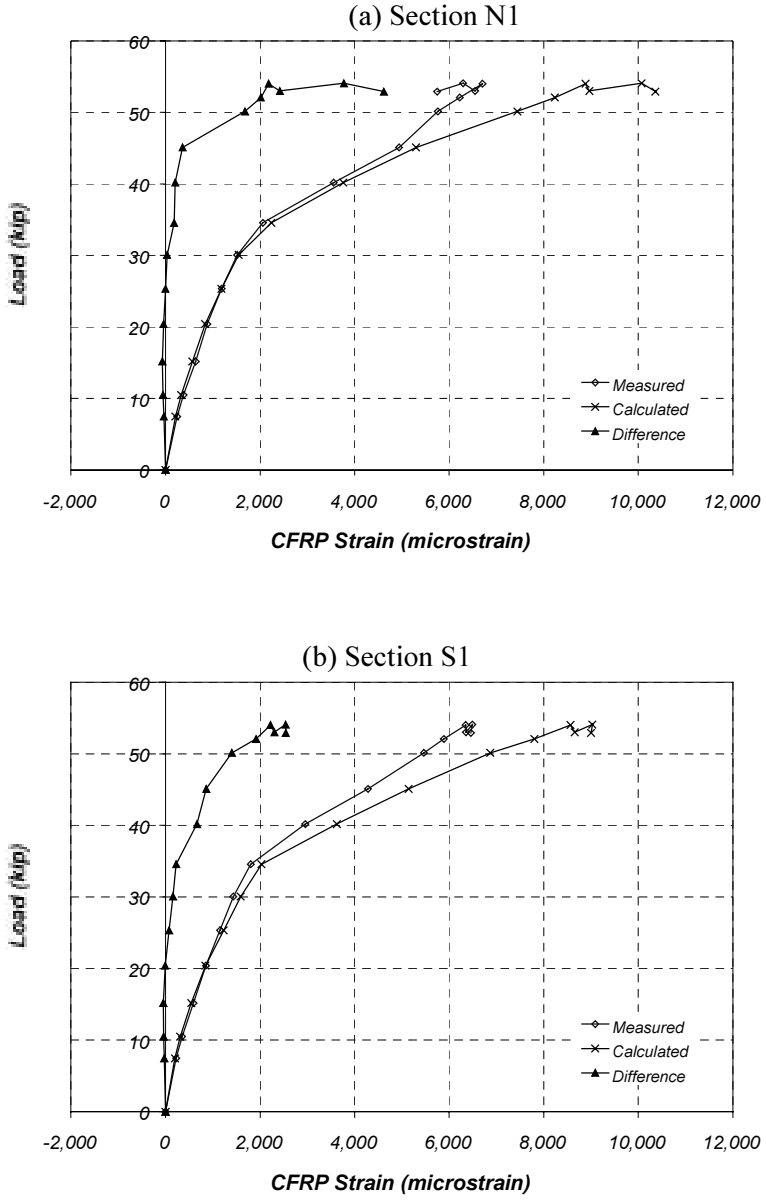

Figure 8.7 Comparison of Measured and Calculated CFRP Strains for Specimen FS-1

(a) Section N1

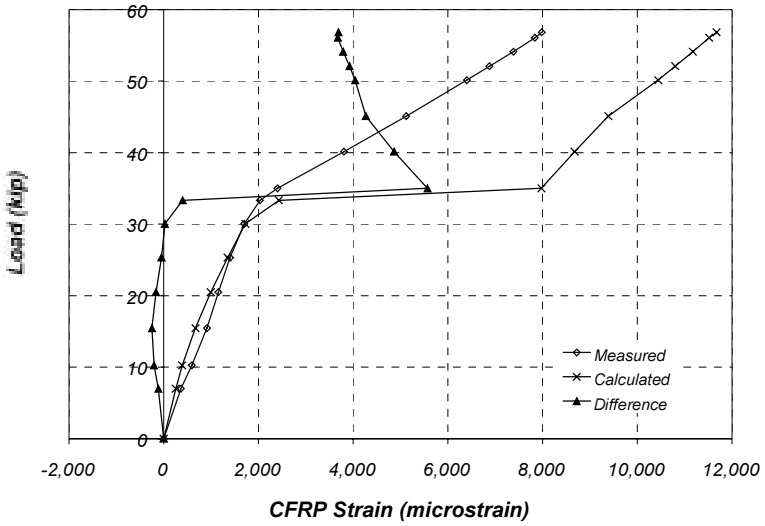

(b) Section S1

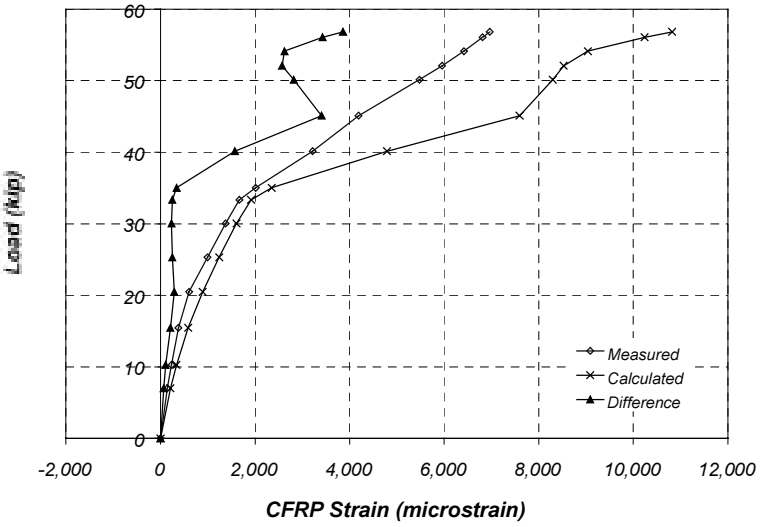

Figure 8.8 Comparison of Measured and Calculated CFRP Strains for Specimen FS-2

For specimen FS-1, the difference in measured and calculated strains increases suddenly at a load of approximately 45 kip. The maximum difference between the measured and calculated CFRP strains was approximately 5,000 microstrain. For section S1, the difference in strains increased gradually for loads above the observed yield load (34 kip). The maximum difference at failure was approximately 3,000 microstrain. The difference between measured and calculated CFRP strains gives an indication that the composites began to debond from the surface of the concrete. A comparison between the strains in sections N1 and S1 for specimen FS-1 indicates that debonding is largely dependent on local surface and cracking conditions. The difference in strains is larger in section N1 than section S1, consistent with the observed progression of debonding of the CFRP plates toward the north end (Chapter 7). The maximum measured CFRP strain at failure was approximately 7,000 microstrain in sections N1 and S1.

For specimen FS-2, the behavior was dramatically different at sections N1 and S1. The effect of the accumulation of plastic strains in the reinforcing steel at section N1 on the calculated CFRP strains is observed in Figure 8.8 (a). This plot indicates that large plastic strains cause the composite to debond locally at the location of cracks. Once the reinforcing bar strains stabilize, the composite strains increase as the cross section deforms until failure. The calculated strains at section S1 also show the effect of reinforcing bar yielding but to a lesser extent. The maximum measured CFRP strain at failure was approximately 8,000 microstrain. Strains in the composites for both flat-slab specimens were approximately equal to the strain value assumed for design (7,000 microstrain).

8.3 EVALUATION OF MOMENT-CURVATURE RESPONSE

The measured strains were used to calculate the relationship between moment and curvature for the test specimens. Moment-curvature response derived from the measured strains is compared with the results of the analytical model in Section 8.3.3.

The procedures used to calculate internal forces and moments from the measured strains were similar to those used in the analytical model. Internal forces were calculated following the same basic steps that were used for the pan-girder specimens (Chapter 5). In the case of the flat-slab specimens, the composites were bonded to the bottom surface of the concrete so the calculation of internal forces followed directly the procedure outlined for specimen J-1 (Section 5.3.1). The only modification was the position of the composites on the cross section. Therefore, the methodology is not repeated in this chapter, and only the results from the calculations are presented.

The calculation of internal forces for specimens FS-1 and FS-2 is presented in two separate sections because the measured strains were significantly different. The discussion of the results for the two specimens needs to be addressed separately because there was a large accumulation of plastic strains in the reinforcement for section N1 in specimen FS-2.

8.3.1 Internal Forces Calculated from Measured Strains for Specimen FS-1

Internal force equilibrium was verified by comparing the total compressive force with the total tensile force at different load levels. The sum of the internal forces in compression is plotted as a function of the sum of the internal forces in tension in Figure 8.9. It can be observed that the sum of the internal compressive forces consistently exceeded the sum of the internal tensile forces, although the difference remained fairly constant below the observed yield load. Above yielding, the differences between the compressive forces and tensile forces increased at a higher rate.

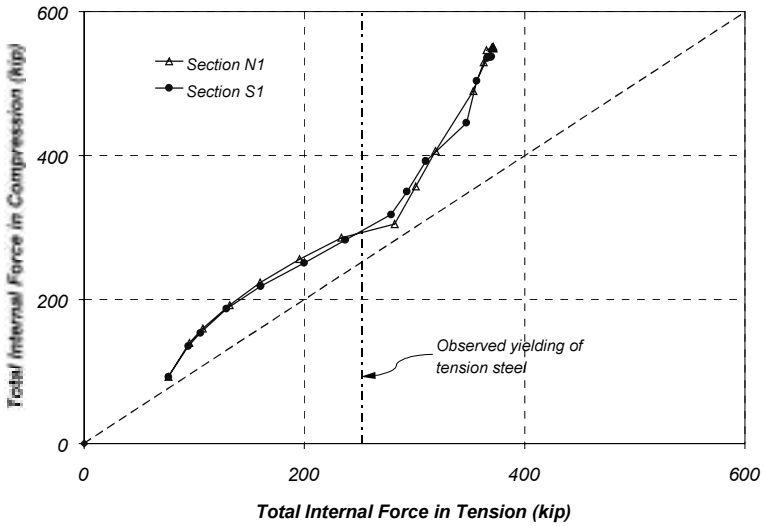

Figure 8.9 Internal Force Resultants for Specimen FS-1

The factors that could have affected the readings used to obtain the tensile and compressive forces on the cross section were discussed in Section 5.3.1. Local perturbations at the sections of applied load, distance from the gage to cracks on the concrete surface, and bending of the reinforcement at large deformation levels could have affected the gage readings at different load levels.

To be consistent with the approach used for the pan-girder specimens, the neutral axis position was shifted to achieve equilibrium of internal forces. This procedure was based on revising the value of the concrete strains and using the measured strains in the reinforcement to define the neutral axis depth that satisfied equilibrium. The methodology is described in detail in Chapter 5.

The revised peak compressive strain is compared with the measured peak compressive strain in Figure 8.10. The differences in strain tended to increase as the applied load increased, and reached a maximum at failure. However, the revised neutral axis depth was modified less than 20% from the measured depth throughout the test to achieve equilibrium, except after the failure sequence initiated (Figure 8.11). The revised values of strain and neutral axis depth were used in the subsequent calculations.

The normalized tensile force components in the cross section are plotted as a function of the ratio of the applied load to the yield load in Figure 8.12. The contribution of the concrete to the total tensile force represented approximately 18% of the total tensile force and decreased constantly to almost zero at a load equal to the observed yield load. At the same time, the CFRP plates increased steadily up to the yield load and the reinforcing steel contribution remained fairly constant at about 85% up to this load level. After yielding, the portion of the total internal tensile force carried by the CFRP plate increased at a higher rate until failure. Prior to failure, the contribution of the reinforcing steel was close to 75% and the contribution of the CFRP composite was approximately 25%.

(a) Section N1

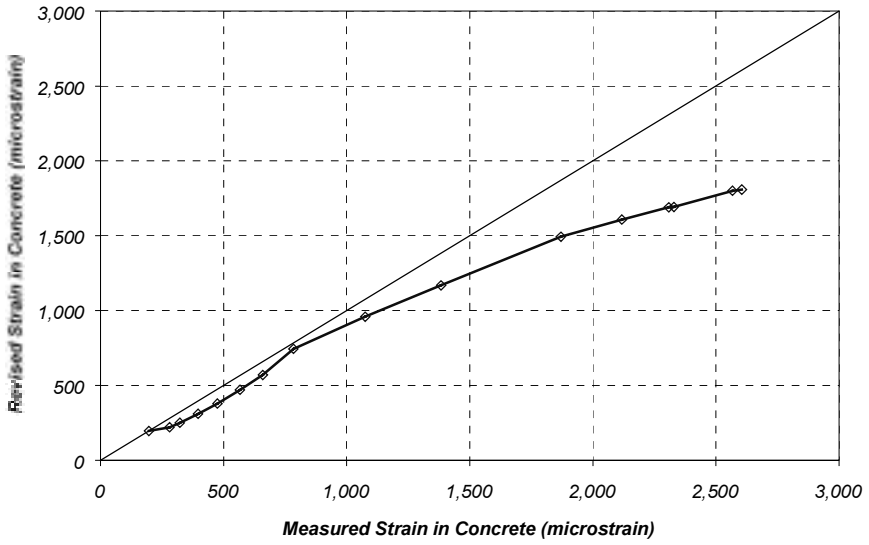

(b) Section S1

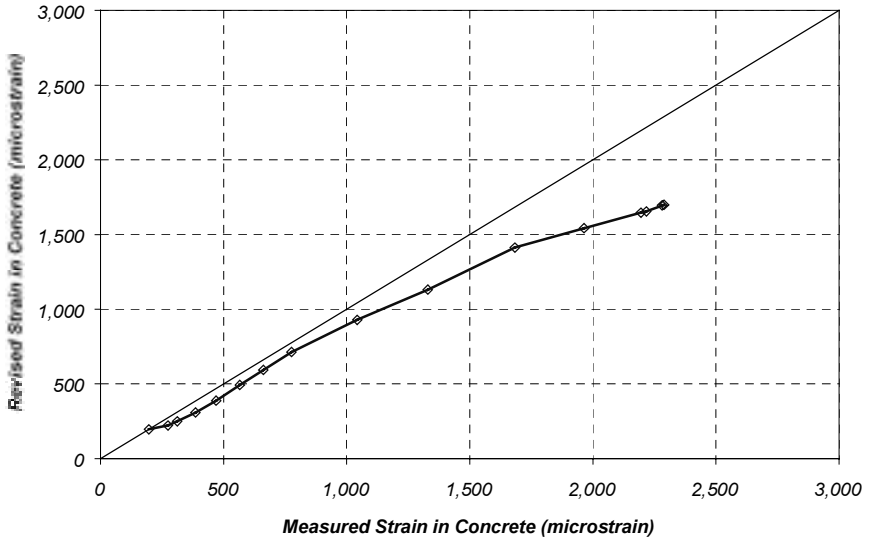

Figure 8.10 Comparison of Revised and Measured Peak Compressive Strains for Specimen FS-1

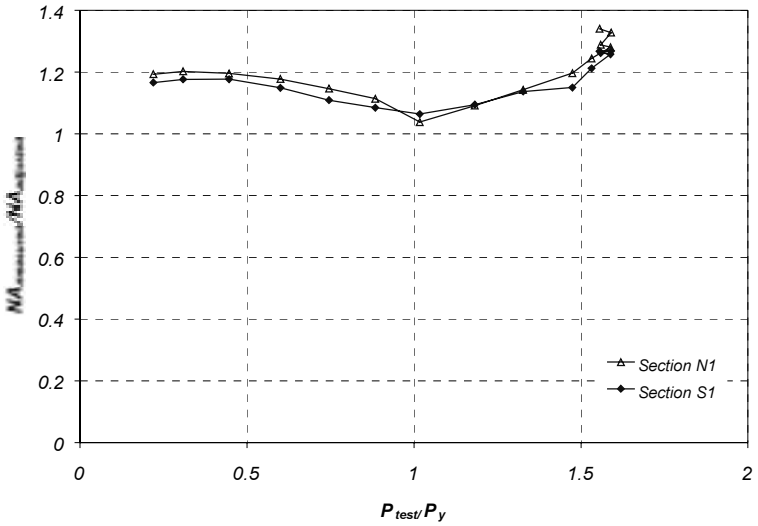

Figure 8.11 Comparison of Neutral Axis Depth from Revised and Measured Strain Profiles

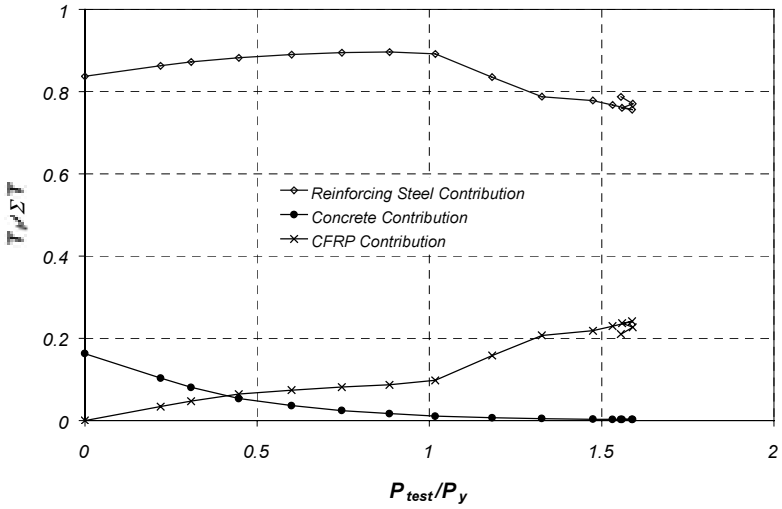

Figure 8.12 Variation of Tensile Force Components at Section N1 for Specimen FS-1

8.3.2 Internal Forces Calculated from Measured Strains for Specimen FS-2

Internal forces were calculated in specimen FS-2 as described in Section 5.3.1. A comparison of the total internal compressive force and the total tensile force for Specimen FS-2 is shown in Figure 8.13. Below yielding of the reinforcing steel, the total internal compressive force exceeded total internal tensile force. However, unlike the distribution of internal forces of specimen FS-1, tensile forces either exceeded or were nearly equal to the compressive forces at load levels. The large drop in the total compressive force is probably caused by the reduction of the neutral axis depth as plastic strains were accumulated during the cycles at yield load. This effect is more pronounced in section N1, consistent with the observation of accumulation of plastic strains shown in Figure 8.5(a). To be consistent, however, the neutral axis depth was adjusted to satisfy force equilibrium using the same approach presented for specimen FS-1 and the pan-girder specimens.

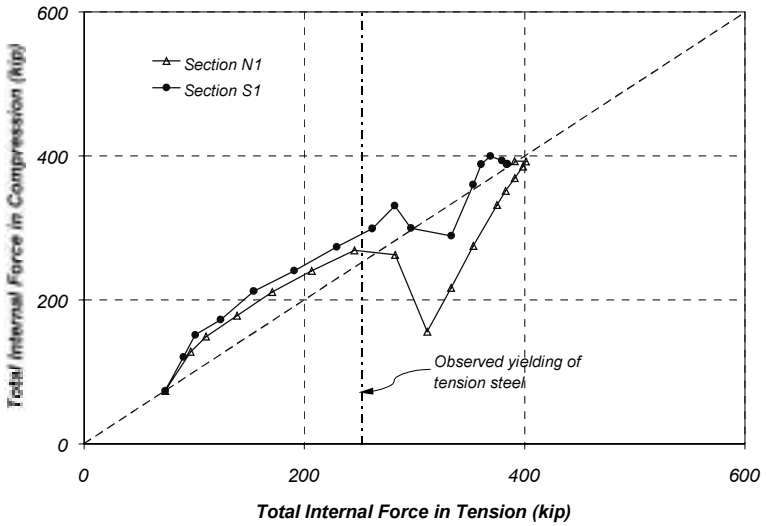

Figure 8.13 Internal Force Resultants for Specimen FS-2

Figure 8.14 shows the revised peak compressive strains as a function of measured peak compressive strains in the concrete. The largest difference between measured and revised strains is approximately 500 microstrain in section N1. Only minor adjustments were required in section S1 throughout the loading history. A comparison between sections N1 and S1 reveals that the change in magnitude of the concrete strains required to reach equilibrium was different at sections that were subjected to the same applied moment, supporting the observation that strain readings are largely influenced by local conditions occurring at each section.

The change in neutral axis position required to achieve internal force equilibrium is presented in Figure 8.15. The maximum change that was required was within 20% of the measured value calculated from the measured strain data, except at the observed yield load. Typically, the change in neutral axis depth was approximately 10% throughout the loading sequence.

The distribution of the total internal tensile force among the different force components at different load stages is illustrated in Figure 8.16. The trends are very similar to those observed in Specimen FS-1. Prior to failure, the CFRP composites contributed in approximately 30% to the total tensile force, while the reinforcing steel contributed approximately 70%. The contribution of concrete to the total tensile force was negligible at load levels above the yield load.

(a) Section N1

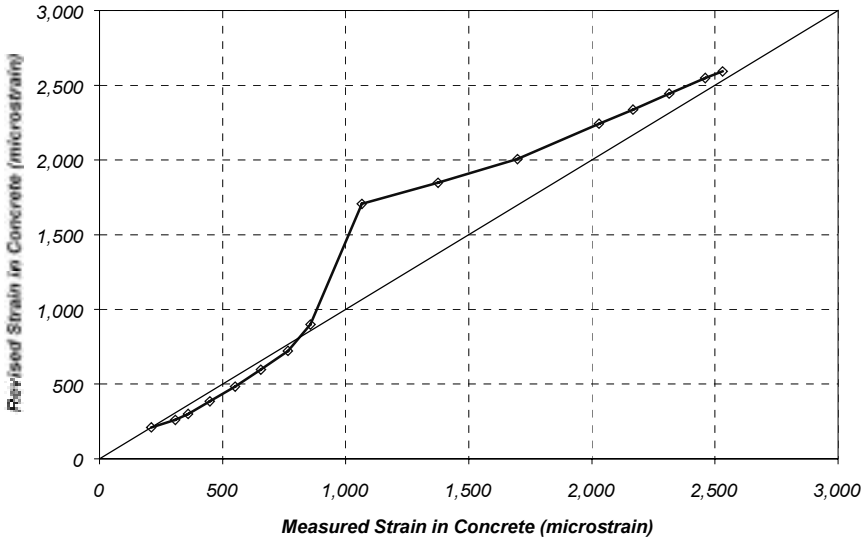

(b) Section S1

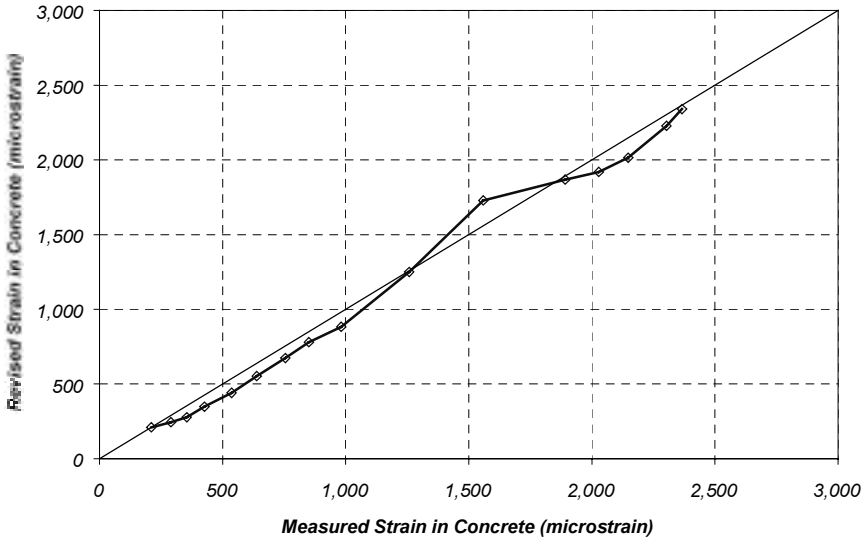

Figure 8.14 Comparison of Revised and Measured Peak Compressive Strains for Specimen FS-2

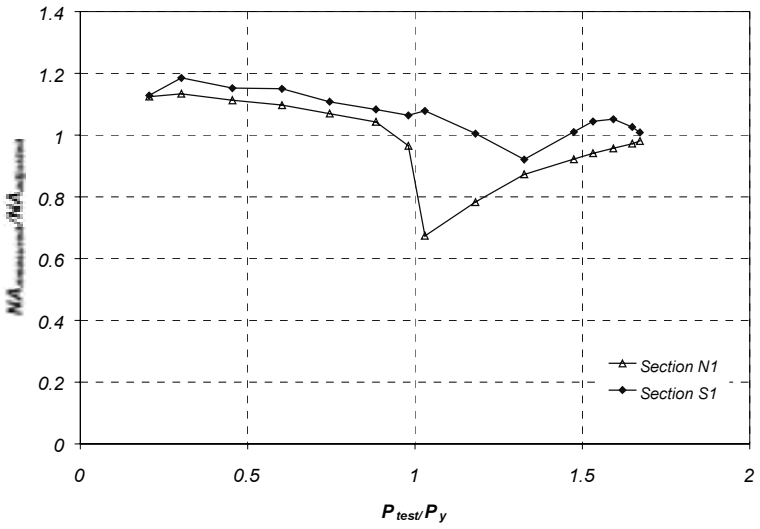

Figure 8.15 Comparison of Neutral Axis Depth from Revised and Measured Strain Profiles

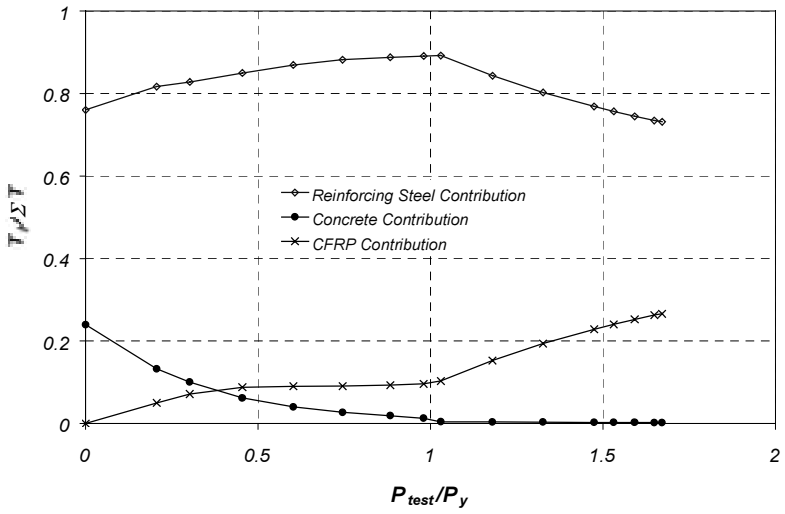

Figure 8.16 Contribution of the CFRP Sheets to the Total Internal Moment at Section N1 for Specimen FS-2

8.3.3 Moment-Curvature Response

Internal moments and curvature were calculated in both specimens using the internal forces that satisfied equilibrium. The moment and curvature corresponding to dead loads (Table 8.1) were then subtracted from each of the calculated values to obtain the relationship between moment and curvature for the applied loads. This response is compared with the results from the analytical model in Figure 8.17 and Figure 8.18 for specimens FS-1 and FS-2, respectively. Debonding was not included in the analytical model at this point.

(a) Section N1

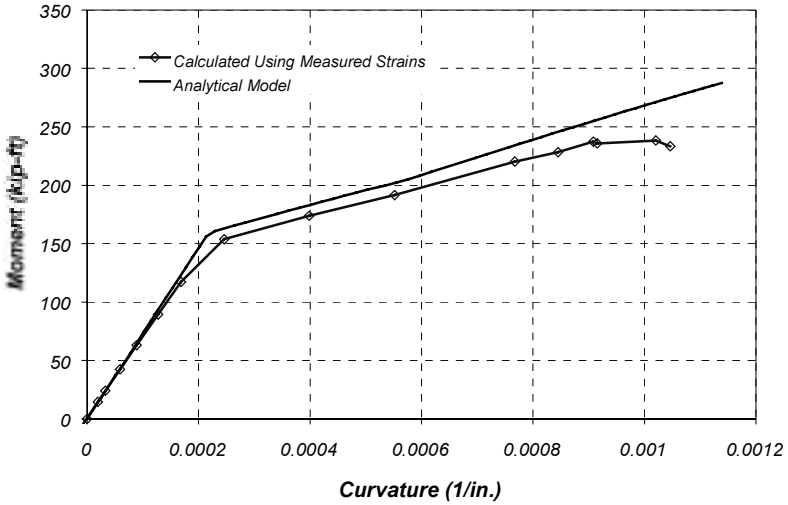

(b) Section S1

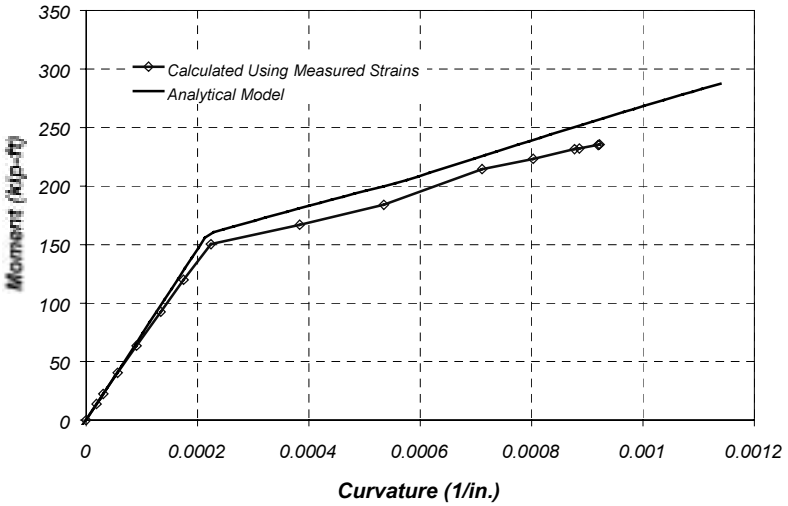

Figure 8.17 Comparison of Measured and Calculated Moment-Curvature Response for Specimen FS-1

(a) Section N1

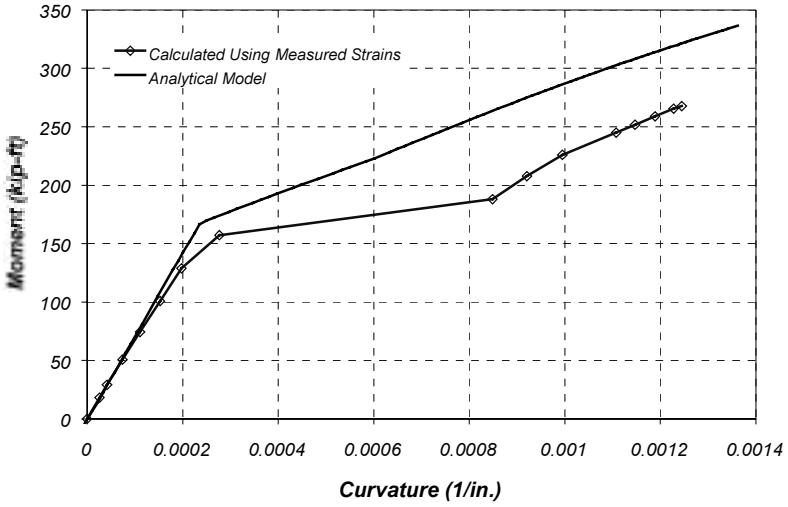

(b) Section S1

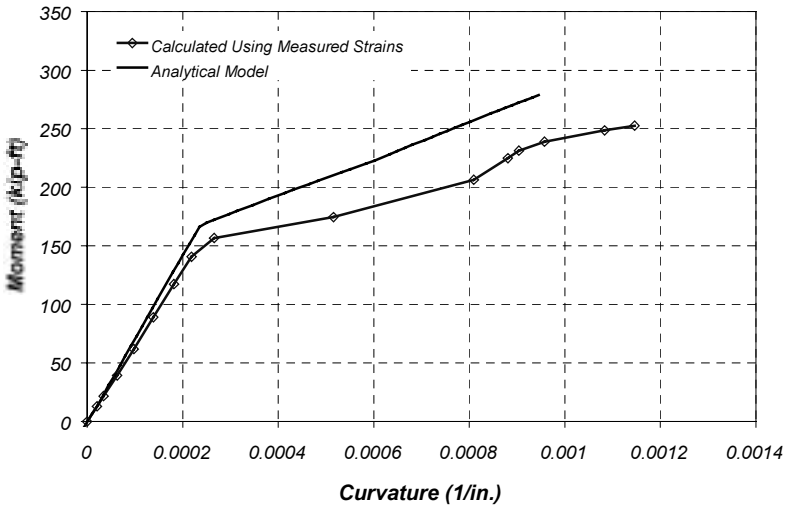

Figure 8.18 Comparison of Measured and Calculated Moment-Curvature Response for Specimen FS-2

The moment-curvature response calculated from the measured strains is well represented by the results of the analytical model. The trends obtained from the analytical model and the measured data were similar for specimen FS-1. At the same moment, the curvature inferred from the measured strains tended to be slightly higher than the calculated curvature, but the differences were small. The calculated curvature capacity was larger than the curvature obtained from measured strains at both sections.

In contrast curvatures obtained from measured strains were much larger than the calculated values using the analytical model for specimen FS-2, particularly at load levels above the yield load. This again was caused by the inability of the model to account for the accumulation of plastic strains in the reinforcement after cycling to yield. However, the prototype bridges are not expected to yield, much less experience cycles of large inelastic deformations during their service life. Therefore, the analytical model should be adequate to calculate the response in these cases.

8.3.4 Comparison of Internal and External Moments

The applied load is plotted as a function of the maximum internal moment due to live load obtained from the measured strains in Figure 8.19. Also shown in the figure is the external midspan moment determined from static equilibrium with a span equal to 24 ft. Both specimens exhibited the same general response. The internal moment at the two instrumented sections was consistently smaller than the external moment at low load levels. The difference between internal and external moments decreased at load levels above yielding, but the internal moment was never equal to the external moment in three out of the four sections. Only the internal moment at section N1 in specimen FS-2 was approximately equal to the external moment at applied loads above the yield level (34 kip).

(a) Specimen FS-1

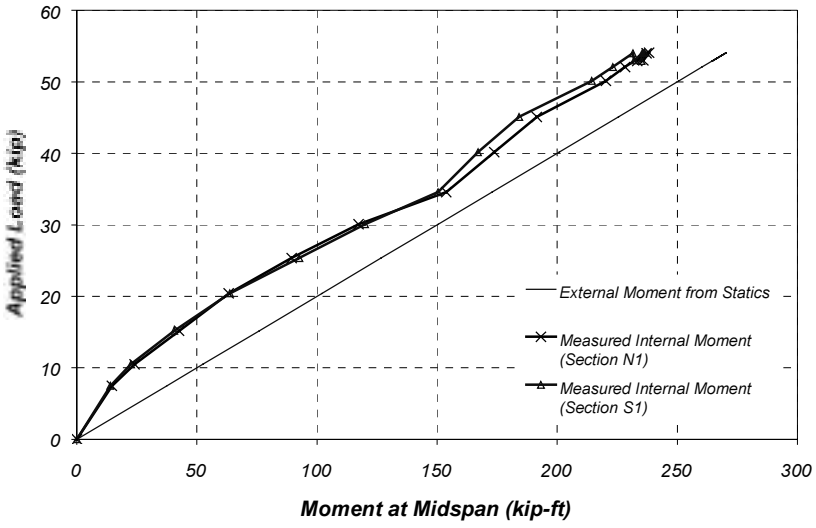

(b) Specimen FS-2

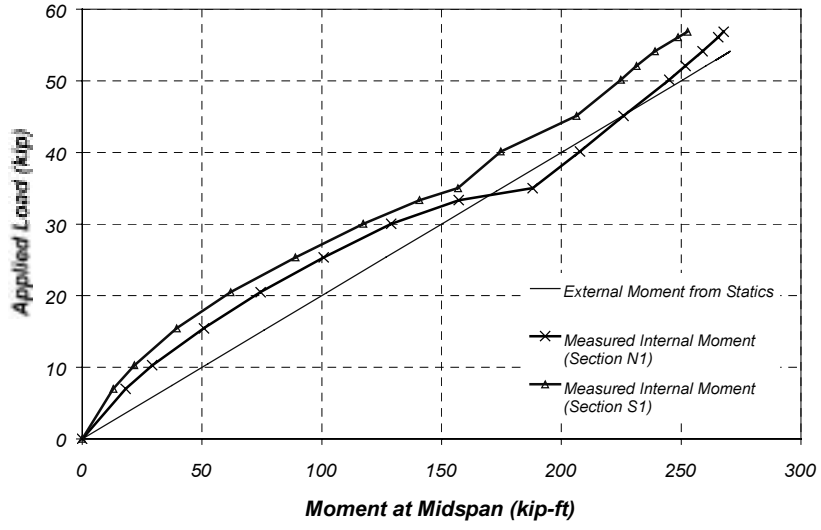

Figure 8.19 Comparison of Internal and External Moments

8.4 EVALUATION OF LOAD-DEFLECTION RESPONSE

The global response of the strengthened specimens is first evaluated by comparing the measured response of the two specimens. The response of each specimen was then compared with the calculated response obtained using the analytical procedure presented in a companion report. The displacement response of the strengthened specimens is compared with the bare reinforced concrete elements at the end of this section.

The displacement response was obtained by averaging the displacement measurements from midspan of the east and west sides of the slabs. The measurements were adjusted by subtracting the average vertical displacement at the supports. The load-deflection behavior of specimens FS-1 and FS-2 is shown in Figure 8.20. It can be seen that the overall behavior of both specimens was similar throughout the loading history. The main difference between the response of specimens FS-1 and FS-2 was observed at failure. While specimen FS-1 exhibited an increase in displacement under almost constant load, specimen FS-2 showed a uniform increase in load until failure. This behavior was caused by the progressive debonding of the CFRP plates in specimen FS-1 at the peak load.

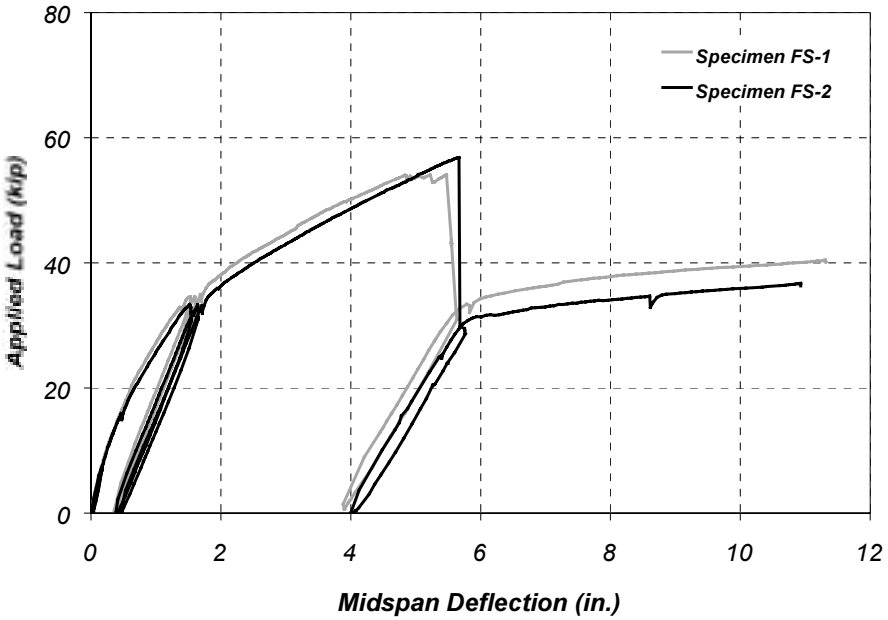

Figure 8.20 Measured Load-Deflection Response of Flat-Slab Specimens

At failure, the load dropped suddenly and the residual load was carried by the bare reinforced concrete elements. The maximum deformation capacity of the bare specimens was approximately equal.

The measured response of the specimens at large deflection levels is compared with the calculated response in Figures 8.21 and 8.22 for specimens FS-1 and FS-2, respectively. The comparisons show that the model was capable of reproducing the response of the bare reinforced specimens at large deflections, after the composites debonded from the surface of the concrete. This result implies that the material models used for the concrete and steel were appropriate for the comparison with the strengthened specimens. From these plots, the strengthening effect of the CFRP composites on the specimens is also apparent.

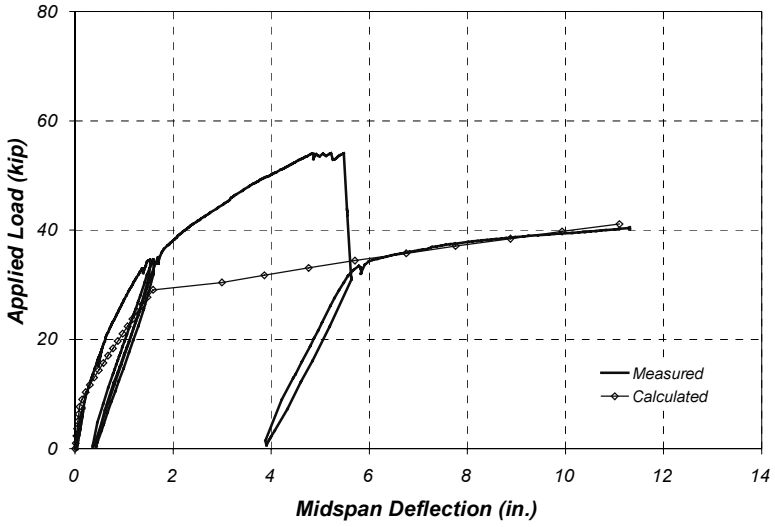

Figure 8.21 Comparison of Measured and Calculated Load-Deflection Response of Specimen FS-1 (Bare Section)

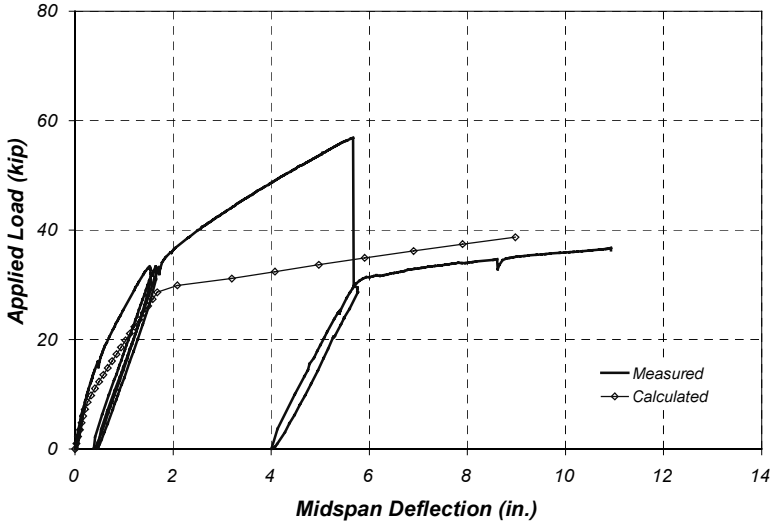

Figure 8.22 Comparison of Measured and Calculated Load-Deflection Response of Specimen FS-2 (Bare Section)

The measured response of the test specimens is compared with the calculated load-deflection response in Figures 8.23 and 8.24 for specimens FS-1 and FS-2, respectively. A 24-ft span was used for the calculated load-deflection response. The results presented show that the analytical model was able to reproduce the displacement response adequately for both specimens. However, the analytical model overestimated the peak load because debonding was not included in the calculations.

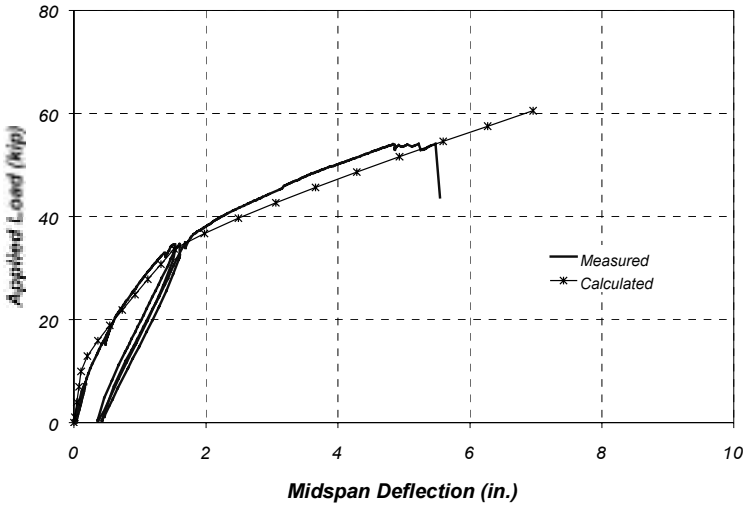

Figure 8.23 Comparison of Measured and Calculated Load-Deflection Response of Specimen FS-1 (Strengthened Section)

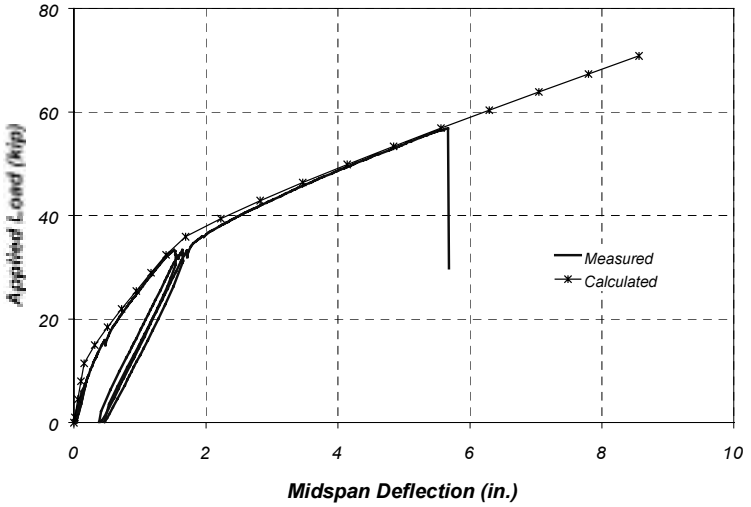

Figure 8.24 Comparison of Measured and Calculated Load-Deflection Response of Specimen FS-2 (Strengthened Section)

8.5 SUMMARY

The measured response of specimens FS-1 and FS-2 was compared to the response calculated using the analytical model presented in Chapter 3 of the companion report [Breña, et al., 2001], with the modifications indicated in Chapter 2 of this report. The comparisons show that the model was able to reproduce the measured global response of the test specimens accurately at all levels of loading.

As was the case for the pan-girder specimens, local effects such as cracking of the concrete, debonding of the CFRP composites, and accumulation of plastic strains in the reinforcement were not adequately represented with the analytical model. Local effects controlled the response at a particular section and were highly variable at different sections subjected to the same moment level.

Chapter 9: Design Recommendations

9.1 INTRODUCTION

The design recommendations presented in this chapter are based on strength theory for reinforced concrete structures for members subjected to flexure. This philosophy of design is consistent with the bridge load rating procedure currently used by TxDOT (Appendix B). These recommended procedures are based on the results of the laboratory tests of the strengthened full-scale bridge components discussed in Chapters 3 through 8. Therefore, it is intended that the response of elements strengthened using the recommended procedures outlined in this chapter will be similar to the observed response of the laboratory specimens.

The CFRP composites were bonded to laboratory specimens in which the condition of the concrete surface was not deteriorated. The performance of the strengthened elements may be significantly different from the response measured in the laboratory if the composite systems are attached to a deteriorated concrete surface. Therefore, the design provisions contained in this chapter should be used only for cases where the surface of the concrete is clean and sound.

The procedure to calculate the nominal capacity of a strengthened section is summarized in Section 9.2. The strength reduction factor is discussed in Section 9.3, serviceability issues are summarized in Section 9.4, and recommended details are presented in Section 9.5.

9.2 CALCULATION OF NOMINAL FLEXURAL CAPACITY OF STRENGTHENED SECTIONS

The procedures discussed in this section are based on the observed and calculated response of the laboratory specimens presented in Chapters 4 and 5 for the pan-girder specimens, and Chapters 7 and 8 for the flat-slab specimens. The objective is to present a set of design and analysis provisions for safe and reliable strengthening of reinforced concrete bridges using CFRP composites. The behavior of the strengthened bridge should be similar to the observed response of the laboratory specimens.

The assumptions used in the calculations for the flexural capacity of the strengthened sections are similar to current design practice for reinforced concrete members. The recommended design procedure is illustrated using a rectangular reinforced concrete element to facilitate the presentation. Nevertheless, the procedures can easily be modified to accommodate other shapes. However, the calculations can become quite involved so the use of a computer may be required.

Different modes of failure have been identified by other investigators for strengthened reinforced concrete elements using CFRP composites [Meier et al., 1992; Arduini and Nanni, 1997]. The failure mode depends primarily on the characteristics of the bare reinforced concrete section and the amount of CFRP composite used to strengthen the existing element. For the types of elements that were tested in this research project, failure was always governed by debonding of the CFRP from the concrete surface. Debonding occurred after yielding of the reinforcing bars, before concrete crushing in the extreme compression fiber. Adequate deformation capacity and ample indications of impending failure were observed in the laboratory tests conducted in this research project. Therefore, this mode of failure was considered to be adequate, and the design recommendations were developed to duplicate this mode of failure.

9.2.1 Strain Distribution within Strengthened Sections

The distribution of strains across the depth of the cross section ultimately defines the internal forces within the strengthened reinforced concrete member. Strains in each material are related to the internal stresses through the stress-strain relationships. The same material relationships used for the analytical model presented in Chapter 3 of the report documenting the first phase of this project [Breña et al., 2001] can be used for design. An elasto-plastic stress-strain relationship is considered adequate for the reinforcing steel.

As was discussed in Chapters 5 and 8, the bridge elements are subjected to dead-load moments before the CFRP composites are applied to the surface of the concrete. Therefore, the existing dead-load strain distribution on the existing reinforced concrete section needs to be determined before the capacity of the strengthened sections can be calculated. In some cases, the moments caused by dead loads do not exceed the cracking moment of the cross section. However, it is recommended that cracked section properties be used in the calculations because it is likely that the section has been cracked due to the application of service live loads during the lifetime of the structure.

The calculation of the strains in the concrete and reinforcing bars caused by dead load moments is illustrated graphically for a cracked reinforced concrete beam with a rectangular cross section in Figure 9.1. In this figure, the transformed area concept is used to calculate the neutral axis depth required to achieve equilibrium with the external dead-load moment. The basic assumptions and methodology to calculate stresses and strains along the cross section using the transformed area concept is presented in detail by Ferguson [1958]. For these calculations, a linear relationship between stresses and strains for the concrete and reinforcing bars may be assumed. The figure only shows the contribution of the reinforcement in tension, but the effect of the compression reinforcement can be included if necessary.

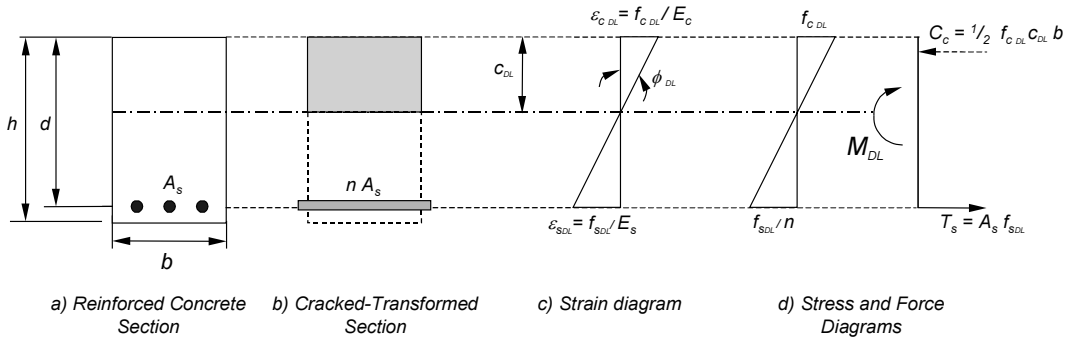

Figure 9.1 Calculation of Strains Caused by Dead-Load Moments

At capacity, the strengthened cross section is subjected to a strain increment corresponding to the factored dead and live-load condition. The strain distribution caused by service dead loads is added to the increase in strains on a strengthened rectangular cross section caused by factored loads in Figure 9.2. The figure illustrates a cross section strengthened with a CFRP plate attached to the bottom fiber, but the approach can be modified to accommodate composites bonded to the sides. The incremental strains in the concrete, reinforcement and CFRP composite are assumed to vary linearly with depth (Figure 9.2c). Therefore, an apparent incompatibility exists on the total strain profile between the CFRP composite and the original cross section because the composite was bonded while the reinforced concrete section was subjected to dead loads.

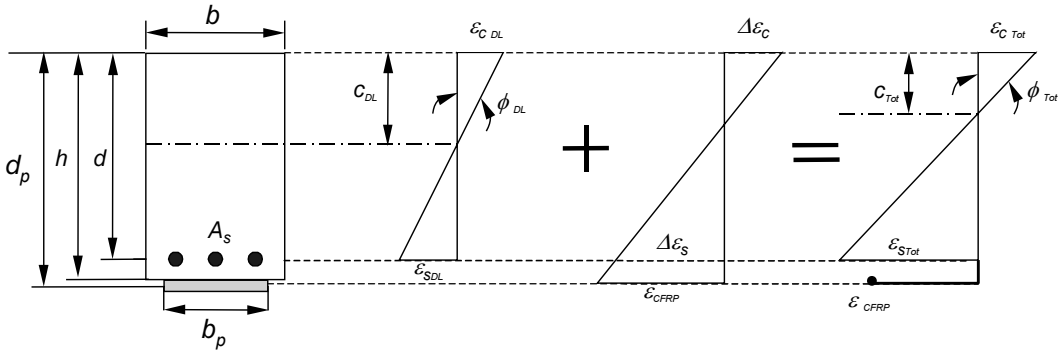

Figure 9.2 Increment of Strains on Strengthened Reinforced Concrete Section

9.2.2 Preliminary Estimate of the Area of CFRP Composite

A procedure to estimate a preliminary area of CFRP composite to reach the target strength is presented in this section. The procedure is based on an assumed distribution of compressive stresses in the concrete based on results of the experimental tests conducted in this project. Again, the procedure is demonstrated using a rectangular cross section. However, the general procedure may be applied to other cross sectional shapes.

The distribution of internal stresses within the cross section is calculated in Figure 9.3 based on the total strain distribution shown in Figure 9.2. The stress distribution shown in Figure 9.3(c) corresponds to the condition at nominal flexural capacity, defined as the capacity of the cross section when the CFRP composite debonds from the surface of the concrete.

The area of the CFRP can be calculated for preliminary design based on an assumed distribution of compressive stresses in the concrete. The material model for concrete implemented in the analytical model is used in this discussion. The maximum measured concrete strain before debonding of the CFRP composite from the surface of the concrete during the laboratory tests was approximately 0.002. This value is equal to the commonly assumed value of strain corresponding to the peak compressive stress, ε_{co}. This value was chosen to provide an estimate of the compressive stress distribution in the concrete. At this strain value, the stress in the extreme compressive fiber in the concrete is equal to f''_c (Figure 9.3c). The resultant of compressive stresses in the concrete, C_c, can then be calculated by integrating the assumed compressive stress distribution:

$$f_c = f''_c \left[\frac{2\varepsilon_c}{\varepsilon_{c0}} - \left(\frac{\varepsilon_c}{\varepsilon_{c0}} \right)^2 \right] \tag{9.1}$$

with

ε_c = 0.002
f''_c = $0.9 f'c$
f'_c = Concrete compressive strength

For a rectangular cross section and the assumed value of ε_c equal to 0.002, the resultant compressive force and its position from the top surface can be calculated as:

$$C_c = \frac{2}{3} f''_c \, c_{Tot} b \tag{9.2}$$

and

$$z = \frac{3}{8} c_{Tot} \tag{9.3}$$

It should be emphasized that the use of the equivalent rectangular stress block that is commonly used for the design of reinforced concrete flexural members is not applicable in this case because the selected failure mode is by debonding of the composites from the surface of the concrete. The distribution of compressive stresses in the concrete depends on the total tensile force developed by the reinforcing steel and CFRP composite when the failure condition is reached. However, the strain in the extreme compression fiber will not have reached the maximum usable strain in the concrete, ε_{cu}. The maximum recommended area of CFRP composite to guarantee this mode of failure is discussed in Section 9.2.3.

At the nominal strength condition, the reinforcing bars are assumed to have reached yield. The maximum strain in the CFRP composite is assumed to be equal to ε^*_{CFRP}, the strain corresponding to debonding from the surface of the concrete. As was discussed in Chapters 5 and 8, the maximum measured CFRP strain was highly dependent on the distance from the critical section to the nearest crack. Therefore, a conservative value of ε^*_{CFRP} equal to 0.007 is recommended for design. The tensile force from the individual components can be calculated with:

$$T_s = A_s f_y \tag{9.4}$$

$$T_p = A_p f_p = A_p \varepsilon^*_{CFRP} E_p \tag{9.5}$$

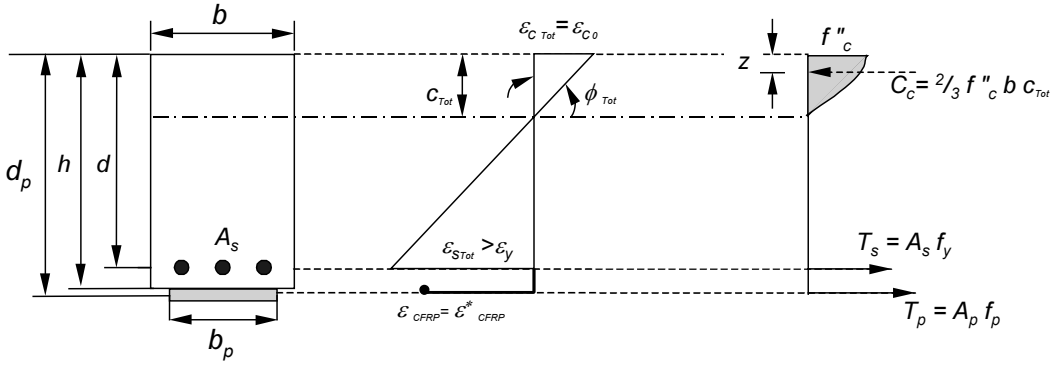

a) Strengthened Reinforced Concrete Section *b) Strains at Capacity* *c) Stresses at Capacity*

Figure 9.3 Internal Stress Distribution for a Strengthened Rectangular Section at Capacity

The initial estimate of required area of CFRP, A_p, can be calculated by solving the equations of equilibrium of horizontal forces and moments simultaneously:

$$A_s f_y + A_p \varepsilon^*_{CFRP} E_p = \frac{2}{3} f''_c \, c_{Tot} b \tag{9.6}$$

and

$$M_{n\,req} = A_s f_y \left(d - \frac{3}{8} c_{Tot} \right) + A_p \varepsilon^*_{CFRP} E_p \left(d_p - \frac{3}{8} c_{Tot} \right) \tag{9.7}$$

where

$M_{n\,req}$ = Required nominal capacity of the strengthened section, kip-in
A_s = Existing area of reinforcing steel, in^2
f_y = Specified yield stress of the reinforcing steel, ksi
c_{Tot} = Neutral axis depth due to total loads, in
A_p = Required area of CFRP composite, in^2
ε^*_{CFRP} = Strain in the CFRP composite before debonding from the concrete surface = 0.007
E_p = Tensile modulus of elasticity of the CFRP composite, ksi
d = Distance from extreme compression fiber to centroid of existing reinforcing steel, in
d_p = Distance from extreme compression fiber to centroid of CFRP composite, in

With the initial estimate of the required area of CFRP composite, the procedures in Chapter 3 of the companion research report [Breña, et al., 2001] can be used to calculate the capacity of the strengthened section. A revised distribution of compressive stresses in the concrete is obtained and the area of CFRP can be adjusted to guarantee that the maximum strain in the composite does not exceed the recommended value.

9.2.3 Maximum Recommended Area of CFRP Composite

The procedure used to estimate the area of CFRP composite required to develop the required nominal flexural capacity was outlined in the previous section. However, no limitation was set on the maximum area that can be used in a section to prevent concrete crushing at the extreme compressive fiber. The criterion to calculate the maximum area of CFRP composite is similar to the limit set on the maximum area of reinforcing steel in current design of reinforced concrete members [ACI 318, 1999]. The procedure is illustrated for a rectangular concrete section in Figure 9.4, where the maximum usable concrete strain, ε_{cu}, is developed at the extreme compressive fiber simultaneously as the strain in the CFRP composite, ε^*_{CFRP}, reaches the value equal to 0.007 assumed for debonding.

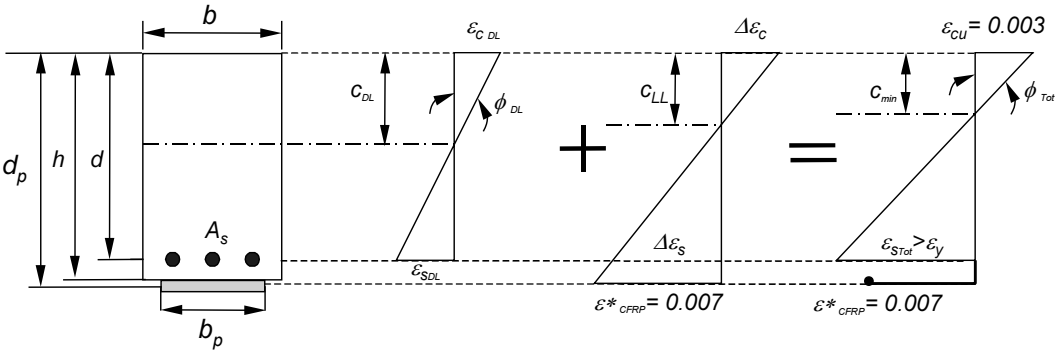

Figure 9.4 Strain Profile for Maximum Recommended Area of CFRP Composite

The maximum recommended area of CFRP composite can be calculated from horizontal force equilibrium, assuming that the distribution of compressive stresses can be represented by the commonly used rectangular stress block. In this calculation, the reinforcing steel is assumed to have yielded. Horizontal force equilibrium yields:

$$A_{p\max} = \frac{0.85 f'_c \, b a_{\min} + A_s f_y}{\varepsilon^*_{CFRP} E_p} \tag{9.8}$$

where

a_{min} = Depth of the equivalent compressive stress block corresponding to concrete crushing at the same time the CFRP debonds from the surface of the concrete, in

$A_{p\,max}$ = Area of CFRP composite that generates concrete crushing and debonding at the same time, in^2

and other variables were defined previously.

The depth of the rectangular stress block is assumed to be equal to β_1 times the neutral axis depth, c_{min} [ACI 318, 1999]. The neutral axis depth can be determined from compatibility of strains using:

$$c_{\min} = \left(\frac{\varepsilon_{cu}}{\varepsilon_{cu} + \varepsilon_{sTot}} \right) d \tag{9.9}$$

where

$$\varepsilon_{sTot} = \frac{\varepsilon^*_{CFRP} \, d + \Delta\varepsilon_c \, d_p}{d_p \left(1 - \Delta\varepsilon_c\right)} + \varepsilon_{sDL} \tag{9.10}$$

The first term in Eq. (9.10) represents the increment in strains, $\Delta\varepsilon_s$, generated at capacity of the cross section. This value was calculated using the strain diagram presented in Figure 9.4. As discussed in Section 9.2.1, the existing strain condition caused by dead loads must be established for the calculation of the maximum area of CFRP composite.

The area of CFRP calculated with this procedure would cause the member to simultaneously fail by debonding and concrete crushing at the design capacity. The capacity of the strengthened member is reached after yielding of the reinforcement so adequate deformation capacity is expected. For design purposes, however, to insure debonding prior to concrete crushing, the maximum area of CFRP composite for a specific cross section is recommended to be limited to 90% of $A_{p\,max}$.

9.3 RECOMMENDED STRENGTH REDUCTION FACTOR FOR USE IN THE BASIC DESIGN EQUATION

Current design practice for reinforced concrete design uses load and resistance factors in the basic design equation. The basic design equation contained in the *AASHTO Standard Specifications* [1996], expressed in terms of flexural actions can be written as:

$$M_u = \gamma_{DL} M_{DL} + \gamma_{LL} M_{LL} \left(1 + I\right) \le \phi \, M_n \tag{9.11}$$

where

M_{DL} = Maximum moment caused by dead loads, kip-in
M_{LL} = Maximum moment caused by live loads, kip-in
M_u = Maximum factored moment generated on the element, kip-in
M_n = Nominal flexural resistance, kip-in
I = Impact factor = 0.3
γ_{DL} = Load factor for dead load effects = 1.3
γ_{LL} = Load factor for live load effects = 2.17
ϕ = Strength reduction factor used for design

Therefore, the required nominal moment capacity, $M_{n\ req}$, to resist the design moment can be determined by writing Eq. 10.11 in terms of M_n:

$$M_{n\ req} = \frac{M_u}{\phi} \tag{9.12}$$

The value that was used for the strength reduction factor, ϕ, in the design of the laboratory specimens was 0.85. The observed deflection response of the laboratory specimens was considered adequate and consistent with the current design philosophy implicit in the design of reinforced concrete flexural members. Therefore this value is recommended for the design of strengthening systems until more information is available to support the use of a higher value.

It is important to note that the use of this value was only evaluated for the failure mode that was observed in the laboratory. The failure sequence involved yielding of the reinforcing steel prior to debonding of the CFRP composites from the surface of the concrete. Therefore, this value for ϕ should only be used in designs similar to those presented for the laboratory specimens in this report, where yielding of the steel reinforcement precedes debonding of the CFRP composites from the surface of the concrete.

9.4 SERVICEABILITY CONSIDERATIONS

The bridge sections that were studied in this research project exhibited adequate response under service-load conditions. No indications of distress along the composite-concrete interface were observed during the tests. Debonding always initiated at load levels that were above yielding.

Therefore, the yield capacity of the strengthened section should not be exceeded under the increased service loads to prevent damage to the composite-concrete interface. For the design conditions that were encountered in this research project, increased service loads on the bridge elements represented a maximum of approximately 70% of the yield capacity. The procedures described in Chapter 3 of the companion report [Breña et al., 2001] should be used to determine the yield capacity of the strengthened sections.

9.5 DETAILING RECOMMENDATIONS

The recommendations presented in this section are not supported by engineering calculations, but are based on experience gained from the laboratory tests of the strengthened specimens. These detailing practices are suggested based on the observation of adequate response of the strengthened test specimens.

9.5.1 Anchoring Straps

As discussed previously the observed failure of the strengthened elements was characterized by debonding of the CFRP composites from the surface of the concrete. However, local debonding was observed before total debonding of the composite elements. Debonding was observed only after the longitudinal reinforcement yielded. The longitudinal CFRP composites were restrained from debonding by CFRP straps positioned at a space equal to h/2 along the length of the beam.

An analytical model to determine the required width, length, spacing, and position of the anchoring straps was not developed because debonding is a complicated phenomenon that is greatly influenced by the tensile strength of the concrete and the extent of cracking. These conditions vary greatly in the field and are essentially impossible to quantify in an existing reinforced concrete bridge. The straps were provided where debonding was expected to start, and this was always near the section of maximum moment. However, for a real structure, the section of maximum moment is generated under the axle of a moving truck and therefore, this section can vary depending on the span and loading configuration. Therefore, it is suggested that straps be provided along the entire length of the longitudinal composites used for flexural strengthening.

Strap spacing was based on the assumption that diagonal cracks would be oriented 45° from horizontal and that these cracks would trigger local debonding of the CFRP composite. Therefore, the strap spacing was selected such that at least one strap would cross a potential diagonal crack in the reinforced concrete bridge element. A maximum spacing equal to the height of the cross section divided by two (h/2) was thus established.

The length of the straps can be determined by extending them beyond mid-depth to ensure that the potential diagonal crack is crossed by a strap. The length of the extension should be determined so that the full tensile strength of the strap is developed at the crack location. Experimental studies conducted by other investigators [Bizindavyi and Neale, 1999] concluded that the maximum strength of 1-ply CFRP composites bonded to a concrete surface can typically be developed within a distance of approximately 3 to 4 in. measured from the free end. In these tests, the CFRP composites were attached to the concrete surface and subjected to direct shear by pulling with a force parallel to the bond surface at the free edge of the composite. Based on these results and the observations from this research project, it is recommended that the minimum strap length should extend at least 4 in. beyond the element mid-depth.

Finally, the width of the straps was selected based on the width of the longitudinal CFRP composites, bonded to either the bottom or side of the specimens. This dimension is recommended for use in design.

9.5.2 Length of CFRP Composites

The determination of the length for the composites that were used to strengthen the laboratory specimens was discussed in Chapters 4 and 7 for the pan-girder and the flat-slab specimens, respectively. This length was based on the loading configuration that was used in the laboratory tests. The length of the CFRP composites required in an actual bridge, however, depends on the factored moment diagram acting on the bridge. This moment diagram is controlled by the live loads generated by the design vehicle. The procedure to determine the cut-off point on one side of the bridge is illustrated schematically in Figure 9.5. The CFRP composites should be extended at least a distance equal to the height of the member, h, from the theoretical cut-off point. However, this point will be located very close to the support in many cases for the bridges considered in this research study because of their short span length. In these cases, it is recommended that the CFRP composites be attached along the entire bridge span.

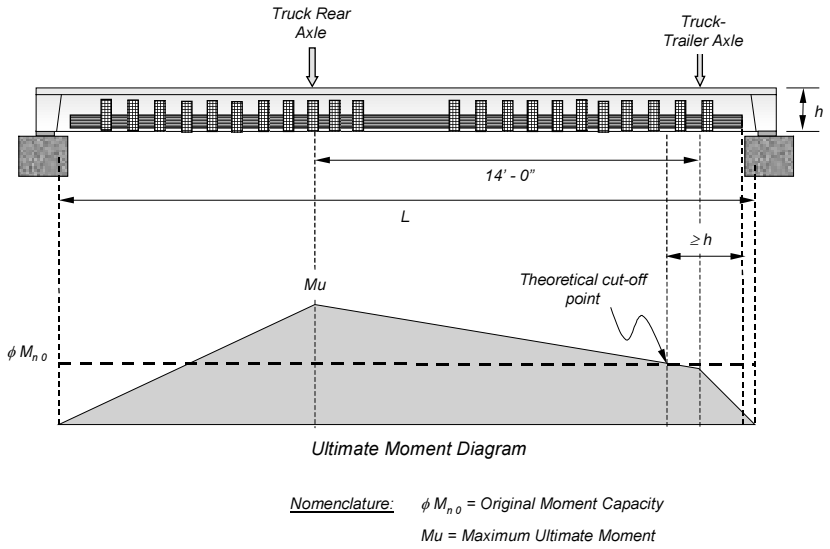

Figure 9.5 CFRP Composite Length Determined Based on Ultimate Moment Diagram

9.6 SUMMARY

Recommendations for the design of flexural strengthening techniques for reinforced concrete elements using CFRP composites were presented in this chapter. These recommendations were based on the results of the experimental portion of this research project and engineering judgment. Therefore, the procedures that are outlined in this chapter are only strictly applicable to similar situations encountered in the field.

Chapter 10: Summary and Conclusions

10.1 SUMMARY

Laboratory tests were conducted on four full-scale reinforced concrete bridge specimens that were strengthened using carbon fiber reinforced polymer composites. The specimens represent two types of bridge construction that were very common in Texas approximately 50 years ago: pan-girder bridges and flat-slab bridges. The measured response of the laboratory specimens was compared with the calculated response using an analytical model that was developed to study the flexural behavior of reinforced concrete beams strengthened with CFRP composites.

The response of the strengthened specimens was excellent, and the design objectives were fully accomplished. The CFRP composites had little influence on the response of the specimens below the yield load. A marginal increase in stiffness was observed after strengthening under low load levels; however, the yield load of the reinforced concrete element was not increased significantly.

However, the post-yield behavior of the specimens was drastically different from the response of a reinforced concrete element. The stiffness of the specimens after yielding was much higher than the stiffness expected of a bare reinforced concrete element. Also, the measured strength exceeded the nominal capacity calculated during design of the test specimens.

Examination of the measured load-deflection response during the tests demonstrated that CFRP composites are effective in increasing the flexural strength of existing reinforced concrete elements. The maximum strength of the specimens was always controlled by CFRP debonding from the surface of the concrete. CFRP straps were attached transversely along the longitudinal composites to control the propagation of debonding and increase the deformation capacity of the specimens before failure. These straps also provided ample warning of impending failure due to debonding of the longitudinal composites.

An analytical model was developed to calculate the moment-curvature response for a strengthened cross section using the nonlinear properties of the materials. The global load-deflection response of the laboratory specimens was well represented with the analytical model. However, the calculated response at the section level sometimes departed from the measured response. This was mainly attributed to local effects such as the concentration of strains at a section caused by its proximity to cracks in the concrete. Local debonding of the CFRP composites from the surface of the concrete also affected the measured response. However, the analytical model was considered to be appropriate for reproducing the general trends in the behavior of the strengthened elements, and was therefore recommended for use in design.

The controlling mode of failure in all four full-scale specimens was debonding of the composites from the concrete surface. The maximum strain that was developed in the CFRP composites prior to debonding was measured during the tests at discrete locations. This value was compared with the maximum expected strain assuming perfect bond to the surface of the concrete. The large variations in the difference between calculated and measured values indicated that strain measurements are largely influenced by local effects. Therefore, it is recommended to use a conservative estimate of the maximum strain that can be developed before debonding in design.

Design recommendations were developed based on the results of the laboratory tests and on the comparisons of the measured and calculated response. The design procedures are based on the assumption that the original reinforced concrete cross section is under-reinforced and that the steel will yield before the CFRP debonds in the strengthened cross section.

10.2 CONCLUSIONS

The results of earlier phases of this investigation [Breña et al, 2001] demonstrated that CFRP composites represent a viable means of increasing the flexural strength of reinforced concrete beams. The four different CFRP systems that were investigated in these phases performed satisfactorily. Fatigue loading, sustained service-level loads, and exposure to wetting and drying cycles did not affect the behavior of the strengthened beams. Therefore, CFRP composites should be considered seriously for strengthening existing reinforced concrete bridges that were proportioned using lighter design vehicles, but do not exhibit any signs of deterioration after many years in service.

While most of the strengthened beams failed after the CFRP composites debonded from the surface of the concrete, this mode of failure was delayed by using transverse CFRP straps. In addition, placement of the longitudinal CFRP on the sides of the cross section, rather than on the bottom, reduced the tendency of the CRFP composites to pry off the surface of the concrete at locations where the laminates crossed existing cracks.

The prototype pan-girder and flat-slab bridges selected for study in phase 3 of this investigation were both designed to carry two, H-10 loading vehicles. The CFRP composites selected for the pan-girder test specimens were designed to increase the inventory rating for the bridge to HS-20. When the curbs were removed from the prototype flat-slab bridge, the inventory rating for the bare slab was HS-6. In this case, the CFRP composites for the flat-slab specimens were designed to increase the inventory rating of the slab to HS-10.

The design procedures developed during this study were successful, and the strengthened specimens exceeded the desired capacities. All specimens exhibited significant inelastic behavior before the CFRP composites debonded from the surface of the concrete. The transverse straps began to exhibit distress after the longitudinal reinforcement in the specimens yielded and provided ample warning of imminent failure.

In accordance with accepted flexural design procedures [ACI, 1999; AASHTO, 1996], the amount of longitudinal CFRP composites applied to a reinforced concrete beam should be limited such that the reinforcing steel yields before failure. For traditional reinforced concrete beams, failure is defined by crushing of the concrete, while failure is defined by debonding of the composites for the strengthened beams. In addition, transverse straps should be provided along the entire length of the reinforced concrete beam at a spacing not to exceed one-half the depth of the cross section in order to control debonding.

The two CFRP systems that were used to strengthen the laboratory specimens in this phase of the research project achieved similar performance. The strengthening techniques were designed for the same target strength. The laboratory tests revealed that any of the systems may be used to achieve similar response of the strengthened structures.

Application of CFRP composites to reinforced concrete beams that were cracked under service loads did not adversely influence the performance of the strengthened beams. However, the concrete surface was sound for all beams tested, and the design procedures described in this report should not be used for bridges with damaged or deteriorated concrete.

10.3 AREAS FOR FUTURE RESEARCH

Throughout this investigation, it was observed that, in order to be able to calculate the capacity of strengthened members, adequate strain limits at which the CFRP composites debonded from the surface of the concrete need to be determined. The strain limit recommended for use in design in Chapter 9

represents a conservative estimate that was established based on the particular conditions of the tested specimens in this project. Several factors are believed to affect the maximum strain that can be developed before debonding, such as conditions of the surface of the concrete at the time of bonding, stiffness of the CFRP composite, position of the CFRP composites on the element, supplemental anchorage of the composite to the concrete element, and the shear span of the element. Clarification on the influence of these factors on the maximum strain developed before debonding requires further investigation.

In this study, the CFRP composites were used to increase the flexural capacity of the reinforced concrete elements. Transverse CFRP straps were positioned along the longitudinal composites to prevent sudden failure of the strengthening system after initial debonding. However, no attempt was made to consider the effect of these straps in the shear capacity of the strengthened member. The loading configuration used in the laboratory precluded shear failure before reaching the flexural strength of the specimens and, therefore, the composites oriented transversely were not required for shear strength. It is believed, however, that composites can be used effectively to strengthen elements for shear. Further research is required to develop design guidelines for the use of composites in this area.

Appendix A: Measured Material Properties

This appendix is divided into three sections. Concrete material properties are summarized in Section A.1, reinforcement steel properties are summarized in Section A.2, and CFRP properties are summarized in Section A.3. Concrete cylinders and steel coupons were tested as part of this research program to determine the material properties. Material properties reported by the manufacturers are summarized for the composite material systems.

A.1 CONCRETE

Concrete cylinders (6 in. diameter by 12 in. in height) were fabricated using standard ASTM procedures as specified in ASTM C-40 [ASTM, 1996]. Eighteen cylinders were cast for each specimen and cured under ambient conditions in the laboratory next to the specimens. Three cylinders were tested in compression 3, 7, 14, and 28 days after casting to evaluate the change in strength with time for the concrete used in each specimen. Also, compression tests and split cylinder tests were conducted within 24 hours of testing each specimen to establish the concrete strength at the time of testing. Table A.1 and Table A.2 summarize the results of the compressive strength tests and split cylinder tests respectively for all specimens.

A.1.1 Pan-Girder Specimens

Concrete compressive strength vs. time curves for Specimens J-1 and J-2 are shown in Figure A.1 and Figure A.2, respectively. Stress-strain curves for Specimens J-1 and J-2 are shown in Figure A.3 and Figure A.4, respectively. Cylinder strains were measured using a compression meter with an 8-in. gage length. The cylinders were tested under force control using a 600-kip Forney testing machine at an average loading rate of 800 lb/sec.

The concrete model [Hognestad, 1950] used to calculate internal stresses for all specimens is superimposed in each of these figures. This model was adjusted using the individual material properties for each specimen (maximum compressive strength, f'_c, and strain at maximum strength, ε_{co}). The stress-strain parameters are summarized in Table A.1.

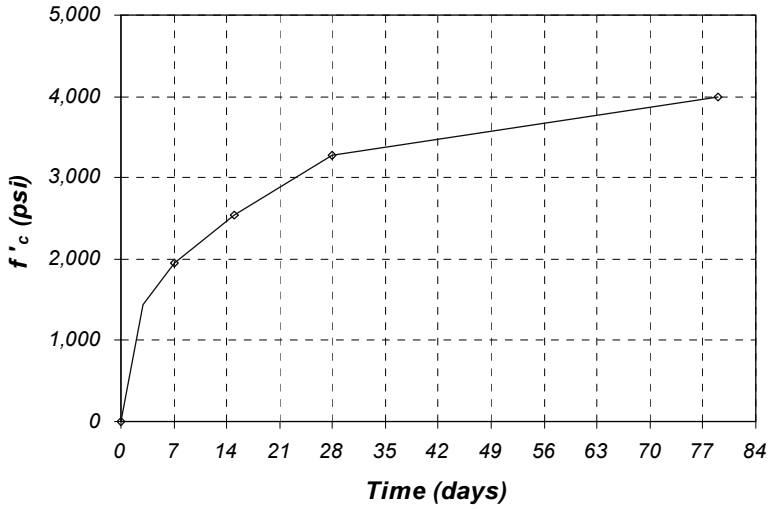

Figure A.1 Variation of Concrete Compressive Strength with Time for Specimen J-1

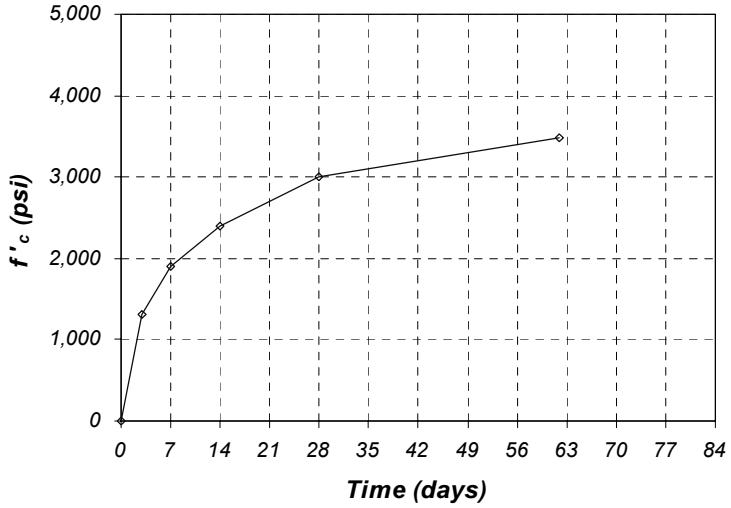

Figure A.2 Variation of Concrete Compressive Strength with Time for Specimen J-2

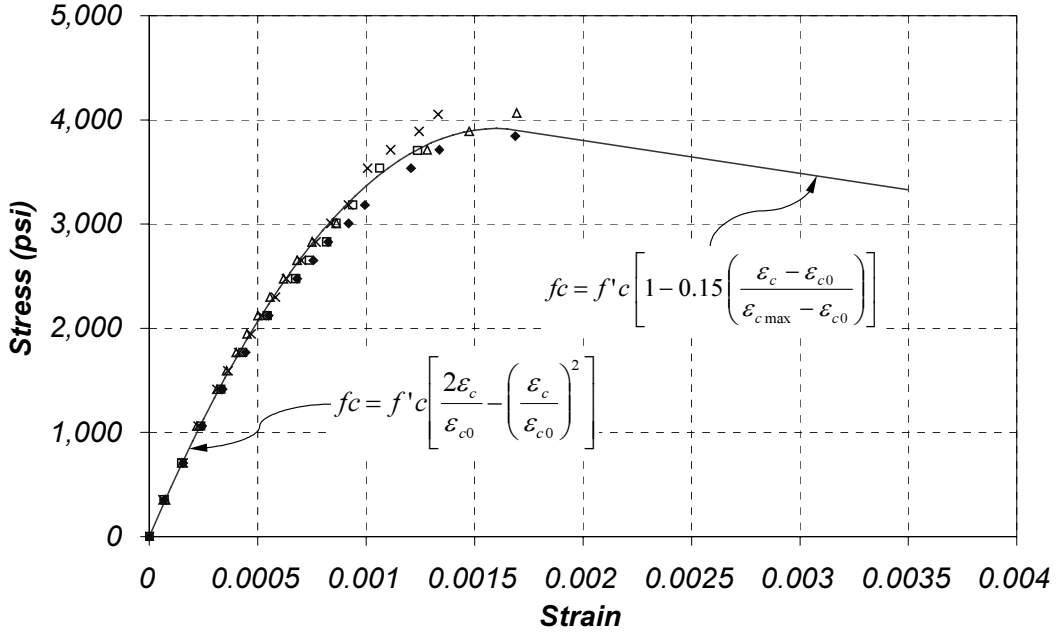

Figure A.3 Concrete Stress-Strain Curve for Specimen J-1

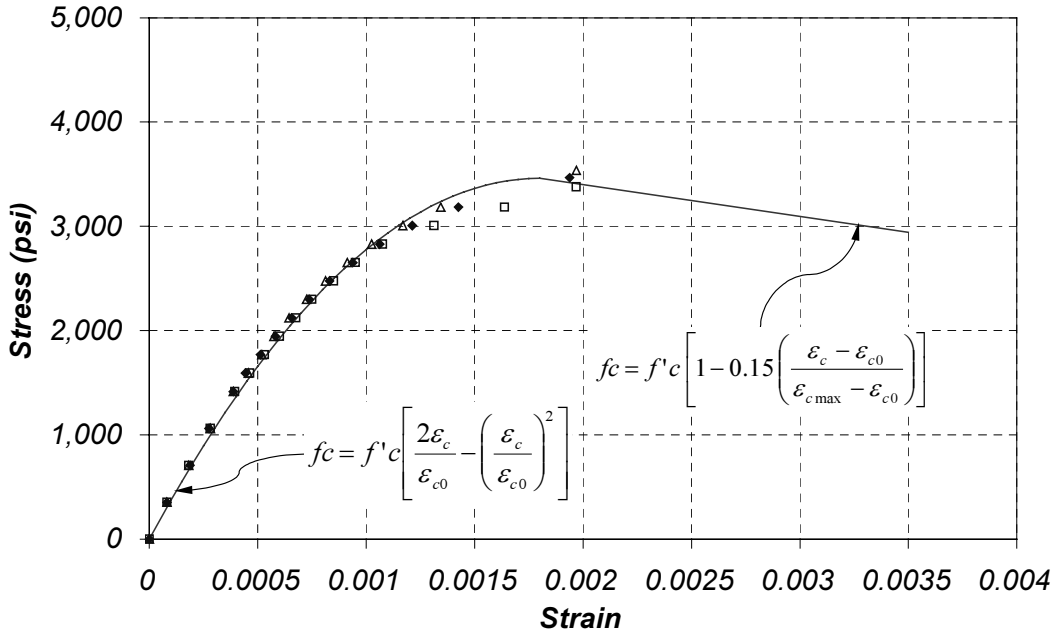

Figure A.4 Concrete Stress-Strain Curve for Specimen J-2

A.1.2 Flat Slab Specimens

Concrete compressive strength vs. time curves for Specimens FS-1 and FS-2 are shown in Figure A.5 and Figure A.6, respectively. In the case of Specimen FS-2, the specimen was tested before reaching its 28-day compression strength, so no cylinders were tested at this age. Concrete stress-strain curves for the flat slab specimens are shown in Figure A.7 and Figure A.8 respectively. These curves were obtained in the same manner as those for the joist specimens.

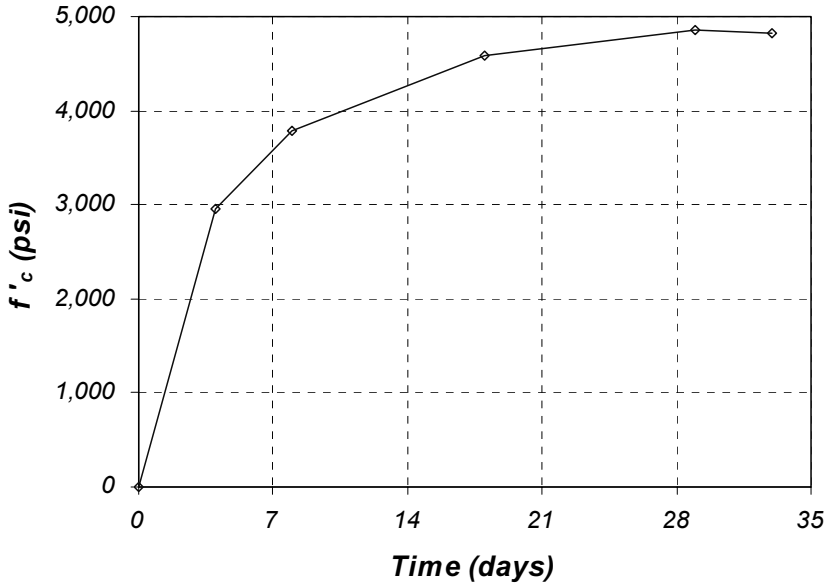

Figure A.5 Variation of Concrete Compressive Strength with Time for Specimen FS-1

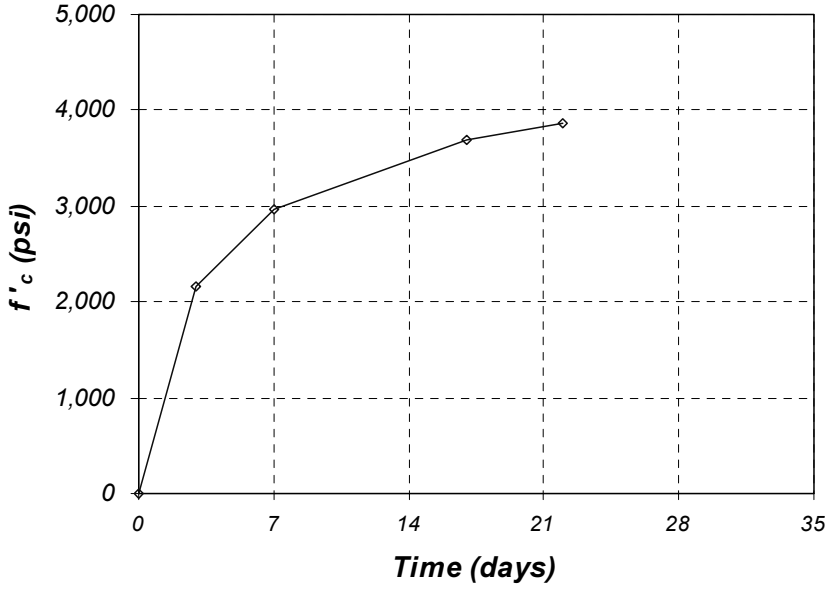

Figure A.6 Variation of Concrete Compressive Strength with Time for Specimen FS-2

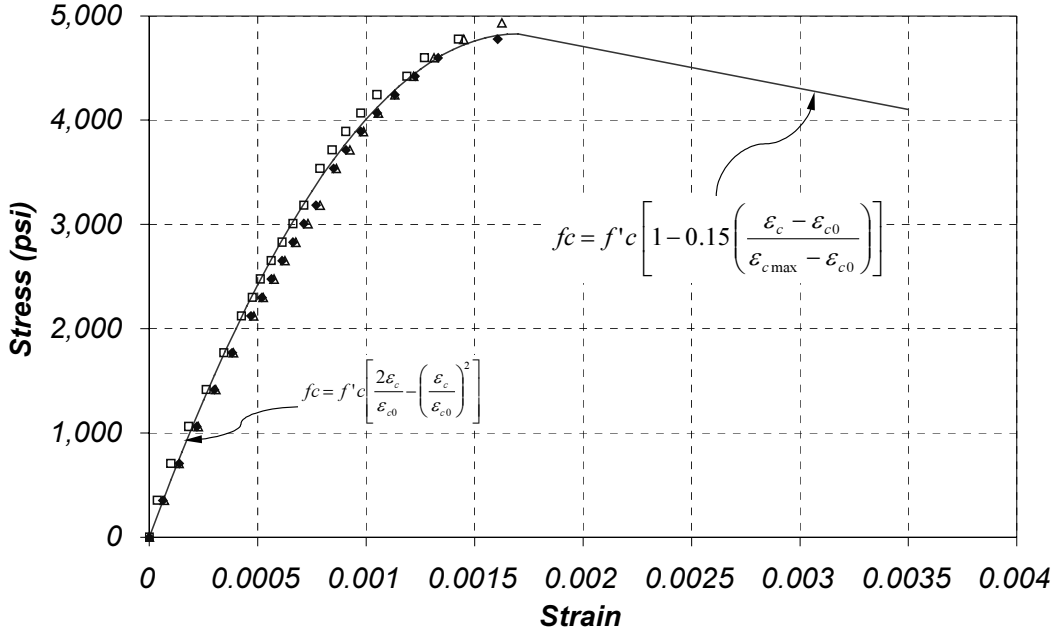

Figure A.7 Concrete Stress-Strain Curve for Specimen FS-1

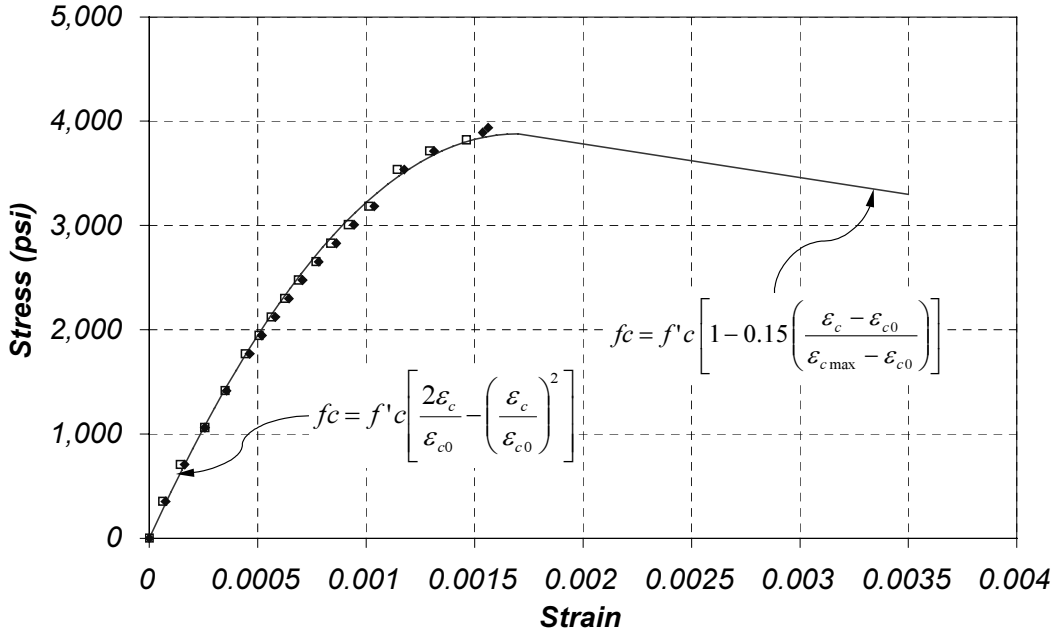

Figure A.8 Concrete Stress-Strain Curve for Specimen FS-2

Table A.1 Concrete Compression Tests and Parameters Used for Material Models

Specimen	Age, days	Compressive Strength, psi				Avg. f'_c, psi	Std. Dev., psi	ε_{co}
		Test 1	Test 2	Test 3	Test 4			
J-1	79	3,850	3,710	4,070	4,050	3,920	170	0.0016
J-2	62	3,470	3,540	3,380	-	3,460	80	0.0018
FS-1	33	4,780	4,780	4,930	-	4,830	87	0.0017
FS-2	22	3,820	3,940	-	-	3,880	85	0.0017

Table A.2 Tensile Strength of Concrete Determined from Split Cylinder Tests

Specimen	Age, days	Tensile Strength, psi			Average f_t, psi	Standard Dev., psi
		Test 1	Test 2	Test 3		
J-1	79	450	380	-	415	50
J-2	62	390	360	-	375	21
FS-1	33	470	370	360	400	61
FS-2	22	390	470	350	400	61

A.2 REINFORCING STEEL

Tension tests were conducted to determine the stress-strain curves for all sizes of reinforcing bars used to fabricate the specimens. Bar elongation was measured using a clip-on extensometer with an 8-in. gage length. The bars were tested in a 120-kip Tinius Olsen testing machine at a strain rate of 0.00125/min. The extensometer was removed from the bars at a strain of approximately 0.04 to avoid damage.

Both dynamic yield and static yield stresses were measured during these tests. For bars with a well-defined yield plateau, the dynamic yield stress was defined as the stress measured with the testing running at the strain rate specified above. In bars that did not show a well-defined yield point, the yield stress was determined using the 0.2% offset method.

The static yield stress was determined by stopping the machine after the yield plateau was reached and holding the load during two minutes. After the two-minute hold had elapsed, the stress in the bar was determined and the machine was started and stopped again once the stress-strain plot leveled-off. This process was repeated three times. The static yield stress was defined as the average of the three readings after the load holds. Table A.3 summarizes the static and dynamic yield stresses measured during the tests and the average values used in the calculations.

A.2.1 Pan-Girder Specimens

Four sizes of reinforcing bars were used to construct the pan-girder specimens. Stress-strain curves for this reinforcement are shown in Figures A.9 through A.12.

The measured stress-strain curves for the #8 bars are shown in Figure A.9. A mathematical model proposed by Menegotto and Pinto [Stanton and McNiven, 1979] was used to mimic the stress-strain behavior of these bars. The stress-strain response using this model is compared with the average measured stress-strain curves in part (d) of this figure along with the parameters for the mathematical expression that defines the model. Details of the material model are presented in Chapter 3.

a) Test 1 - #8 Bars

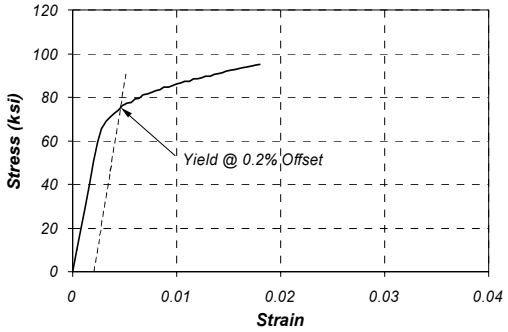

c) Test 3 - #8 Bars

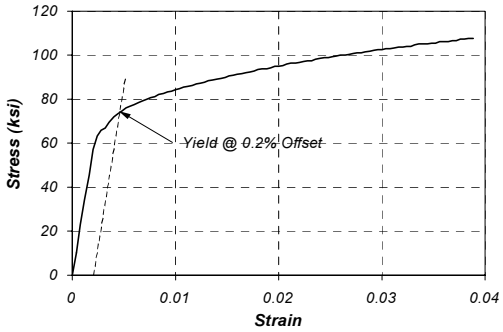

b) Test 2 - #8 Bars

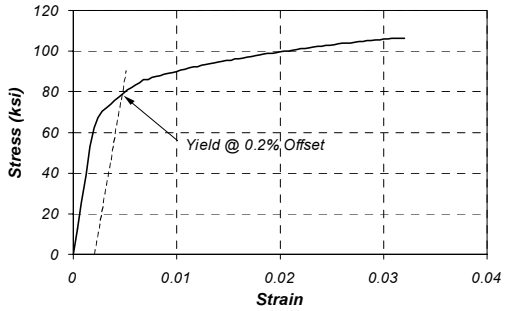

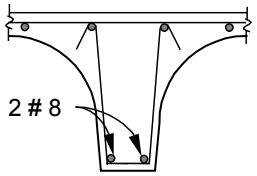

d) Menegotto-Pinto Model

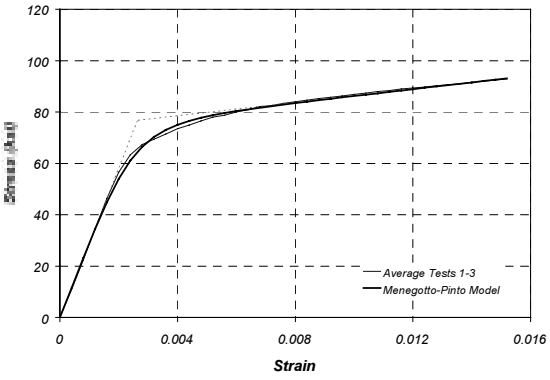

$$\frac{f}{f_0} = b\frac{\varepsilon}{\varepsilon_0} + \frac{(1-b)\frac{\varepsilon}{\varepsilon_0}}{\left[1+\left(\frac{\varepsilon}{\varepsilon_0}\right)^n\right]^{\frac{1}{n}}}$$

$b = 0.045$

$\varepsilon_0 = 0.0026$

$f_0 = 76.8\,ksi$

$n = 3.83$

Figure A.9 Stress-Strain Curves for #8 Bars in Joist Specimens

a) Test 1 - #3 Bars

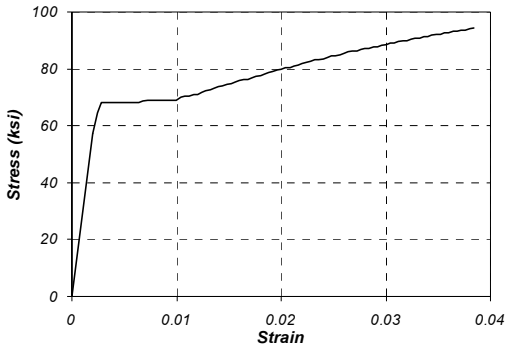

b) Test 2 - #3 Bars

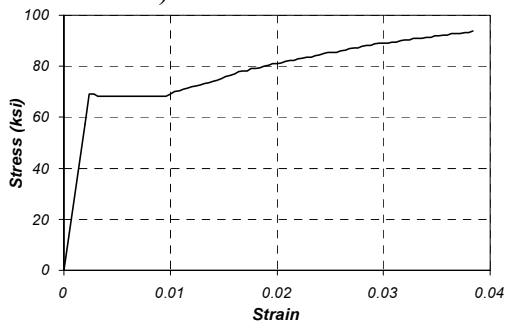

c) Test 3 - #3 Bars

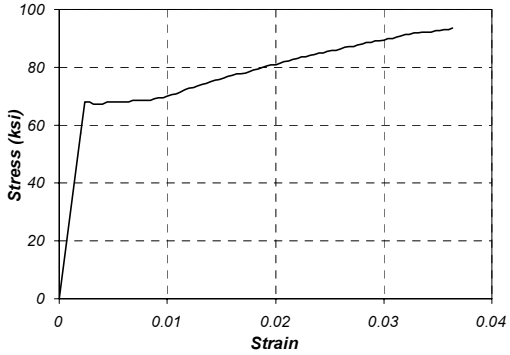

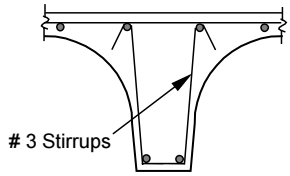

Figure A.10 Stress-Strain Curves for #3 Bars in Joist Specimens

a) Test 1 - #4 Slab Longitudinal Bars (#4 L)

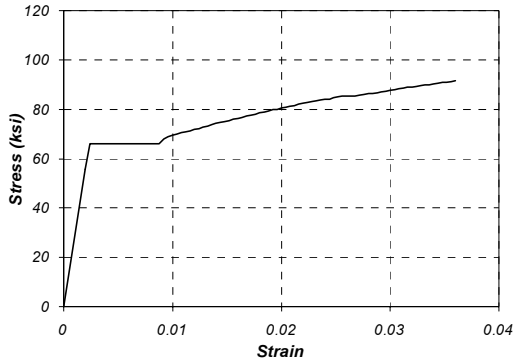

b) Test 2 - #4 Slab Longitudinal Bars (#4 L)

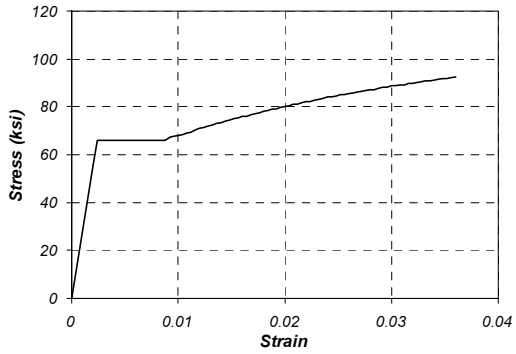

c) Test 3 - #4 Slab Longitudinal Bars (#4 L)

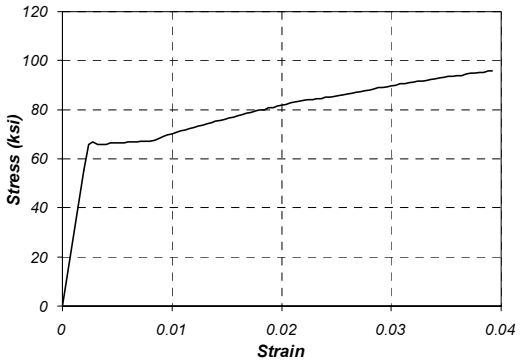

d) Test 4 - #4 Slab Transverse Bars (#4 T)

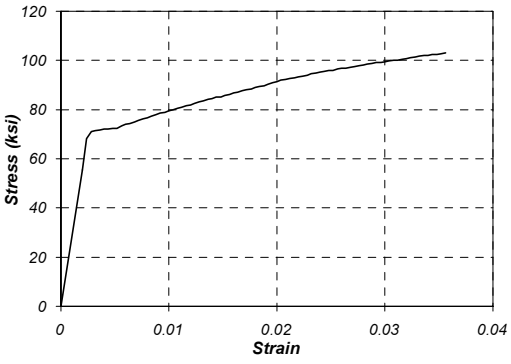

e) Test 5 - #4 Slab Transverse Bars (#4 T)

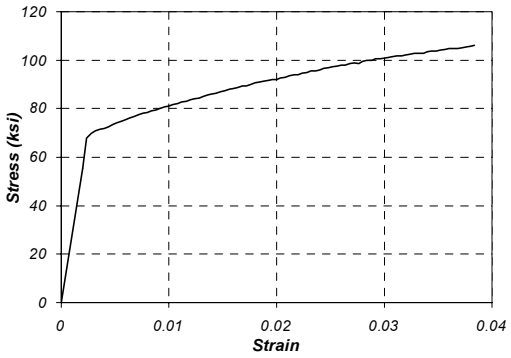

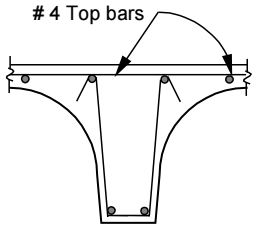

Figure A.11 Stress-Strain Curves for #4 Bars in Joist Specimens

a) Test 1 - #5 End Diaphragm Bars

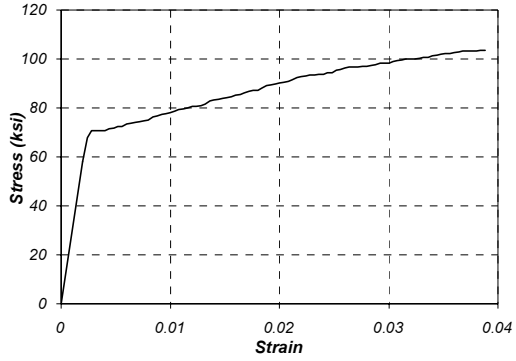

c) Test 3 - #5 End Diaphragm Bars

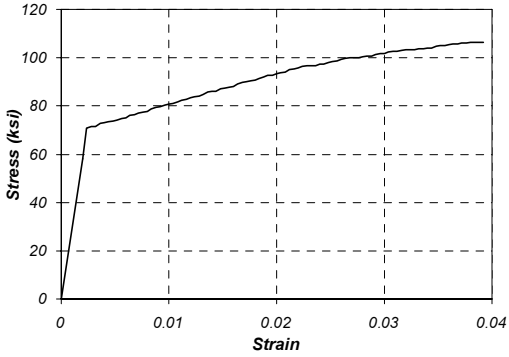

b) Test 2 - #5 End Diaphragm Bars

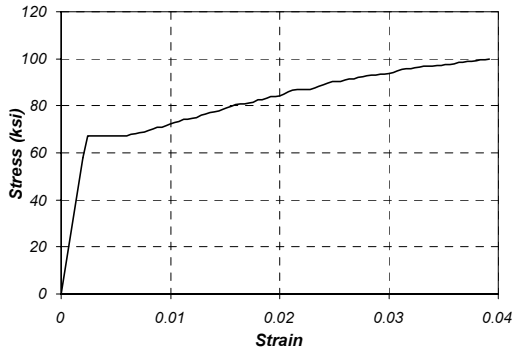

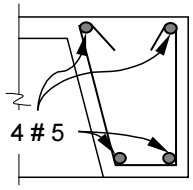

Figure A.12 Stress-Strain Curves for #5 Bars in Joist Specimens

A.2.2 Flat-Slab Specimens

Three sizes of reinforcing bars were used to construct the flat-slab specimens. Strain-stress curves for this reinforcement are shown in Figures A.13 through A.15.

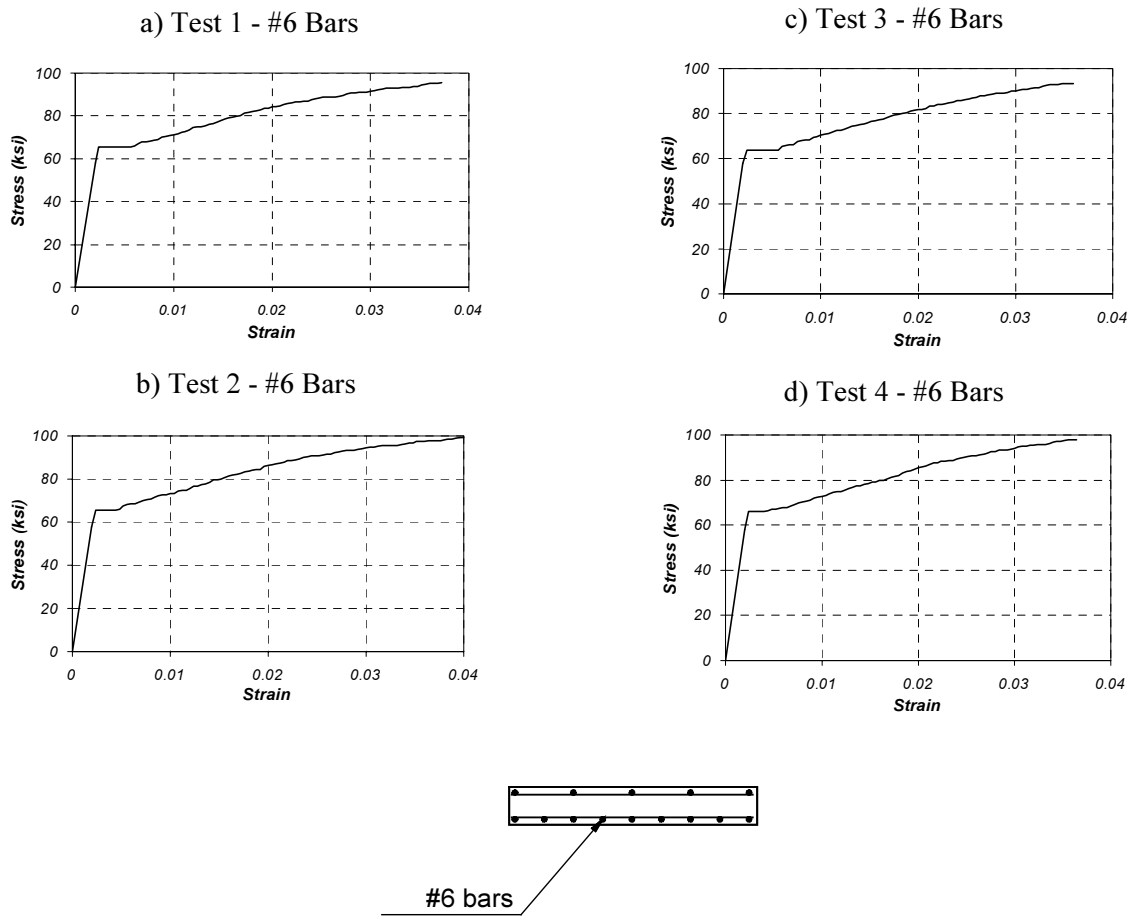

Figure A.13 Stress-Strain Curves for #6 Bars in Flat-Slab Specimens

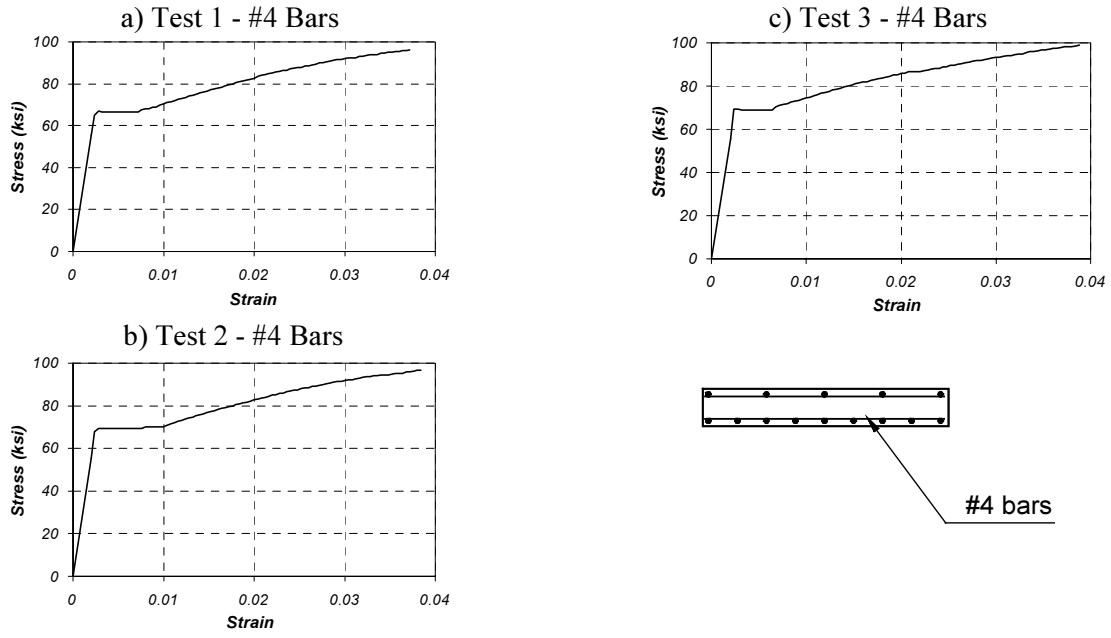

Figure A.14 Stress-Strain Curves for #4 Bars in Flat-Slab Specimens

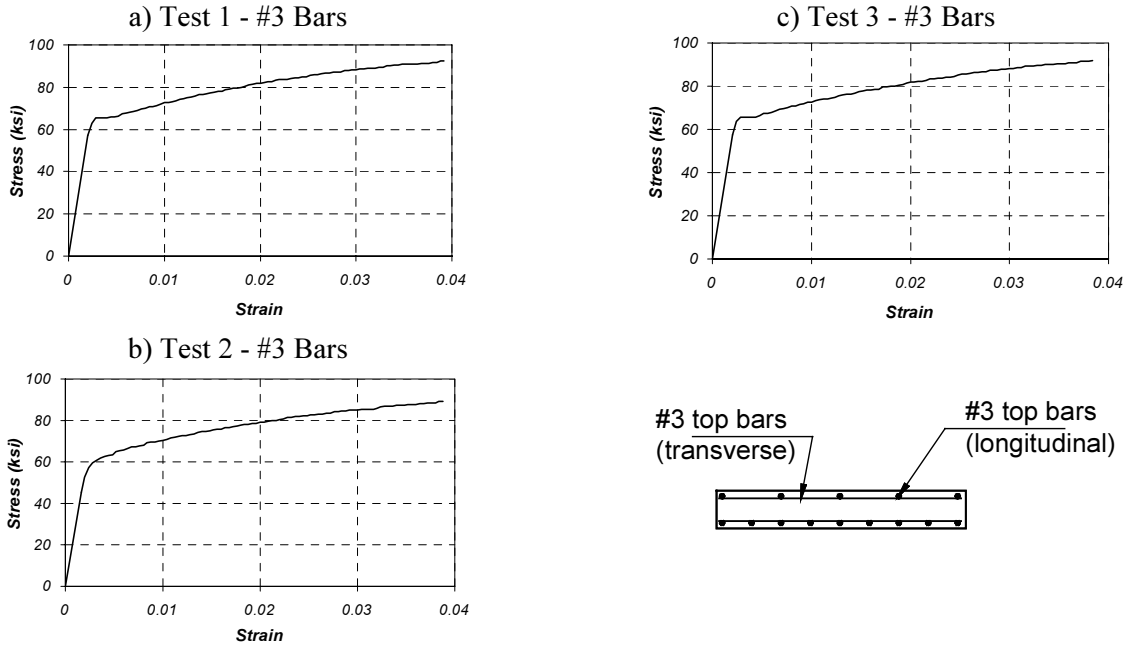

Figure A.15 Stress-Strain Curves for #3 Bars in Flat-Slab Specimens

Table A.3 Measured Yield and Ultimate Stresses for Reinforcing Bars

Bar No.	f_y static, ksi				$f_{y\ avg}$, ksi	Std Dev, ksi	f_y dynamic, ksi				$f_{y\ avg}$, ksi	Std Dev, ksi	$f_{u\ avg}$, ksi	Std Dev, ksi
	Test 1	Test 2	Test 3	Test 4			Test 1	Test 2	Test 3	Test 4				
Pan-Girder Specimens														
#8	75.3	70.0	72.8	68.5	71.7	3.0	77.7	72.2	74.6	70.3	73.7	3.2	114.0	1.9
#3	66.3	64.8	65.1	-	65.4	0.8	69.0	68.8	68.2		68.7	0.4	106.4	0.5
#4L	63.2	63.1	63.8	-	63.4	0.4	66.1	66.3	66.7		66.4	0.3	105.1	0.8
#4T	69.6	68.7	69.3	-	69.2	0.5	72.1	71.1	71.6		71.6	0.5	113.6	0.8
#5	70.2	65.7	71.2	-	69.0	2.9	70.9	67.2	71.7		69.9	2.4	112.7	2.7
Flat-Slab Specimens														
#6	63.1	64.2	62.4	64.4	63.5	0.9	65.0	65.8	64.4	66.3	65.4	0.8	106.1	1.5
#4	63.8	67.1	66.6	-	65.8	1.8	67.0	69.7	69.5		68.7	1.5	107.4	0.9
#3	63.2	60.9	63.2	-	62.4	1.3	65.8	63.1	65.7	-	64.9	1.5	99.2	1.8

A.3 CFRP PLATES AND SHEETS

Properties for the CFRP systems were not determined in the laboratory. However, it is recommended that the CFRP systems be tested in future laboratory experiments. Coupons can be removed from the strengthened specimens after failure to determine the actual properties of the complete CFRP/epoxy system.

The values that were used in calculations are listed in Table A.4 and are the values reported in each of the manufacturers' literature. The systems used in this research project are proprietary so only the mechanical properties of the composites were available. For the composites formed using unidirectional carbon fibers, the manufacturer publishes the stress-strain parameters based on the dimensions of the fibers only and not on the thickness of the formed composite (see bottom row in Table A.4). This is the reason why the thickness of this system is smaller than the thickness of the other two types of composites listed in the table.

The mechanical properties for the resins used to impregnate and bond the different composite systems to the surface of the concrete are listed in Tables A.5 through A.7. These data were also obtained from the literature published by the manufacturer of each proprietary system.

Table A.4 Properties of CFRP Composite Systems Used for Specimen Strengthening Published by Manufacturers [Master Builders, 1998; Sika, 1997]

Composite Type	Manufacturer and System	t_p, in.	f_{pu}, ksi	E_p, ksi	ε_{max} (rupture)
Pultruded	Sika, Corp. (Sika® Carbodur®)	0.047	348	22,500	0.015
Woven Fabric	Sika/Hexcel (SikaWrap® Hex 103 C)	0.040	139	10,600	0.013
Unidirectional Fiber	Master Builders (Mbrace™ CF 130)	0.0065*	505	33,000	0.015

* Thickness used for design calculations. Actual thickness after fabrication ranges from 0.03 to 0.06 in. per ply.

Table A.5 Mechanical Properties of Resin (Mbrace™ Saturant) Used for Mbrace™ System [Master Builders, 1998]

Property	Tension[1]	Flexure[2]	Compression[3]
Maximum Stress (psi)	8,000	20,000	12,500
Stress at Yield (psi)	7,800	20,000	12,500
Stress at Rupture (psi)	7,900	18,000	-
Strain at Maximum Stress	0.030	0.042	0.050
Strain at Yield	0.025	0.038	0.050
Strain at Rupture	0.035	0.050	-
Elastic Modulus (psi)	440,000	540,000	380,000
Poisson's Ratio	0.40	-	-

Notes: Properties determined at 72° F and 40% relative humidity after curing for 7 days.
[1]ASTM D-638 [ASTM, 2000a]
[2]ASTM D-790 [ASTM, 2000b]
[3]ASTM D-695 [ASTM, 1996]

Table A.6 Mechanical Properties of Epoxy Paste (SikaDur® 30) Used to Bond Pultruded Plates [Sika, 1997]

Property	Tension[1]	Flexure[2]	Compression[3]
Maximum Stress (psi)	3,600	6,800	8,600
Strain at Maximum Stress	0.010	-	-
Elastic Modulus (psi)	650,000	1,700,000	390,000

Notes: Properties determined at 73° F and 50% relative humidity after curing for 7 days.
[1]ASTM D-638 [ASTM, 2000a]
[2]ASTM D-790 [ASTM, 2000b]
[3]ASTM D-695 [ASTM, 1996]

Table A.7 Mechanical Properties of Impregnating Resin (SikaDur Hex 300/306) for SikaWrap Hex 103 C Woven Fabric [Sika, 1999]

Property	Tension[1]	Flexure[2]
Maximum Stress (psi)	10,500	17,900
Strain at Maximum Stress	0.048	-
Elastic Modulus (psi)	459,000	452,000

Notes: Properties determined at 73° F and 50% relative humidity after curing for 7 days.
[1]ASTM D-638 [ASTM, 2000a]
[2]ASTM D-790 [ASTM, 2000b]
[3]ASTM D-695 [ASTM, 1996]

Appendix B: Bridge Load Rating Procedure

B.1 INTRODUCTION

The bridge load rating method contained in the AASHTO *Manual for Condition Evaluation of Bridges* [AASHTO, 1994] is summarized in this appendix. There are two rating methods as described in the AASHTO *Manual* [1994]: an allowable stress method and a load factor method. The method that was chosen for this research study is presented in Section B.4 and is based on the use of load factors.

The first step to determine the load rating of the prototype bridges used in this research project was to calculate the dead and live-load moments acting on the structural components. For the pan-girder prototype bridge, the dead-load moment was based on the self-weight of each joist and a weight provision for a ½ in. overlay. Live-load moments were calculated based on the distribution of wheel loads to individual joists depending on the joist spacing. The procedure is described in detail in Chapter 3.

For the flat-slab prototype bridge, the procedure to distribute the dead and live-load moments to the flat-slab and curbs was based on empirical coefficients developed from research conducted at the University of Illinois in the 1940s. Coefficients to distribute moments to the slab and curbs were obtained from the analysis of edge-stiffened plates using elastic plate theory [Jensen et al., 1943]. This procedure is summarized in Section B.3.

B.2 DESCRIPTION OF DESIGN TRUCKS USED FOR LOAD RATING

Load rating is used as a measure of the load-carrying capacity of a bridge. Therefore, the load rating of a bridge is specified in terms of the same trucks that are used for design. Two different design trucks are used to specify the load rating of a bridge: H-truck and HS-truck. The characteristics of the design vehicles are illustrated in Figure B.1 [AASHTO, 1996].

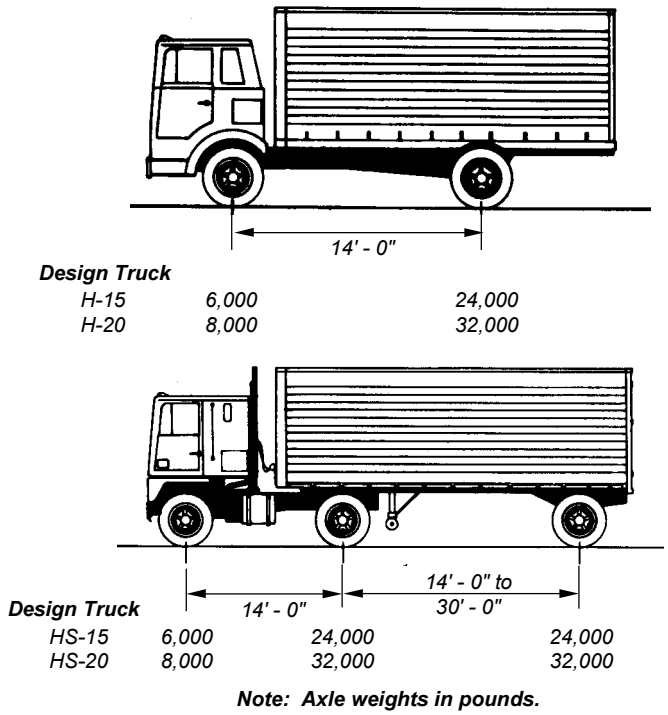

Figure B.1 Design Trucks used for Bridge Load Rating

B.3 DISTRIBUTION OF MOMENTS ON FLAT-SLAB BRIDGES

The total maximum moment at midspan on a short-span, simply-supported, flat-slab bridge can be calculated using:

$$M_{total} = m\frac{Pl}{4} + \frac{pbL^2}{8} + \frac{2qL^2}{8} \qquad \textbf{(B.1)}$$

where

m = Number of wheel loads on bridge
P = Live load due to one rear wheel
L = Span length of the bridge from center to center of bearing areas
p = Dead load per unit area between inside faces of curbs
b = Width of the roadway between inside faces of curbs
q = Dead load per unit length along curb

The first term in Eq. B.1 represents the moment due to live load from wheel loads at midspan, the second term represents the moment due to the dead load of the slab, and the third term represents the moment due to the dead load of the curbs. Equation B.1 assumes that the maximum live-load moment occurs when the rear axle of an H-design truck is located at midspan. However, when multiple axles of the HS-truck configuration generate moments that are larger than the moments from the H-truck configuration at midspan, the live-load moment at midspan from a single axle is increased to the live-load moment caused by multiple axles on the bridge.

The total moment across the bridge is distributed to the curbs and slab using empirical coefficients. The moment distributed to the curbs can be calculated using:

$$M_{curb} = C_1 \frac{PL}{4} + C_2 \frac{pbL^2}{8} + C_3 \frac{2qL^2}{8} \quad \textbf{(B.2)}$$

with the empirical coefficients, C_i, determined from:

$$C_1 = \left(\frac{12}{2.5 + G} \right) \frac{4 - (\nu / L)}{4 + 28(\nu / L)} \quad \textbf{(B.3)}$$

$$C_2 = \frac{0.5(L/b)}{0.47G + \sqrt[3]{1.15 + (L/b)^3}} \quad \textbf{(B.4)}$$

$$C_3 = \frac{\sqrt[3]{1.15 + (L/b)^3}}{0.47G + \sqrt[3]{1.15 + (L/b)^3}} \quad \textbf{(B.5)}$$

where

G = Stiffness parameter = $\dfrac{Lh^3}{12I}$

h = Overall depth of slab

I = Moment of inertia of the gross section of the curb outside the roadway width

ν = Axle width, center to center of truck tires

The moment distributed to the slab is then calculated by subtracting the moment distributed to the curbs, M_{curb}, from the total static moment, M_{total}. However, the moment calculated from Eq. B.2 is based on a wheel load located 2 ft from the curb to generate the maximum effect on the curb. Therefore, the term corresponding to live-load moment in Eq. B.2 is first reduced by 25% before subtracting the moment from the two curbs from the total moment across the bridge, M_{total}. This reduction reflects a truck location closer to the centerline of the roadway to generate maximum effects on the slab:

$$M_{es} = (m - 1.5C_1)\frac{PL}{4} + (1 - 2C_2)\frac{pbL^2}{8} + (2 - 2C_3)\frac{qL^2}{8} \quad \textbf{(B.6)}$$

Therefore, the average moment per unit width of slab can be calculated as:

$$M_{slab} = (m - 1.5C_1)\frac{PL}{4b} + (1 - 2C_2)\frac{pL^2}{8} + (1 - C_3)\frac{qL^2}{4b} \quad \textbf{(B.7)}$$

The studies used to develop these provisions indicated that a portion of the slab adjacent to the curbs acted compositely and forming an L-shaped section on each side of the bridge. The recommended width

acting compositely with the curbs was equal to 4 times the slab thickness. Therefore, the moment that needs to be resisted by the L-shaped curbs can be calculated as:

$$M_{L-curb} = M_{curb} + 4hM_{slab} \quad \textbf{(B.8)}$$

Finally, for load rating, dead and live-load effects have to be considered separately on the individual components. The separate effects due to dead loads and live loads can be calculated from:

$$\left(M_{slab}\right)_{DL} = \left(1-2C_2\right)\frac{pL^2}{8} + \left(1-C_3\right)\frac{qL^2}{4b} \quad \textbf{(B.9)}$$

$$\left(M_{slab}\right)_{LL} = \left(m-1.5C_1\right)\frac{PL}{4b} \quad \textbf{(B.10)}$$

$$\left(M_{L-curb}\right)_{DL} = C_2\frac{pbL^2}{8} + C_3\frac{qL^2}{8} + 4h\left(M_{slab}\right)_{DL} \quad \textbf{(B.11)}$$

$$\left(M_{L-curb}\right)_{LL} = C_1\frac{PL}{4} + 4h\left(M_{slab}\right)_{LL} \quad \textbf{(B.12)}$$

B.4 BRIDGE LOAD RATING

The moments distributed to the individual structural members according to Section 4.2.3 for pan-girder bridges or Section B.3 for flat-slab bridges are used to calculate the overall bridge rating. The load rating procedure is based on calculating a rating factor for each of the structural elements. This procedure gives two rating levels depending on the load factors used to calculate the rating factor: operating and inventory rating. The inventory-rating level represents the load that a bridge can withstand, with an adequate margin of safety, under service conditions. The operating-rating level represents the load that can be supported under unusual bridge overloads. The rating levels are expressed in terms of an AASHTO design truck.

For the pan-girder bridge rating, the difference between the two rating levels is only due to the load factors that are used for the live load effects. The factors used for live-load effects are equal to 2.17 and 1.30 for inventory-rating and operating-rating levels, respectively.

For the flat-slab bridge rating, the different rating levels depend not only on the load factors used for live-load effects, but also on the manner in which the element that controls the rating is identified. For the inventory-rating level, the overall bridge rating is controlled by the element that has the lowest rating. For the operating level, the overall bridge rating is calculated using a weighted average of the individual element ratings. The weighting factors that are used are calculated based on the tributary width of each structural component on the bridge.

The rating factor equation is [AASHTO, 1994]:

$$RF = \frac{C - A_1 D}{A_2 L (1 + I)} \qquad \textbf{(B.13)}$$

where

RF = Rating factor for the live-load carrying capacity of the bridge
C = Strength reduction factor times nominal capacity of member
A_1 = Factor for dead load effects = 1.3 for inventory and operating rating
D = Dead-load effect on the member
A_2 = Factor for live-load effects = 2.17 for inventory rating and 1.3 for operating rating
L = Live-load effect on the member
I = Impact factor = 0.3

Once the rating factor is determined for all members that contribute to the structural capacity of the bridge, the rating of each member is determined with:

$$RT = (RF) W \qquad \textbf{(B.14)}$$

where

RT = bridge member rating, tons
W = weight of the first two axles of the design truck used in determining the live load effect, tons

The load rating results for the pan-girder prototype bridge are shown in Table B.1 and those for the flat-slab prototype bridge are shown in Tables B.2 and B.3. These were obtained using a spreadsheet developed at TxDOT by their BRINSAP Division [TxDOT, 1999]. It should be noted, however, that these sheets only contain the rating results for flexural effects and shear effects for the pan-girder prototype bridge had to be considered separately. For the flat-slab prototype bridge, the rating was first calculated considering the structural curbs and then calculated based on the flat-slab acting alone to examine the effect of curb removal on the bridge rating.

Table B.1 Load Rating of Pan-Girder Prototype Bridge

Pan Girder Bridge Rating

To Print - Ctrl P

Note: Ratings should include any structural deterioration that affects the load capacity of the structure.

System Information	
Date	05/28/00
Engineer Initials	SFB
Program Version Number	3.0

Bridge Information	
District	District (#)
County	County (#)
Structure #	CCCC-SS-SSS
CSJ ®	CCCC-SS-JJJ
Year Built	1951
Location	PROTOTYPE BRIDGE

® Cont-Sec-Job used for this analysis

USER INPUT	
Overall Span (ft)	30.00
Beam+Slab Depth = 24 or 33 (in)	24.00
Misc Dead Load per Beam (k/ft)	
Top Layer of Long. Steel	
Total Area of Steel (in^2)	
Distance from bottom (in)	
Bottom Layer of Long. Steel	
Total Area of Steel (in^2)	3.12
Distance from bottom (in)	2.375

Recommended Material Properties			
Fy (ksi)	33.0	f'c (ksi)	2.5

HS RATING	
Inventory Rating	HS- 12.2
Operating Rating	HS- 20.4
Legal HS Equivalent §	HS- 24.2

§ Based on Span Length & Texas Legal Load

SYSTEM DEFAULT INPUT	
Span bearing length deduct (ft)	2.00
Fy (ksi)	33.00
f'c (ksi)	3.00
Overlay (in)	0.50

Recommendation	
Posting	None
Inspection Frequency	12 months

Moments (kip-ft)	
Mdl	41.7
Cu	162.7
Undistributed Mll (H-20)	113.4
Undistributed Mll (HS-20)	126.0

H RATING	
Inventory Rating	H- 13.6
Operating Rating	H- 22.6

Calculated Values	
Distribution Factor	0.50
Impact Factor	1.30
a (in) *	1.12

* Depth of concrete ultimate stress block

See formula 6-1a (Manual for Condition Evaluation Bridges) for Rating Formula.

ADDITIONAL NOTES BELOW :

Table B.2 Load Rating of Flat-Slab Prototype Bridge Including the Contribution of Structural Curbs

Slab Bridge Rating

To Print - Ctrl P

Note: Ratings should include any structural deterioration that affects the load capacity of the structure.

System Information	
Date	08/02/00
Engineer Initials	SFB
Program Version Number	3.0

See below for input notes and assumptions.

USER INPUT	
Overall Span along Roadway (ft)	25.00
Overall Bridge Width (ft)	21.33
Skew (deg)	0.00
Slab Thickness (in)	11.00
Slab Steel Direction (P or N)	P
P = Parallel to rdwy, N = Normal to supports	
Area of Slab Tension Steel (in2/ft)	1.110
Distance from bottom of Slab (in)	1.75
Left (C)urb, (B)eam, or (N)one	**c**
Curb Height above Slab (in)	18.00
Top of Curb Width (in)	8.00
Bottom of Curb Width (in)	12.50
Misc. Dead Load on Curb (k/ft)	0.00
Area of Curb Tension Steel (in2)	3.720
Distance from bottom of Slab (in)	1.75
Area of Curb Comp. Steel (in2)	3.120
Distance from top of Curb (in)	2.00
Right (C)urb, (B)eam, or (N)one	**c**
Curb Height above Slab (in)	18.00
Top of Curb Width (in)	8.00
Bottom of Curb Width (in)	12.50
Misc. Dead Load on Curb (k/ft)	0.00
Area of Curb Tension Steel (in2)	3.720
Distance from bottom of Slab (in)	1.75
Area of Curb Comp. Steel (in2)	3.120
Distance from top of Curb (in)	2.00

SYSTEM DEFAULT INPUT	
Span bearing length deduct (ft)	1.00
Fy (ksi)	40.00
f'c (ksi)	3.00
Overlay (in)	0.50
Number of Live Load Lanes	2

Moments		
Slab		
(M slab)DL	(kft/ft)	5.18
(M slab)LL HS-20	(kft/ft)	16.03
(M slab)LL H-20	(kft/ft)	15.97
Cu slab	(kft/ft)	28.39
Left Curb		
(M l-curb)DL	(kft)	92.73
(M l-curb)LL HS-20	(kft)	187.05
(M l-curb)LL H-20	(kft)	186.40
Cu l-curb	(kft)	559.06
Right Curb		
(M l-curb)DL	(kft)	92.73
(M l-curb)LL HS-20	(kft)	187.05

Bridge Information	
District	
County	
Structure #	
CSJ ®	
Year Built	1945
Location	Flat-Slab Prototype Bridge

® Cont-Sec-Job used for this analysis

Structure # must be in format CCCC-SS-SSS

Recommended Values			
Fy (ksi)	33.0	f'c (ksi)	2.5
Number of Live Load Lanes			2

HS RATING		
Inventory Rating	HS-	12.4
Operating Rating	HS-	27.5
Legal HS Equivalent §	HS-	26.5

§ Based on Span Length & Texas Legal Load

Recommendation	
Posting	None
Inspection Frequency	12 months

H RATING		
Inventory Rating	H-	12.5
Operating Rating	H-	27.6

Calculated Values	
Analysis Method	Illinois Bulletin 346
Impact Factor	1.30
Effective Slab Width(in)	44.00
a-slab (in)	1.45
a-curb,left (in)	8.13
a-curb,right (in)	8.13

"a" = depth of concrete ultimate stress block

Effective slab width is that portion acting integra with curb or beam = 4 times slab thickness

Additional CSJ's For This Structure	
Cont-Sec-Job	
Cont-Sec-Job	
Cont-Sec-Job	

ADDITIONAL NOTES BELOW :

Table B.3 Load Rating of Flat-Slab Bridge Without the Contribution of Structural Curbs

Slab Bridge Rating

To Print - Ctrl P

Note: Ratings should include any structural deterioration that affects the load capacity of the structure.

System Information	
Date	08/02/00
Engineer Initials	SFB
Program Version Number	3.0

See below for input notes and assumptions.

Bridge Information	
District	
County	
Structure #	
CSJ ®	
Year Built	1945
Location	Flat-Slab Prototype Bridge

® Cont-Sec-Job used for this analysis

Structure # must be in format CCCC-SS-SSS

USER INPUT	
Overall Span along Roadway (ft)	25.00
Overall Bridge Width (ft)	21.33
Skew (deg)	0.00
Slab Thickness (in)	11.00
Slab Steel Direction (P or N)	P
P = Parallel to rdwy, N = Normal to supports	
Area of Slab Tension Steel (in2/ft)	1.110
Distance from bottom of Slab (in)	1.75
Left (C)urb, (B)eam, or (N)one	**n**
	18.00
	8.00
	12.50
	0.00
	3.720
	1.75
	3.120
	2.00
Right (C)urb, (B)eam, or (N)one	**n**
	18.00
	8.00
	12.50
	0.00
	3.720
	1.75
	3.120
	2.00

Recommended Values			
Fy (ksi)	33.0	f'c (ksi)	2.5
Number of Live Load Lanes			2

HS RATING		
Inventory Rating	HS-	6.0
Operating Rating	HS-	10.0
Legal HS Equivalent §	HS-	26.5

§ Based on Span Length & Texas Legal Load

Recommendation	
Posting	Required
Inspection Frequency	24 months

H RATING		
Inventory Rating	H-	6.0
Operating Rating	H-	10.0

SYSTEM DEFAULT INPUT	
Span bearing length deduct (ft)	1.00
Fy (ksi)	40.00
f'c (ksi)	3.00
Overlay (in)	0.50
Number of Live Load Lanes	2

Calculated Values		
Analysis Method	AASHTO	3.24.3.2
Impact Factor		1.30
a-slab (in)		1.45

"a" = depth of concrete ultimate stress block

Moments		
Slab		
(M slab)DL	(kft/ft)	10.33
(M slab)LL HS-20	(kft/ft)	23.02
(M slab)LL H-20	(kft/ft)	22.94
Cu slab	(kft/ft)	28.39

Additional CSJ's For This Structure	
Cont-Sec-Job	
Cont-Sec-Job	
Cont-Sec-Job	

ADDITIONAL NOTES BELOW :

Appendix C: Application of CFRP Composite Systems to Existing Reinforced Concrete Elements

C.1 INTRODUCTION

Two types of composite systems were used to strengthen the reinforced concrete specimens that were part of the experimental portion of this research project. These systems differ primarily in the method that is used for their fabrication and also on the procedure that is used to bond them to the concrete surface. A description of the procedures that were used to attach these systems to the laboratory specimens is presented in this appendix. These procedures were based on the recommendations provided by the manufacturer of each of the composite systems.

C.2 PULTRUDED CFRP SYSTEM

C.2.1 Description of Composite System

The CFRP pultruded system used in this research project consisted of plates that were fabricated using the pultrusion process. In this process, continuous carbon fiber roving is impregnated in a resin bath and pulled through a forming die at an elevated temperature. The carbon fibers were oriented along the plate longitudinal axis (unidirectional carbon fibers). The resin bath is usually mixed with a curing agent so that curing initiates simultaneously as the fibers are pulled through the die. The temperature, pulling speed, and length of the die are controlled to ensure that the resin fully cures before the fiber-reinforced element exits the die [Mallick, 1993]. The member is cooled with air or water after exiting the forming die. The elements are then cut to the required length using a diamond saw at the end of the pultrusion line (Figure C.1).

A limitation of this fabrication process is that only elements that have a constant cross section can be manufactured economically. An advantage of using this procedure is that the elements are fabricated in a controlled environment and better quality control is achieved. Also, large volume contents of fibers can be used in the composites fabricated using this procedure.

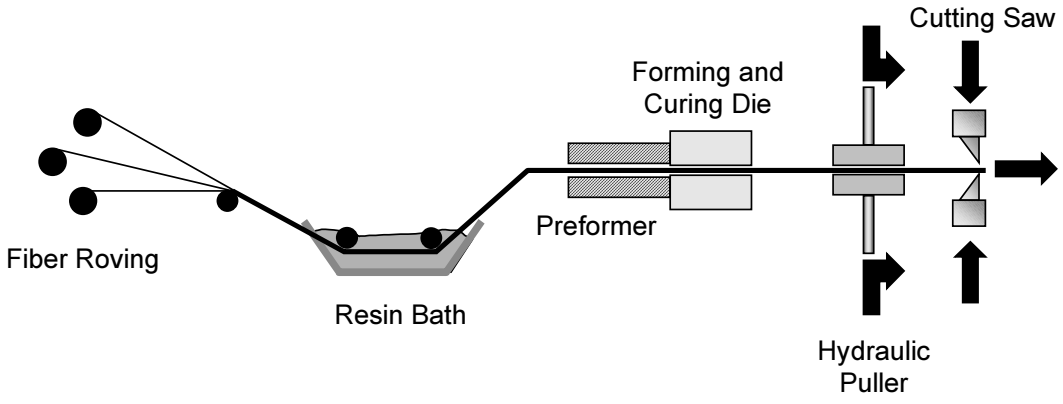

Figure C.1 Schematic Representation of the Fabrication of a Fiber Reinforced Polymer Plate using the Pultrusion Process [Mallick, 1993]

C.2.2 Application to Reinforced Concrete Element

The application of the pultruded CFRP system that was used to strengthen the reinforced concrete laboratory specimens can be summarized in the following steps and is illustrated in Figure C.2:

a) Preparation of concrete surface and CFRP plate

- Prepare concrete surface by grinding or light sandblasting to expose aggregates.
- Remove loose concrete particles generated during surface preparation using pressurized air.
- Clean concrete surface and CFRP pultruded plates with acetone until a white cloth remains white after wiping.

b) CFRP system application

- Mix epoxy paste and hardener for three minutes at approximately 400 to 600 RPM. The mixing proportions should follow the values recommended by the manufacturer.
- Apply a thin layer (approximately 1/16-in.) of mixed epoxy paste to the concrete surface, covering the area where the pultruded plates will be installed.
- Apply a layer of epoxy paste to the clean CFRP plate. The epoxy paste should have a triangular section after application on the plate
- Place CFRP plate on concrete surface and apply hand pressure to force epoxy paste out of the plate.
- Clean excess epoxy from sides of plates.

A woven carbon fiber sheet was used to fabricate straps to wrap the CFRP pultruded plates at discrete locations and avoid premature debonding of the pultruded plates. These straps were applied using the procedures described for the CFRP wet-layup system in Section C.3. The procedure is illustrated in Figure C.3.

The thickness of the pultruded plates system was approximately 1/8 in. after placement on the concrete surface. Therefore, to place the woven fabric straps and avoid having a sharp bend at the plate boundary, epoxy paste was built up, forming a ramp. The woven fabric straps were placed on the reinforced concrete element after the epoxy paste that formed the ramps had hardened.

a) Surface grinding

d) Applying epoxy to surface

b) CFRP plate cleaning

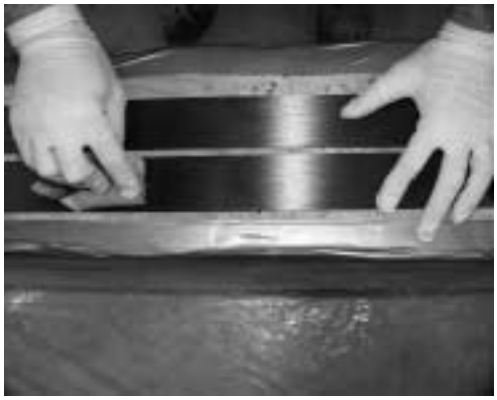

e) Positioning CFRP plate on beam

c) Mixing epoxy paste

f) Strengthened beam

Figure C.2 Application of CFRP Pultruded Plates to Reinforced Concrete Beam

a) Cutting Woven CFRP mat

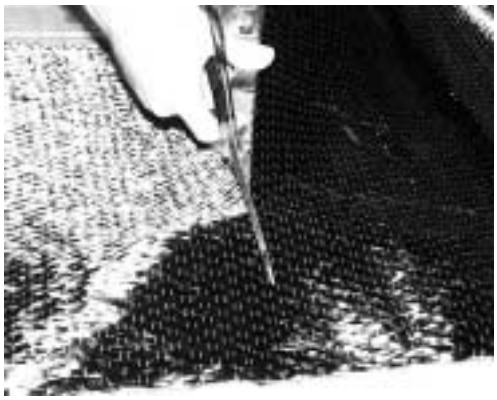

c) Placing woven straps around beam

b) Applying epoxy on concrete surface

d) Final configuration of beam

e) Final configuration of full-scale joist after strengthening

Figure C.3 Application of Woven Straps Around CFRP Pultruded Plates

C.3 WET-LAYUP CFRP SYSTEM

C.3.1 Description of Composite System

The CFRP composite system that was used in this research project consisted of dry unidirectional carbon fiber sheets that were impregnated with an epoxy resin to form the composite in the laboratory. The fabrication process is termed "wet-layup process" because the carbon fiber sheets are impregnated sequentially as they are positioned on the concrete element.

The main disadvantage of this composite system is caused by the large variability introduced by the manufacturing process. Because the epoxy resin that forms the matrix of the composite is applied manually, significant variations in the composite thickness can result. For the composites that were used in this study, the actual composite thickness ranged from 0.04 to 0.06-in. per carbon fiber ply. Recognizing this inherent variability, the manufacturer of this system suggests using the carbon fiber thickness for design calculations because the uniaxial tensile stress behavior is controlled by the carbon fibers.

C.3.2 Application to Reinforced Concrete Element

The procedure that was used in this research project to apply this CFRP composite system is summarized below. These steps were followed according to recommendations from the manufacturer of the system (Figure C.4):

a) Preparation of concrete surface

- Remove loose concrete particles from surface using a grinding tool. Remove dust generated during grinding using compressed air.
- Fill concrete voids with epoxy putty.

b) CFRP system application

- Apply epoxy primer to seal the concrete surface. Wait until primer reaches a tack-free condition before applying epoxy on the concrete surface.
- Mix two-component epoxy resin using the mixing ratio specified by the manufacturer. Mix using a power drill at a low speed (approximately 400 RPM) using an epoxy paddle.
- Apply a coat of mixed epoxy resin on the concrete surface. This layer will partially impregnate the carbon fibers after they are placed on the concrete element.
- Cut carbon fiber sheets to the required width and length.
- Place carbon fiber sheets on concrete surface over area that was previously coated with epoxy resin. Placement should begin on one end of the concrete element and continue toward the other end.
- Remove backing paper and use a ribbed roller to remove air bubbles that are trapped behind the carbon fiber sheet. Let carbon fibers impregnate in the epoxy resin for approximately 30 minutes.
- Apply a coat of epoxy resin on top of the carbon fibers to enhance impregnation and to form the composite matrix.
- Apply subsequent layers (plies) of carbon fiber sheets and epoxy coat, if required by design, following the procedure described above.

a) Unidirectional carbon fiber sheet

b) Cutting carbon fiber sheets

c) Applying epoxy to surface

d) Placing carbon fiber sheet on joist

e) Eliminating air bubbles from sheets

f) Coating placed sheets with epoxy

Figure C.4 Application of CFRP Wet-Layup System to Reinforced Concrete Element

Appendix D: Measured Strains

Measured readings from strain gages located at four different sections for the test specimens are presented in this appendix. The instruments were positioned on the reinforcing bars, CFRP composites and concrete surface.

For the pan-girder specimens, each instrumented section contained four strain gages on the reinforcing bars, four strain gages on the CFRP composite, and five concrete gages in specimen J-1 or three concrete gages in specimen J-2. For the flat-slab specimens, three strain gages were attached to the reinforcing bars, four to the CFRP composites, and three to the concrete surface at each instrumented section. The location of the instrumented sections for the pan-girder specimens and the flat-slab specimens is shown in Figures D.1 and D.2, respectively. Only the concrete gages are indicated in these figures, but the positions of gages on the reinforcement and CFRP composites are indicated in each of the corresponding strain plots. Characteristics of the strain gages are listed in Table D.1.

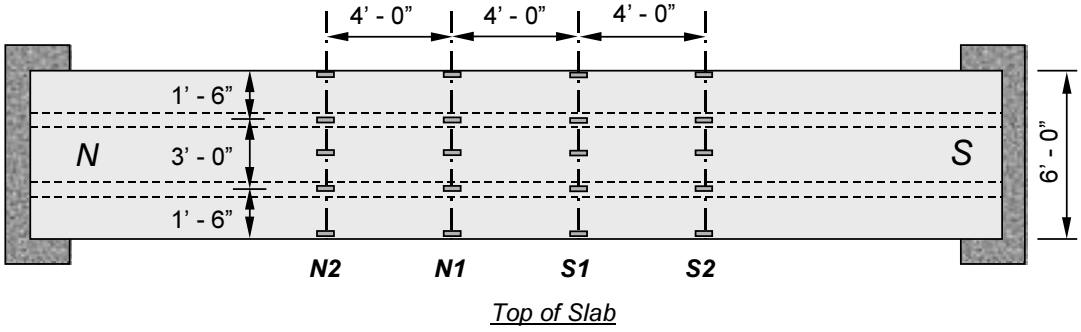

Figure D.1 Position of Instrumented Sections for Pan-Girder Specimens

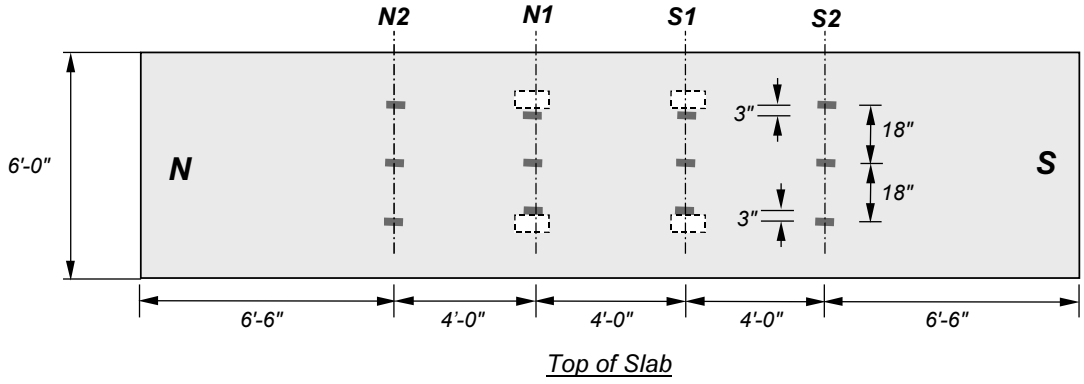

Figure D.2 Position of Instrumented Sections for Flat-Slab Specimens

Table D.1 Characteristics of Strain Gages

Material	Strain Gage Type	Nominal Resistance, Ohms	Gage Length, mm	Gage Factor
Steel	Foil	119.5±0.5	6	2.12±1%
CFRP	Foil	119.5±0.5	6	2.12±1%
Concrete	Wire	120±0.5	60	2.09±1%

Strain gage readings were used to compute internal stresses and forces and to determine the location of the neutral axis during the tests. These results are presented in Chapter 5 for the pan-girder specimens and in Chapter 8 for the flat-slab specimens. Only the outputs from the instruments as were recorded during the tests without any modification are presented in this appendix.

Figures D.3 to D.14 show load vs. strain plots for the four instrumented sections in specimen J-1. Measured strains on the reinforcement are contained in Figures D.3 to D.6, on the CFRP plates in Figures D.7 to D.10, and on the concrete slab in Figures D.11 to D.14, respectively.

Figures D.15 to D.26 show load vs. strain plots for the four instrumented sections in specimen J-2. Measured strains on the reinforcement are contained in Figures D.15 to D.18, on the CFRP sheets in Figures D.19 to D.22, and on the concrete slab in Figures D.23 to D.26, respectively.

Figures D.27 to D.30 show load vs. strain plots for the four instrumented sections in specimen FS-1. Measured strains on the reinforcement are contained in Figures D.27 to D.30, on the concrete slab in Figures D.31 to D.34, and on the CFRP plates in Figures D.35 to D.38, respectively.

Finally, Figures D.39 to D.50 show load vs. strain plots for the four instrumented sections in specimen FS-2. Measured strains on the reinforcement are contained in Figures D.39 to D.42, on the concrete slab in Figures D.43 to D.46, and on the CFRP plates in Figures D.47 to D.50, respectively.

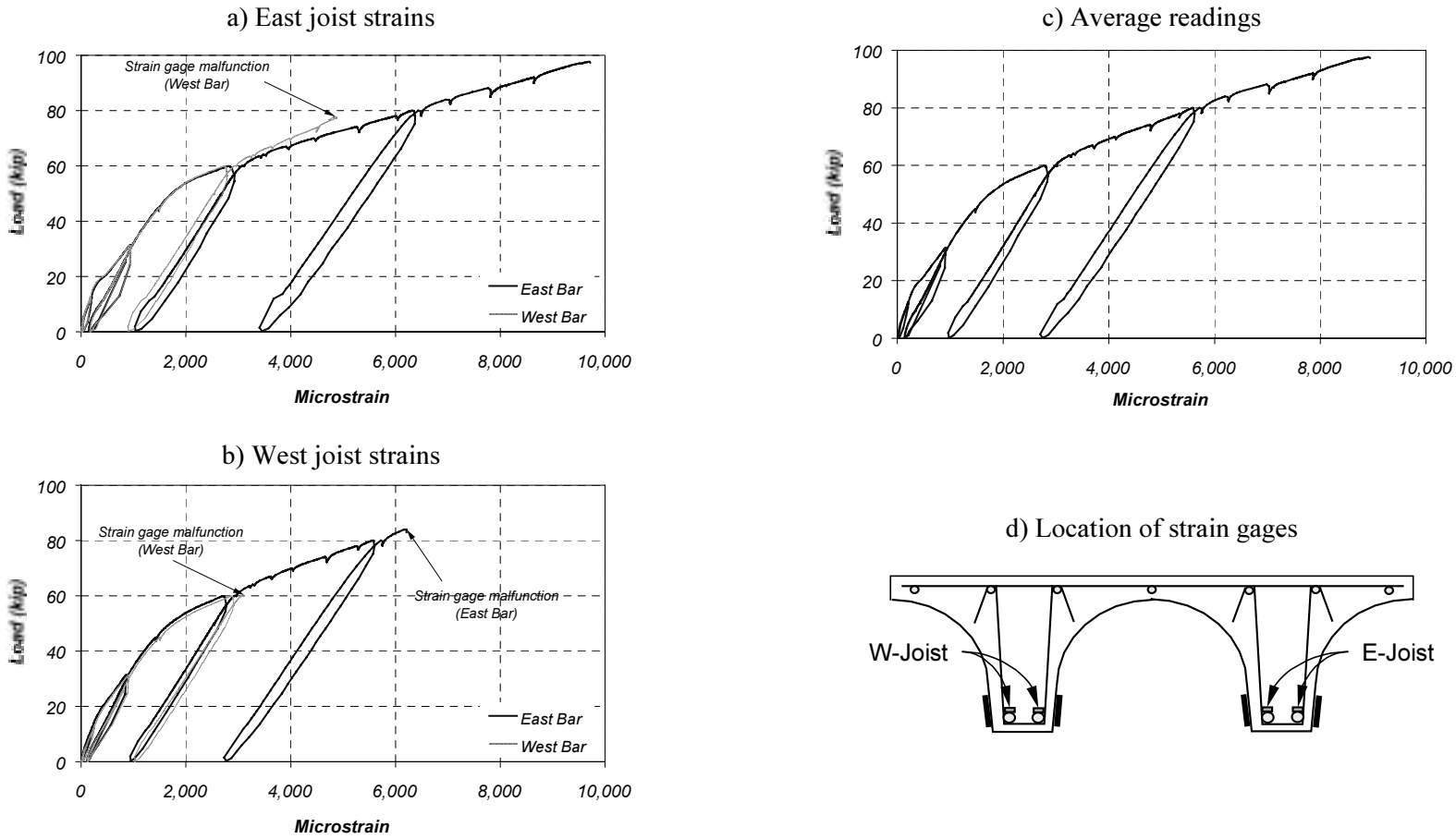

Figure D.3 Measured #8 Reinforcing Bar Strains in Specimen J-1 (Section N1)

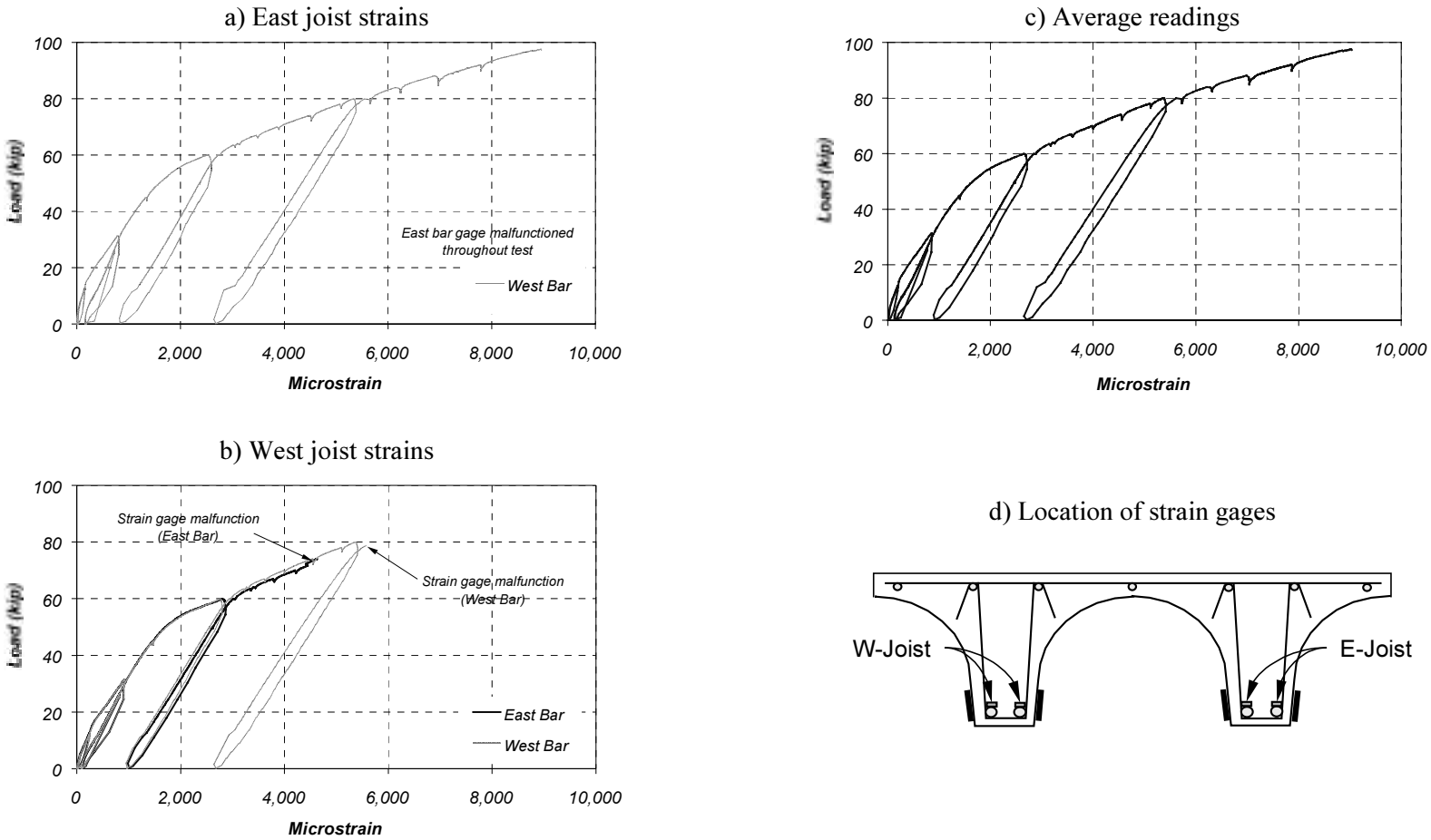

Figure D.4 Measured #8 Reinforcing Bar Strains in Specimen J-1 (Section S1)

a) East joist strains

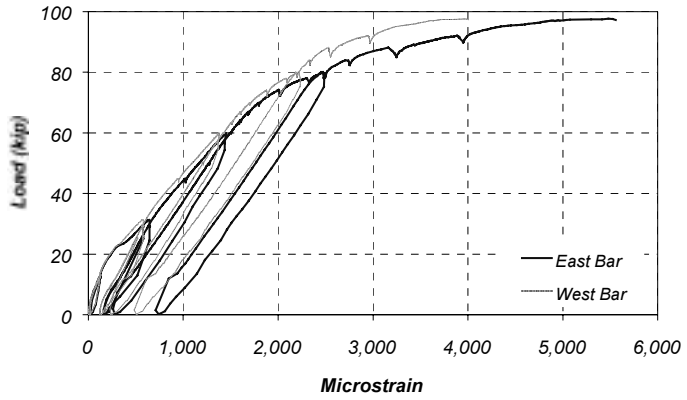

b) West joist strains

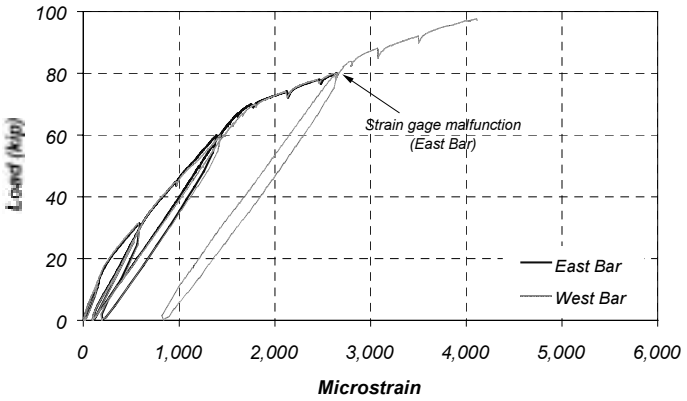

c) Average readings

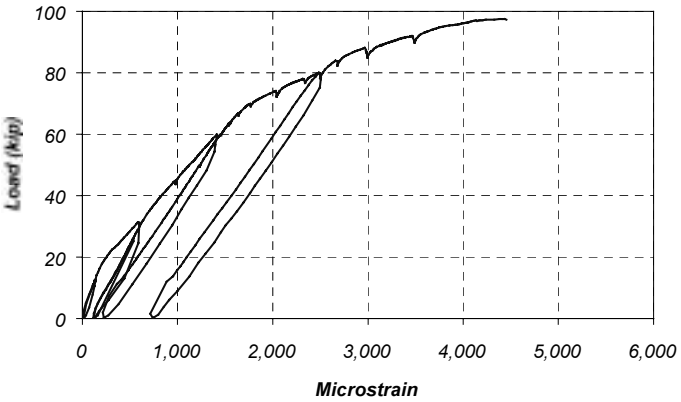

d) Location of strain gages

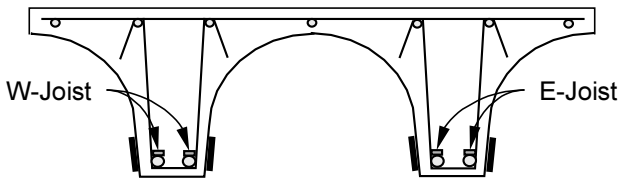

Figure D.5 Measured #8 Reinforcing Bar Strains in Specimen J-1 (Section N2)

a) East joist strains

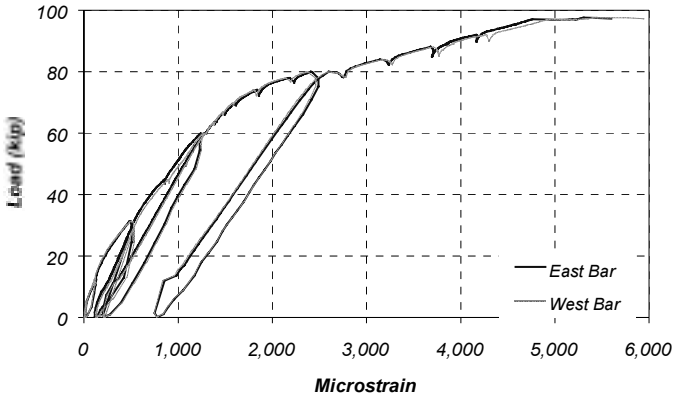

b) West joist strains

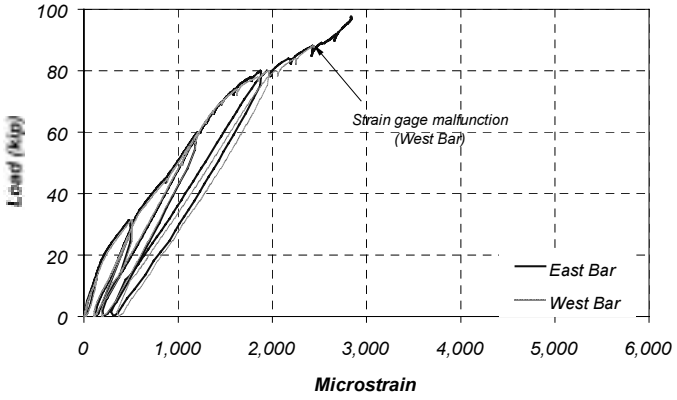

c) Average readings

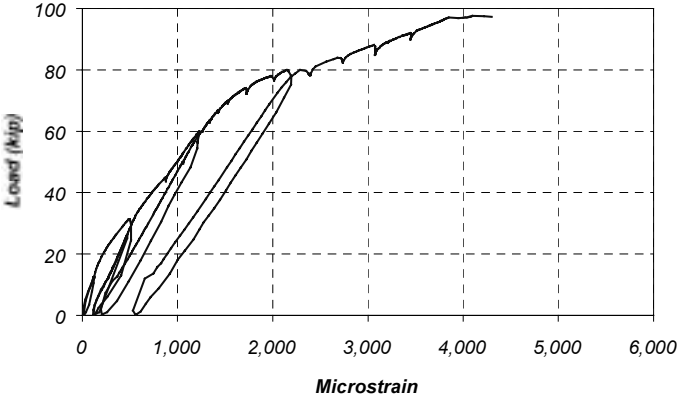

d) Location of strain gages

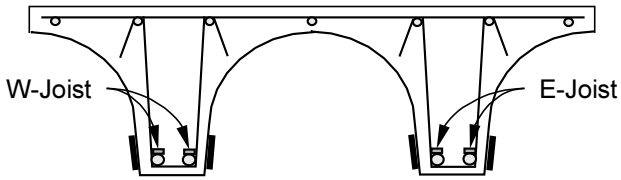

Figure D.6 Measured #8 Reinforcing Bar Strains in Specimen J-1 (Section S2)

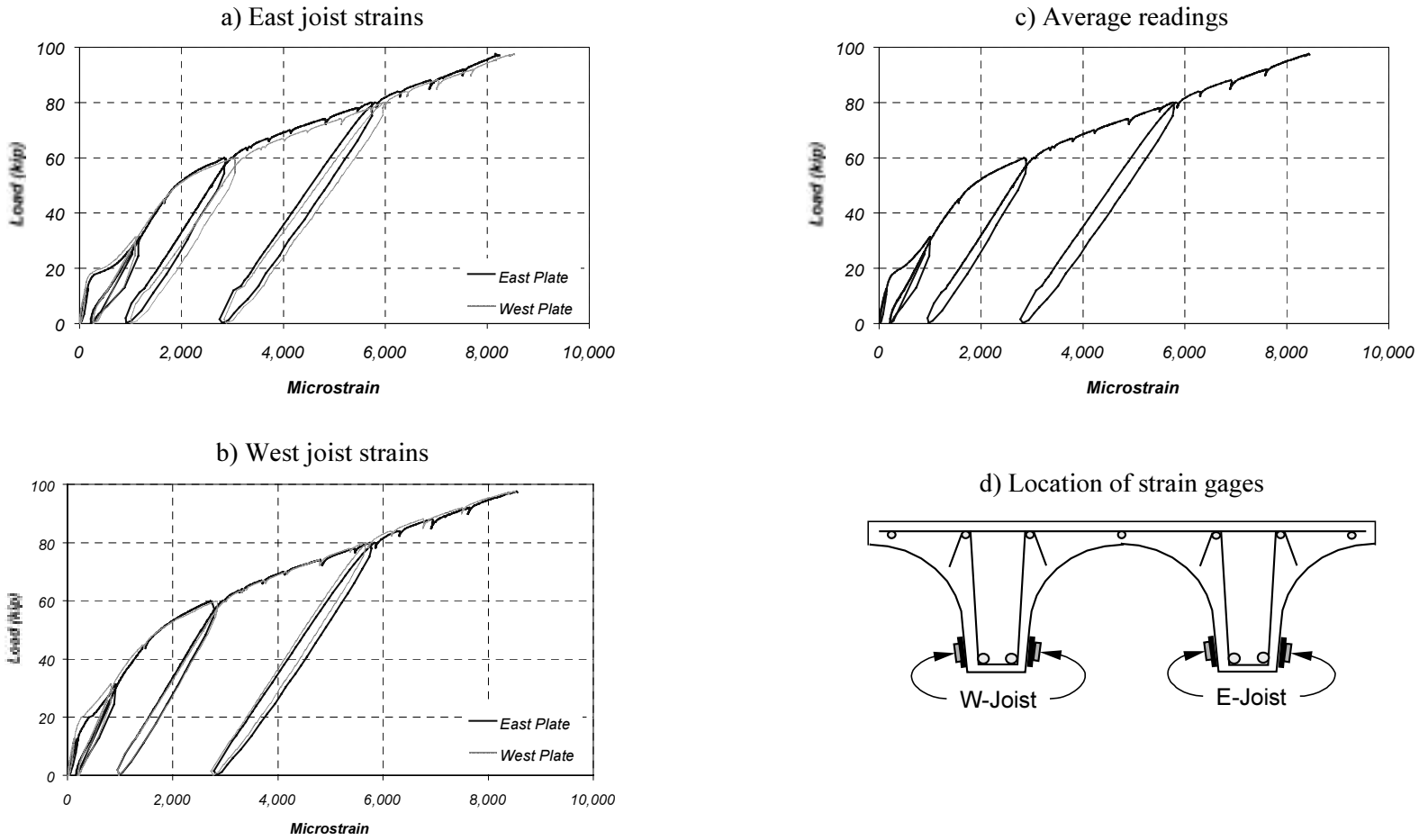

Figure D.7 Measured CFRP Strains in Specimen J-1 (Section N1)

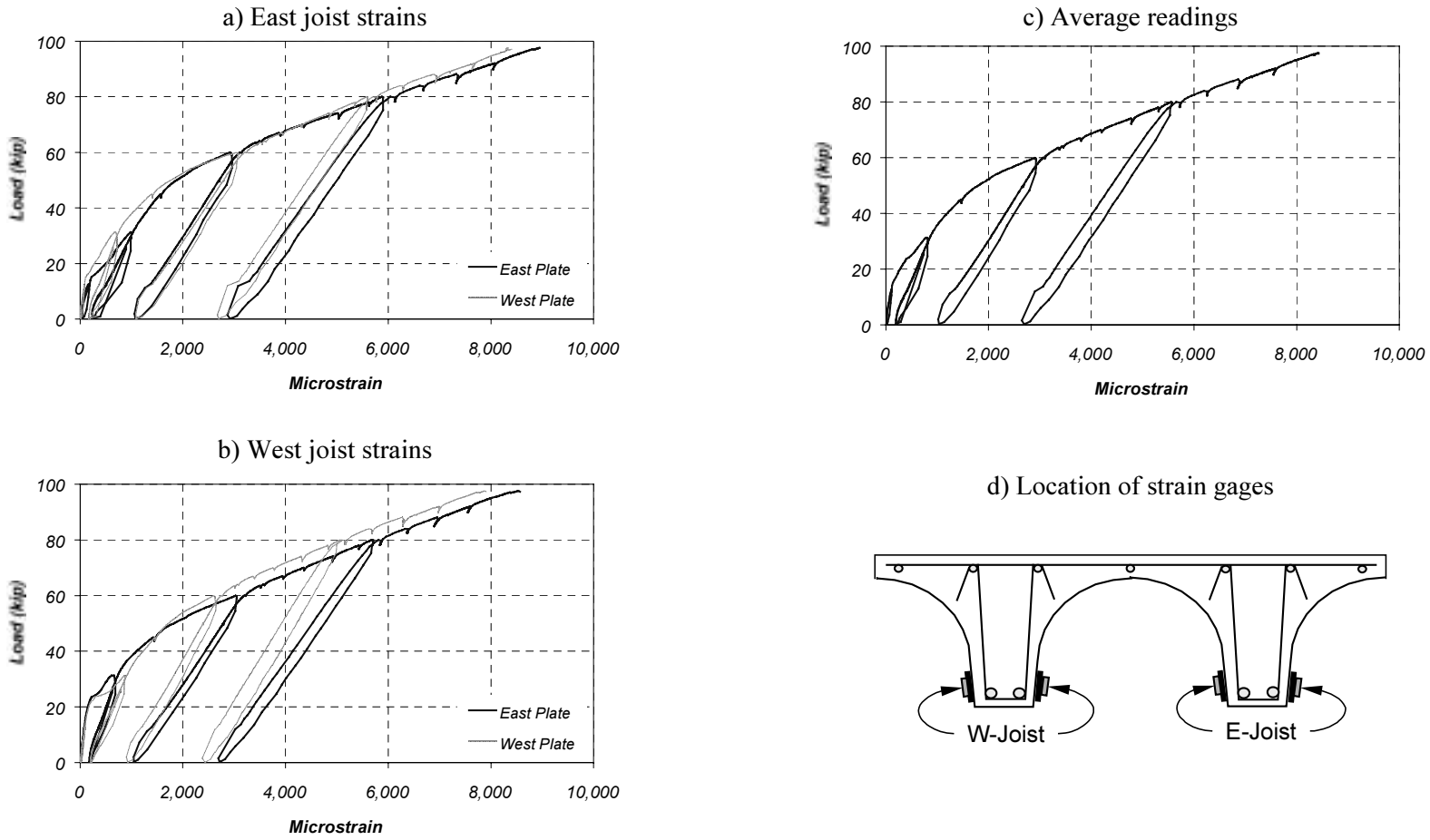

Figure D.8 Measured CFRP Strains in Specimen J-1 (Section S1)

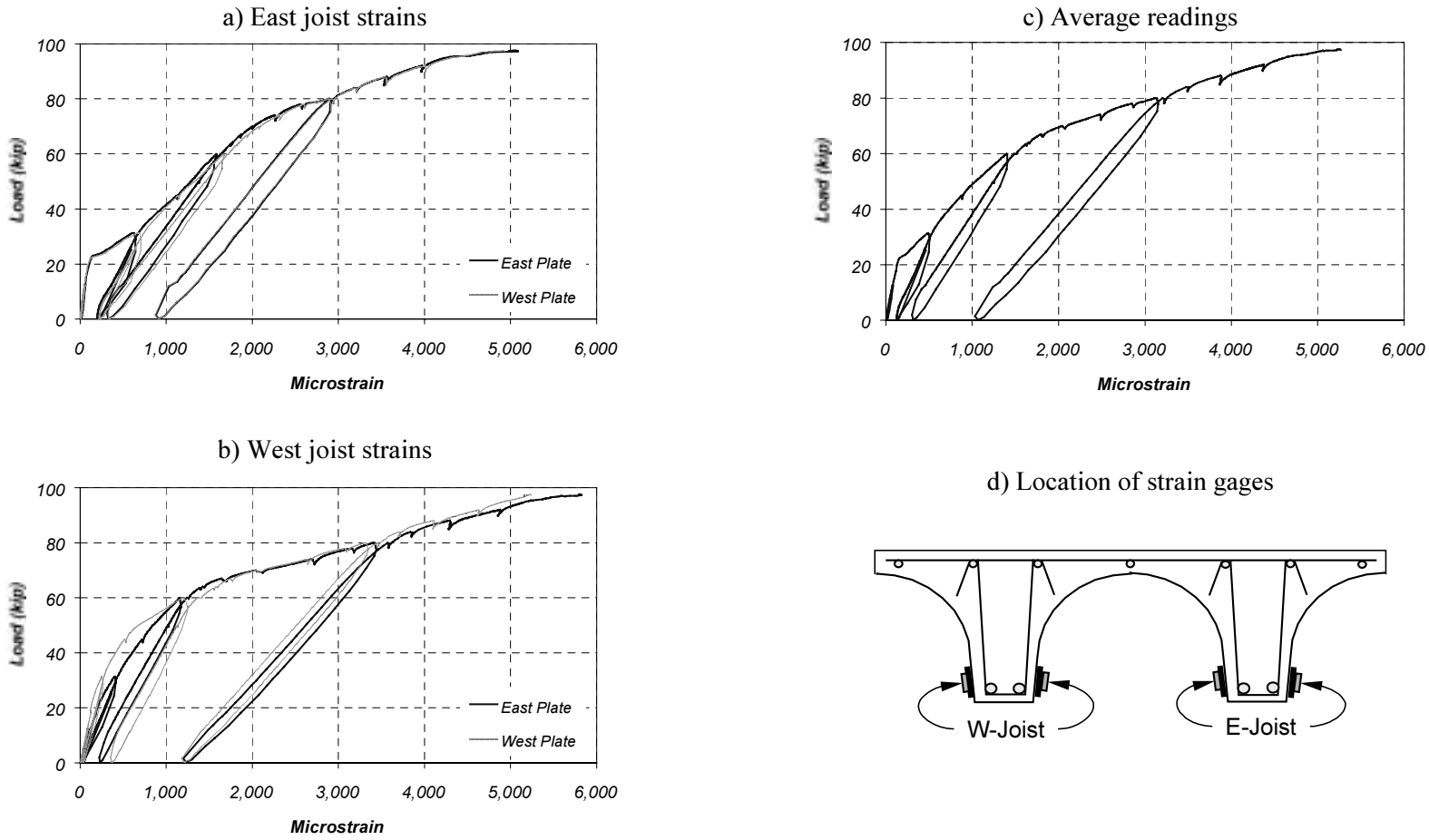

Figure D.9 Measured CFRP Strains in Specimen J-1 (Section N2)

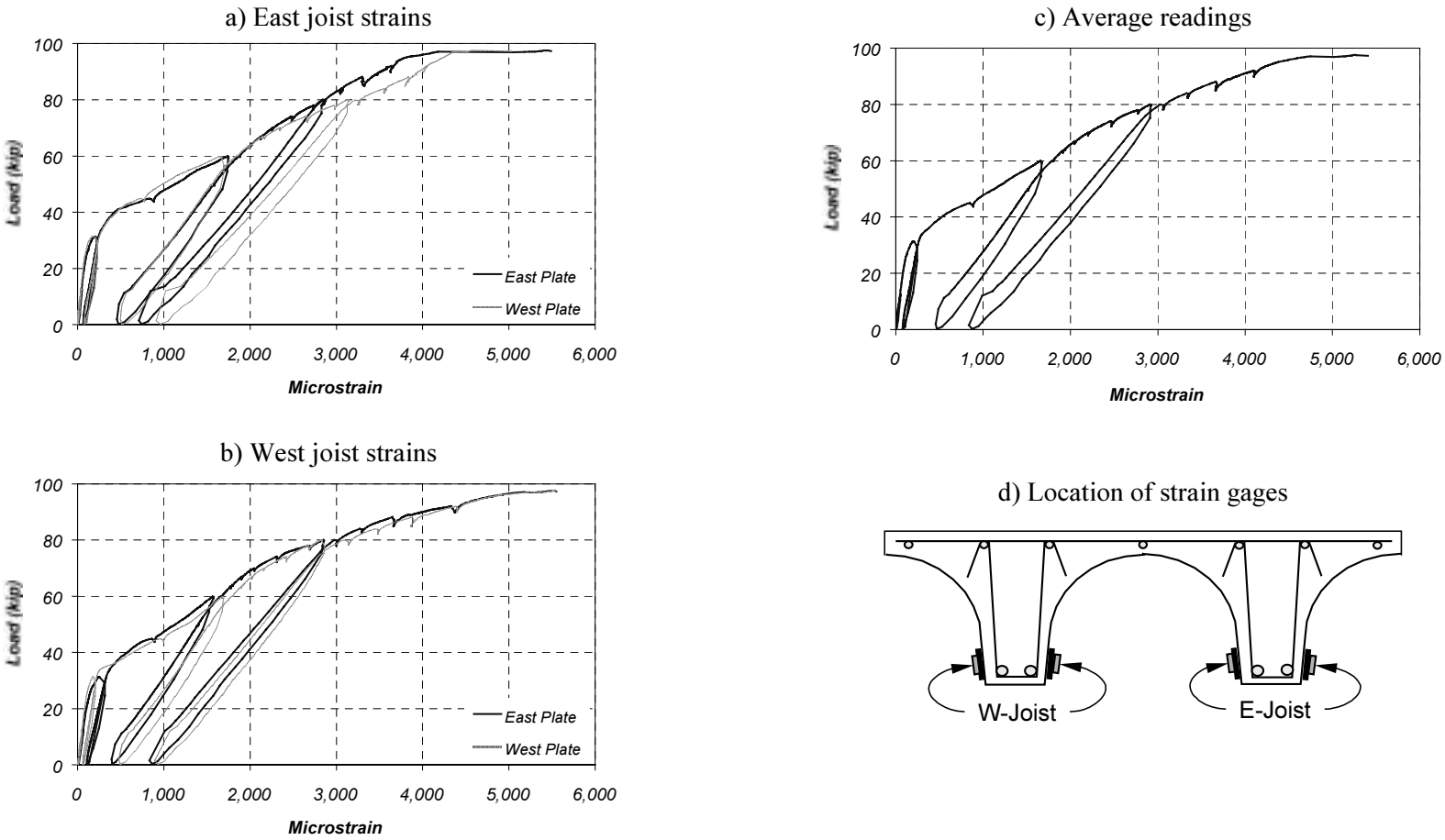

Figure D.10 Measured CFRP Strains in Specimen J-1 (Section S2)

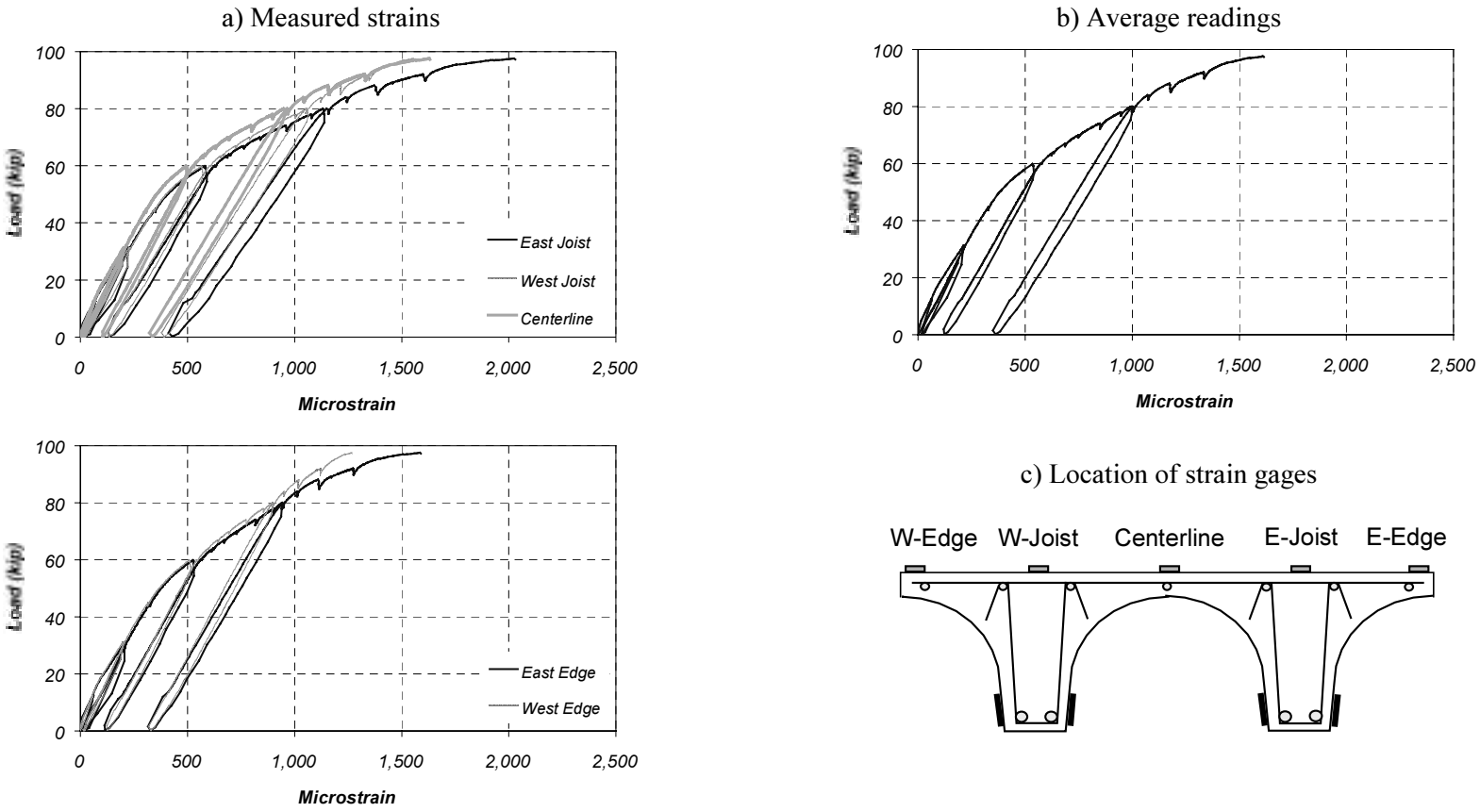

Figure D.11 Measured Strains on Concrete Slab in Specimen J-1 (Section N1)

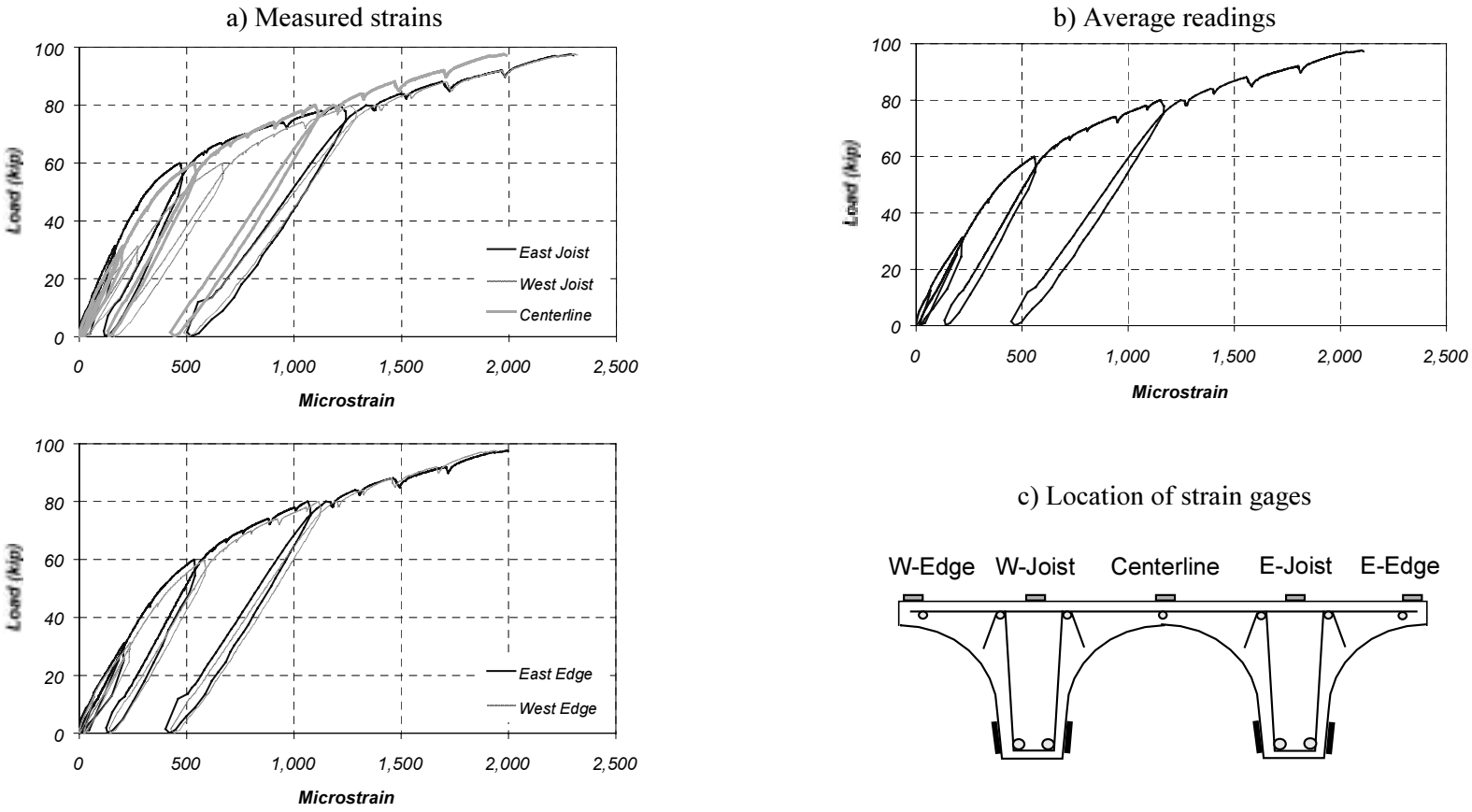

Figure D.12 Measured Strains on Concrete Slab in Specimen J-1 (Section S1)

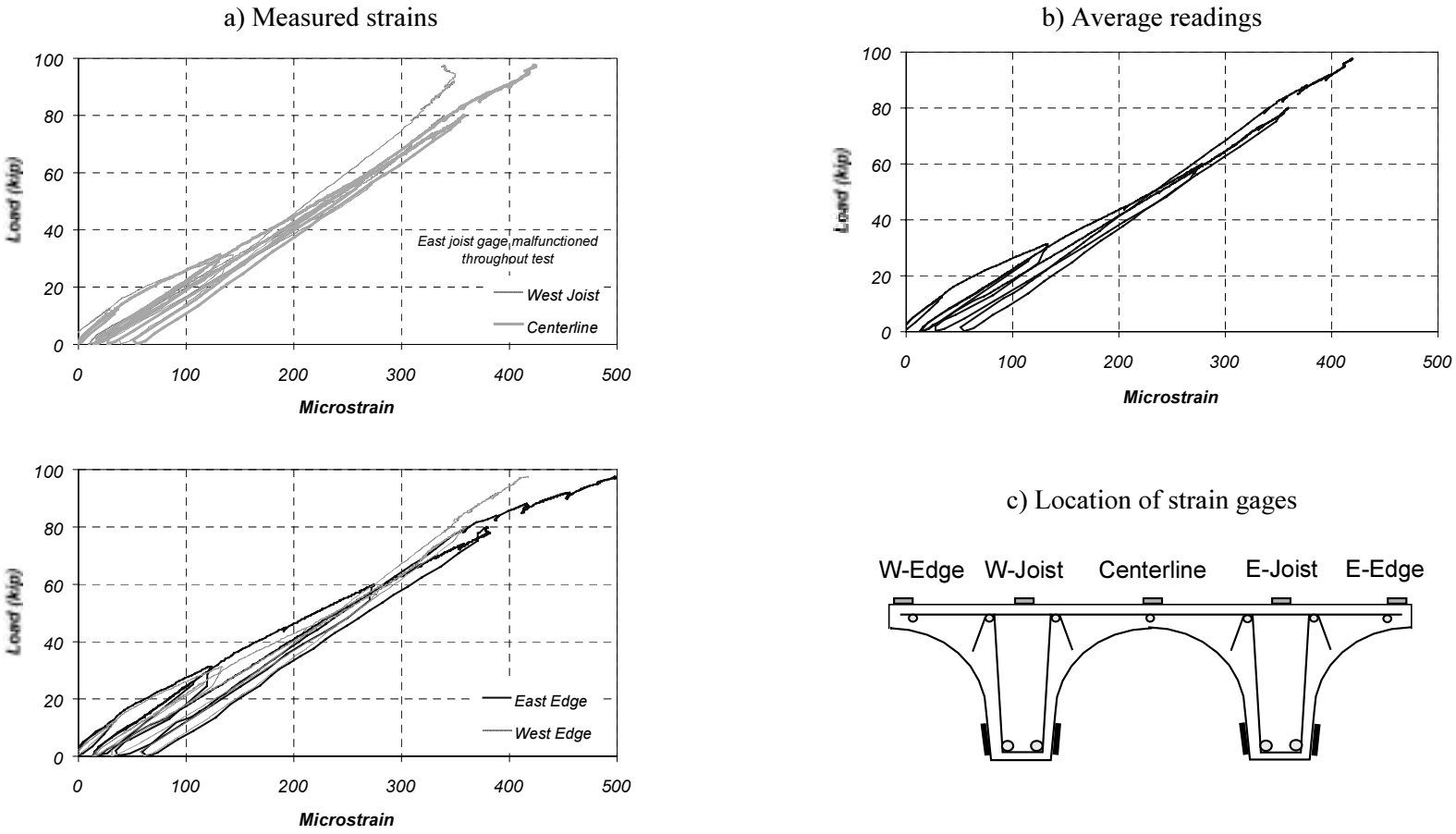

Figure D.13 Measured Strains on Concrete Slab in Specimen J-1 (Section N2)

a) Measured strains

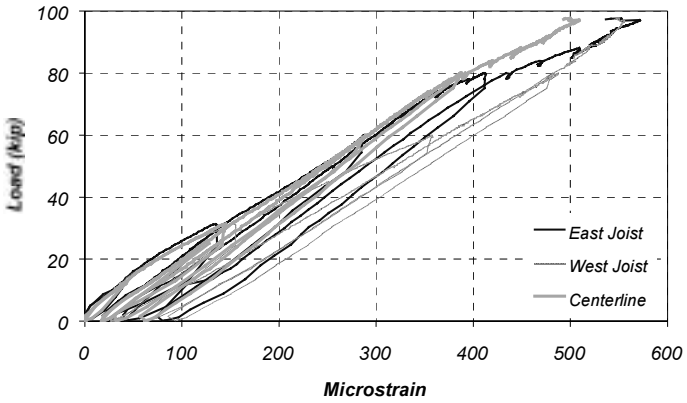

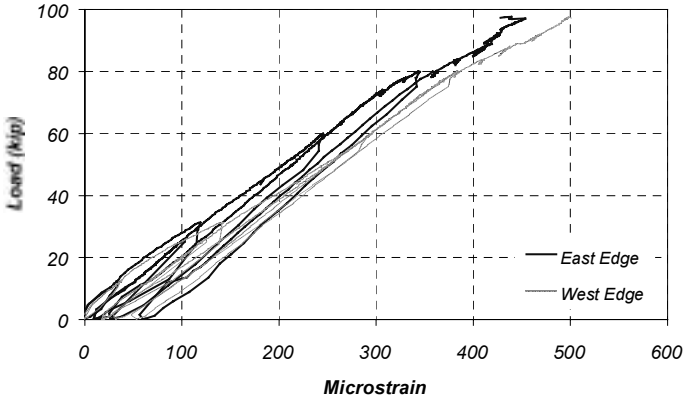

b) Average readings

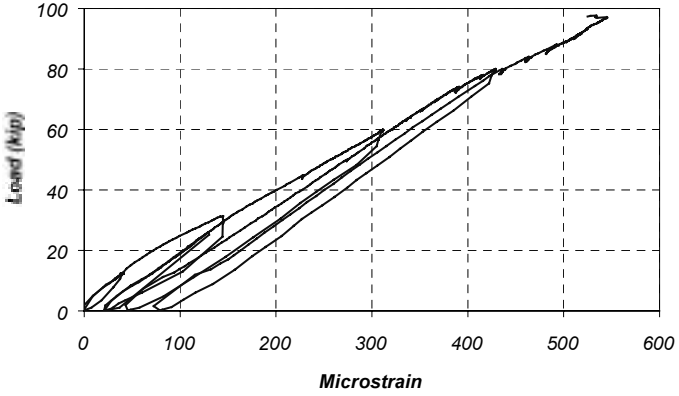

c) Location of strain gages

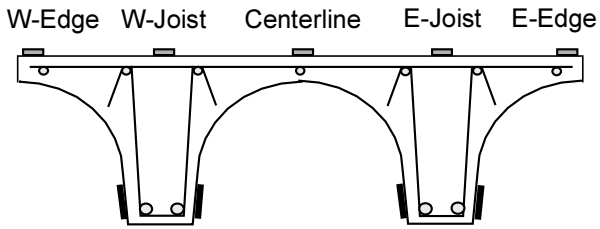

Figure D.14 Measured Strains on Concrete Slab in Specimen J-1 (Section S2)

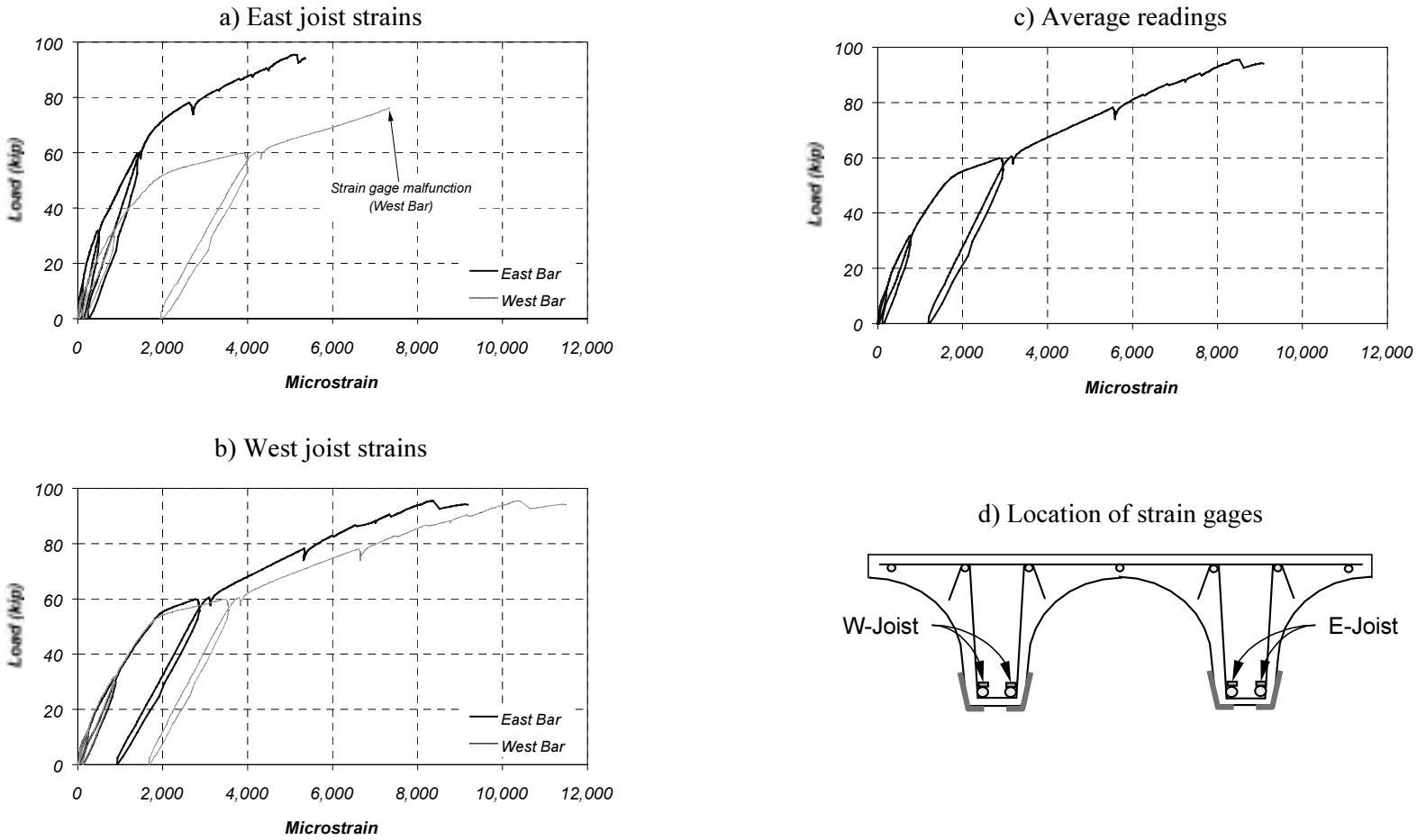

Figure D.15 Measured #8 Reinforcing Bar Strains in Specimen J-2 (Section N1)

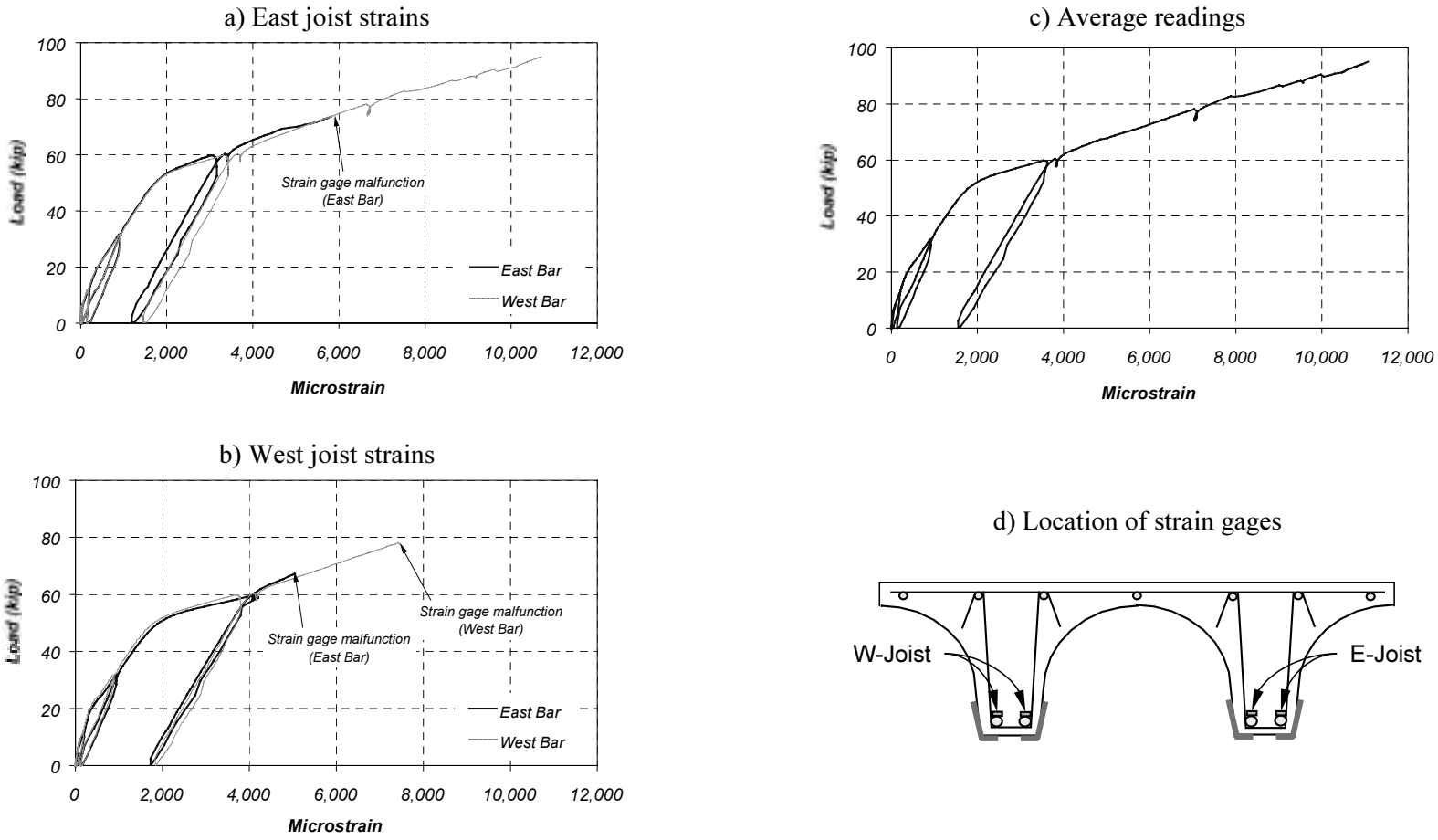

Figure D.16 Measured #8 Reinforcing Bar Strains in Specimen J-2 (Section S1)

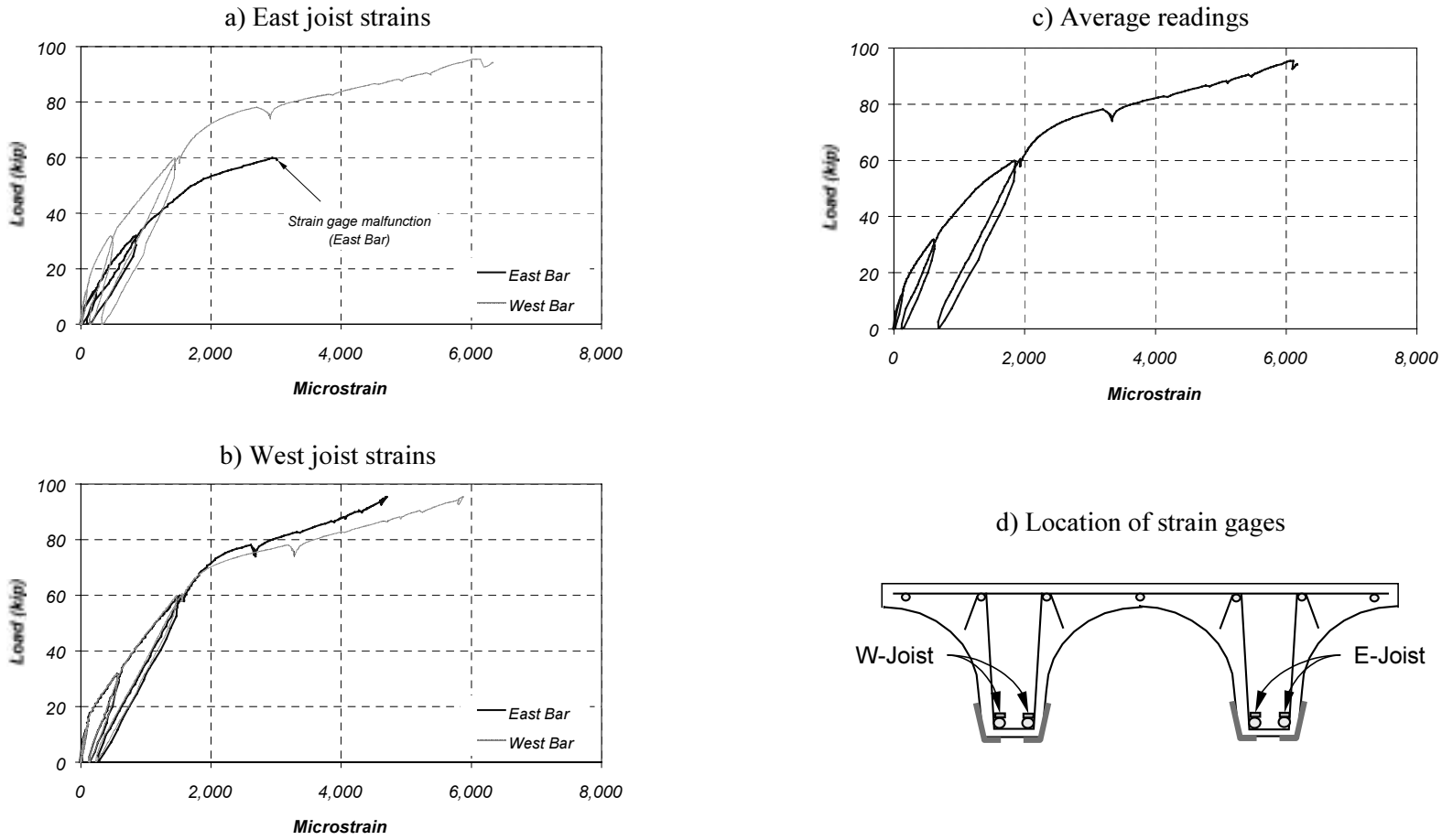

Figure D.17 Measured #8 Reinforcing Bar Strains in Specimen J-2 (Section N2)

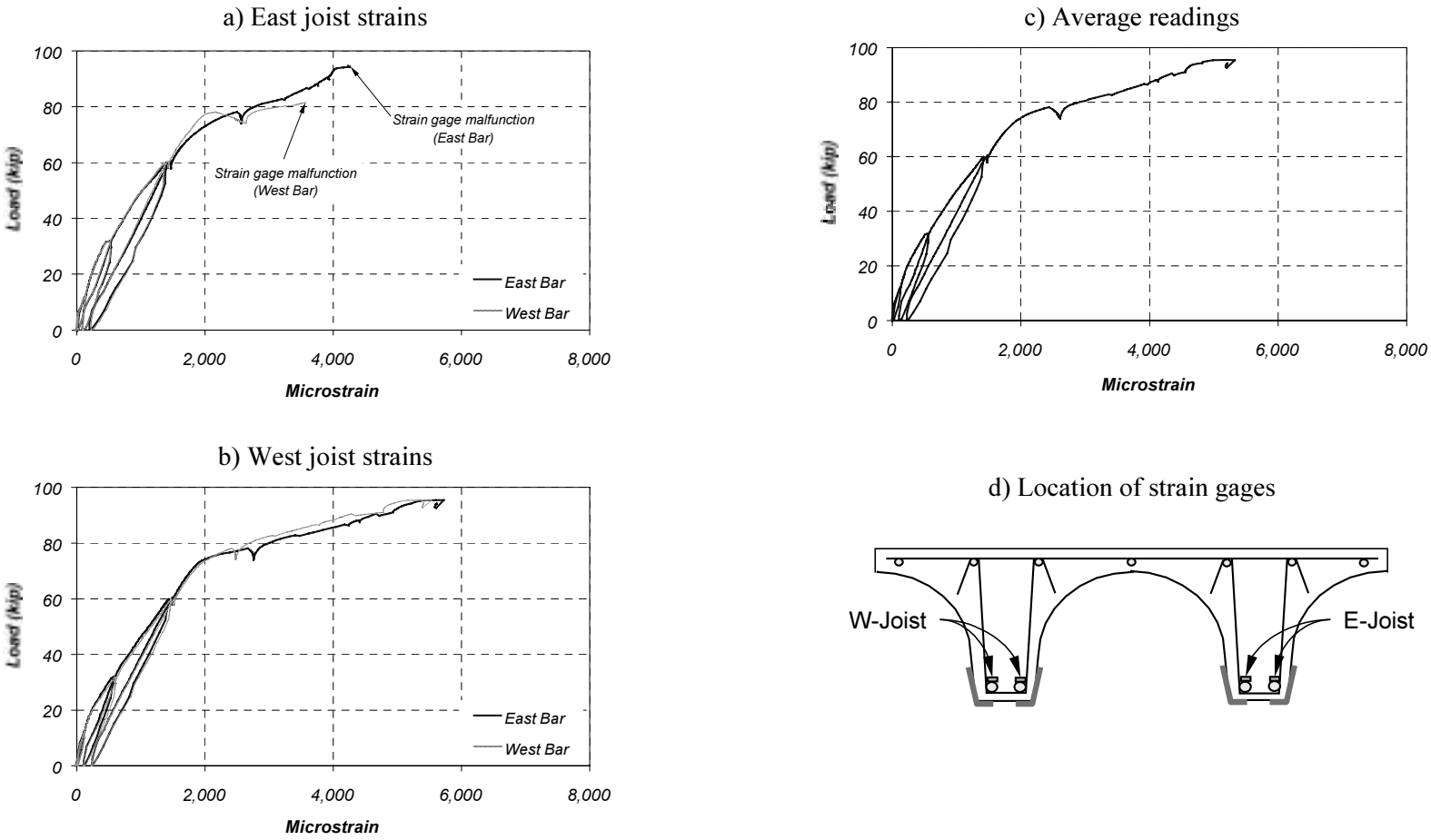

Figure D.18 Measured #8 Reinforcing Bar Strains in Specimen J-2 (Section S2)

a) East joist strains

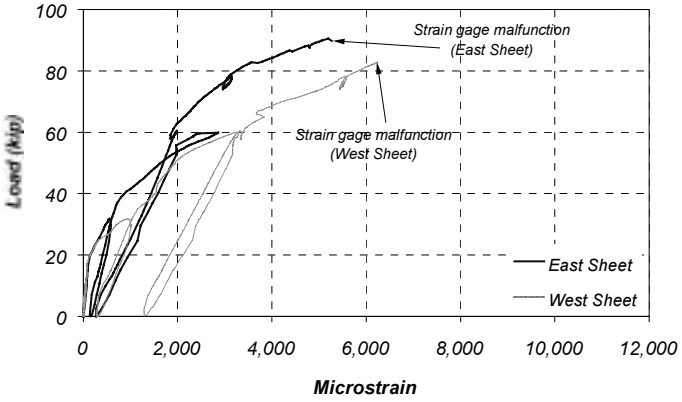

c) Average readings

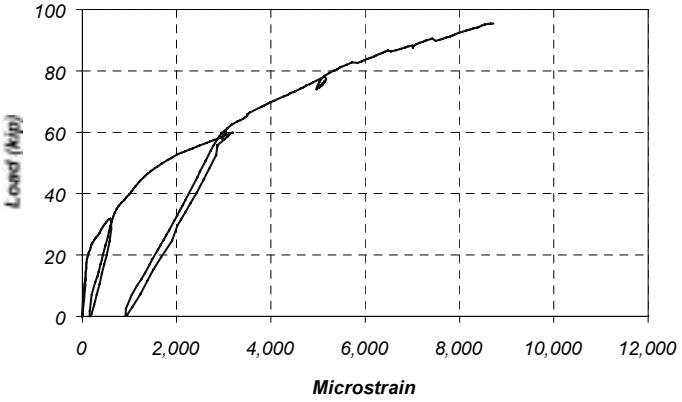

b) West joist strains

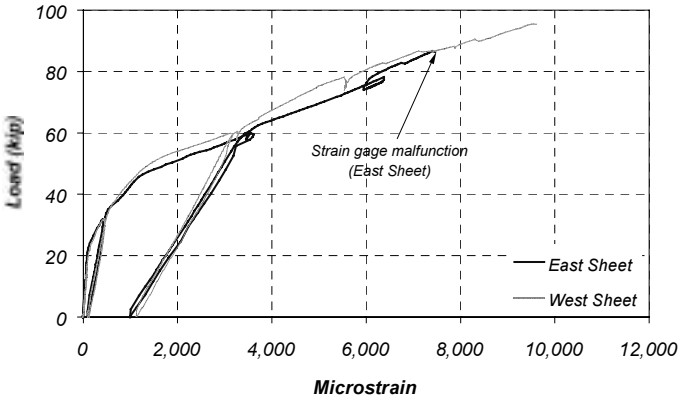

d) Location of strain gages

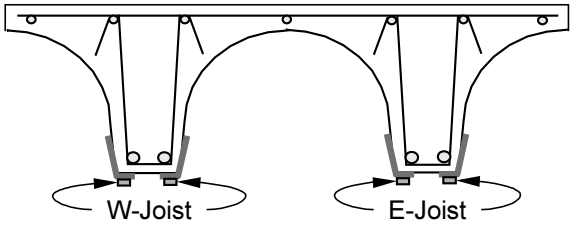

Figure D.19 Measured CFRP Strains in Specimen J-2 (Section N1)

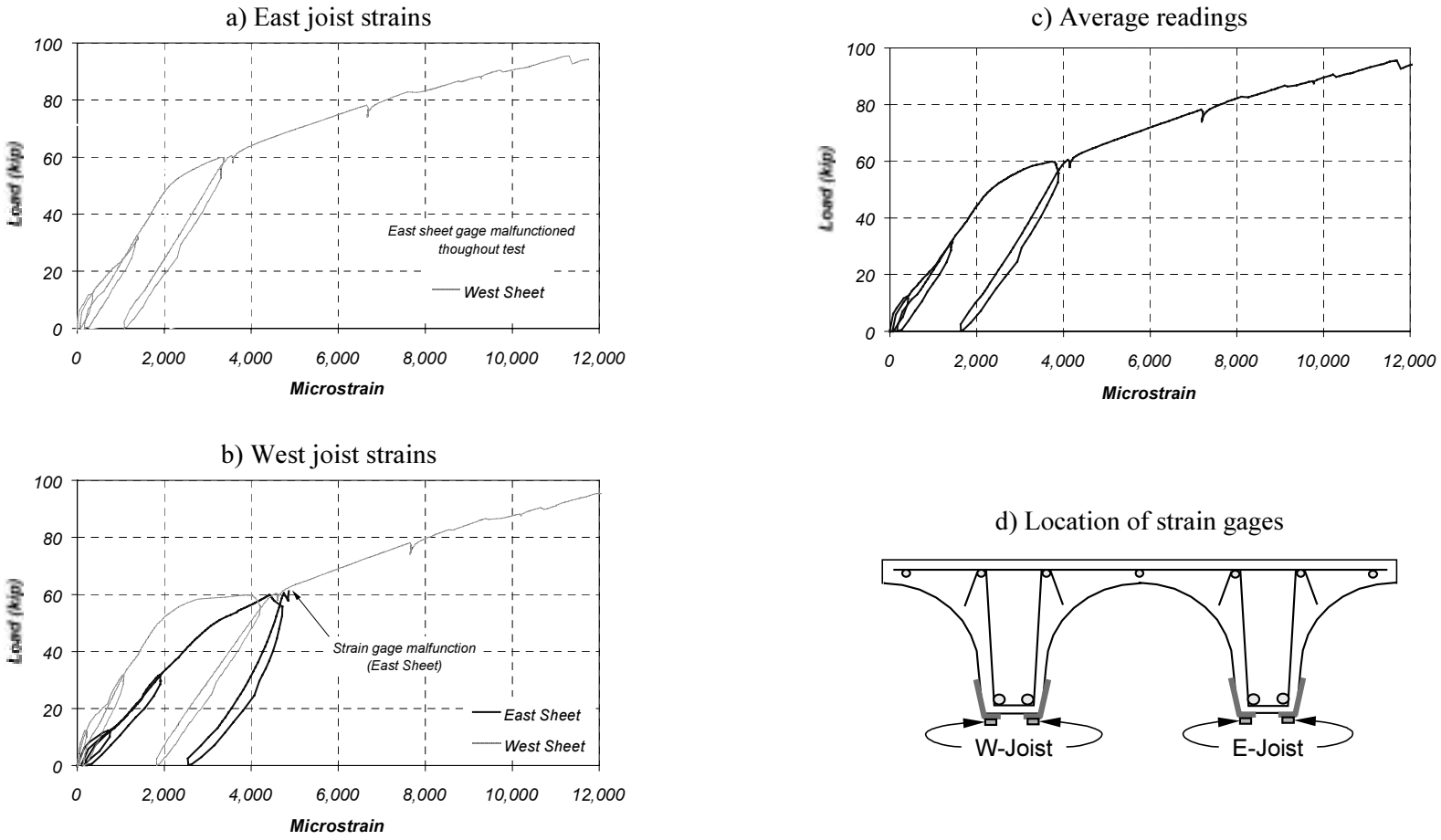

Figure D.20 Measured CFRP Strains in Specimen J-2 (Section S1)

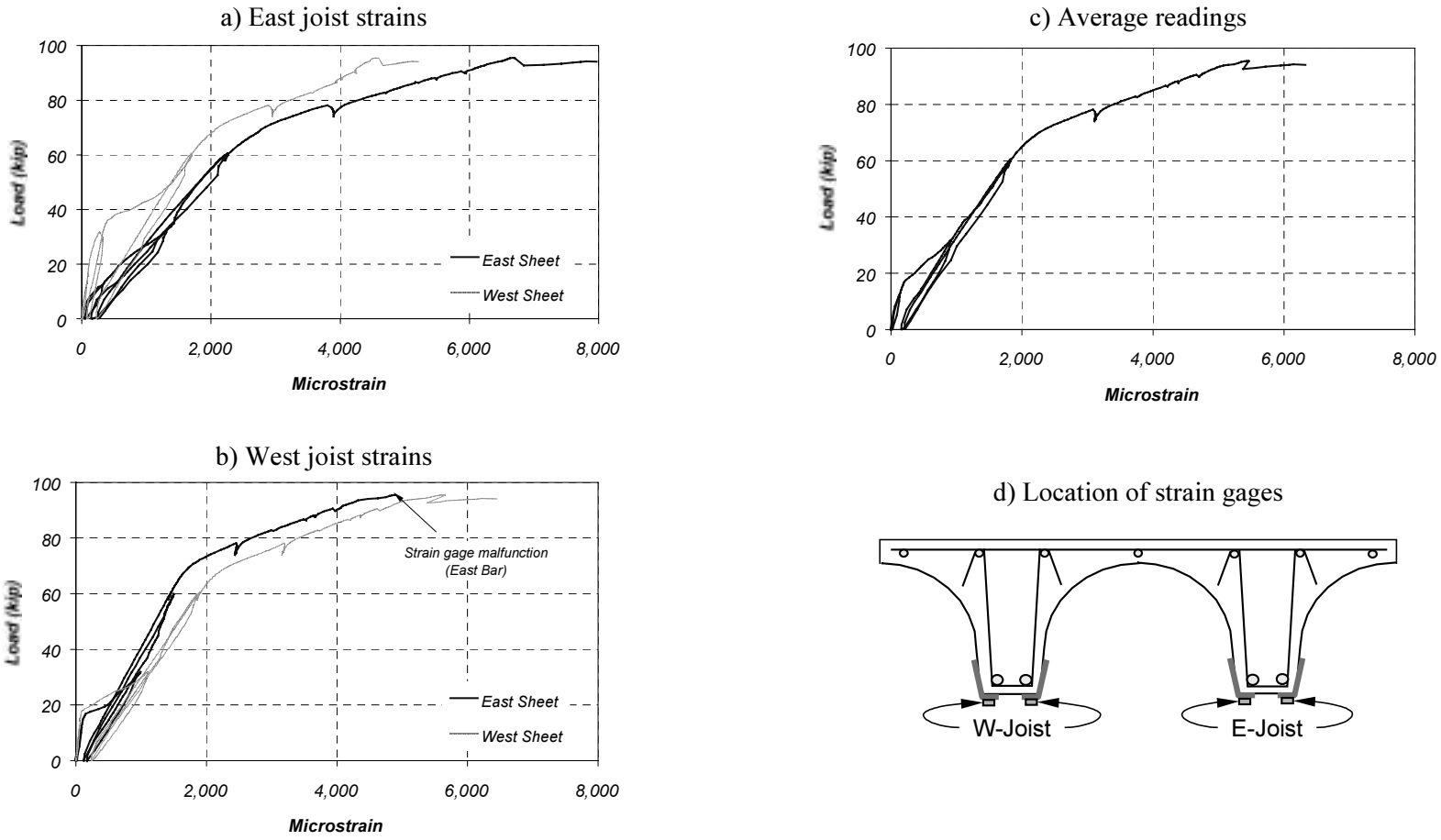

Figure D.21 Measured CFRP Strains in Specimen J-2 (Section N2)

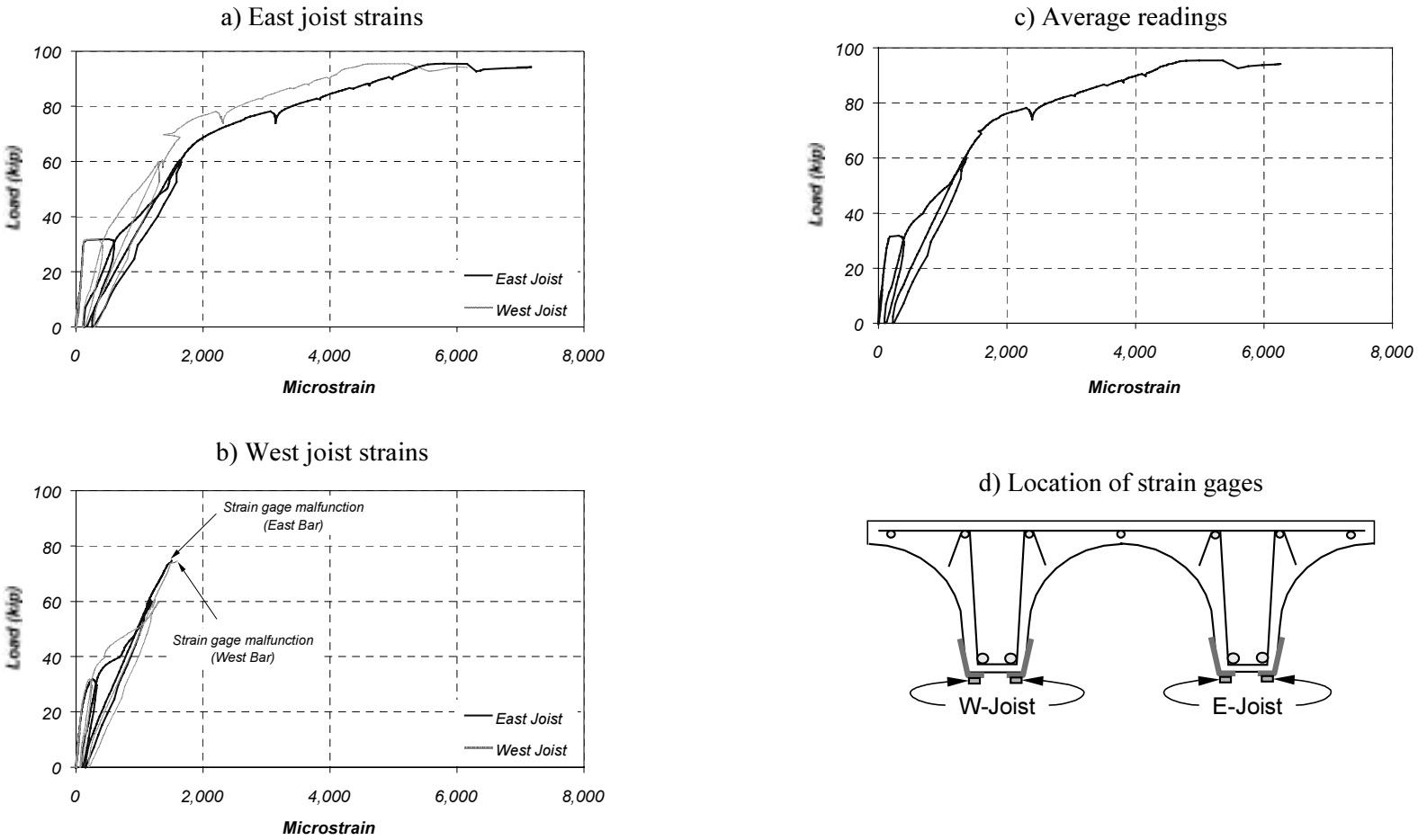

Figure D.22 Measured CFRP Strains in Specimen J-2 (Section S2)

a) Measured strains

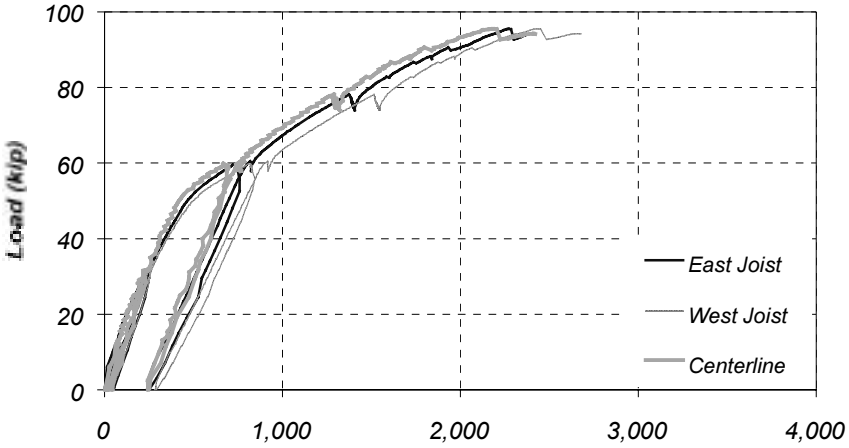

b) Average readings

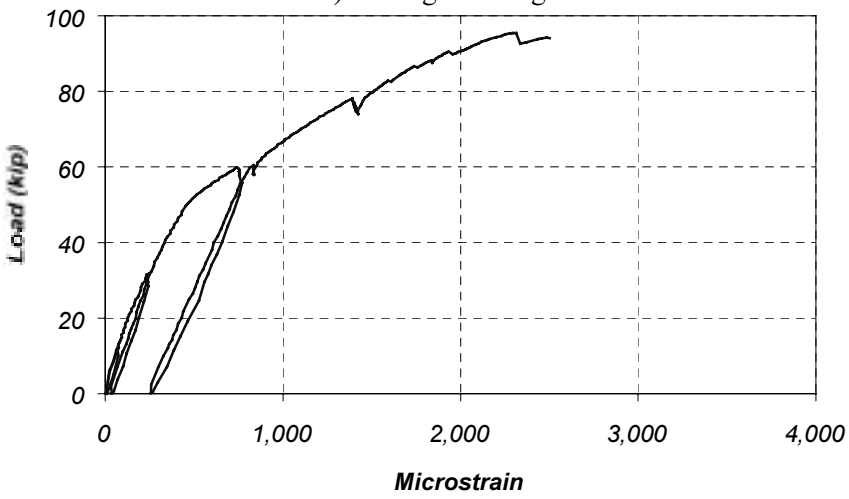

c) Location of strain gages

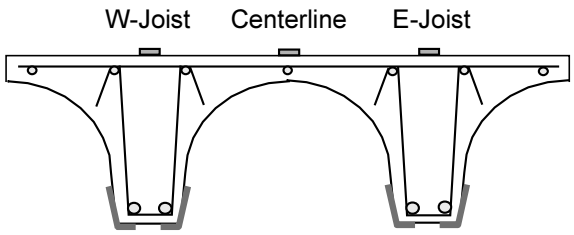

Figure D.23 Measured Strains on Concrete Slab in Specimen J-2 (Section N1)

a) Measured strains

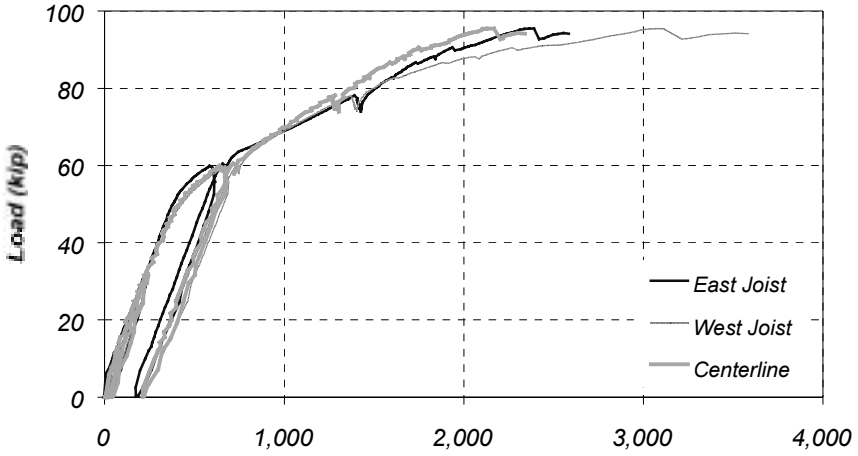

b) Average readings

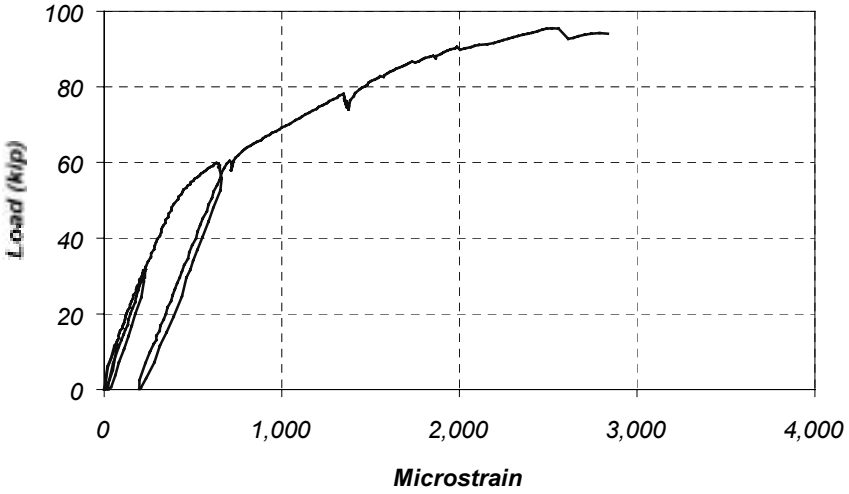

c) Location of strain gages

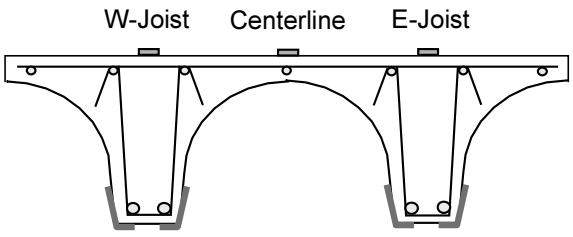

Figure D.24 Measured Strains on Concrete Slab in Specimen J-2 (Section S1)

a) Measured strains

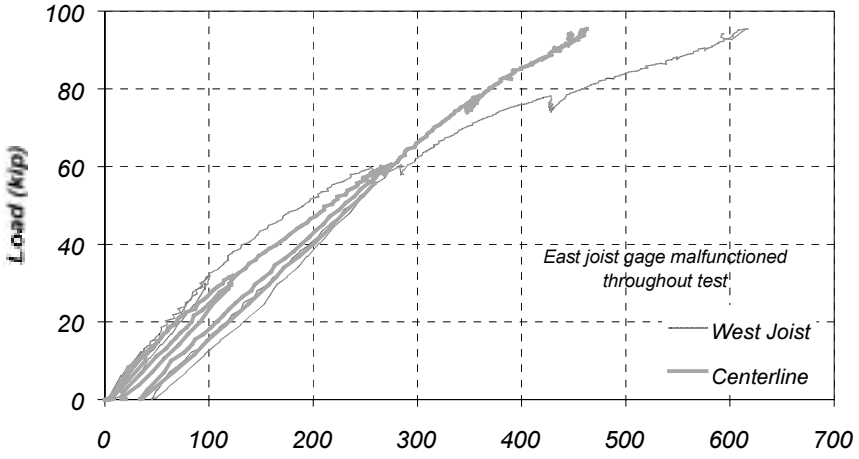

b) Average readings

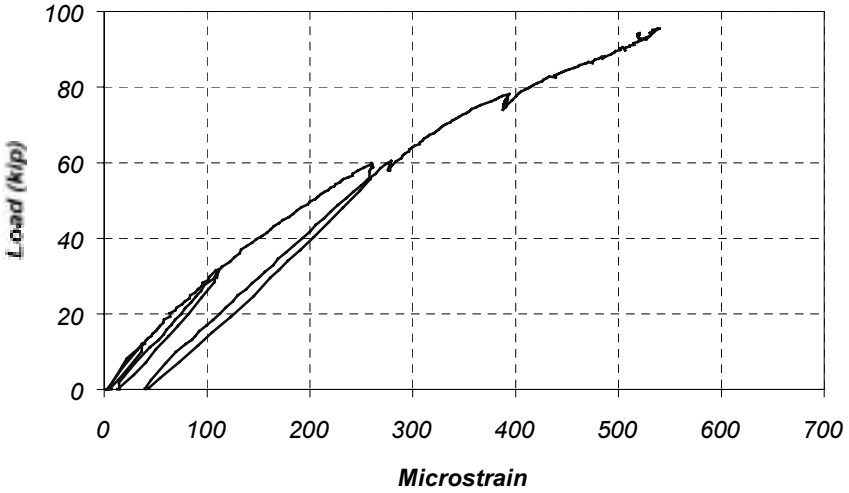

c) Location of strain gages

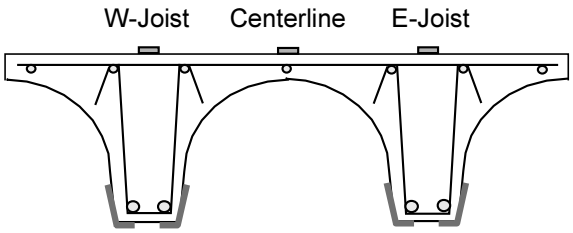

Figure D.25 Measured Strains on Concrete Slab in Specimen J-2 (Section N2)

a) Measured strains

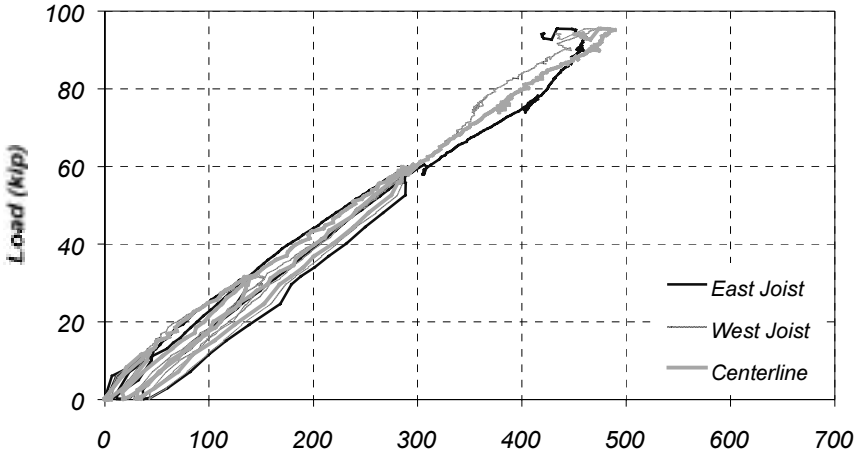

b) Average readings

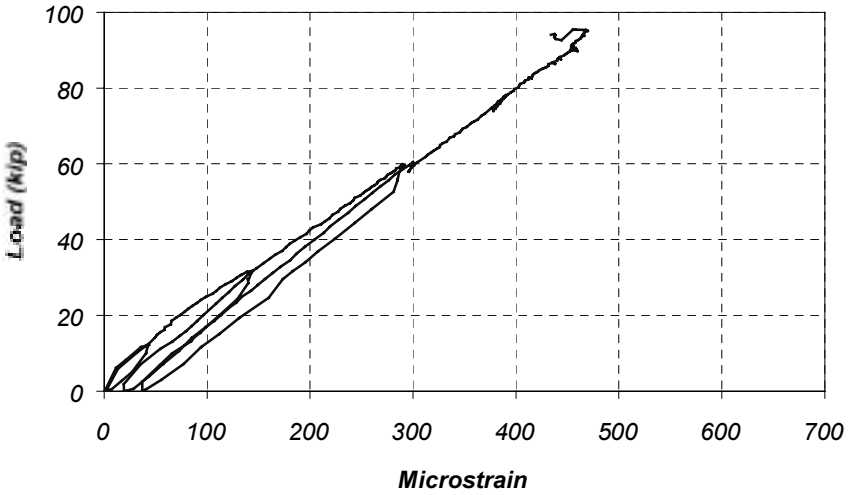

c) Location of strain gages

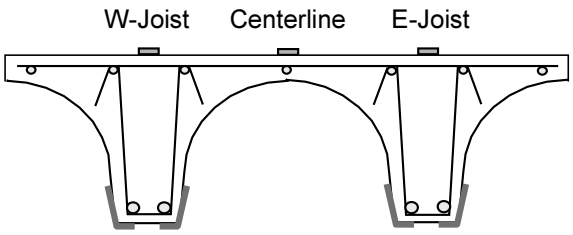

Figure D.26 Measured Strains on Concrete Slab in Specimen J-2 (Section S2)

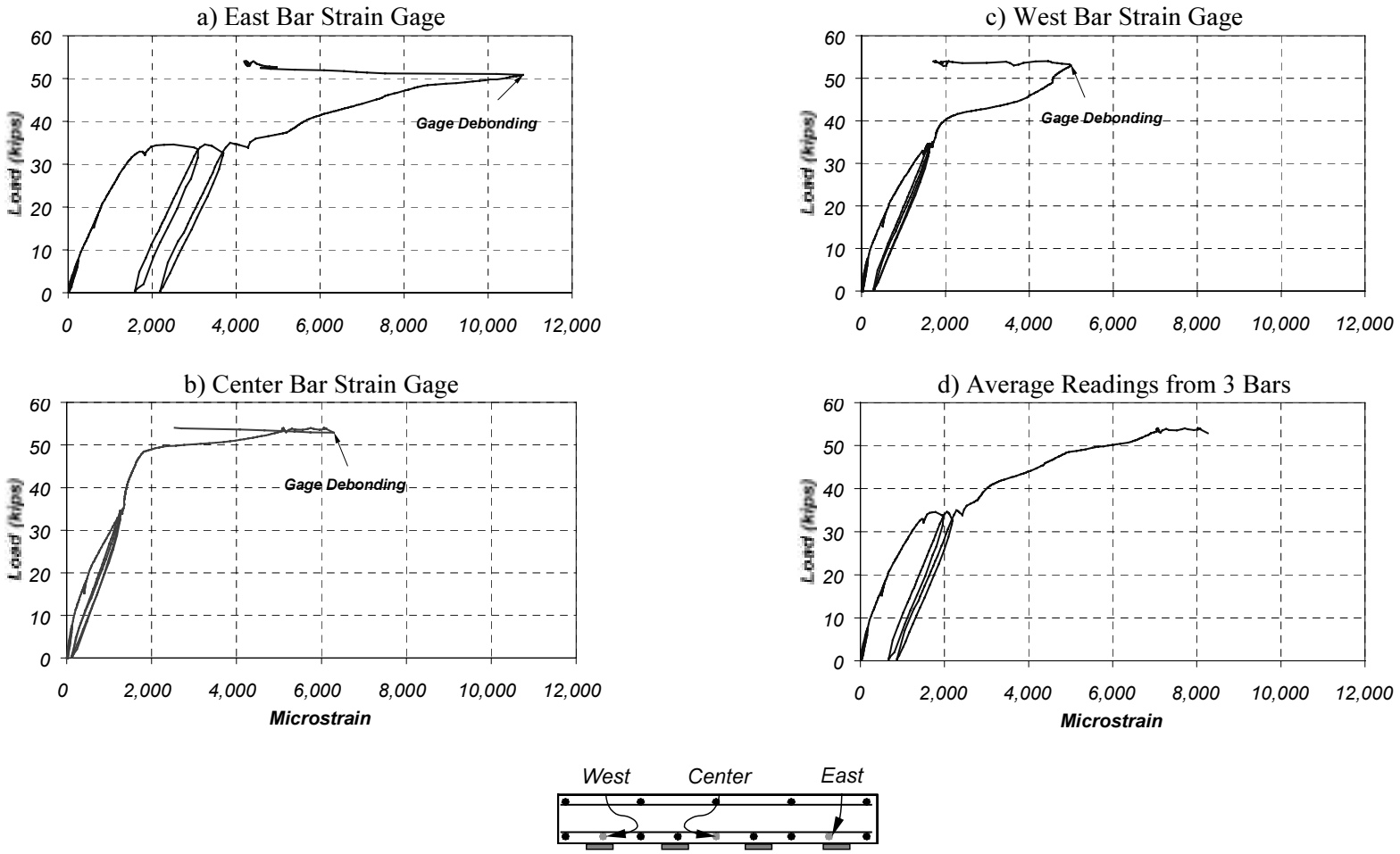

Figure D.27 Measured Reinforcing Bar (#6) Strains on Specimen FS-1 (Section N1)

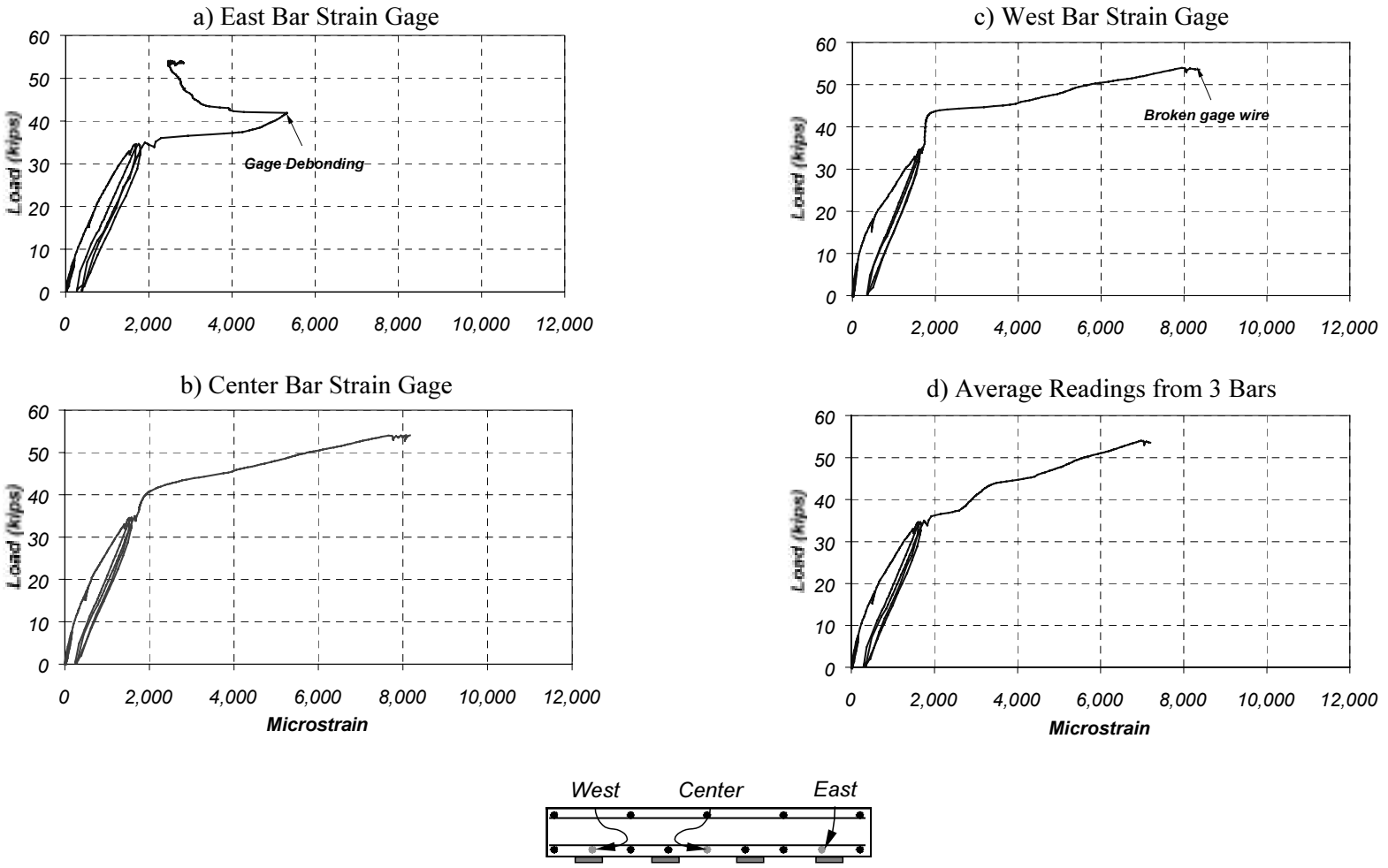

Figure D.28 Measured Reinforcing Bar (#6) Strains on Specimen FS-1 (Section S1)

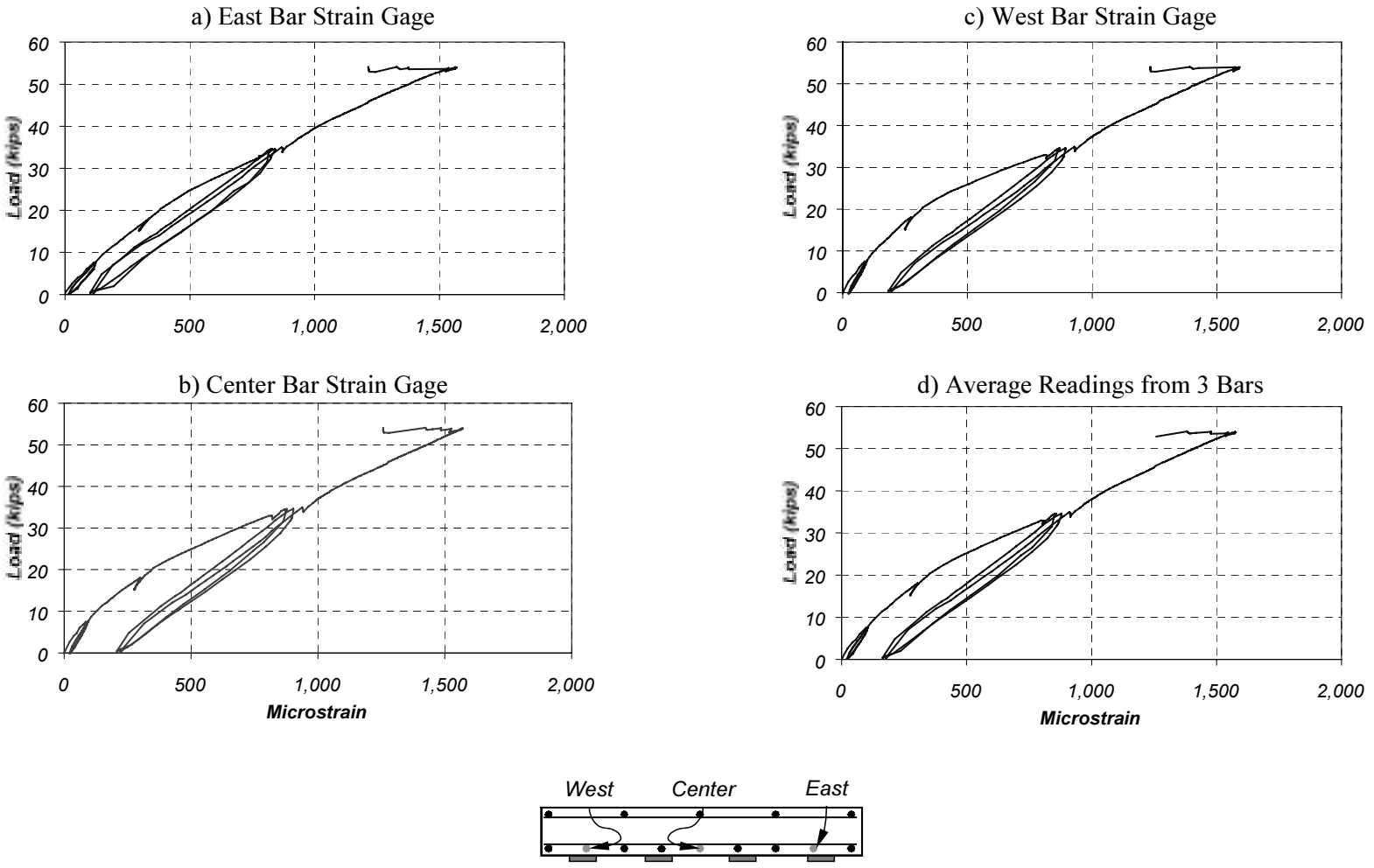

Figure D.29 Measured Reinforcing Bar (#6) Strains on Specimen FS-1 (Section N2)

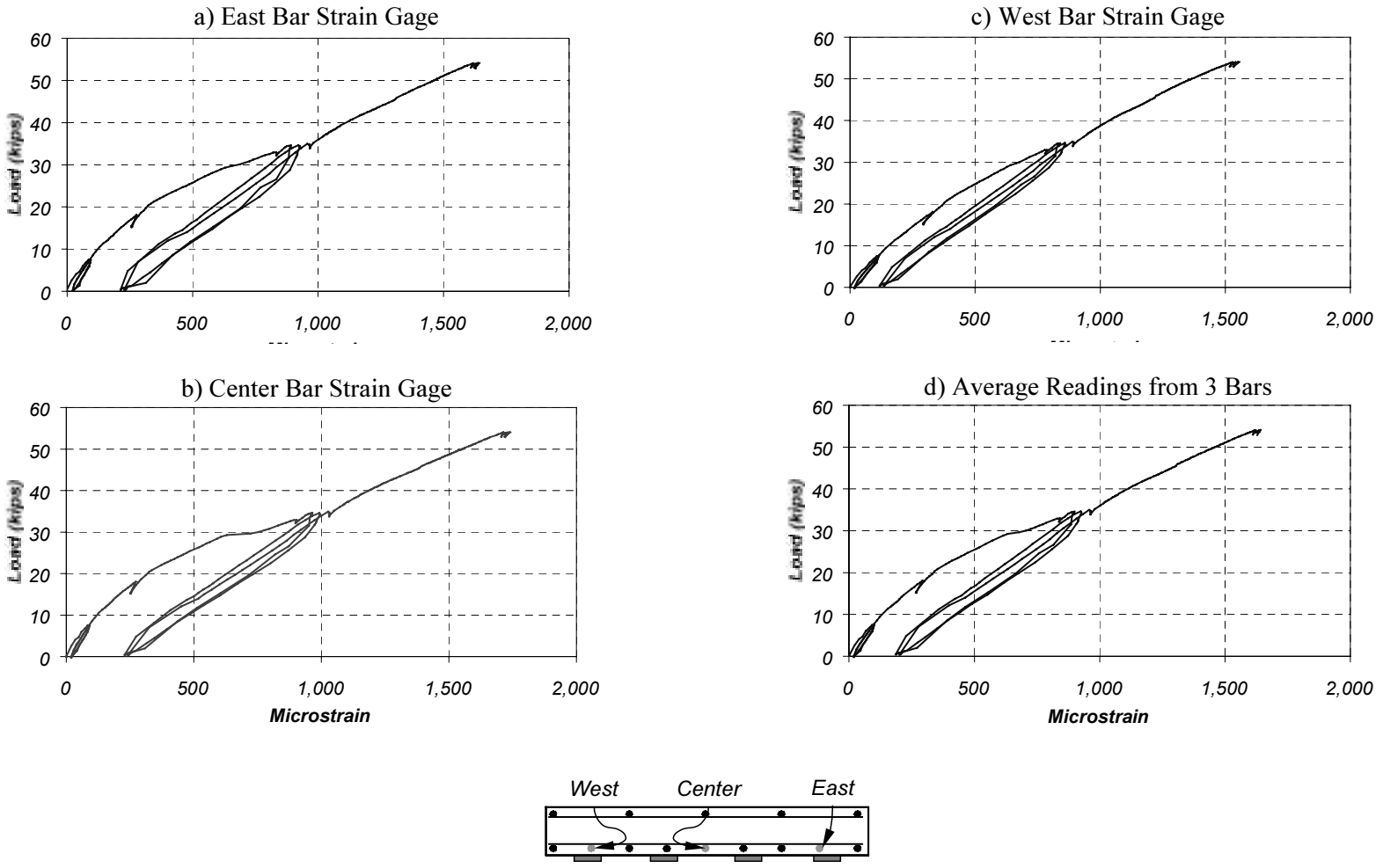

Figure D.30 Measured Reinforcing Bar (#6) Strains in Specimen FS-1 (Section S2)

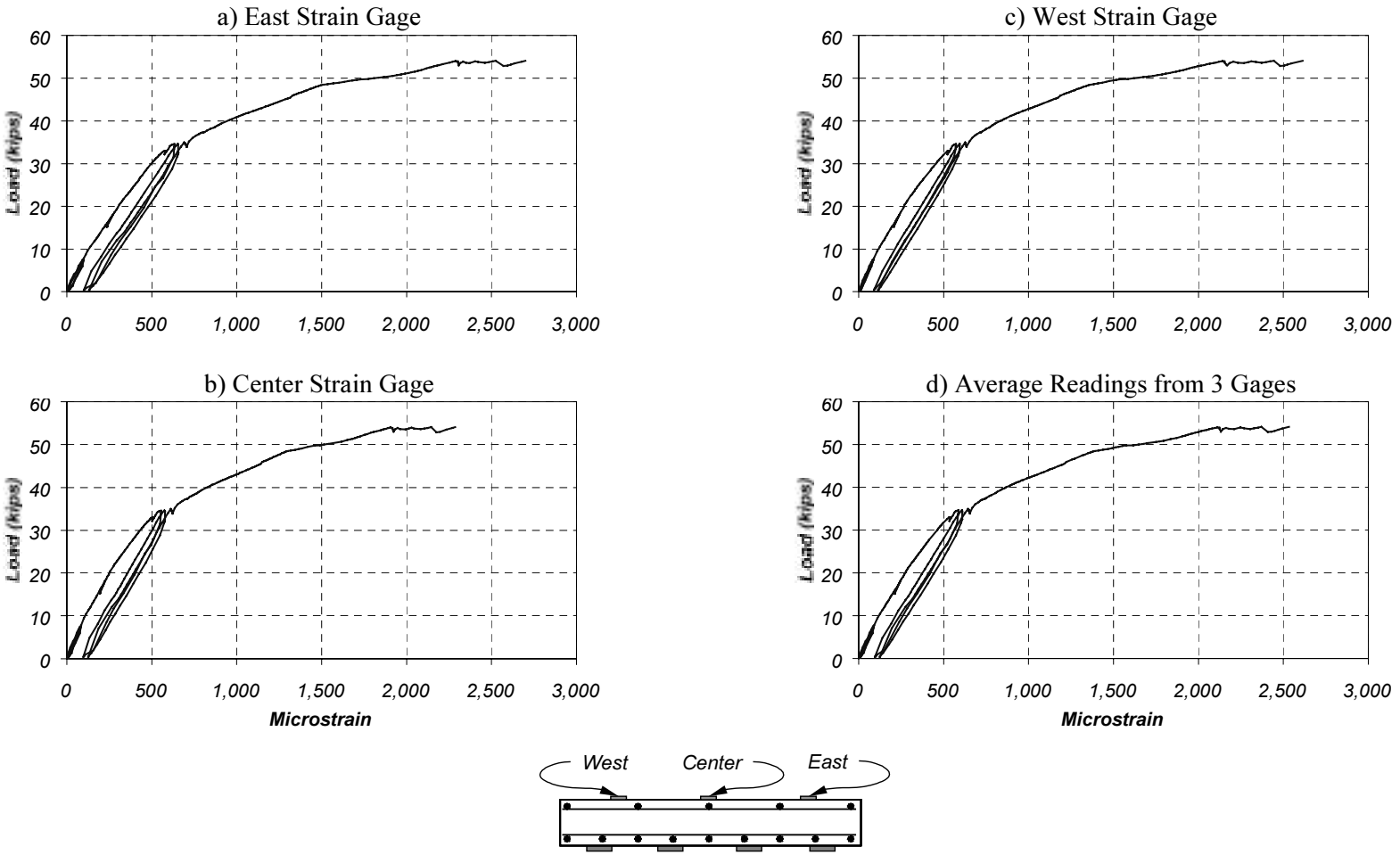

Figure D.31 Measured Strains on Concrete Slab in Specimen FS-1 (Section N1)

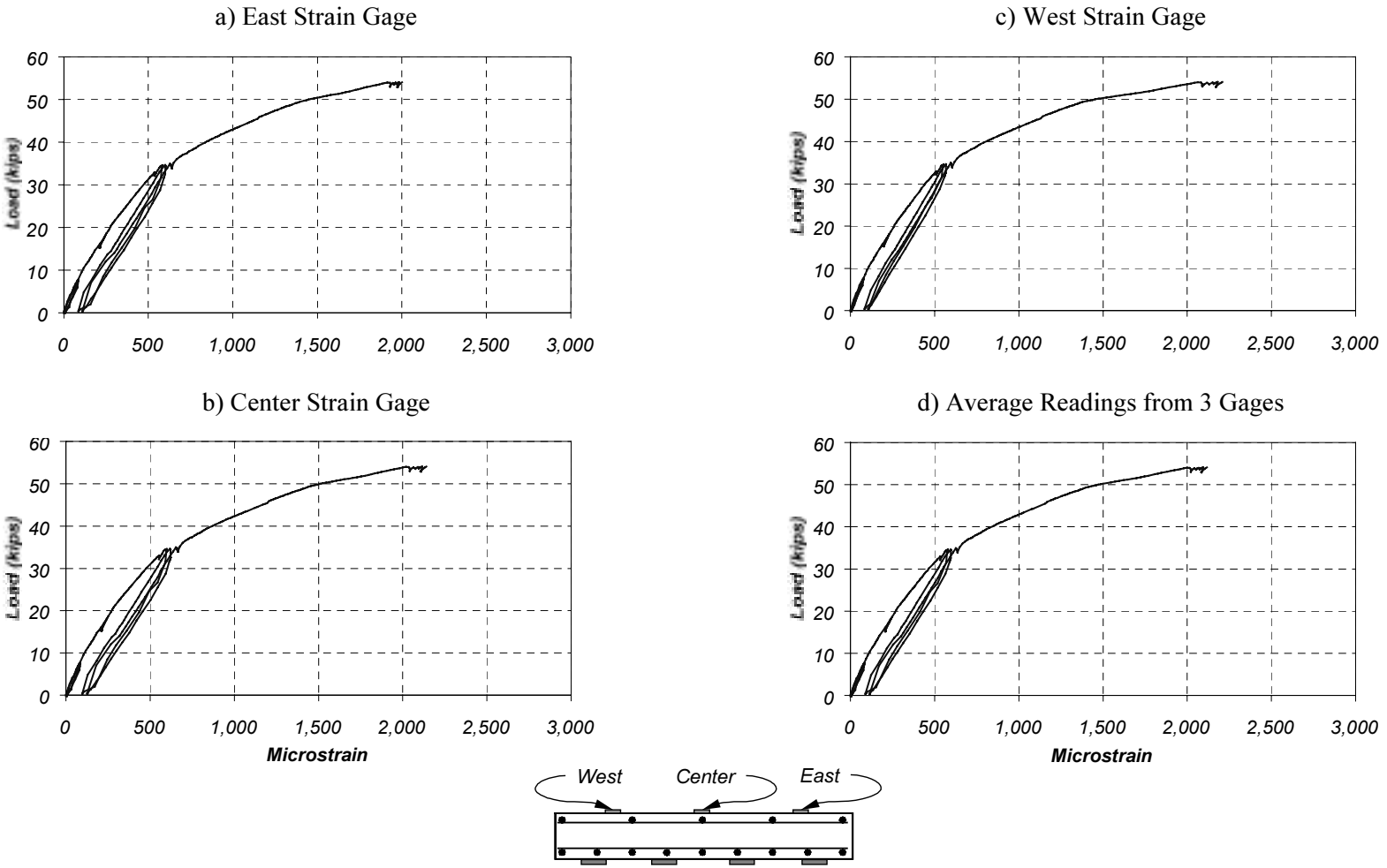

Figure D.32 Measured Strains on Concrete Slab in Specimen FS-1 (Section S1)

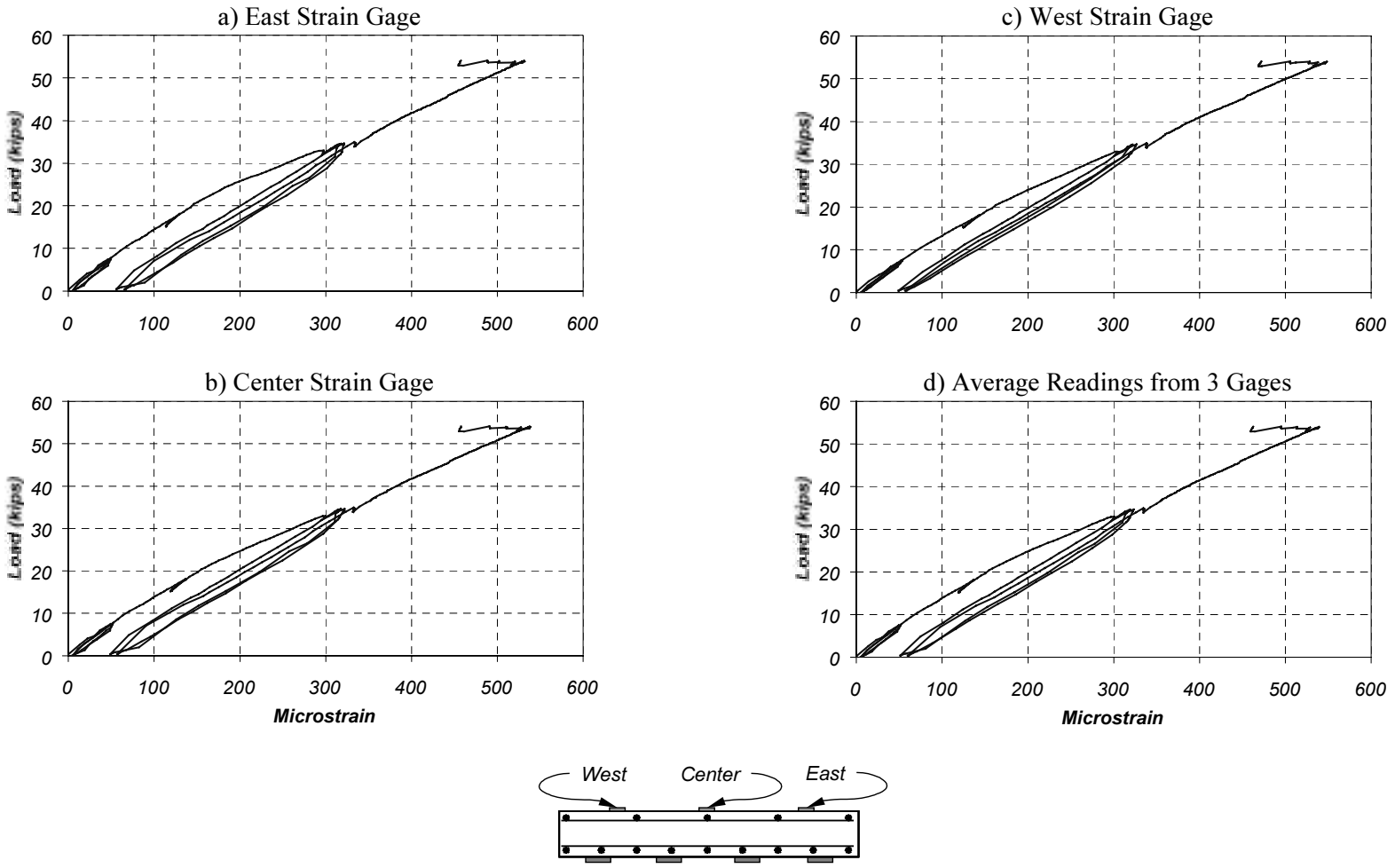

Figure D.33 Measured Strains on Concrete Slab in Specimen FS-1 (Section N2)

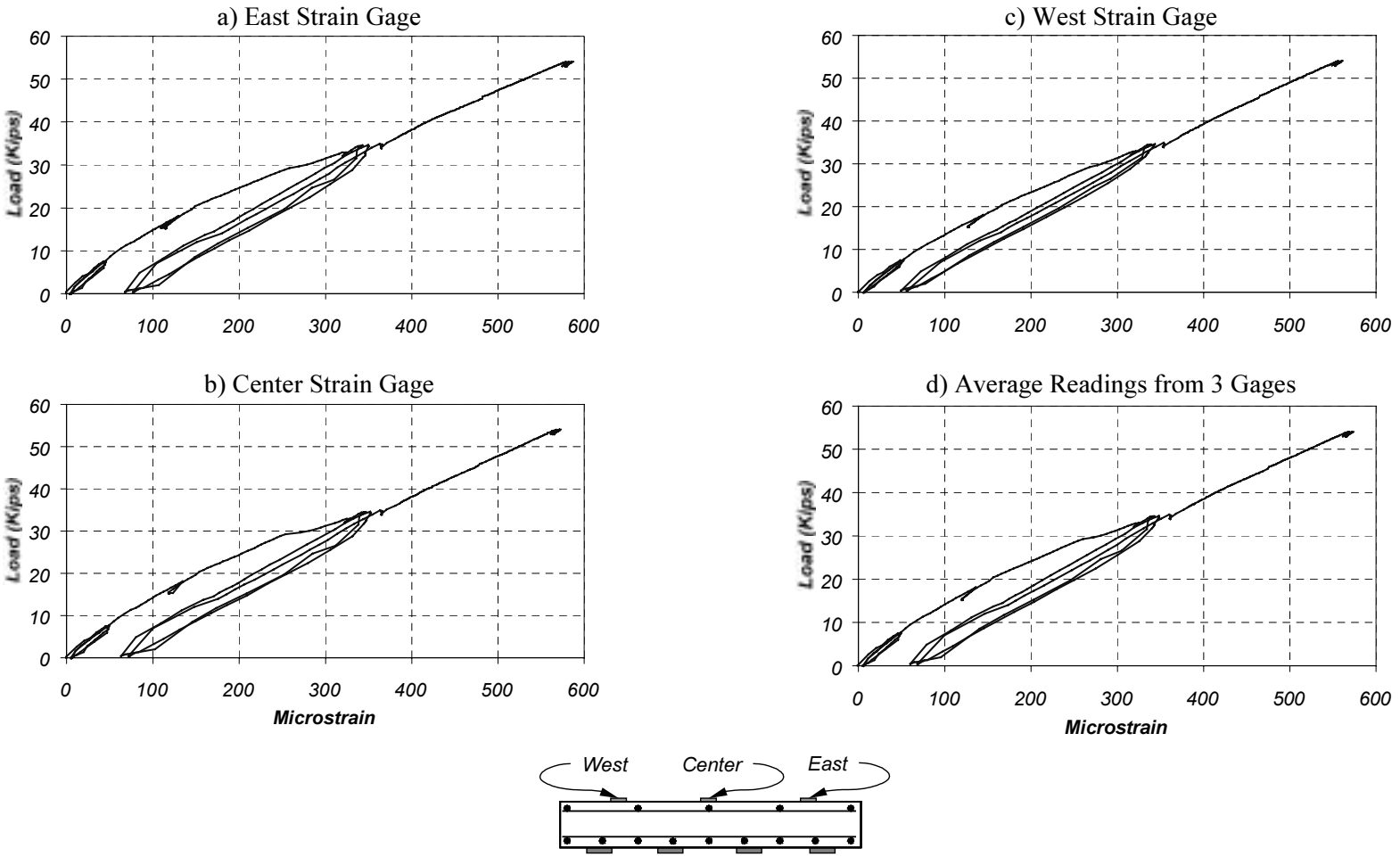

Figure D.34 Measured Strains on Concrete Slab in Specimen FS-1 (Section S2)

a) E-Plate Strain Gage

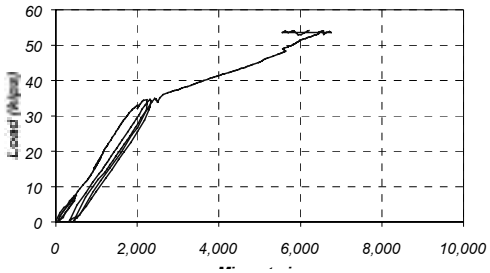

c) W-Plate Strain Gage

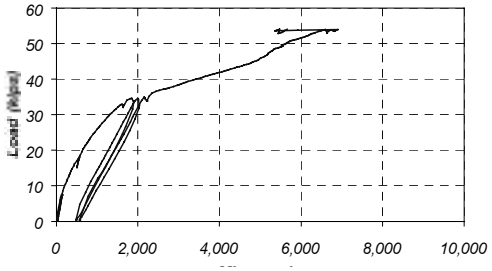

b) E-Center Plate Strain Gage

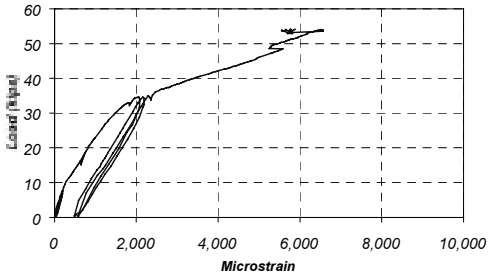

d) W-Center Plate Strain Gage

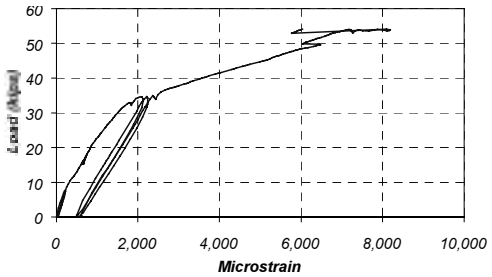

e) Average Readings from 4 Plates

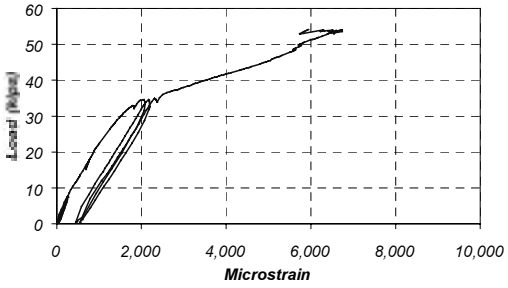

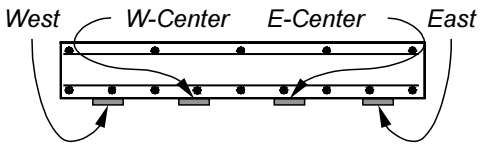

Figure D.35 Measured Strains on CFRP Plates in Specimen FS-1 (Section N1)

a) E-Plate Strain Gage

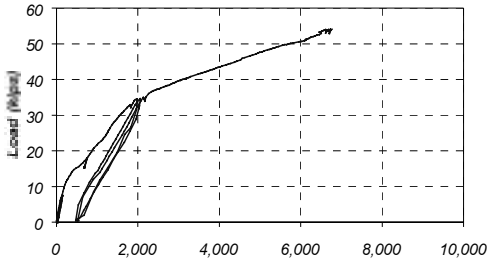

c) W-Plate Strain Gage

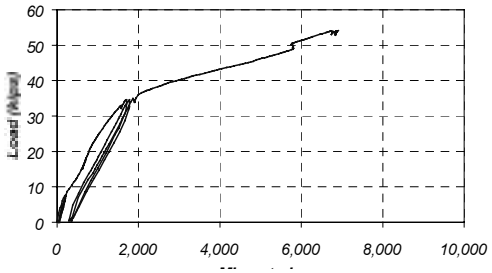

b) E-Center Plate Strain Gage

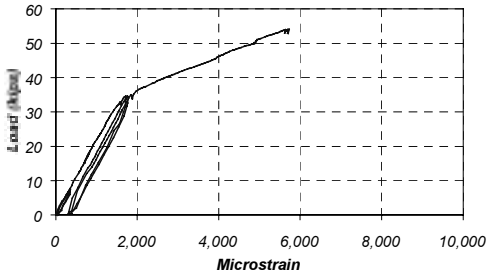

d) W-Center Plate Strain Gage

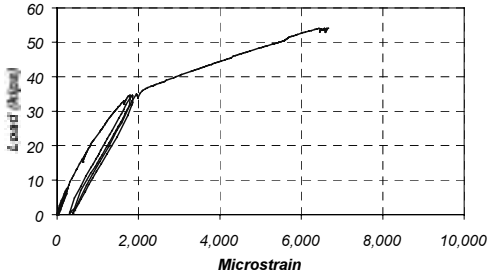

e) Average Readings from 4 Plates

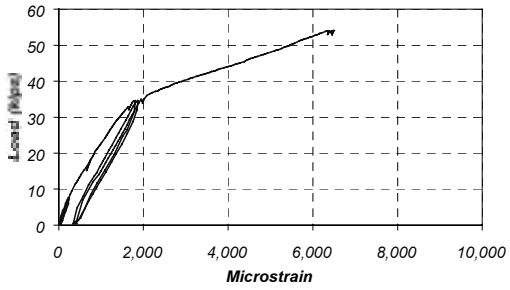

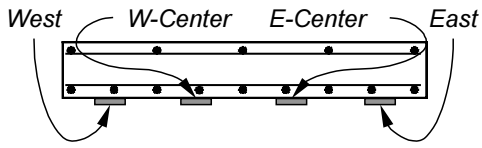

Figure D.36 Measured Strains on CFRP Plates in Specimen FS-1 (Section S1)

a) E-Plate Strain Gage

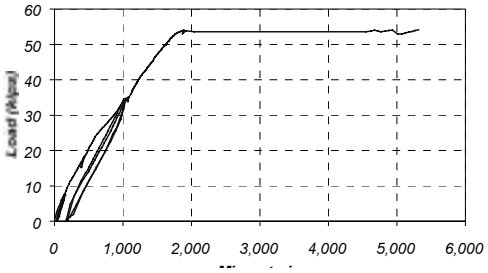

c) W-Plate Strain Gage

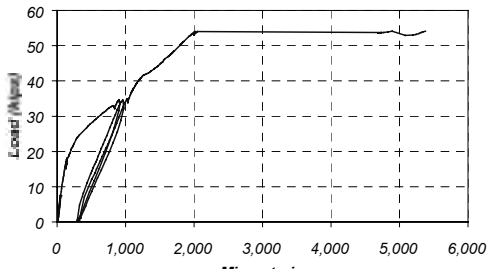

b) E-Center Plate Strain Gage

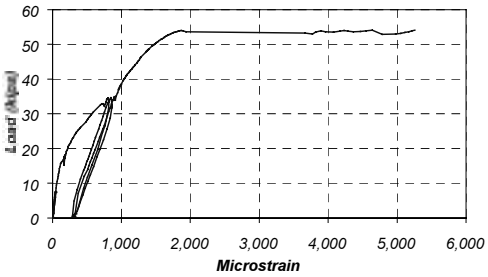

d) W-Center Plate Strain Gage

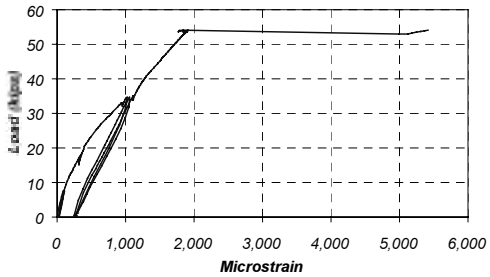

e) Average Readings from 4 Plates

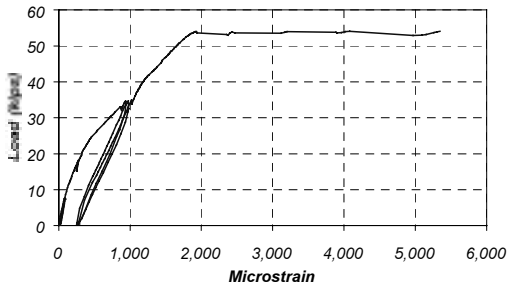

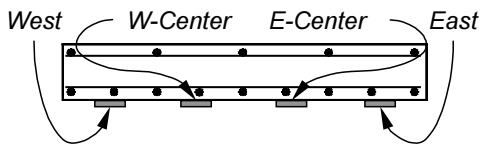

Figure D.37 Measured Strains on CFRP Plates in Specimen FS-1 (Section N2)

a) E-Plate Strain Gage

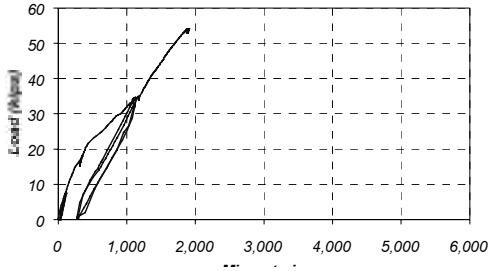

c) W-Plate Strain Gage

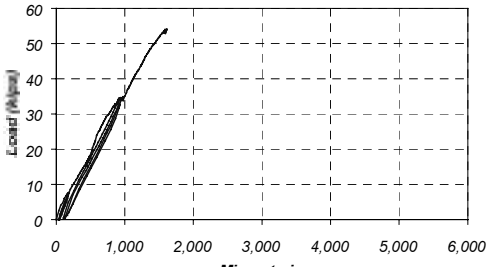

b) E-Center Plate Strain Gage

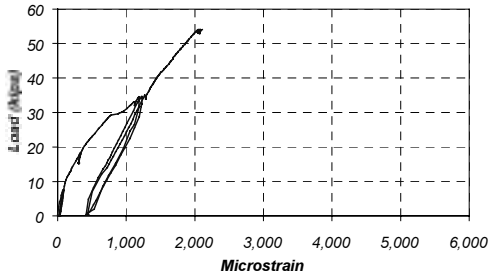

d) W-Center Plate Strain Gage

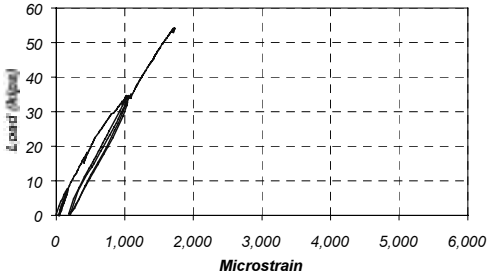

e) Average Readings from 4 Plates

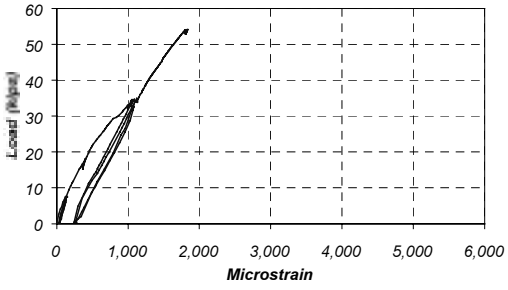

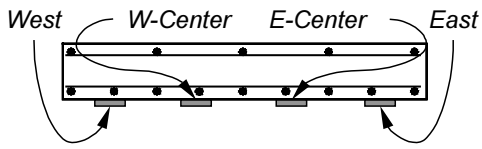

Figure D.38 Measured Strains on CFRP Plates in Specimen FS-1 (Section S2)

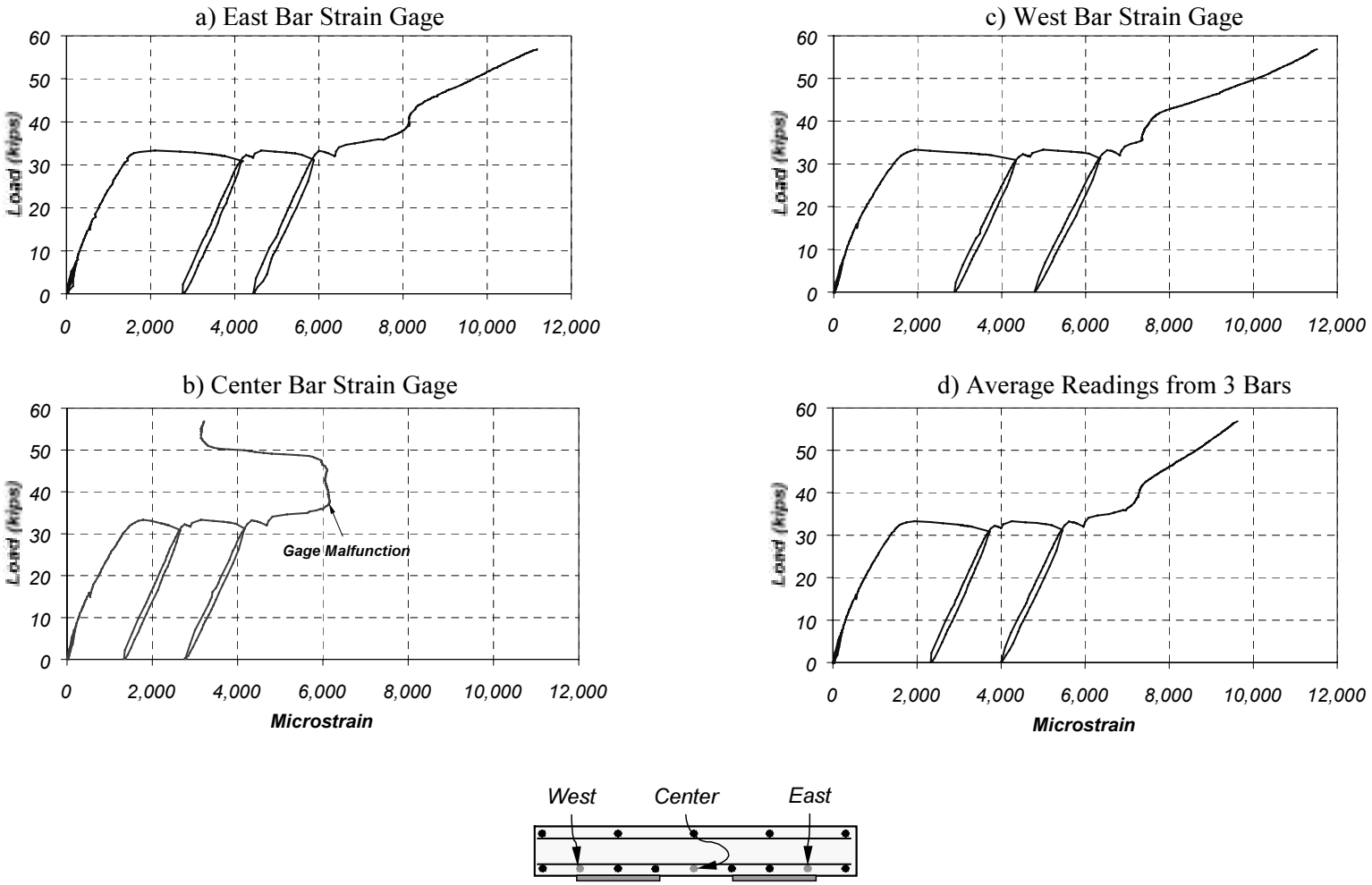

Figure D.39 Measured Reinforcing Bar (#6) Strains in Specimen FS-2 (Section N1)

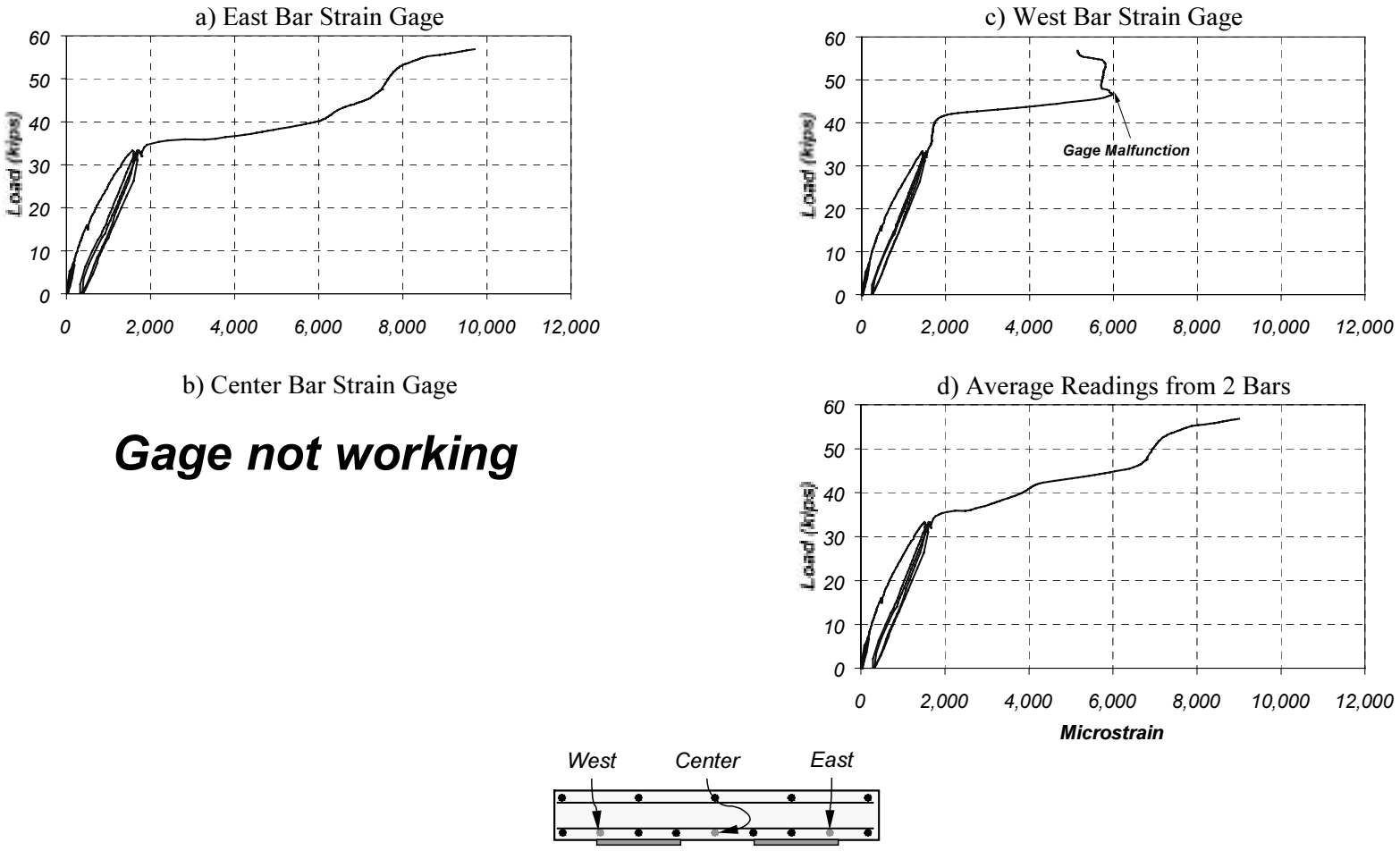

Figure D.40 Measured Reinforcing Bar (#6) Strains in Specimen FS-2 (Section S1)

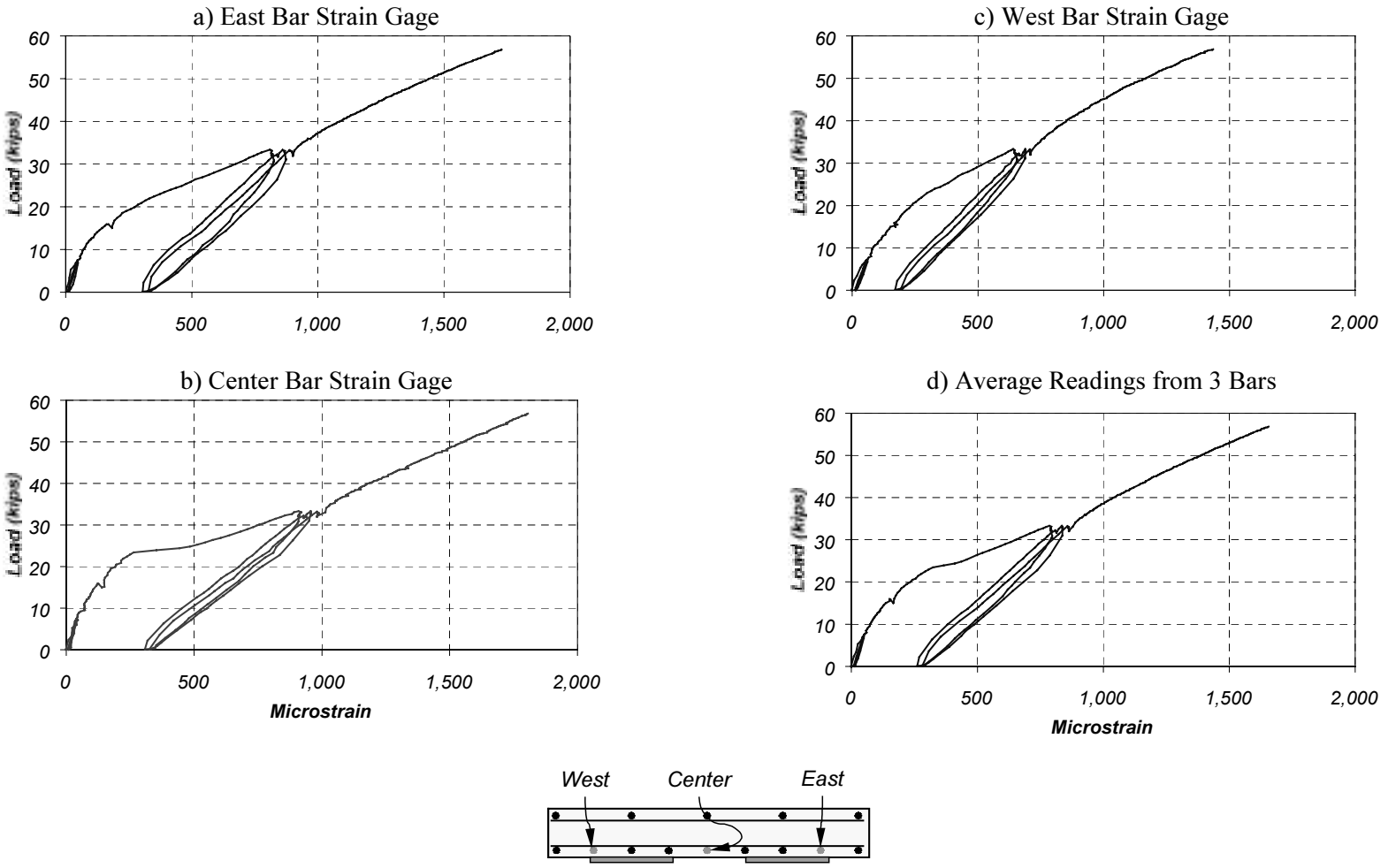

Figure D.41 Measured Reinforcing Bar (#6) Strains in Specimen FS-2 (Section N2)

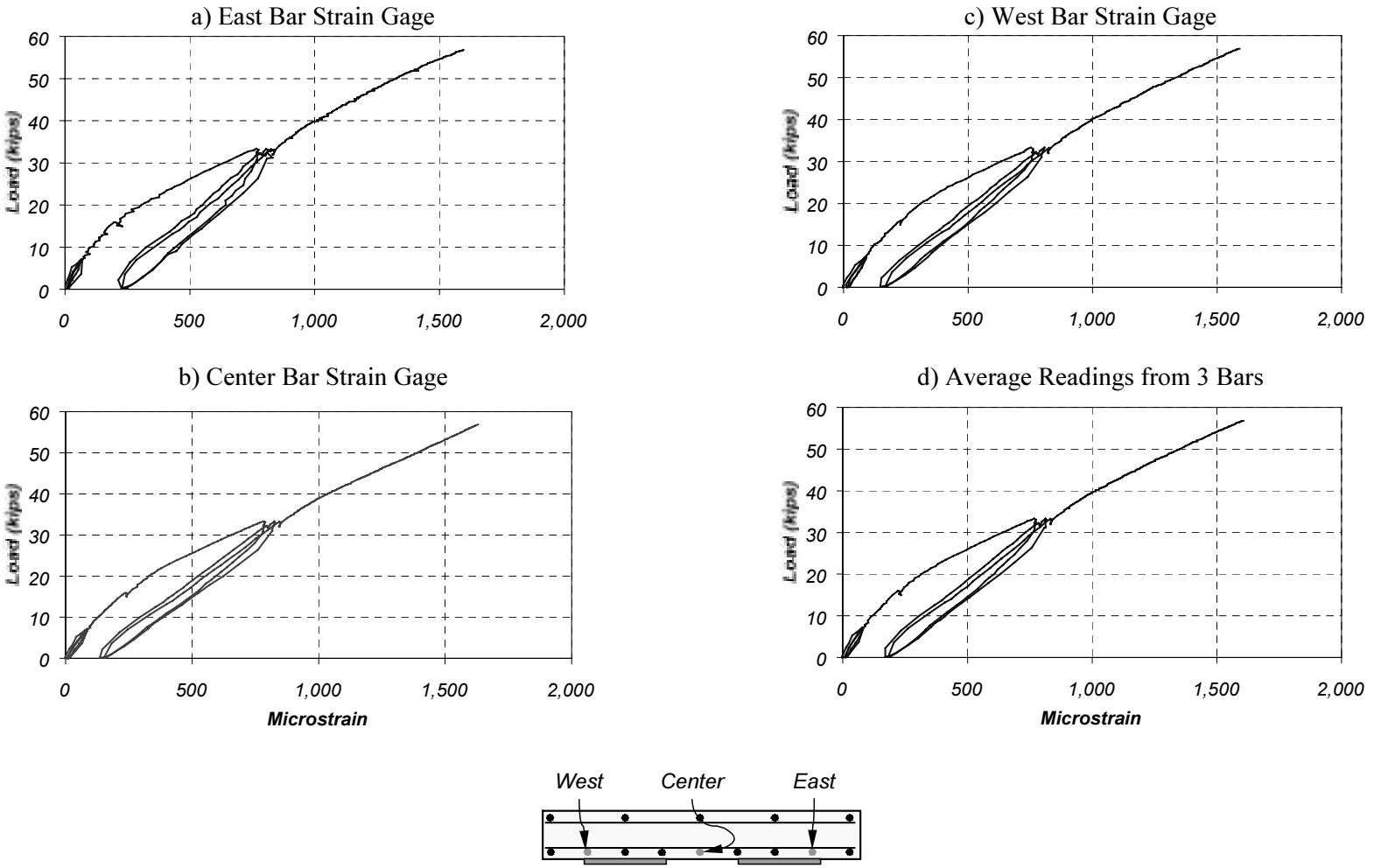

Figure D.42 Measured Reinforcing Bar (#6) Strains in Specimen FS-2 (Section S2)

a) East Strain Gage

Gage not working

c) West Strain Gage

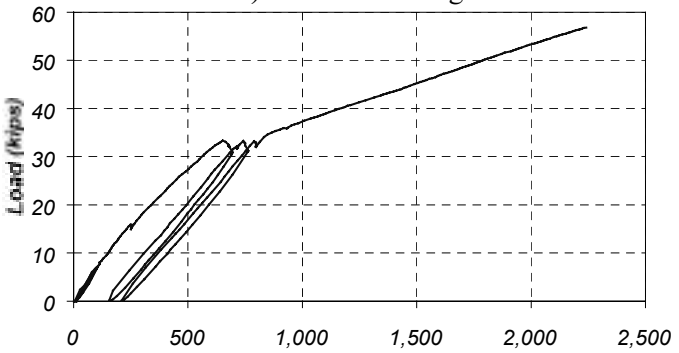

b) Center Strain Gage

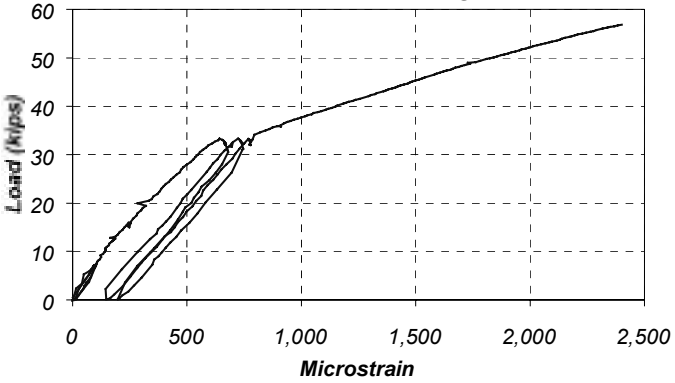

d) Average Readings from 2 Gages

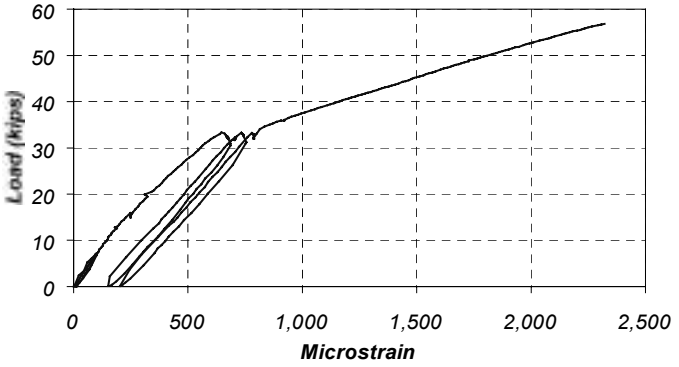

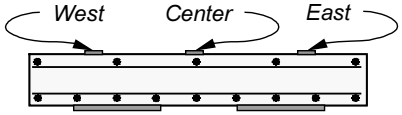

Figure D.43 Measured Strains on Concrete Slab in Specimen FS-2 (Section N1)

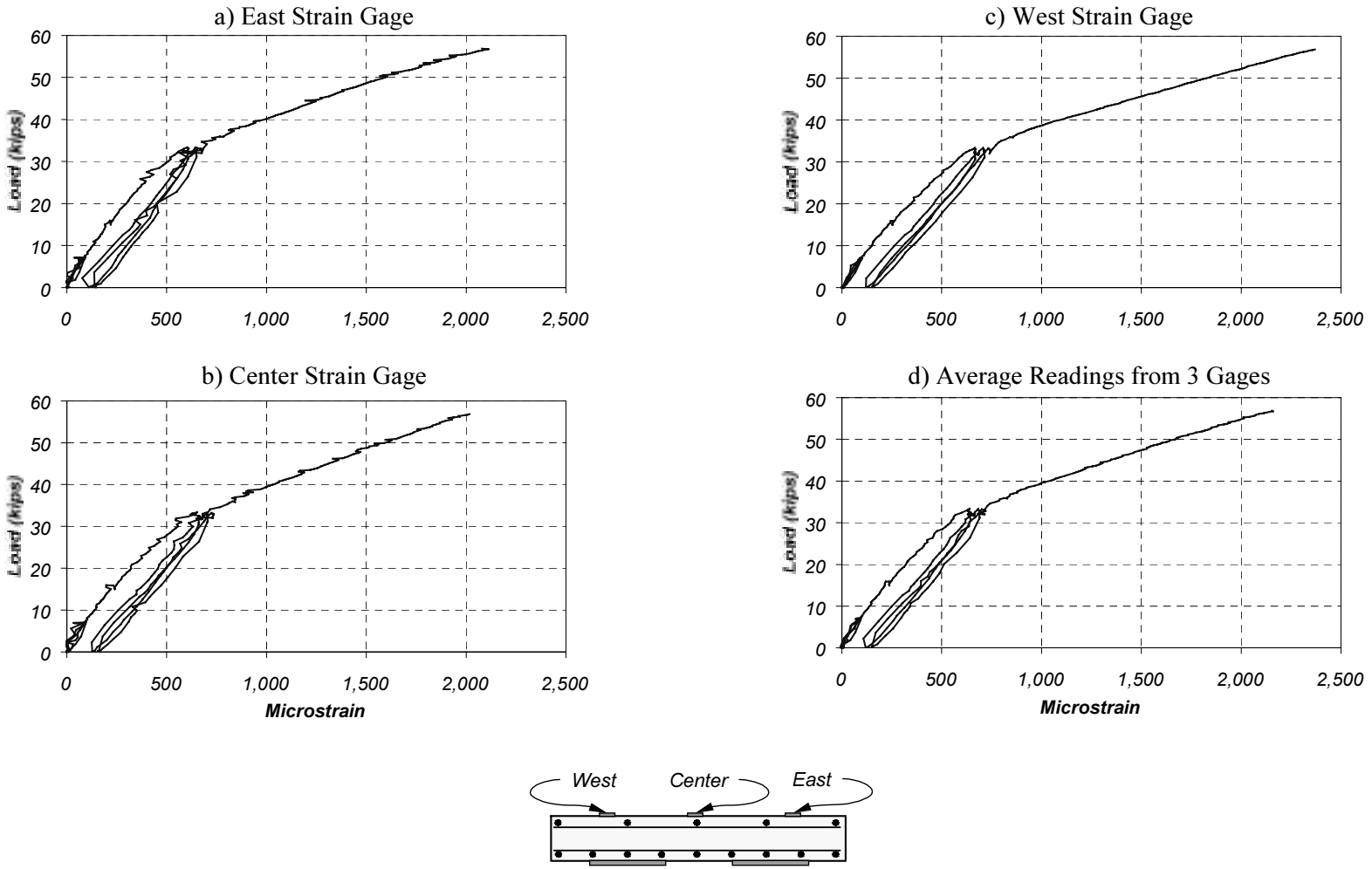

Figure D.44 Measured Strains on Concrete Slab in Specimen FS-2 (Section S1)

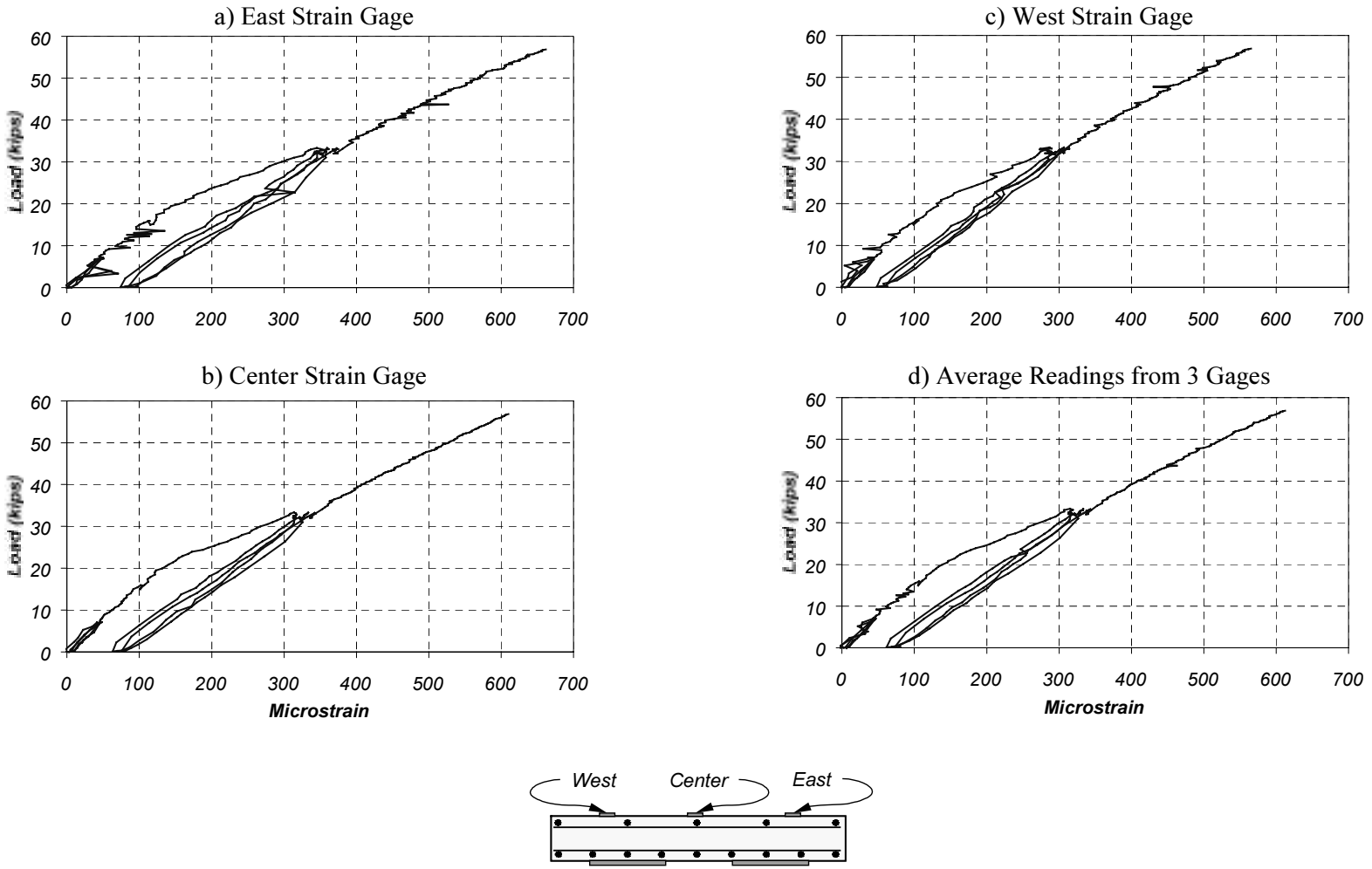

Figure D.45 Measured Strains on Concrete Slab in Specimen FS-2 (Section N2)

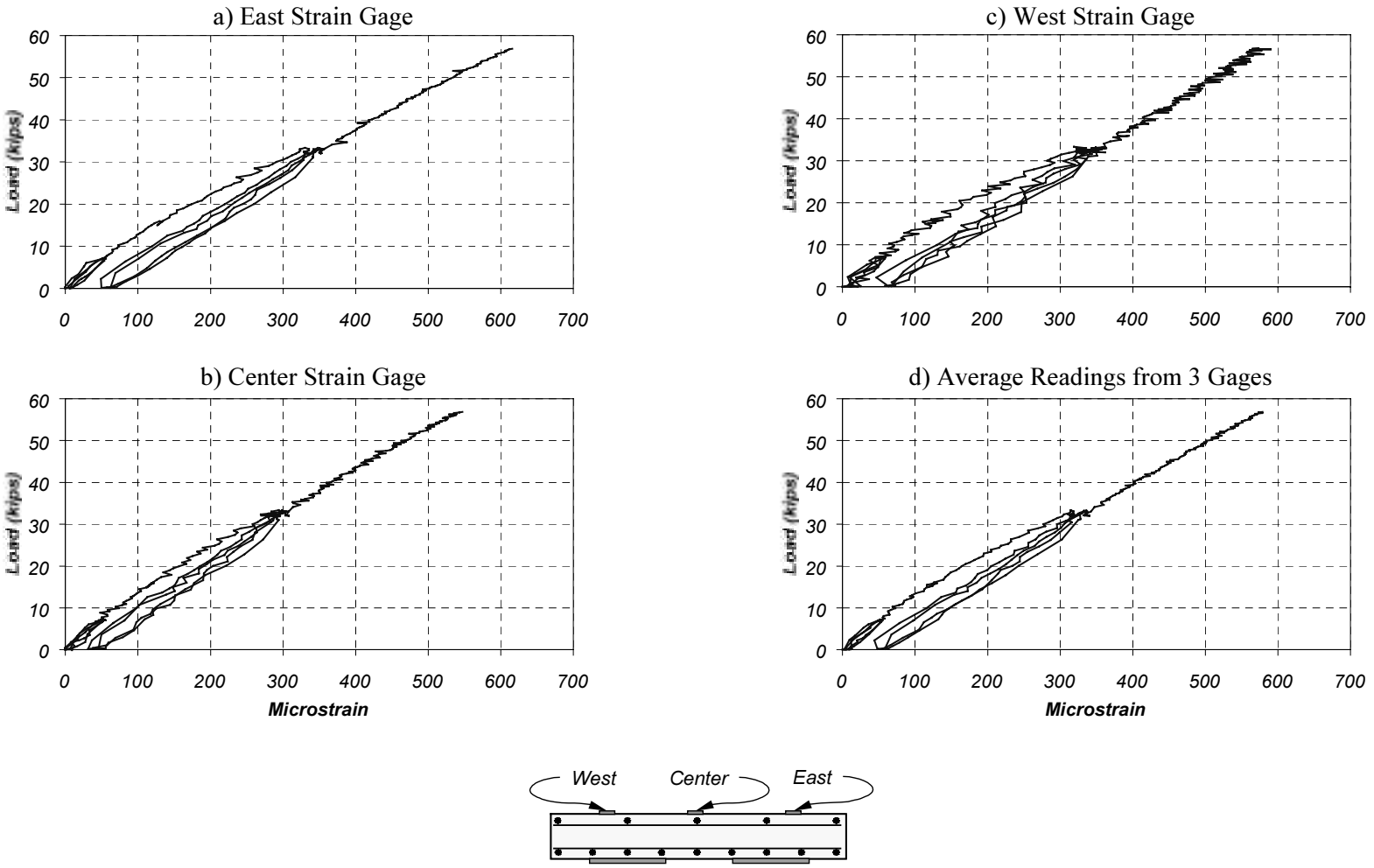

Figure D.46 Measured Strains on Concrete Slab in Specimen FS-2 (Section S2)

a) E-Sheet Strain Gage

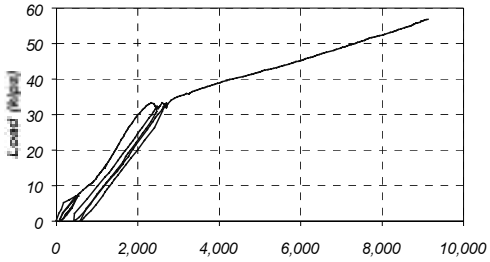

c) W-Sheet Strain Gage

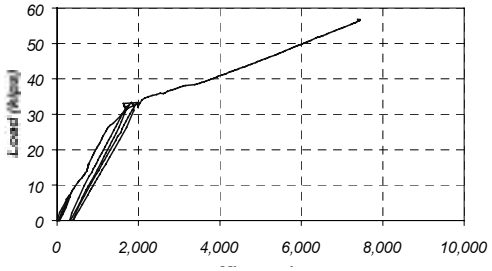

b) E-Center Sheet Strain Gage

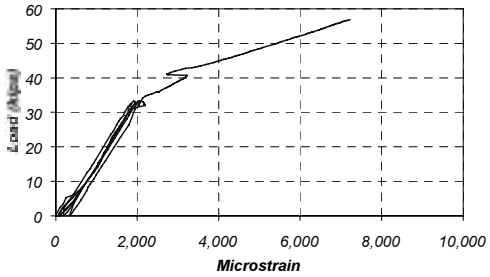

d) W-Center Sheet Strain Gage

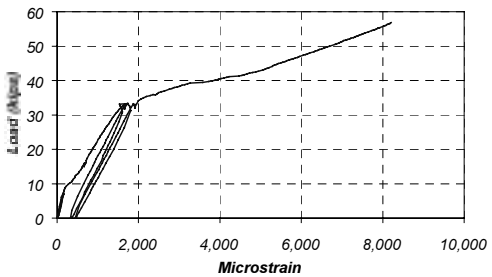

e) Average Readings from 4 Strain Gages

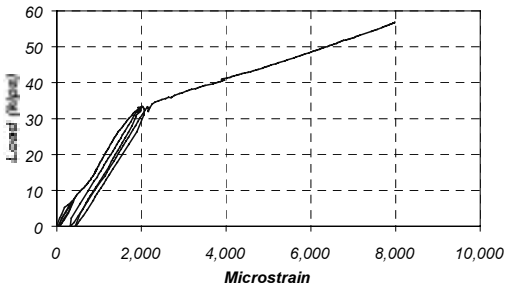

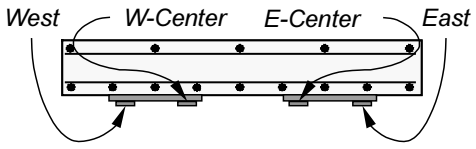

Figure D.47 Measured Strains on CFRP Sheets in Specimen FS-2 (Section N1)

a) E-Sheet Strain Gage

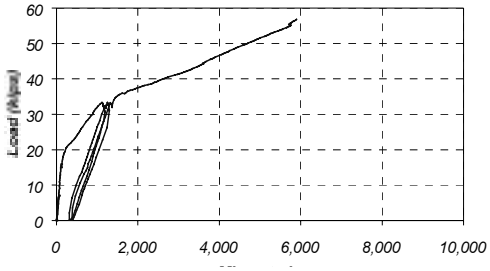

c) W-Sheet Strain Gage

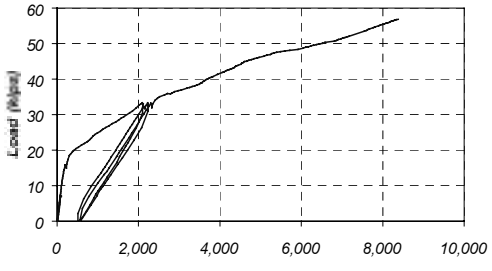

b) E-Center Sheet Strain Gage

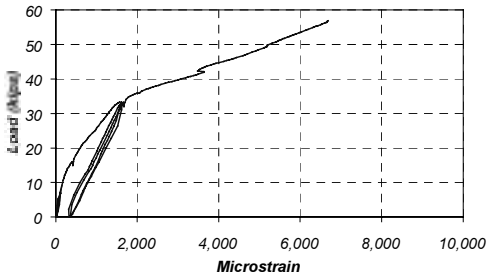

d) W-Center Sheet Strain Gage

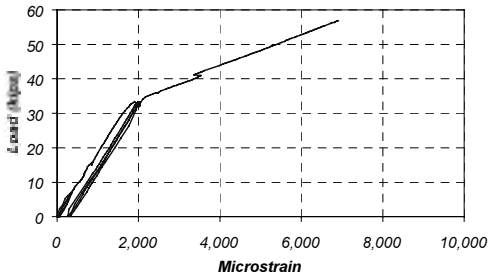

e) Average Readings from 4 Strain Gages

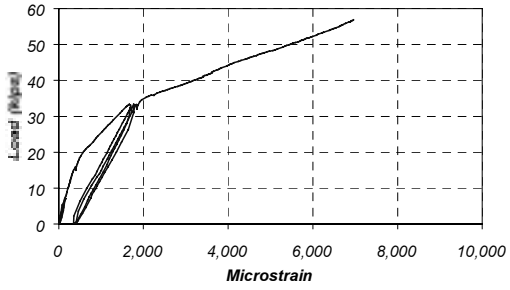

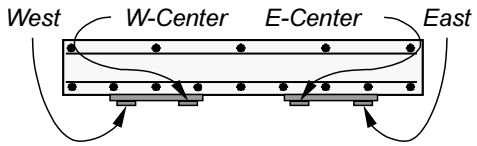

Figure D.48 Measured Strains on CFRP Sheets in Specimen FS-2 (Section S1)

a) E-Sheet Strain Gage

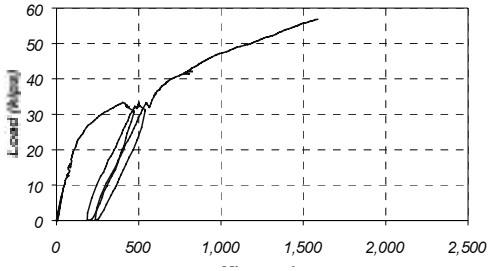

c) W-Sheet Strain Gage

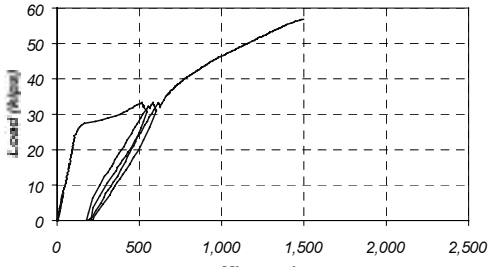

b) E-Center Sheet Strain Gage

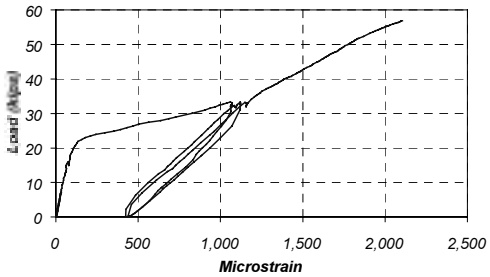

d) W-Center Sheet Strain Gage

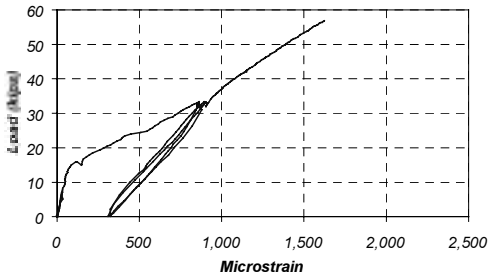

e) Average Readings from 4 Strain Gages

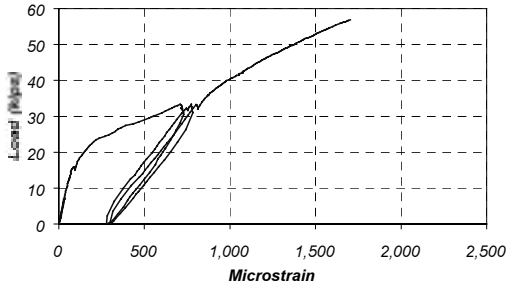

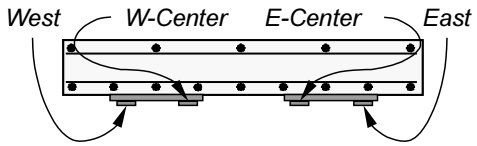

Figure D.49 Measured Strains on CFRP Sheets in Specimen FS-2 (Section N2)

a) E-Sheet Strain Gage

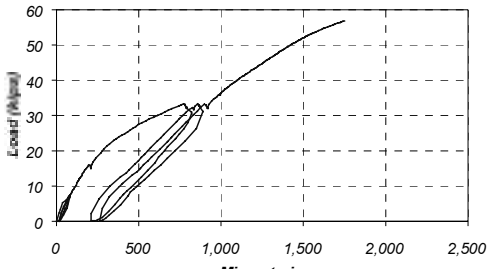

c) W-Sheet Strain Gage

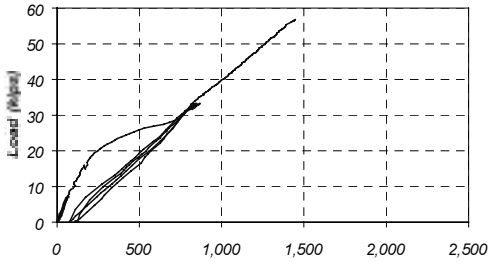

b) E-Center Sheet Strain Gage

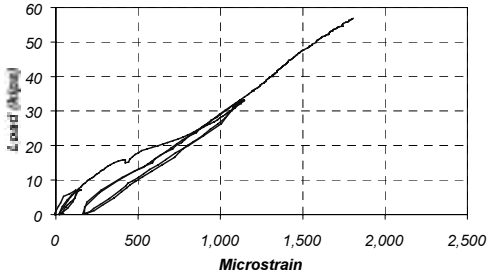

d) W-Center Sheet Strain Gage

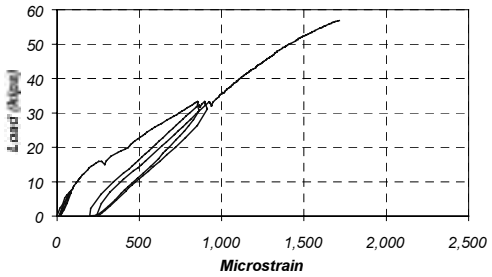

e) Average Readings from 4 Strain Gages

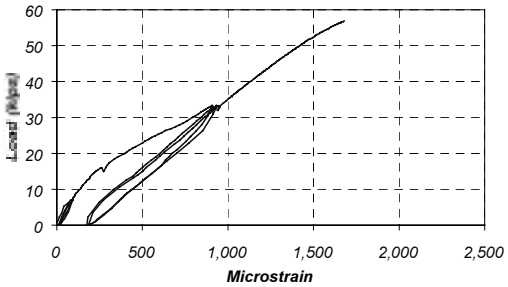

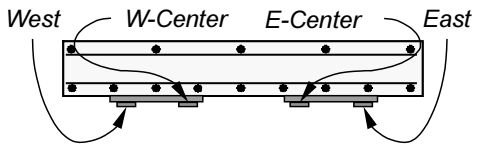

Figure D.50 Measured Strains on CFRP Sheets in Specimen FS-2 (Section S2)

References

American Association of State Highway and Transportation Officials (AASHTO 1994), *Manual for Condition Evaluation of Bridges*, Washington, D.C., 1994.

American Association of State Highway and Transportation Officials (AASHTO 1996), *Standard Specifications for Highway Bridges*, 16th Edition, Washington, D.C., 1996.

American Concrete Institute (ACI 318-99), Building Code Requirements for Structural Concrete (318-99) and Commentary (318R-99), Farmington Hills, Michigan, 1999.

American Society for Testing and Materials (1996), *Standard Test Method for Compressive Properties of Rigid Plastics,* Annual Book of ASTM Standards, Vol. 08.01, Designation: D 695-96, 1996.

American Society for Testing and Materials (2000a), *Standard Test Method for Tensile Properties of Plastics, Annual Book of* ASTM Standards, Vol. 08.01, Designation: D 638-99, 2000.

American Society for Testing and Materials (2000b), *Standard Test Methods for Flexural Properties of Unreinforced and Reinforced Plastics and Electrical Insulating Materials,* Annual Book of ASTM Standards, Vol. 08.01, Designation: D 790-99, 2000.

Arduini, M. and Nanni, A. (1997), "Parametric Study of Beams with Externally Bonded FRP Reinforcement", *ACI Structural Journal*, Vol. 94, No. 5, September-October 1997.

Breña, S.F., Bramblett, R.M., Benouaich, M.A., Wood, S.L, and Kreger, M.E. (2001), "Use of Carbon Fiber Reinforced Polymer Composites to Increase the Flexural Capacity of Reinforced Concrete Beams," Research Report 1776-1, Center for Transportation Research, University of Texas, Austin, TX, April 2001.

Bizindavyi, L. and Neale, K.W. (1999), "Transfer Lengths and Bond Strengths for Composites Bonded to Concrete", *Journal of Composites for Construction*, Vol. 3, No. 4, November 1999, pp. 153-160.

Bussell, L. C. (1997), *Diagnostic Testing for Improved Load Rating of Reinforced Concrete Slab Bridges,* Thesis presented to the Graduate School in partial fulfillment of the requirements for the degree of Master of Science in Engineering, The University of Texas at Austin, May 1997.

Ferguson, P.M. (1958), *Reinforced Concrete Fundamentals*, 3rd Ed., John Wiley & Sons, 1958.

Hognestad, E. (1950), *An Experimental Study of Combined Bending and Axial Load in Reinforced Concrete Members*, University of Illinois, Engineering Experiment Station, Bulletin 399, October 1950.

Jensen, V.P., Kluge, R.W., and Williams, C.B. (1943), *Highway Slab-Bridges with Curbs: Laboratory Tests and Proposed Design Method*, University of Illinois, Engineering Experiment Station, Bulleting 346, July 1943.

Master Builders, Inc. (1998), *MBrace™ Composite Strengthening System-Engineering Design Guidelines,* Cleveland, OH, 1998.

Meier, U., Deuring, M., Meier, H., and Schwegler, G. (1992), "Strengthening of Structures with CFRP Laminates: Research and Applications in Switzerland", *Advanced Composite Materials in Bridges and Structures*, Canadian Society for Civil Engineering, 1992.

Menegotto, M. and Pinto, P. (1973), "Method of Analysis for Cyclically Loaded Reinforced Concrete Plane Frames Including Changes in Geometry and Nonelastic Behavior of Elements Under Combined Normal Force and Bending", *IABSE Symposium on the Resistance and Ultimate Deformability of Structures Acted on by Well-Defined Repeated Loads,* Lisbon, 1973.

Sika Corporation (1997), *Engineering Guidelines for the Use of CarboDur® (CFRP) Laminates for Structural Engineering,* Lyndhurst, NJ, 1997.

Sika Corporation (1999), *Sika Carbodur®– Structural Strengthening Systems*, Lyndhurst, NJ, 1999.

Stanton, J. F. and McNiven, H. D. (1979), *The Development of a Mathematical Model to Predict the Flexural Response of Reinforced Concrete Beams to Cyclic Loads, Using System Identification,* Earthquake Engineering Research Center, Report No.UCB/EERC-79/02, January 1979.

Texas Department of Transportation (TxDOT 1999), Bridge Inventory, Inspection, and Appraisal Program (BRINSAP) Load Rating Spreadsheet, 1999.

Timoshenko, S.P. and Goodier, J.N. (1970), *Theory of Elasticity*, 3rd Edition, McGraw-Hill, 1970.

Velázquez, B. M. (1998), *Diagnostic Load Tests of a Reinforced Concrete Pan-Girder Bridge*, Thesis presented to the Graduate School in partial fulfillment of the requirements for the degree of Master of Science in Engineering, The University of Texas at Austin, August 1998.